Durham E-Theses

A geochemical and petrological study of the tertiary minor intrusions of Rhum, northwest Scotland

Forster, R. M.

How to cite:

Forster, R. M. (1980) *A geochemical and petrological study of the tertiary minor intrusions of Rhum, northwest Scotland*, Durham theses, Durham University. Available at Durham E-Theses Online: http://etheses.dur.ac.uk/7948/

Use policy

A geochemical and petrological

study of the Tertiary minor intrusions of

Rhum, Northwest Scotland.

A thesis submitted for the degree of
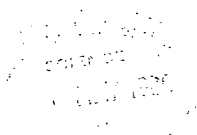Doctor of Philosophy

by

R.M. Forster, B.Sc.

Graduate Society   February, 1980

Petrogenesis? - God made them.

                          N.A. Matthew.

Dedicated to my parents, without whom
none of this would have been possible.

ABSTRACT

The Rhum minor intrusion suite is petrographically and compositionally variable, the majority of the basic rocks are aphyric dolerites but olivine phyric (picritic) and plagioclase phyric (big feldspar) dolerites are also present. In addition, several medium to coarse grained gabbro and peridotite plugs occur. Intermediate rocks are not abundant and acid dykes are rare.

The basic and intermediate intrusions occur in a variety of structural environments all over the island, the gabbros and peridotites are generally emplaced as plugs in the northern and southern Torridonian tracts, while the few acid dykes are usually closely associated with the plutonic acid rocks.

Twelve classes of dolerite (Groups 1-12) and five classes of gabbro have been distinguished on geochemical and petrographic grounds. The suite as a whole is characterised by high MgO levels when compared with rocks of analogous differentiation in other Tertiary suites of North-West Britain. Several of the group 1 picrites are believed to have existed as mafic liquids with 15-20 wt% MgO at high crustal levels. In addition the basic members (dolerite groups 2 to 4) and several of the gabbros are characterised by higher Ni and Cr and lower Al_2O_3 than comparable British Tertiary rocks. Discriminant Function analysis of the compositional variation within the basic members of the Rhum

minor intrusion suite has shown that the majority of these rocks are completely transitional between alkali olivine basalt and tholeiite basalt and contrast with the mildly alkaline Skye Main Lava Series and the mildly tholeiitic Ardnamurchan cone sheets. In contrast, the dolerite groups 5 and 6 are very similar to some of the Skye magma types and consequently are believed to be outlying members of the Skye regional dyke swarm. Of the intermediate rocks, the dolerite groups 8 and 9 and the gabbroic differentiates are tholeiitic in affinity and the dolerite groups 10 to 12 are alkalic in affinity.

Detailed field and geochemical investigation has shown there is a progression from tholeiitic basic magmas to high MgO more alkalic composition with time. Despite the known presence of a large upper crustal magma chamber on Rhum, the geochemical variation of the majority of the basic rocks is compatible with processes operating below 15 km within the lower crust, or in the upper mantle at depths up to 80 km. In contrast the big feldspar (group 7) dolerites and the magmas which gave rise to the peridotite plugs are believed to have been tapped from a high level crustal magma chamber. In addition the divergence towards more extreme alkalic and tholeiitic compositions in the intermediate rocks coupled with their general porphyritic nature and their major oxide and trace element variation suggests that they are the product of low pressure fractionation processes.

Acknowledgements

producing various photographs and photographic plates.

The Nature Conservancy Council staff on the Island of Rhum also deserve mention and I wish to thank the Wardens, Mr. C. Brown and Mr. J. Sutton and the other inhabitants, especially Mr. and Mrs. A. McIntosh, for their help. I am also grateful to several members and past members of this department, Dr. C.H. Emeleus, Dr. B. Beddoe-Stephens, Mr. R.H. Hunter and Mr. T. McKay for their companionship during my field work.

This study has benefitted from active discussion with many people at Durham. In this respect I wish to thank Dr. D.M. Hirst, Dr. A. Peckett and also Dr. J.G. Holland for use of unpublished data, and my contemporaries Mr. R.H. Hunter, Mr. A.P. Jones, Mr. M. Ozcelick, Mr. Y. Panjasawatwong, Dr. I.T. Williamson, Mrs. A. Allwright and Mr. Christodoulou for their criticism and advice. In addition discussion on many aspects of Rhum geology with Mr. D. Kitchen (Queens University, Belfast) and Miss J. McClurg (Edinburgh University) has also proved fruitful.

Finally I wish to thank Mrs. C.L. Mines and Mrs. H. Wynn for typing the manuscript with speed and efficiency.

Page

LIST OF CONTENTS

LIST OF FIGURES

Page

LIST OF PLATES (ALL PHOTOMICROGRAPHS)

LIST OF TABLES   Page

CHAPTER ONE

THE GEOLOGY OF RHUM

Introduction

Rhum has received attention from geologists for

nearly 170 years, but was first mapped and described

in detail by A. Harker (1908, 1908b). Our present under-

standing of Rhum geology is based on several major

contributions including and postdating Bailey's (1945)

work in which the major dislocation enclosing the

Tertiary intrusive igneous rocks was interpreted as a

ring fault. Both Stewart (in Craig, 1965) and Dunham

and Emeleus (1967) have reviewed the history of research

on Rhum, to which publications the reader is referred for

further details. Of the investigations over the past 30

years, the importance of Brown's (1956) and Wadsworth's

(1961) demonstration that the layered ultrabasic rocks

of Rhum are cumulus in origin and the contributions by

Hughes (1960) and Dunham (1965a, 1968) on both the acid

rocks and the structure of the complex in general, are

outstanding.

I) General outline

Rhum is divided into two major portions by an

arcuate fault, the Main Ring Fault, which separates the

Torridonian and Triassic sediments of northern and

eastern Rhum from the Lewisian gneisses, the Torridonian grits and shales and the Tertiary intrusive rocks of central and western Rhum (Fig. 1.1). Lewisian gneiss and basal Torridonian grits only occur within the Main Ring Fault indicating uplift of these rocks and their associated intrusives within the confines of this fault (Bailey,1945). The majority of the Tertiary rocks are intrusive. However a small area of lavas occurs in western Rhum, these lavas are younger than the westerly extension of the Main Ring Fault in this area as they can be seen to overlap the fault on Bloodstone Hill (NM318998) and Bealach a' Bhraig Bhig (NG340.000) (Black, 1952; Emeleus and Forster, 1979).

The intrusive rocks can be divided into two main groups, one consisting essentially of acidic rocks, the other of layered ultrabasic and associated gabbroic rocks. The acid rocks and associated breccias have been subdivided into four types (Hughes, 1960; Dunham, 1968), these being granophyre, felsite, explosion breccia and tuffisite. They occur along with Lewisian and basal Torridonian in two main areas these being the Southern Mountains Complex (Hughes, 1960), in southeastern Rhum and the Northern Margin Complex (Dunham, 1965a, 1965b, 1968) in east-central Rhum. There is also an area composed almost entirely of granophyre in western Rhum (Black, 1952). Much

of central and southern Rhum consists of a sequence of layered peridotites and gabbros.

The Geological sequence on Rhum

The geological succession on Rhum as generally understood at the present day is presented in Table 1.1. It only differs from the sequence outlined by Dunham and Emeleus (1967, Table 1.2b) by the insertion of the Papadil Gabbro pre-dating the layered peridotites and by the insertion of ultrabasic intrusion breccias prior to the intrusion of the later gabbros and peridotites (see p. 10). These ultrabasic breccias generally have poorly exposed contacts, thus Harker (1908) speculated they were intrusive contacts whilst Wadsworth (1961, 1973) considered them to be fault scarp deposits. Mapping by Donaldson (1975) revealed two better exposed breccias with intrusive contacts which led him to reinterpret all the breccia contacts as intrusive. The eastern contact of the Harris Bay breccia (Donaldson, op.cit.) was examined as part of the present study and the breccia matrix is certainly intrusive into the adjacent peridotite. Following Donaldson the ultrabasic breccias on Rhum are considered to be later intrusions into the peridotite as opposed to contemporaneous fault scarp screes.

Pre-Tertiary

Lewisian gneiss outcrops in three main areas, the largest mass lies on the western side of the Southern Mountains Complex (Hughes, 1960), another strip occurs southeast of this on the lower slopes of Sgurr nan Gillean, the third major outcrop is west of the Long Loch in the Northern Margin Complex (Dunham, 1968). Smaller outcrops are located north of the Long Loch, south of Priomh Lochs, north of Meall Breac, on the summit of Ard Nev and between Ard Nev and Ard Mheall.

The Torridonian sequence has been divided into five major groups (Black and Welsh, 1961). The lowest member, the Basal grits, consisting of grits and shales, occurs entirely within the Main Ring Fault. However, the Bagh na h Uamha shale outcrops on both sides of the Main Ring Fault to the east of Dibidil Glen. The three remaining groups occur entirely outside the Main Ring Fault. The highest of these, the Guirdil Arkose Group, is uncon- formably overlain by an outlier of Triassic sediments to the north of Glen Shellesder (Fig.1.1).

Tertiary

The earliest known Tertiary rocks on Rhum are basic igneous fragments contributing to the explosion breccia in the Northern Margin Complex. Although locally important (e.g.

northeast of Loch Gammich NM 380989) the vast majority
of the explosion breccia in both the Northern Margin and
Southern Mountains igneous complexes consists of comminuted
Torridonian with rare, but locally abundant Lewisian
fragments (Hughes, 1960; Dunham, 1968).

Tuffsites which invariably cut the explosion breccias
occur as masses up to 0.5 km long in the Southern Mountains
(Hughes op.cit.) and as thin sheets with every angle from
vertical to horizontal in the Northern Margin Complex.
They are characterised by a matrix of devitrified glass
with xenocrystic quartz and plagioclase. A diverse xenolith
assemblage of Lewisian, Torridonian, dolerite, felsite
granophyre and gabbro have been located in the Southern
Mountains tuffisites but only Torridonian and occasional
Lewisian fragments have been recorded in the Northern
Margin Complex.

The felsites in both areas chill against and intrude
the explosion breccias, although Hughes (1960) records a
single fragment of felsite in an explosion breccia south
of Sgurr nan Gillean which is cut by later felsite,
showing more than one intrusion of felsite magma has
occurred (cf. Emeleus and Forster, 1979, p.23). Whilst
tuffisite is generally earlier than felsite in the
Northern Margin Complex the Southern Mountain tuffisites
both contain blocks of felsite and are themselves cut by

later felsites. Thus whilst the explosion breccias are generally of earlier formation the periods of tuffisite and felsite intrusion overlapped.

The age relationships of the granophyre to the other acid intrusions are obscure as the contacts are badly exposed. In the Southern Mountains the critical contact between the Papadil granophyre and the tuffisites and felsites is unfortunately scree covered (Hughes, 1960).

Hughes (op.cit.) commented on the development of an intrusion breccia between felsite and gabbro at the head of Glen Dibidil which he believed was due to rheomorphic melting of the felsite by later gabbro and also commented on the truncation of dykes within the felsite by gabbro in Dibidil Glen. Dunham (1964) presented a more detailed study of rheomorphic melting of felsite by gabbro in the Northern Margin complex. The granophyre-peridotite contact at Harris Bay also shows veining of the more basic rock by acid veins which were attributed to rheomorphic melting by both Bailey (1956) and Wadsworth (1961).Thus the Western Granophyre predates the ultrabasic and basic rocks.

The age relationship between the Papadil granophyre and the gabbros and peridotites is less clear. Hughes (1960) noted that the gabbros from this contact possessed plagioclase clouded with magnetite dust and that magnetite

had also exsolved along the augite cleavages, features he attributed to reheating of the gabbros. Although he noted amphibole veinlets cutting the gabbro he found no evidence of the type of backveining he had encountered in Dibidil and suggested the granophyre postdated the gabbro. However, Dunham and Emeleus (1967) found re-crystallisation textures in the granophyre from this contact identical to those from Harris Bay and south of Minishal where back-veining had occurred. Furthermore. they pointed out that the gabbro and peridotites cross (and thus probably postdate) the Main Ring Fault and the Lewisian-granophyre boundary (Fig. 1.2).

The contact in question was examined as part of the present study to ascertain which body was the earlier intrusion. Two critical pieces of evidence suggest the gabbro post-dates the granophyre. Firstly, the contact is exposed 100 m north of the granophyre-Torridonian-gabbro triple junction (Fig. 1.2) and the gabbro here chills towards the granophyre. Secondly, basic minor intrusions 50 m north of this locality are back-veined (with veins up to 2 cm thick) in a distinctive angular manner by the enclosing granophyre. This type of veining is a common occurrence at the contacts of the major acid and basic bodies on Rhum and can help produce extensive breccias with increased rheomorphic melting (Emeleus and Forster, 1979, p.9).

Thin sections reveal that <u>both</u> the gabbro and the
granophyre show features attributable to reheating, the
granophyre in particular exhibits marked fingerprint textures
in the relict plagioclase phenocrysts. Fig. 1.2 shows
that the peridotite mass northeast of Papadil is in
direct contact with Torridonian sandstone and appears to
cut out the gabbros which lie both north and east of
this contact. A later peridotite body of this size
would provide a viable heat source to account for the
reheating of both the Papadil granophyre and the gabbro
at the contact under discussion. In addition the gabbro
at Papadil is atypical when compared with other gabbros
marginal to the layered peridotites, as the latter are
often deeply weathered and lack the abundant xenoliths
found in the Papadil gabbro. The Papadil gabbro is cut
by many dykes whereas the adjacent peridotites are
relatively dyke free suggesting the latter are younger.

The next event in the Tertiary sequence was the
intrusion of elongate tongues of peridotite which cut
Lewisian gneiss, Torridonian, explosion breccia and
granophyre in the Northern Margin Complex. The eastern-
most tongue also cuts the Main Ring Fault (Dunham, 1965b).
The tongues are petrographically distinct from peridotites
of the layered series and are believed by Dunham (<u>op.cit</u>.)
to be separated from the layered series by a drift-

covered fault marking the westerly continuation of the
fault along which the main ultrabasic mass was emplaced.

The age relationships of the layered peridotites and
the associated gabbros to other geological events on
Rhum has been assessed by several authors. Bailey (1945)
believed the ultrabasic rocks post-dated the development
of the Main Ring Fault, this view was supported by
Brown (1956), Wadsworth (1961), and Wager and Brown (1968);
the age relationships to the adjacent acid rocks have
been discussed previously. Both Brown (1956) and Wadsworth
(1961) considered the layered series peridotites were
emplaced in their present position as an essentially solid
mass lubricated by a marginal gabbro. This gabbro is
continuous along the margins of the Eastern Layered
Series (Brown, 1956). However Wadsworth (1961) commented
on its discontinuous nature along the margins of the
Western Layered Series. Wadsworth (op.cit.) suggested
the lack of faulting in those country rocks which are in
direct contact with the peridotites could be explained
by firstly, the differential displacement of the lubricating
basic magma and secondly, the subsequent annealing of any
fractured country rocks by the adjacent hot peridotite.

The layered series peridotites are frequently cut
by later gabbros and eucrites These can occur in every
attitude from steeply transgressive dyke-like bodies

(e.g. Fiachinis eucrite dyke, Wadsworth 1961, Fig.2) or
as sheets more or less conformable with the peridotite
layering (e.g. Askival Plateau gabbro, Brown 1956, Fig.1).
The sequence of gabbro intrusion is rarely determinable in
the field, however Wadsworth (op.cit. p.55) suggested the
gabbro west of the Long Loch fault (NM367958) postdated
the Glen Harris eucrite. In addition, both Brown and
Wadsworth indicate their lubricating marginal gabbro
postdates many of the gabbros associated with the layered
series and this marginal gabbro is also cut by a fine-
grained olivine gabbro on Cnapan Breaca.

The relative ages of the ultrabasic breccias and the
gabbros cannot be stated with any certainty. However
Wadsworth (1961, Fig.2) shows the Lag Sleitir breccia
apparently cut out by elongate gabbroic bodies on its
northwestern and northeastern margins suggesting the
gabbros postdate the breccias, similarly the Fiachnis
eucrite dyke (Wadsworth op.cit.) may cut the north-western
margin of the Ruinsival breccia.

Lavas

The lavas of western Rhum are the youngest major
igneous body on Rhum. The age relationships of the lavas
on Orval to the underlying granophyre were firmly
established by Black (1952) who showed that they rested

unconformably on an eroded granophyre surface. The lavas
are underlain by and are interbedded with conglomerates
which contain cobbles of Lewisian, Torridonian,tuffisite,
explosion breccia, granophyre,dolerite,basalt and gabbro
(Dunham and Emeleus, 1967).Subsequent investigation has
also revealed cobbles of felsite (Emeleus et al., 1971;
Emeleus and Forster, 1979) and allivalite (Emeleus and
Forster op.cit.). The presence of the ultrabasic rocks
confirms that the emplacement and subsequent erosion with
unroofing of the layered peridotites occurred prior to
the extrusion of the lavas.

II) Previous research on the minor intrusions of Rhum

Introduction

Two major works form the basis of our understanding
of the minor intrusions of Rhum at the present day. The
first major contribution was made by Harker (1908) who
collated several points of interest in his Small Isles
Memoir. A more recent contribution was made by Speight
(1972) in a structurally orientated study of dyke distribution
patterns in the Small Isles, Skye and Ardnamurchan. In
addition to these works the contact relationships of some
basic dykes intruded into the Western Granophyre were
studied by Roobol (1971) and brief reference to other
minor intrusions has been made by several authors (Hughes

1960, p.114; Wadsworth, 1961, p.57; Dunham and Emeleus 1967; Emeleus, 1973, p.159).

The two major works differ in scope. Harker incorporated observations on all the minor intrusions including basic sills, rare acid dykes and the gabbro and peridotite plugs. He was concerned with the distribution of the basic dykes over the whole island unlike Speight (1972) who studied only coastal sections within the Torridonian and thus did not deal with dyke relationships within the central complex. A full discussion of the quasi-statistical techniques used in his thesis is given by Speight (1972, Chapter V).

a) Basic Dykes

i) Distribution of the basic dykes as a function of the host rocks.

Harker (1908) had definite views on the intensity of the dyke swarm as a function of the host rock. He believed the granophyres were relatively dyke free and considered the abundance of dykes exposed along the coast northwest of Harris to be a "noteworthy exception". He also maintained that the Torridonian sandstones and the plutonic basic and ultrabasic rocks were intruded by a similar number of dykes. In addition other authors note the truncation of dykes at major contacts on Rhum.

Hughes (1960) and Dunham and Emeleus (1967) mention the occurrence of basic sheets in the felsite in Dibidil and on Cnapan Breaca respectively which do not cut the adjacent gabbros, similarly Wadsworth (1961) noted the truncation of dykes in the Western Granophyre by the later gabbro and peridotite.

ii) Dyke trends

Rhum is sometimes cited as a good example of a volcanic centre with an associated radial dyke swarm (Richey 1948, p.86). This was first asserted by Harker (1908) and has been reiterated by Richey (1961, pp. 96-97), Stewart (1965) and Dunham and Emeleus (1967). However, this view has been recently contested by Speight (1972). His investigations showed that the Torridonian outside the Main Ring Fault contains a linear dyke swarm (see section iii). Fig. 1.3 (taken from Speight 1972, p.334) shows a radial pattern cannot be discerned using the projection of the average trend of groups of ten dykes. The possibility of a radial dyke swarm cutting the ultrabasic rocks is discussed later (Chapter 2, p. 31). Speight (op.cit.) arbitrarily selected dykes trending NE-SW and referred these to a Rhum sub-swarm (a technique he also applied on Skye and Ardnamurchan) the validity of this sub-swarm is discussed in Chapter 2, p. 29 .

iii) The intensity of the dyke swarm

That dykes are numerous on Rhum is evidenced by the accounts of Harker (1908, p.143) who recorded nearly 700 dykes and Speight (op.cit) located approximately 1000 dykes in coastal sections alone. Fig. 1.4 reproduced from Speight (op.cit. Fig.115) shows the dyke distribution is uneven with axes of high intensity running SE from the coast line at Papadil and the Allt nam Ba and NW from Kilmory. The map illustrating dyke intensity as a function of percentage crustal dilation (Speight op.cit., Fig.114) shows similar dyke intensity distribution patterns, the general maximum crustal dilation along the high intensity axes is between three and four percent although over five percent crustal dilation occurs on the coastline near the mouth of the Allt nam Ba.

Fig. 1.4 shows all the characteristics of a linear swarm, this is highlighted by the low dyke intensities on the northeastern coast of Rhum which Speight (1972, p.334) believed was further evidence against a radial dyke distribution pattern on Rhum.

iv) The dips and thicknesses of the dykes

All the previous work on these topics is incorporated in Speight's (1972) thesis. He noted that in general more dykes dipped SW as opposed to NE, an exception being the

dykes of northwestern Rhum and stated that the dykes

varied from 0.2 m to 11.0 m thick with most dykes lying

in the range 0.4-0.8 m.

b) Distribution of the sills and inclined sheets

   Harker (1908) recognised five different varieties

of basic sheet in his classification of the minor

intrusions of Rhum. These generally occur only in the

Torridonian, however one group, the inclined sheets, was

also seen cutting the acid and ultrabasic rocks. A full

account of the inclined sheets is presented later (Chapter

2, p. 38). Another group, the dolerite sills cutting the

Rhum lavas were reinterpreted as the massive dolerite

centres to basaltic lavas by Tomkeiff (1942, p.2).

   In northwest Rhum, Harker (op.cit.) recorded the

presence of a conspicuous sill running SW from Kilmory

which he described as both a "feldspar porphyritic basalt"

and a basic augite andesite without olivine. He also

noted the presence of a different set of aphyric "basic

augite andesites" in the southwestern part of the island.

   The fifth type of sheet was only briefly referred to

by Harker (op.cit.), these were thin sill-like bodies of

limited lateral extent which cut the Torridonian of

northern Rhum.

c) Acid Dykes

Harker (op.cit.) noted the rare occurrence of three acid dykes on Rhum, he also mentioned a pitchstone specimen in the older collections of the Geological Survey labelled as coming from Fionchra, which he failed to relocate. A recent detailed survey in the Fionchra region did not locate any pitchstone dykes (Emeleus pers. comm.) thus the survey specimen was probably either incorrectly labelled or not collected in situ.

d) Gabbro and peridotite plugs

Harker (1908) located approximately 15 peridotite plugs ranging up to 700 m in size. He considered them all to be intrusive with near vertical contacts one exception being the intrusion north of Bealach Mhic Neill (NM380998) which he suggested was lacolithic in form. The two ultrabasic dykes he describes occurring west of Papadil are, in fact, small elongate peridotite plugs. Dunham and Emeleus (1967) pointed out that the peridotite knoll west of Loch Sgoarishal show matrix banding and other features recollective of the tongues in the Northern Margin Complex (Dunham, 1965b) and suggested they could be of similar age.

Approximately 45 intrusive gabbroic bodies were located by Harker (1908) varying in dimension from 700 to 75 m. He distinguished 2 compositional varieties, one

gabbroic and the other eucritic, the latter apparently
cutting only the layered periodites. Dunham and Emeleus
(1967) noted petrographic similarities between gabbros in
the northern Torridonian tract and the early gabbros in the
Northern Margin Complex but stated the postulated early
age of the former could not be demonstrated in the field.

e) The sequence of intrusion

The chronological sequence of both major and minor
intrusions as proposed by Harker (1908) is presented in
Table 1.2a. As Harker considered that the gabbros and
peridotites predated the felsites, it is clear why he
believed there was a greater abundance of dykes in the
former. A revised sequence of both major and minor
intrusion proposed by Dunham and Emeleus (1967) is also
presented in Table 1.2b. The position of both the cone
sheets and the late radial dyke swarm in this second
sequence is in agreement with the more general account of
Stewart (1965).

Sound of Canna

Kilmory

Mullach Mor

Glen Shellesder

Guirdil

Bloodstone Hill

Fionchra

Minishal

road

Kinloch
castle

Loch Scresort

A'Bhrideanach

Orval

Ard Nev

Long Loch

Barkeval

Ard Mheall

road

An Dornabach

Glen Harris

Hallival

Harris Bay

Trallval

Askival

Ruinsival

Dibidil

Allt nam Ba

Sgurr nan Gillean

Sound of Rhum

Inbhir Ghil

Papadil

Tertiary

lavas and sediments

basic sheets

breccia zones in ultrabasic rocks

feldspathic peridotite and allivolite, frequently layered

small plugs of ultrabasic rock

gabbro, of various ages

granophyre and microgranite

porphyritic felsite and tuffisite

explosion breccia

Pre-Tertiary

Triassic sediments   λ = Jurassic limestone

Torridonian sediments { outside Main Ring Fault   fault

inside   loch

Lewisian, gneiss etc.   river

0   1   2   3 km

Fig. 1.1 Geological map of Rhum.

Fig. 1.2 Geological map of Papadil,
Southern Rhum; taken from
Emeleus and Forster (1979,
Fig.16). For relationship
to general geology see Fig.1.

o o o o o o o o	Peridotite
⊞⊞	Gabbro
┼	Granophyre
╱ ╲ ╱ ╲ ╱	Porphyritic felsite
Δ Δ Δ Δ Δ	Explosion breccia
o o o o o o o o o o	Torridonian sandstone
↘ 15	Dip of sediments, in degrees
300	Contours in metres
╱ ╱	Footpath

350

250

─7930

150

100

50

VII1

Inbhir
Ghil

600

500

400

300

200

VII6 15

Papadil
Lodge
(ruin)

VII2

─7920

Loch
Papadil

VII3 VII4

Rubha na
Pairce

Papadil
Pinnacle

VII5

17

to
Dibidil

15

15

0   500m

21

100

370

360

Allt na Gile

Fig. 1.3. Projection of the average trends of groups of ten dykes (redrawn from Speight 1972, Fig.109)
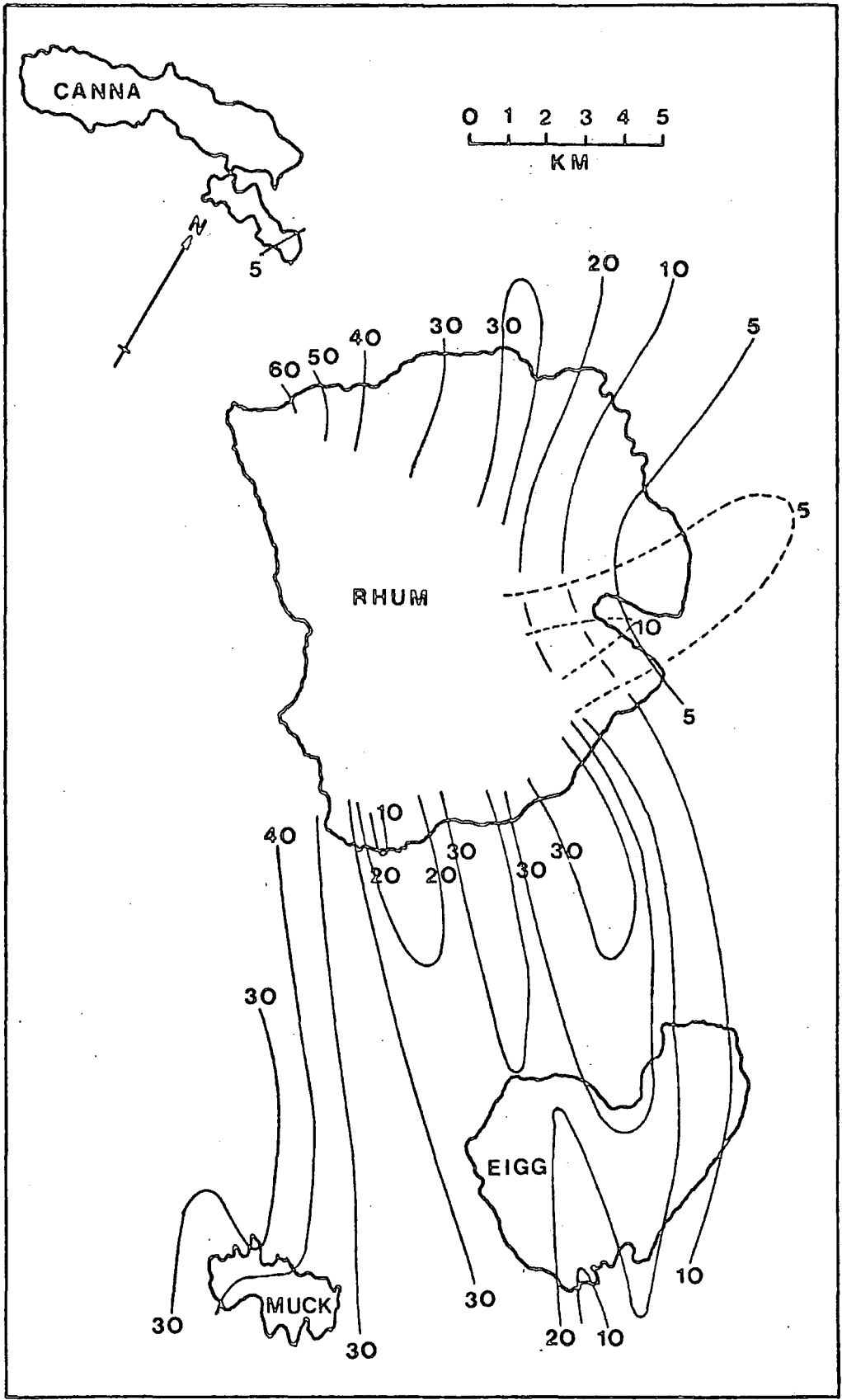
Fig. 1.4. Number of dykes per kilometre in the
coastal strata of Rhum, and the Small
Isles (redrawn from Speight (1972, Fig.115).

Lavas

Fine-grained olivine gabbro

Marginal gabbro

Gabbro and peridotites cutting ultrabasic rocks

Ultrabasic intrusion breccias

Layered peridotites

Ultrabasic tongues)
                   } age relations may be reversed
Papadil gabbro   )

Main Ring Fault

Granophyre

Felsite

Tuffisite

Explosion breccia

Triassic

Torridonian

Lewisian

Table 1.1.   The chronological sequence of major Tertiary

events and pre-Tertiary rocks on Rhum.

A		B	
	Pitchstones	Lavas	
			Radial basic and ultrabasic dykes
	Ultrabasic dykes		
	Basic Andesite Sheets	Fine-grained olivine gabbro	
	Inclined sheets		
		Ultrabasic tongues	Peridotite plugs
Felsite	Quartz felsite dyke		
			Cone sheets
Granophyre			
	Gabbro and peridotite plugs	Granophyre	
Basic rocks			
		Felsite	
Ultrabasic rocks			
			Tachylitic sheets
	Great group of sills		
		Tuffisites	
Basaltic Lavas			
		Explosion breccia	
	Basaltic material in solfataric dykes		
			Early Gabbros

Table 1.2. The sequence of major and minor intrusion envisaged by (A) Harker (1908) and (B) Dunham and Emeleus (1967).

CHAPTER TWO

FIELD RELATIONSHIPS

Introduction

Approximately 4 months fieldwork was undertaken to establish a minor intrusion stratigraphy. This was achieved by detailed mapping of cross-cutting relationships in well exposed areas and assessing the behaviour of minor intrusions along well exposed contacts. Four major categories of minor intrusions were recognised in the field, these are in order of decreasing abundance:

1) Dolerite dykes, sheets and sills.

2) Gabbroic plugs.

3) Peridotite plugs.

4) Acid dykes and sheets.

The Main Ring Fault forms a major break in the Tertiary geological sequence on Rhum and this is reflected in the distribution and the orientation of the minor intrusions. Poor exposure along the line of the fault makes correlation of the sequences of minor intrusions developed on both sides of the fault impossible. The sequence of minor intrusions on each side of the fault is presented in Table 2.1. The location within the sequence of each of the minor intrusion types is discussed in the text.

1. <u>Dolerite dykes, sheets and sills</u>.

These have been divided in the field into four types, these being: dykes, inclined sheets, thin conformable sheets and thick conformable sheets. The term dyke as used in this thesis is defined as an intrusive discordant tabular body which can vary in attitude from approximately 60° to vertical; the term inclined sheets refers to intrusive discordant tabular dolerite bodies which have dips of 60° or less. The term parallel inclined sheet is restricted to a distinct set of intrusions on Rhum as discussed in the text.

a) Dykes and inclined sheets

i) Field and hand specimen characteristics.

This description included all the dolerites except the picritic and big feldspar dykes which are discussed separately. The dykes and inclined sheets are typically aphyric or microporphyritic and thus lack distinctive field characteristics. The vast majority are between 20 cm to 80 cm thick, however dykes up to 18 m thick have been located. Some dykes vary in thickness along strike and can be seen to progressively expand then thin to a tachylitic termination before continuing en echelon along strike. This range in dyke thickness reflects in the grain size of the dykes, some (in particular the thinner dykes) are extremely fine-grained whereas other thicker dykes

have virtually "gabbroic" centres.

The Torridonian sediments adjacent to the contacts of some dykes (eg. a northern trending dyke in Kinloch Glen NG 372005) may be bleached up to 20 cm from the contact. This thermal metamorphism is attributed to passage of magma through the dyke fracture which may have acted as a feeder to overlying lavas and sills (cf. Preston, 1967). These dykes possess only slight chilled margins and contrast with other tachylitic margined dykes (tachylitic sheets of Dunham and Emeleus, 1967), which possess thick chilled margins.

Despite the gross similarity of the bulk of the dolerite hand specimens it is possible to recognise some differences in the field. In general, the dark grey-black specimens tend to be more mafic than the more common dull grey varieties. Increasing differentiation produces mesocratic specimens often characterised by a green-grey colour and the most differentiated specimens are a pale cream-grey colour on fresh faces. Plagioclase, clino-pyroxene and to a lesser extent olivine phenocrysts (in various combinations) can be recognised in some specimens.

Xenoliths have been located in some dykes and inclined sheets but they are extremely sparse. Although Speight (1972) found that xenoliths were more abundant in dykes adjacent to the central complexes, xenoliths in

dykes associated with the central complexes of Arran

(Tyrrel, 1928), Ardnamurchan (Richey and Thomas, 1930)

and Mull (Bailey et al., 1924) are not abundant thus Rhum

is not anomalous in this respect.

Multiple dolerite dykes (those involving two or more

phases of dolerite injection into the same fissure) are

not abundant on Rhum. A simple multiple dolerite involving

two facies, the later central facies possessing a slight

chill can be seen on Dibidil shore (NM 385925) a more

complicated example is located at Papadil (NM 362918).

ii) Distribution and orientation of the dykes and

    inclined sheets.

The strike trends of dykes and inclined sheets

recorded from 11 different areas on Rhum are presented as

rose diagrams on Fig. 2.1. Some duplication of the work

of Speight (1972) has been unavoidable and the data

itemised by Speight (op.cit. p.535, Appendix 18) has

been used to supplement this account when necessary.

The rose diagrams for dykes and inclined sheets

cutting the Torridonian between Papadil and Dibidil and

at the Allt nam Ba (roses 4 and 7, Fig. 2.1) confirm the

linearity and the NW-SE strike of the dykes and inclined

sheets in the southern part of the island. However, the

rose diagrams for dykes and inclined sheets in the northern

part of the island (roses 11,12 and 13, Fig. 2.1) suggest

a more radial distribution. Rose diagrams plotted using Speight's (op.cit.) original data for the northern and eastern part of the island (Fig. 2.2 and 2.3) substantiate this apparent radial distribution, the change in strike trend from NNW through N to NNE, between Glen Shellesder, Kilmory and Rubna na Roinne in particular, suggest a radial dyke distribution.

The dyke intensity map (Fig. 1.4) is clear evidence of the linearity of the Rhum swarm. To account for the anomalous strike directions in the Rubna na Roinne area Speight suggested they represented a separate sub-swarm distinct from the Rhum linear swarm similar to perpendicular sub-swarms he had encountered on Skye. Reference to rose 10 (Fig. 2.1) shows a bimodal distribution of dyke strike trends in the Allt Slugan a Choilich (based on 51 readings) somewhat similar to the trends encountered around Rubna na Roinne (rose 11 Fig.2.1 and RE Fig. 2.2 and 2.3), thus supporting Speight's ideas.

Mapping east of the Long Loch fault in the Mullach Mor area has revealed dykes following N-S fractures in the Torridonian which parallel the Long Loch fault. The only unimodal N-S trending dyke sets on Rhum occur in traverses across the Long Loch fault at Papadil and Kilmory (roses 3 and 12, Fig.2.1 and RD Fig. 2.2). It is likely that the N-S basement fracture which gave rise to

the Long Loch fault has strongly influenced the dyke trends in the Papadil and Kilmory areas.

Examination of the dyke and inclined sheet trends within the Main Ring Fault cutting the sequence Torridonian to tuffisite in Corrie Dubh and the Southern Mountains (roses 5 and 7, Fig. 2.1) show that dykes and inclined sheets of all trends occur, with two trends at NNW and NNE being better represented. Dykes and inclined sheets of all trends have been recorded in the gneisses and Torridonian in lower Dibidil and in the felsite on Beinn nan Stac (rose 6, Fig.2.1). The strong E-W trend defined in this last rose diagram may be in part attributable to the N-S trend of the traverse in the Dibidil river which is more likely to encounter E-W as opposed to N-S dykes.

These diagrams support the impression gained in the field that the numerous dykes and inclined sheets within the Main Ring Fault strike in all directions and testify to a complicated structural history. Analysis of the cross cutting relationships exhibited by the dykes and inclined sheets on Cnapan Breac and in Stony Corrie (Figs. 2.4, 2.5, 2.6) confirms this complicated history, as no simple age relationships of one trend relative to another can be resolved, although dykes or inclined sheets trending $270^\circ - 310^\circ$ generally cut dykes or inclined sheets trending $320^\circ - 335^\circ$ in Stony Corrie.

The northwesterly trend of the dykes cutting the Western Granophyre at Harris (rose 1, Fig. 2.1) is somewhat anomalous and may be due to basement control as postulated for Kilmory and Papadil.

It was suggested in Chapter 1 (p. 13) that the dykes cutting the layered peridotites may have developed a radial distribution. To test this hypothesis the dykes from five different localities were plotted on Fig. 2.7 where the abscissa is the strike trend of the dyke in question and the ordinate is the angular bearing of this dyke outcrop relative to the centre of the ultrabasic mass estimated to be at NM 370960. The diagram is heavily biased from dykes recorded in Harris Bay as the well exposed coastal section revealed relatively abundant dykes when compared with the inland exposures. A perfect radial distribution would result in the dykes plotting along Line A-B in Fig. 2.7. The dykes from the inland exposures (Barkeval etc.) plot fairly close to A-B however the dykes from Harris clearly cover the complete range of possible dyke orientations with the majority lying in the range $40^{\circ}-100^{\circ}$. The Harris Bay section is the best exposed area and thus could possibly be viewed as the most representative data set. However, it is possible that the dyke trends in this area are the product of a radial dyke distribution with a superimposed NW-SE trending set attributable to basement

fractures as postulated for the NW-SE trending dykes in the Western Granophyre.

Despite the limitations of the data and the arbitrary selection of a centre for the ultrabasic mass, the dyke orientations presented in Fig. 2.7 suggest that a radial dyke distribution can be discerned in the ultrabasic rocks of Rhum, a radial dyke swarm will develop when the maximum principal stress (P max) is vertical (Robson and Barr, 1964); thus the radial dyke swarm is supporting evidence for the upward emplacement of the ultrabasic rocks as envisaged by Brown (1956) and Wadsworth (1961).

iii) Age relationships

Detailed mapping along well exposed contacts and the interpretation of the rose diagram trends in Fig. 2.1 has allowed evaluation of the dolerite dykes and inclined sheets relative to the major igneous bodies and other minor intrusions on both sides of the Main Ring Fault (Table 2.1). The change in strike direction across the ring fault at the Allt nam Ba and between Papadil and Dibidil (Fig. 2.1) suggests that the Main Rhum Linear Swarm is truncated by the fault. Although many of the dykes in the linear swarm may be contemporaneous with some of the dykes within the Main Ring Fault, the former were originally emplaced at a higher structural level.

There are several episodes of intrusion within the Rhum Linear Swarm as some dykes in well exposed traverses (e.g. at the foot of Glen Shellesder NG 329016) can be seen to cut older dykes. In addition the thick and thin conformable sheets truncate and are cut by dykes of the Rhum Linear Swarm thus allowing some subdivision of the swarm relative to these stratigraphic indicators. The age relationship of the Rhum Linear Swarm to the layered peridotites and gabbros is demonstrated on Minishal (NG 358005) and at the Allt nam Ba (NM 408943) where the dykes can be seen to be veined and thermally metamorphosed in the Torridonian sediments but are not found in the adjoining mafic rocks which are well exposed in and near Allt nam Ba.

The dykes cutting the post-central complex lavas of western Rhum are the youngest identifiable dolerite dykes on Rhum. The sparse dykes cutting the gabbro and peridotite plugs may be of similar age.

The relative age relationships of dykes and inclined sheets within the Main Ring Fault has been achieved by mapping the contacts between the rock types involved in the early "acid" phase of magmatism and between these and the later basic and ultrabasic igneous rocks. Maps from two of the critical areas are presented in Figs. 2.5 and 2.6.

Dunham (1968, p.330) noted occasional dolerite fragments in the explosion breccias of the Northern Margin Complex which would indicate a "pre-acid" dyke phase. However, the bulk of the explosion breccia consists of Torridonian blocks in a comminuted Torridonian matrix and dolerite fragments are extremely rare. Thus the vast majority of the dykes and inclined sheets postdate the explosion breccias. The presence of a liquid-liquid contact between dolerite and felsite in Stony Corrie, Dibidil (Fig. 2.6) is evidence of contemporaneous acid-basic magmatism but such occurrences are rare.

Mapping along the well exposed explosion breccia-felsite-tuffisite contacts on Cnapan Breaca (Fig. 2.5) and between explosion breccia and felsite in Stony Corrie (Fig. 2.6) has shown that none of the dykes or inclined sheets are truncated at these contacts strongly suggesting the bulk of the dykes and inclined sheets in this area postdate the emplacement of the acid rocks. Supporting evidence comes from several contacts on the island listed in Table 2.2.

As previously stated (Chapter 1, p. 6) the contacts between the granophyre and the earlier "acid phase" rocks on Rhum are not exposed. However, in view of the close temporal and spatial association of the acid rocks proposed by Dunham (1968) it is unlikely that any significant

dyke phase developed in the tuffisite-granophyre interval.

The contact between the Western Granophyre south
of Harris Mausoleum (Fig. 2.8) shows that the abundant
dolerite dykes and inclined sheets in the granophyre are
not found in the adjacent peridotite. Truncation of
dolerite dykes and inclined sheets perpendicular to the
acid-basic and acid-ultrabasic contacts can be clearly
seen at the localities listed in Table 2.3. These
contacts confirm the impression gained in the field that
dykes and inclined sheets are less abundant in the ultra-
basic tract.

In conclusion the majority of the dolerite dykes and
inclined sheets on Rhum appear to postdate the emplacement
of the acid rocks and predate the emplacement of the
gabbros and peridotites.

b) Picritic dykes

Olivine phyric dykes are typically black in hand
specimen. They are generally 30 cm to 60 cm thick and
rarely exceed 1 m. Several (but not all) of the dykes
have olivine enriched centres attributed to laminar flow
differentiation during emplacement, a process believed to
have operated in similar but wider picritic dykes on Skye
(Gibb, 1968).

Picritic dykes have been found at several localities
(see Fig. 2.9). They do not represent a single discrete

magmatic event as several different petrographic types
are represented (Chapter 4, p.94). The petrographic
variation makes assessment of their field relationships
difficult. Some (Type 2 picrites p.96) contribute to
the Rhum Linear Swarm and a dyke petrographically similar
to these cuts Lewisian inside the Main Ring Fault. Another
petrographically similar dyke cuts the peridotite plug
east of Loch Sgoarishal (NG 351023) suggesting a fairly
young age for these dykes.

The picitic dykes in the Allt Slugan a Choilich
(Type 1, p. 94) cut inclined sheets and other dolerite
dykes, a petrographically similar dyke from Rubna nam
Meirlach is cut by a younger dolerite dyke. The picritic
dykes truncated and thermally metamorphosed by the peridotite
body on eastern Minishal (NG 358005) have variolitic
groundmass plagioclase somewhat similar to some of the
dykes in the Allt Slugan a Choilich, thus it is possible
the latter predate the emplacement of the layered series.

In conclusion the picritic dykes postdate the
inclined sheets and some appear to pre-date the emplacement
of the peridotites. They are generally fresh suggesting
that they post-date the dolerite dykes and inclined sheets
which are often altered but are occasionally cut by later
dolerite dykes.

c) Big feldspar dykes

The majority of these dykes occur as 0.5 m to 1.5 m grey-black weathering dykes with abundant (up to 50%) 0.5 cm to 2 cm diameter tabular euhedral plagioclase phenocrysts. The dykes are resistant to erosion and generally form slight topographic highs in areas of outcrop. They show no appreciable flow differentiation as phenocrysts are abundant across the full width of the dyke.

Big feldspar dykes are found on both sides of the Main Ring Fault (see Fig. 2.11) and the dyke on Bealach Mhic Neill (NM 378994) appears to cut the fault. However, another big feldspar dyke on An Mam (NM 382993) located approximately 50 m south of the Main Ring Fault is cut by a minor fault sub-parallel to the Main Ring Fault and is also sheared and crushed suggesting a pre-ring fault age. On balance the extensive occurrence of big feldspar dykes on both sides of the Main Ring Fault suggests they postdate that event and the shearing in the dyke on An Mam may be due to later minor movement along the Main Ring Fault.

That these dykes post-date the acid rocks but pre-date the layered peridotites and associated gabbros is clearly seen at the felsite-gabbro contact on Meall Breac (Emeleus and Forster, 1979, p.18) on the granophyre-peridotite contacts at Papadil and Ard Nev (Emeleus and Forster op cit.,

p.39). A 20 cm thick big feldspar dyke cuts a thick
conformable sheet east of Papadil (NM 376914) and a 1 m
thick dyke cuts a thin conformable sheet north of Glen
Shellesder (NG 349006).

d) Parallel inclined sheets

These sheets are generally composed of a grey weath-
ering aphyric or mildly porphyritic dolerite. Many of
the parallel inclined sheets are very resistant to
erosion and they form a distinctive minor cap rock to
waterfalls in the Allt Slugan a Choilich stream section
SW of Kinloch Castle. When examined in detail, some
sheets can be seen to thin and progressively wedge out
suggesting that individual sheets are not laterally con-
tinuous.

The parallel inclined sheets are abundant in the Allt
Slugan a Choilich stream section and can also be seen
cutting Torridonian sediments north of Corrie Dubh and on
Bealach Mhic Neill. They are not seen in the deep
gully immediately south of the ring fault on the Allt
Slugan a Choilich and thus pre-date the ring fault. They
are cut by picritic and dolerite dykes and by the gabbro
plug east of the Allt Slugan a Choilich (NM 315985).
Their relationship to the Main Rhum Linear Swarm and the
conformable sheets is not known.

Dunham (1962, p.211) noted that two sets of parallel

inclined sheets were present in the Allt Sluggan a Choilich, one dipping towards the southwest, the other westwards. In a later published account (Dunham and Emeleus, 1967, p.401) the authors identified two sets of parallel inclined sheets in the Allt Sluggan a Choilich, one set dipping towards Glen Harris, the other dipping in a southwesterly (as opposed to westerly in the earlier account) direction. The dip directions of all the dolerite sheets exposed in the Allt Slugan a Choilich have been plotted on Fig. 2.10 and only a single dominant SSW trend is represented. It seems possible that in his original account Dunham (1962) incorrectly considered the thin conformable sheets with a regional west to north-west dip exposed in the lower reaches of the stream were structurally analogous to the southwesterly dipping parallel inclined sheets situated nearer the central complex.

Inclined sheets or cone sheets?

The set of dolerite sheets on the northeastern margin of the complex were originally referred to as inclined sheets by Harker (1908) but later workers Hughes (1955), Dunham (1962), Dunham and Emeleus (1967) have used the term cone sheet to describe both these and the other inclined dolerite sheets on the island

The term cone sheet was first used by the authors of the Mull Memoir (Bailey et al., 1924, p.6), these authors plainly state that the term is a synonym of "inclined sheet" as described on Skye by Harker (1908). A more precise definition of the term cone sheet is offered by the authors of the Ardnamurchan Memoir (Richey and Thomas, 1930, p.56) who state:

> "cone sheets consist of relatively thin sheets,
> which viewed as members of a suite, occupy
> conical fissures that have a common apex
> and common vertical axis".

Harker (1908, p.163) considered the dolerite sheets dipping north in Dibidil and dipping WNW in the ultra-basic rocks of Askival to belong to the same set of inclined dolerite sheets on the northeastern margin of the complex. It is clear from his original account he considered these scattered inclined sheets were analogous to the intense inclined dolerite sheets he had encountered on Skye (Harker op cit., p.163).

Later workers using the term cone sheet expanded Harker's (1908) ideas. Hughes (1955, p.132) described three ages of cone sheet; an earlier set dipping 25° N was cut by a later set dipping 40°NNE with another set dipping in a south-westerly direction. He noted that the age relationships could be reversed and there was no

systematic variation in dip. Dunham (1962, p.212) correlated the parallel inclined sheets outside the Main Ring Fault with inclined sheets cutting rocks inside the fault and considered them to be part of a cone-sheet system.

It is clear from these accounts that the distribution of inclined sheets within the Main Ring Fault is erratic. In addition mapping within the fault shows a multiplicity of inclined dolerite sheets and dykes striking and dipping in all directions (see Fig. 2.1, 2.4). The set of parallel inclined sheets on the NE margin of the complex formed at a different structural level to sheets within the central complex as the former are truncated by the Main Ring Fault. In view of the complex and erratic distribution of the inclined dolerite sheets within the Main Ring Fault it seems unlikely that they are analogous to the more regular arrays of concentrically arranged cone sheets in other Tertiary centres. The parallel inclined sheets outside the Main Ring Fault could be part of an incomplete cone-sheet system; however, their role in the structural history of the complex is not clear.

e) Thin conformable sheets

Sheets of dolerite generally conformable with the Torridonian bedding are fairly abundant in the arkosic

Torridonian outside the Main Ring Fault in northern
and southern Rhum but are absent from the shale-rich
horizons of eastern Rhum. They vary from black to grey
in hand specimen and some specimens contain plagioclase
and occasionally olivine macrophenocrysts. They can
range from 2 cm to 1 m in thickness but are generally
less than 0.5 m thick. They generally possess the
regional Torridonian dip of 20-30°NW but can be trans-
gressive along false bedding planes. They produce only
minimal contact alteration in the enclosing sediments.

Although cross-cutting relationships have not been
located it is likely in view of their varied petrography
that they were emplaced in more than one event. Field
evidence supporting this can be seen east of Kinloch
(NM 410998) where two sheets converge with no intervening
Torridonian screen. They both possess chilled margins on
the adjacent dolerite faces and with the Torridonian
suggesting that the earlier sheet had completely cooled
before the later sheet was intruded.

Sheets   both cut and are cut by dolerite dykes and
have been seen to be cut by picritic and big feldspar dykes.
Direct evidence concerning the relative ages of the thick
and thin conformable sheets is available at Kilmory where
a vertical dyke cutting a thin sheet is truncated by an
overlying thick sheet. Thermally metamorphosed thin

conformable sheets occur in the contact aureoles of peridotite and gabbro plugs in Glen Shellesder (NG 351103) and north of Bealach Mhic Neill (NM 380995). In addition the gabbro-Torridonian contact west of Papadil Pinacle (NM 365926) shows truncation of the thin conformable sheets by later gabbros.

Although the age relationships of the thin conformable sheets relative to the Main Ring Fault and the inclined sheets are not exposed, the former appear to be of an early age and may predate the formation of the ring fault.

f) Thick conformable sheets

Two petrographically different sets of 3 m thick conformable sheets have been located on Rhum, one set outcrops SW of Kilmory, the other NNE of Papadil (Fig. 2.11). The former consist of a pale grey plagioclase-clinopyroxene phyric dolerite. The sheets are more resistant to weathering than the enclosing arkoses and produce a distinctive topography in areas of outcrop. The sheets are occasionally transgressive and although the majority are of constant thickness a 0.5 m thick sheet located at Kilmory is petrographically identical to the thicker-sheets.

The Papadil sheets are similar in topographic expression to those near Kilmory but differ as they are aphyric. They usually possess a 30-40 cm thick vesicular

band approximately 1 m below the upper contact, in addition a discontinuous 10 cm thick vesicular band occasionally develops approximately 75 cm below the main vesiculated band.

The Papadil sheets cut dolerite dykes but are themselves cut by later dolerite dykes, a big feldspar dyke and a peridotite plug (NM 379917) but dykes cutting the Kilmory sheets have not been located suggesting they may be younger than the Papadil type. The relative age of the Kilmory and the thin conformable sheets have been discussed previously (p.42). In conclusion the thick conformable sheets are all probably of a similar general age, postdating the thin conformable sheets and much of the Rhum Linear Swarm and predating the gabbro and peridotite plugs.

The thick conformable sheets intrude Torridonian sediments of different stratigraphic height (the Papadil sheets lie approximately 3000 m stratigraphically below the Kilmory sheets). However, this difference in stratigraphic height is probably fortuitous. The Torridonian sediments developed their regional northwest dip prior to the development of the Tertiary complex. The location of the sheets NW and SSE of the central complex is probably related to upwelling of magmas along the NW-SE striking axes identified by Speight (1972, Fig. 1.4). The

ability of the Torridonian to cleave along major
bedding planes allowing sill emplacement in these areas
is probably more important than its location within
the stratigraphic sequence.

2. Gabbro Plugs

Abundant gabbro plugs have been located (Fig. 2.11);
they range in size from 20 m to 150 m diameter and occur
as circular to elongate masses. They are variable in
hand specimen, the majority are medium grained but coarse
grained varieties with pegmatitic patches are found in the
Northern Margin Complex (Dunham and Emeleus, 1967, p. 395).
Differentiated gabbros have been located in the northern
Torridonian tract, they are leucrocratic in hand specimen
but as with the less differentiated gabbros the mafics
have been altered.

The gabbros can induce considerable bleaching in the
enclosing sediments up to 30 m from the contacts. The
sediments adjacent to the contacts often show fritted
textures indicative of partial melting and the gabbros
are unchilled. It seems likely that the gabbros infill a
fracture which previously acted as a conduit to overlying
lavas.

The relative ages of the early and late gabbros in
the Northern Margin Complex were discussed by Dunham and

Emeleus (1967, p.405). The former are characteristically

coarse grained and can contribute to the explosion breccias

whereas the latter are medium grained and cut Lewisian

gneiss, Torridonian explosion breccia, granophyre, the

Main Ring Fault and the peridotite tongues.

Dunham and Emeleus (op.cit) tentatively correlated some

of the altered gabbros outside the Main Ring Fault with the

early gabbros of the Northern Margin Complex on a petrographic

basis. However, the altered early gabbros within the Main

Ring Fault contain both hypersthene and augite and the

plagioclase is characteristically zoned and consequently

contrast with the altered gabbros outside this fault as the

latter lack hypersthene and often contain pseudomorphed olivine.

The early gabbros have a distinctive composition (Chapter 7,

p.241) and three gabbros immediately NE of the Northern

Margin Complex are compositionally similar to the early gabbros

suggesting that they are coeval. However, the compositional

and petrographic dissimilarity of the remaining gabbros outside

the Main Ring Fault suggests they are of different age.

The gabbros outside the Main Ring Fault cut the thick

and thin conformable sheets and are generally dyke free in

areas of known high dyke intensity (e.g. the Sgoarishal

area), thus several of these gabbros are likely to be young

in age and are probably much younger than the compositionally

distinctive early gabbros within the Main Ring Fault.

The geographic distribution of the gabbro plugs on Rhum is shown in Fig. 2.11. There are two main gabbro plug concentrations in northwestern Rhum and along the northeastern margin of the complex. A few gabbros outcrop between Papadil and Dibidil and in the Torridonian of Mullach Mor whilst others cut the layered peridotites.

Many of the gabbro plugs around Loch Sgoarishal and east of Papadil are elongate along a NW-SE trend coincident with the axes of dilation identified by Speight (1972, Fig. 1.4) and their location is probably attributable to regional stress patterns. The structural control on the emplacement of the plugs along the northeastern margin of the central complex is not clear. However, their location may reflect the interaction of the NE-SW trending Rhum sub-swarm axis (p. 29) with the regional stress field or possibly the Main Ring Fault.

3. Peridotite Plugs

The gabbro and peridotite plugs are often in very close association (e.g. the two plugs in Glen Shellesder NG 351103). They tend to be resistant to erosion and form topographic highs in areas of outcrop, an exception being the large plug on the north side of Kinloch Glen (NG 375005). The plugs consist of a medium grained, rusty brown weathering felspathic peridotite in hand specimen and

individual plugs tend to be homogenous. However, felspathic peridotite xenoliths have been found in the peridotite plug east of Loch Sgoarishal (NG 351023) and dunite xenoliths are abundant in a plug north of Minishal (Emeleus and Forster, 1979, p.35).

The peridotites can induce considerable bleaching of the enclosing Torridonian sediments up to 30 m from the contact although the bleaching is often much less pervasive. At well exposed contacts, e.g. the western margin of the plug west of Loch Sgoarishal (NG 342020) the Torridonian sandstones have suffered severe partial melting with acicular quartz crystals (paramorphs after tridymite) embedded in a matrix of acid glass and fritted quartz grains. The peridotite at this contact and at other exposed plug margins is unchilled. Dunham and Emeleus (1967, p.413) suggested these plugs occupied conduits which had previously fed overlying lavas.

The similarity of the banding in some of the peridotite plugs to matrix banding in the tongues east of the Long Loch (Dunham, 1965b) led Dunham and Emeleus (1967) to suggest they could be of similar age. This late age is supported by the cross cutting of the thick conformable sheets and the general lack of dykes in areas of known high dyke intensity.

The distribution of the peridotite plugs on Rhum is

shown in Fig. 2.11, the apparent lack within the layered

series probably reflects the difficulty of locating plugs

intruded into an almost identical country rock as detailed

mapping by McClurg (pers. comm.) has located previously

unmapped plugs in the Barkeval peridotites. The elongation

and distribution of some of the plugs is probably attribut-

able to the controls suggested for the gabbro plug distrib-

ution (p.47).

4. Acid dykes

Four acid dykes have been located on Rhum, two have

been discussed previously by Harker (1908, p.140,177),

the others are previously undescribed. Two occur as

leucrocratic spherulites cutting granophyre and Torridonian.

Another, a pitchstone, occurs in a flow-banded deeply

weathered dyke cutting granophyre whilst another, a felsite,

occurs as a black flinty rock cutting sediments in Dibidil.

They are generally thick varying between 1.5 m to 2 m

however the felsite dyke is less than 50 cm thick. Their

age relationships are obscure, one of the spherulite

specimens is located outside the Main Ring Fault and

the felsite is cut by a dolerite dyke. In view of their

rarity, the close association of two specimens with

the Western Granophyre and the absence of contradictory

evidence it would seem reasonable to suggest they slightly

postdate the plutonic acid rocks of Rhum.
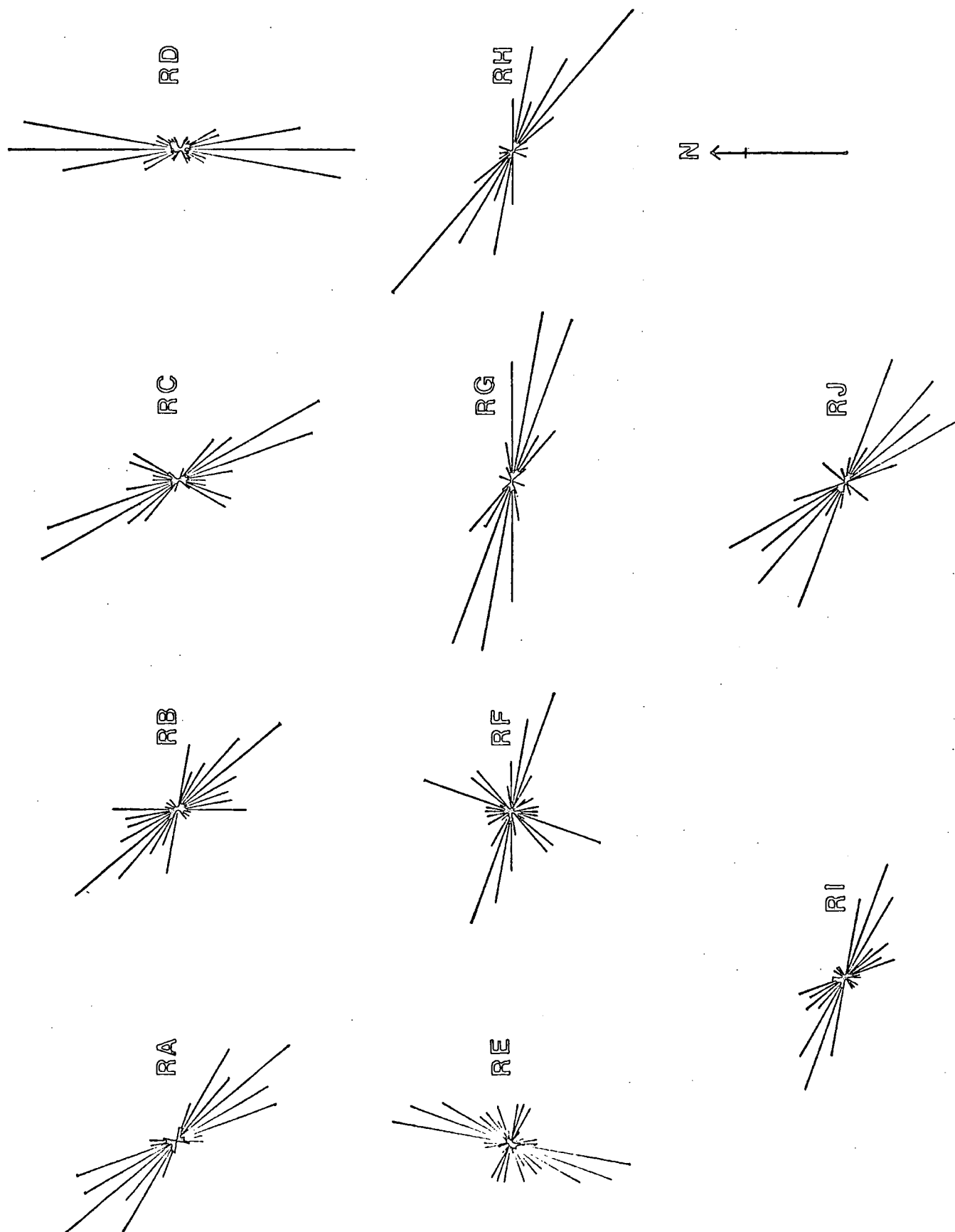
Fig. 2.2 Dyke strike orientations in the coastal Torridonian of Rhum,
see Fig 2.3 for the location of the traverses.(Drawn from
data in Speight 1972 Appendix 18).
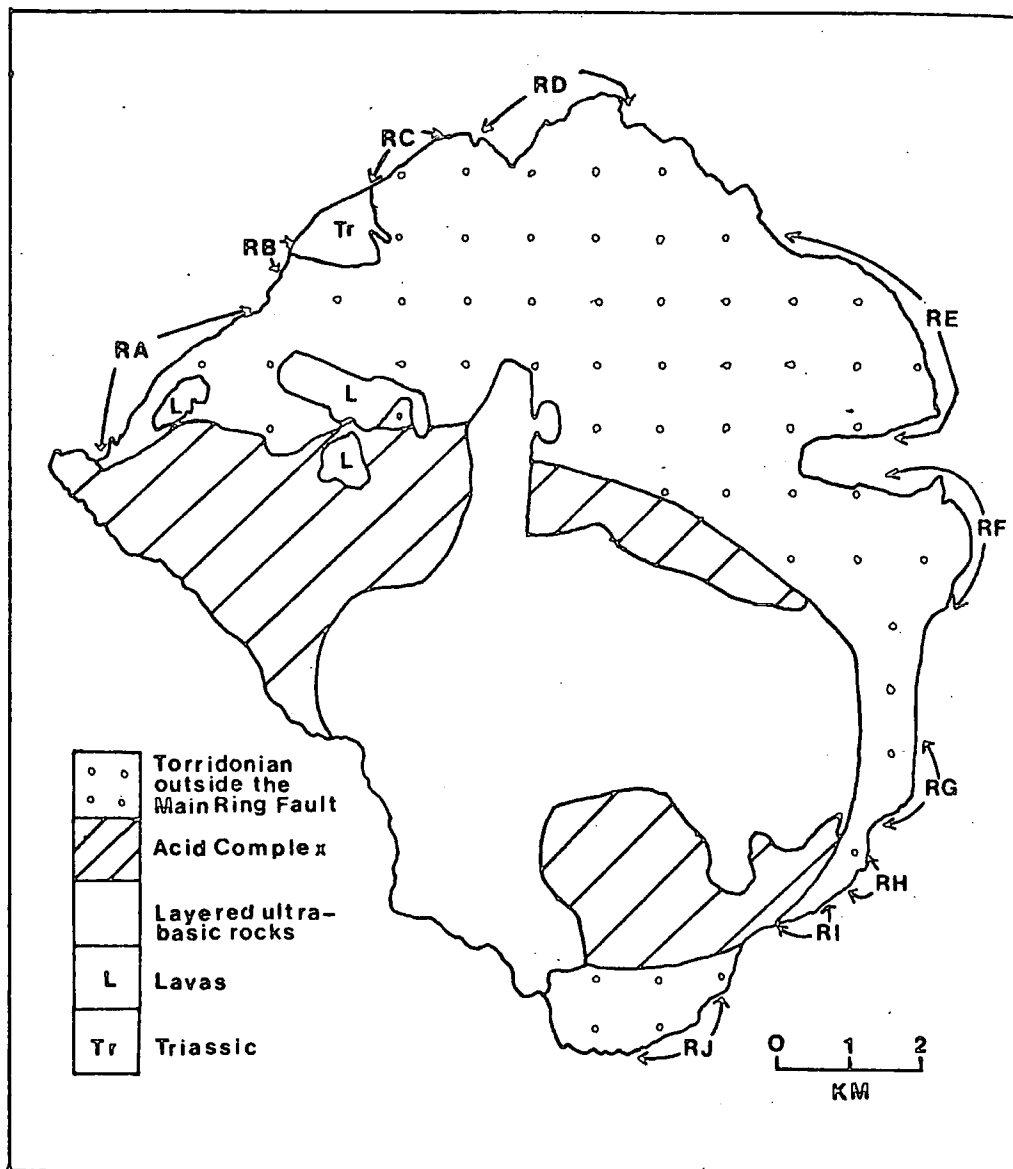
Fig. 2 3 Location of traverses represented in
Fig. 2.2. (Taken from Speight. 1972,
Fig. 107).

Fig. 2.4 Structural analysis of dyke cross-cutting
relationships on (a) Cnapan Breaca (b) Stony
Corrie.
Explanation:
The ordinate and abscissa refer to dyke strike
trends. A circle indicates that a dyke of the
ordinate orientation cuts a dyke of the abscissa
orientation, a cross indicates the reverse
relationship. The small symbols refer to one
observation, the larger symbols indicate two
observations, except the largest cross which
is the product of three observations.
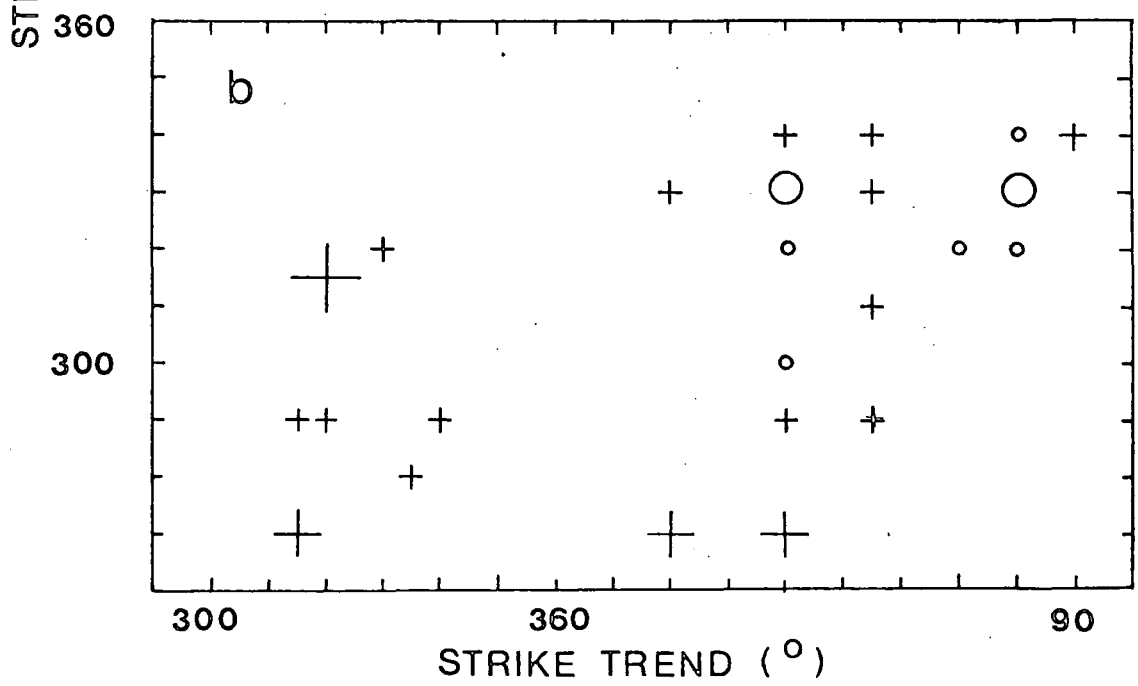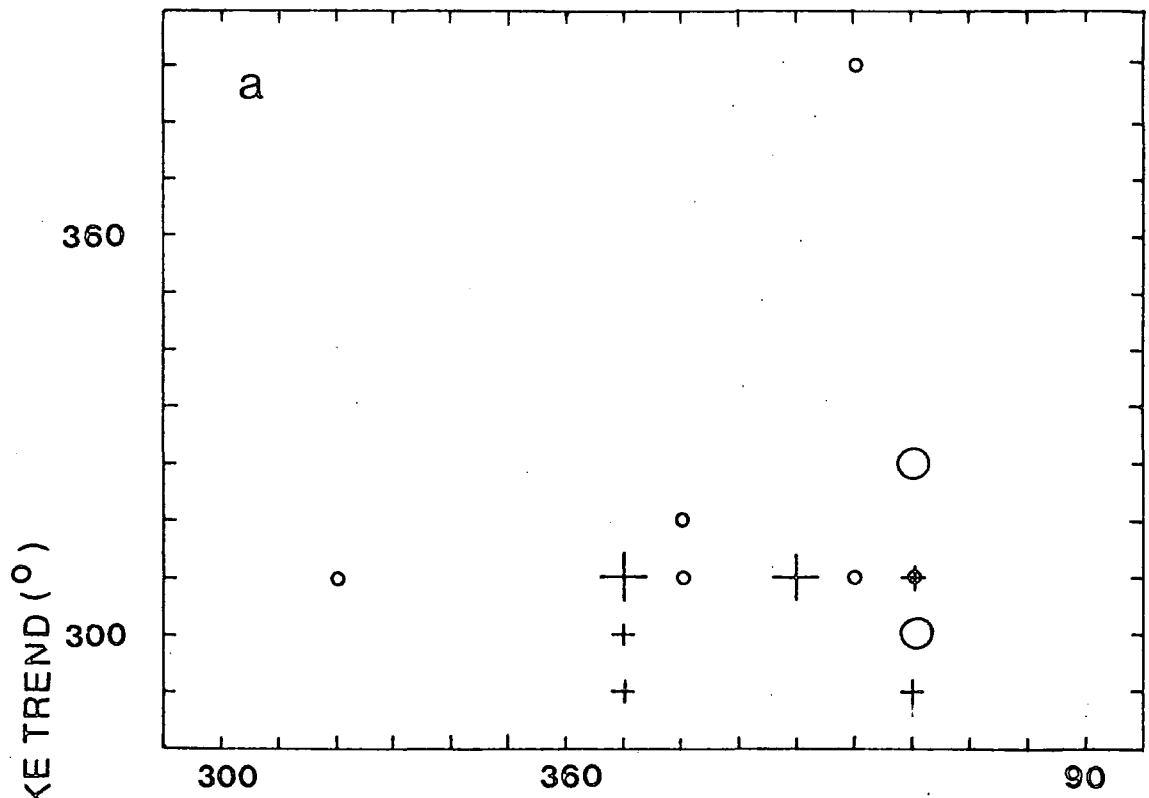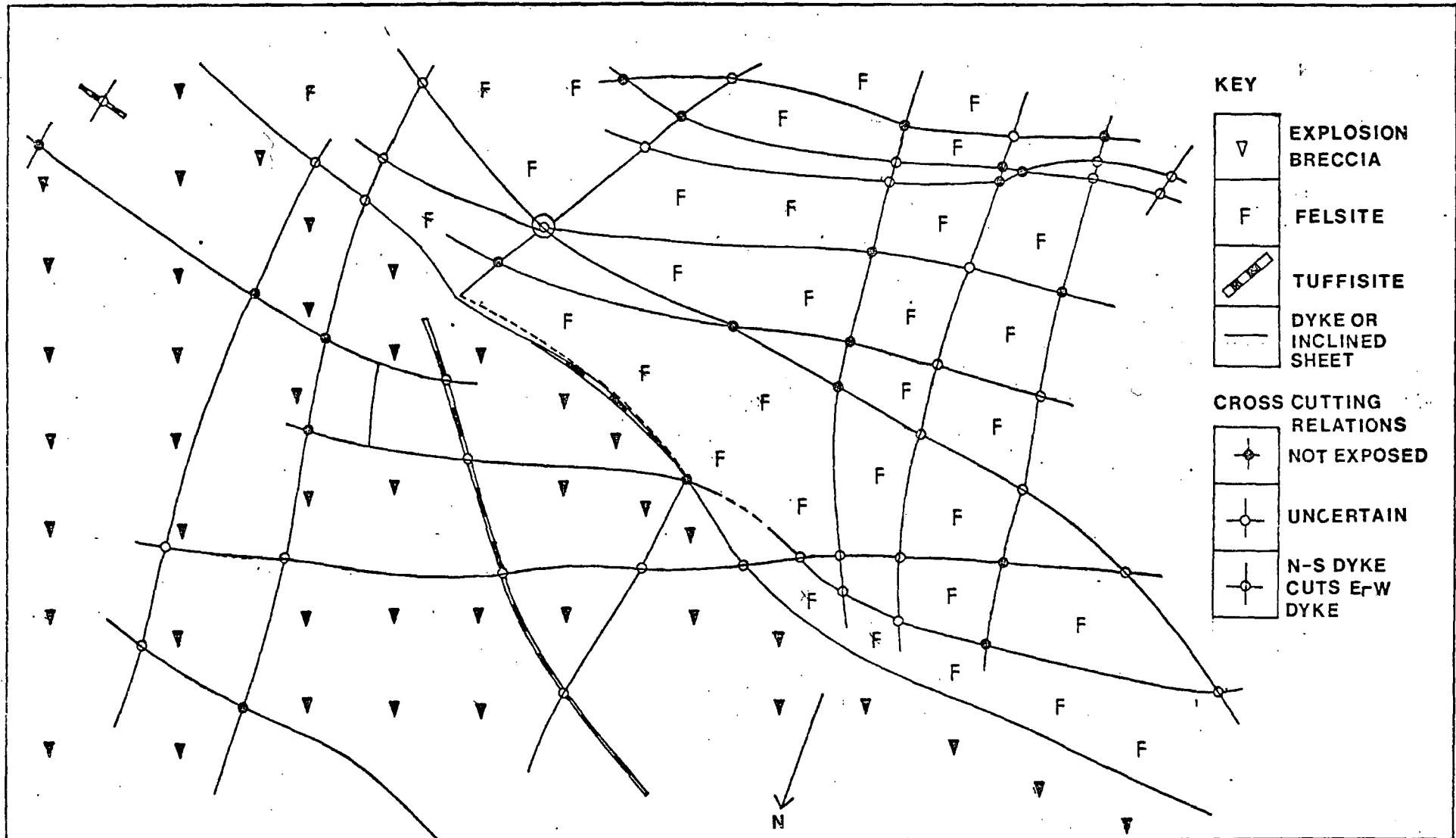
Fig 2.5 Sketch of dyke and country rock relationships on Cnapan Breaca (NM 392968)

KEY

▽	**EXPLOSION BRECCIA**
F	**FELSITE**
(symbol)	**TUFFISITE**
—	**DYKE OR INCLINED SHEET**

CROSS CUTTING RELATIONS

⊕	**NOT EXPOSED**
⊕	**UNCERTAIN**
⊕	**N-S DYKE CUTS E-W DYKE**

N

5/

Several dykes and inclined sheets cut the EX-FE contact 15M SE
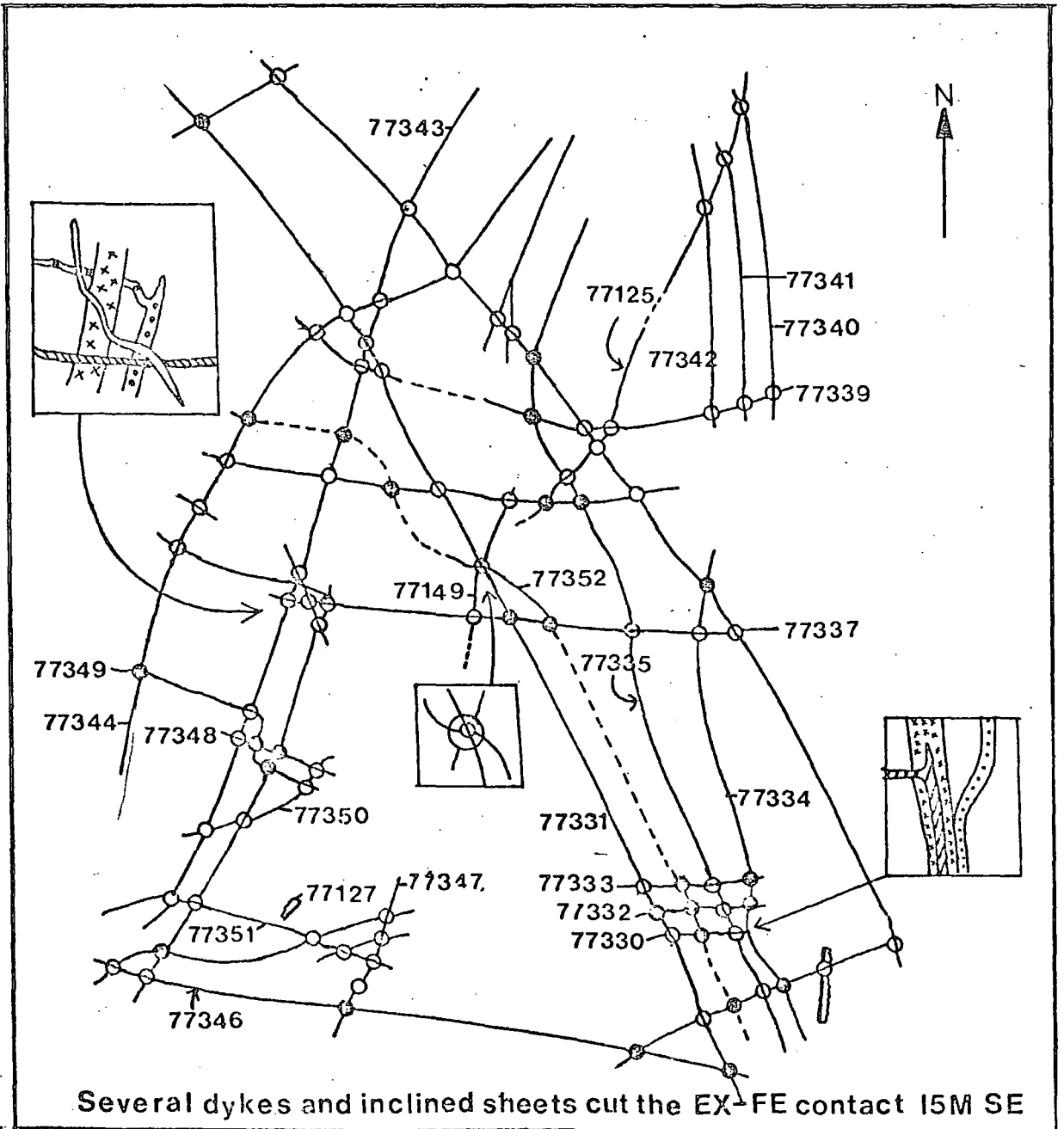
Fig 2.6   Sketch   of dyke and inclined
              sheet cutting felsite in Stony Corrie,
              Dibidil (NM384936) Key on Fig 2.5

NB: Ornament on insets refers to dykes of different age.

Fig 2.7 Structural analysis of dykes cutting the layered
peridotites, relative to the centre of the ultra
-basic mass, estimated to be at NM370960. The
angular bearing of dykes from localities west
of the Long Loch Fault have been corrected for
the 1.5 Km northward movement of the layered per-
idotites west of this fault.
Key to locality symbols.
△ Barkeval
○ Harris bay
□ Corrie nan Grund
▨ An Dornabac
◎ Trollval
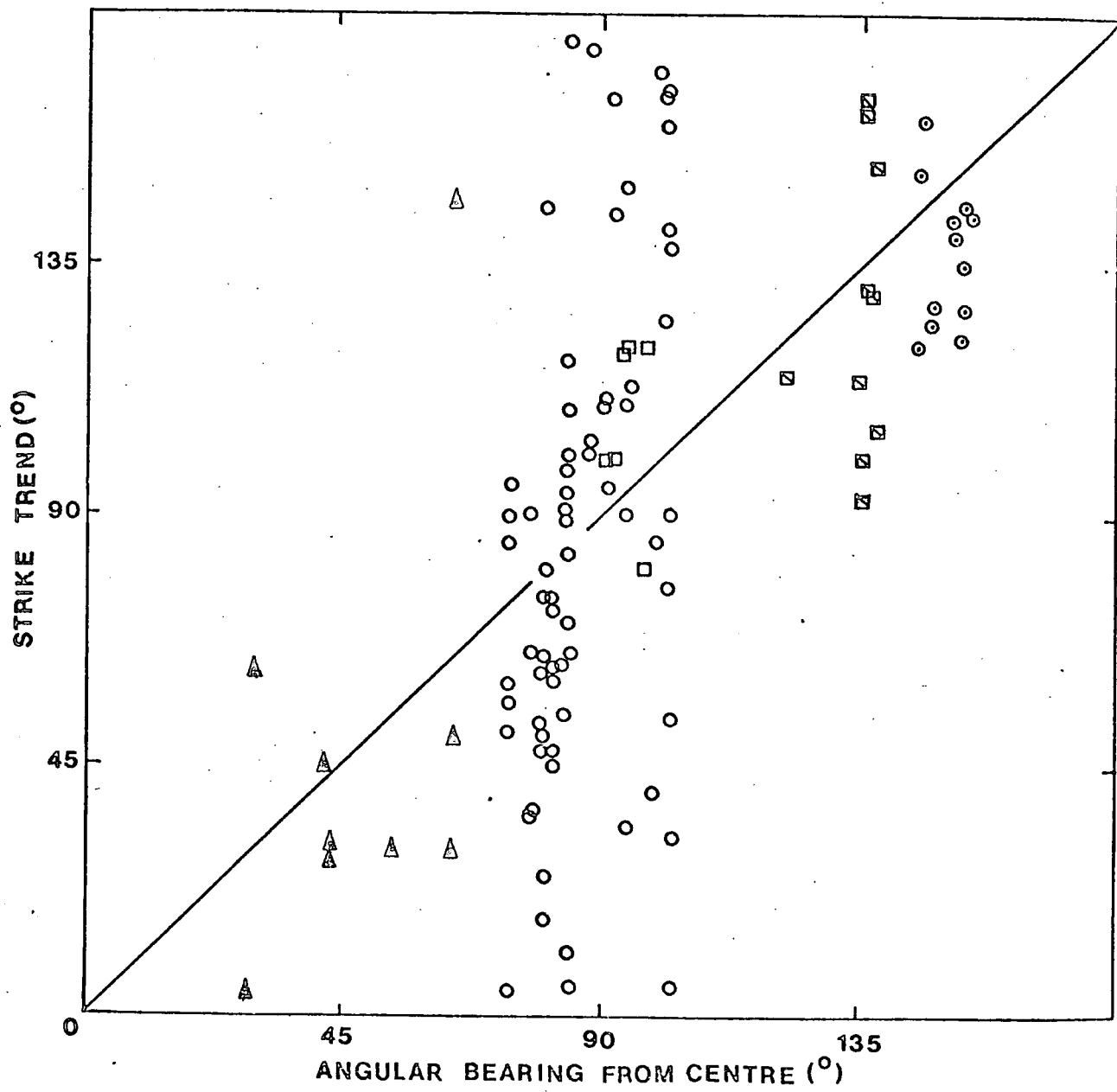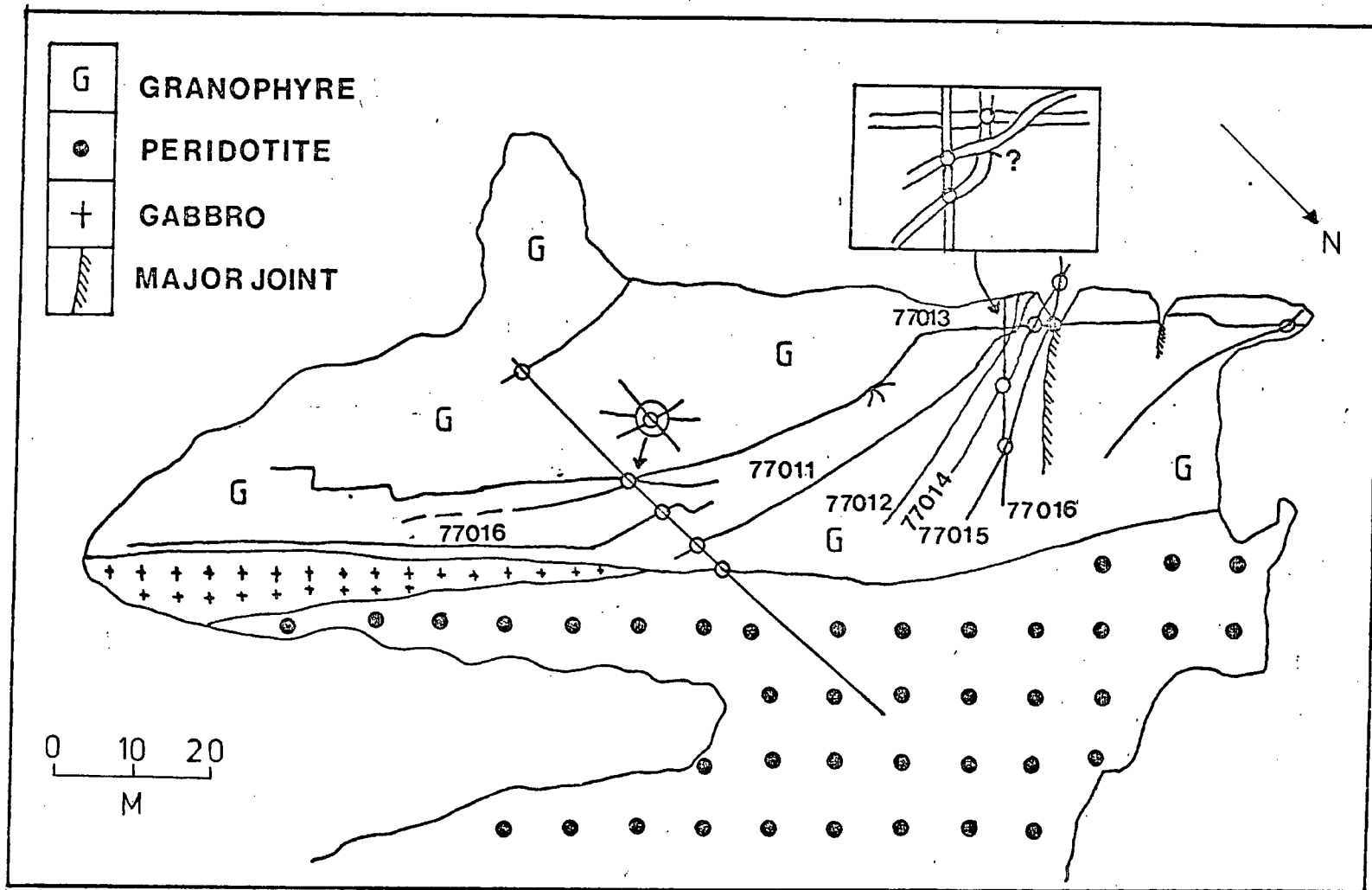
Fig 2.8 Sketch map illustrating some dyke cross-cutting
relationships adjacent to the Granophyre-Peridotite
contact at Harris Bay (NM336995)
For key to dyke intersect relationships see Fig 2.5
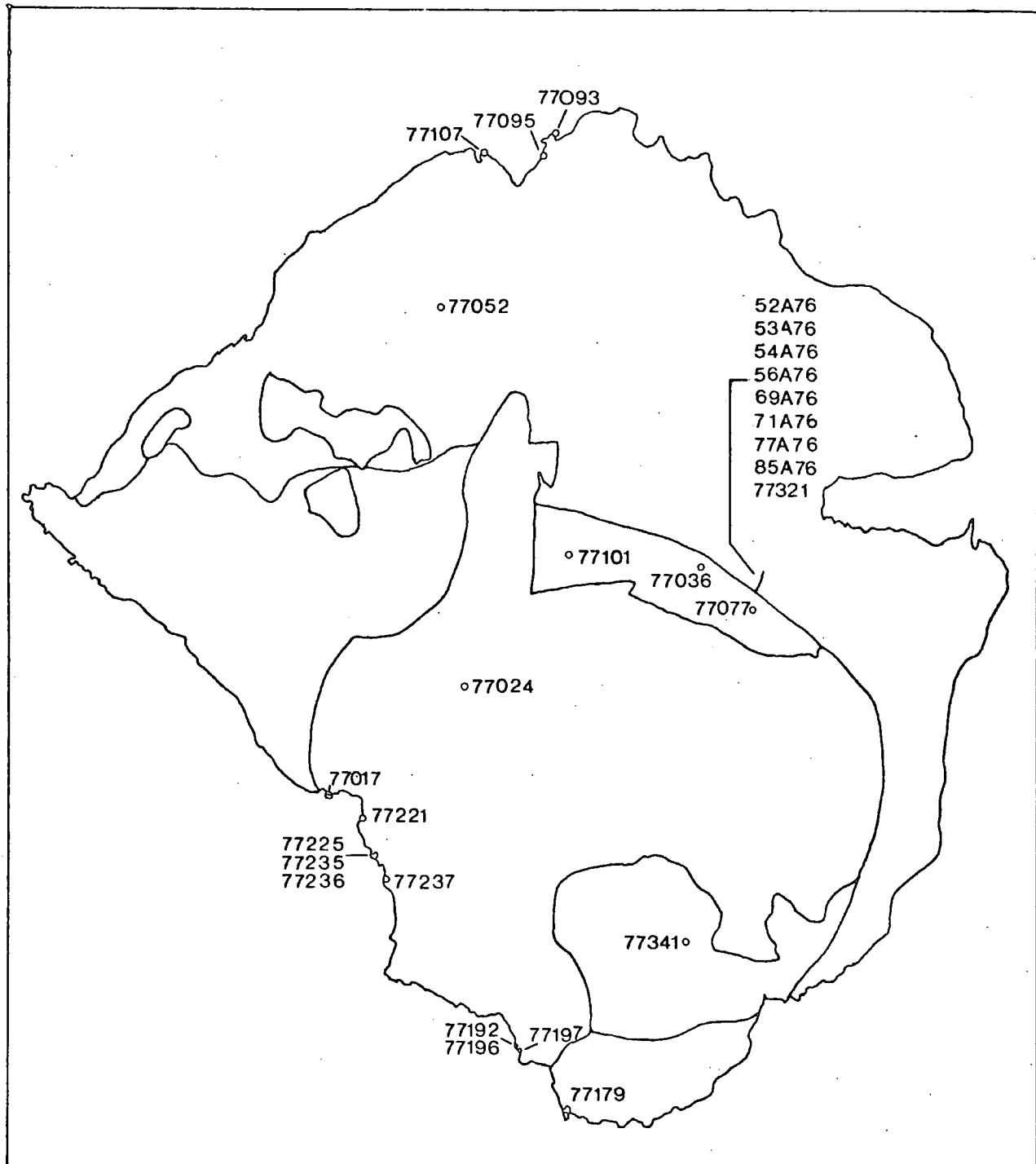
Fig.2.9 Map showing location of the picrite specimens.

Fig 2.10   Stereographic represenation of the inclinations

and dip directions of the inclined dolerite

sheets exposed in the Allt Slugan a Choilich.

The inset is a rose diagram of the dip direct-

ions of the sheets represented in the main

figure.
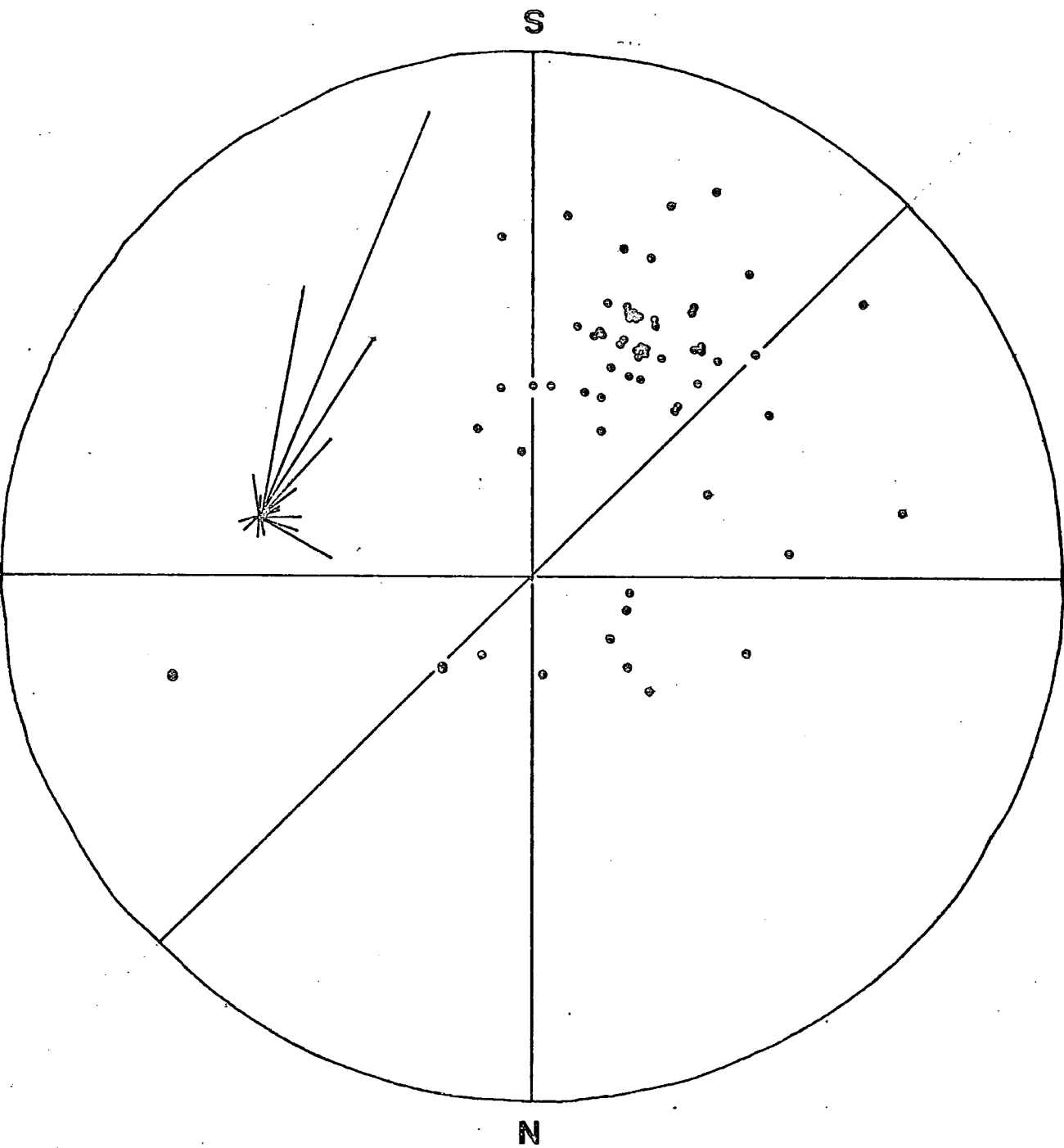
a) Within the Main Ring Fault   b) Outside the Main Ring Fault

	Dykes cutting lavas	Some probably of equivalent age
Dykes (including picritic varieties), inclined sheets and late gabbro plugs possibly some peridotite plugs	Lavas and sediments	
	Dykes cutting the gabbro and peridotite plugs including picritic varieties	
Emplacement of the layered ultrabasic rocks etc.		
Ultrabasic tongues and some plugs, gabbroic plugs.	Gabbro and peridotite plugs	
Big Feldspar Dykes	Big Feldspar Dykes	
	Thick Conformable sheets (two ages) Picritic Dykes	
Main Ring Fault---------------Main Ring Fault		
Intrusion of the majority of the dykes and inclined sheets.	Dykes of the Main Rhum linear swarm (majority of dykes intruded here)	Relative ages not known
Granophyre	Thin conformable sheets	
Dyke with liquid/liquid contact within the felsite.	Inclined Sheets	
Tuffisite, explosion breccia	Some dykes probably pre-date the inclined and thin conformable sheets	
Early Gabbro		

Table 2.1. The sequence of Tertiary minor intrusion
on Rhum

TABLE   2.2

LOCATION AND NUMBER OF DYKES OR INCLINED
SHEETS CUTTING THE SEQUENCE
BASAL TORRIDONIAN TO TUFFISITE.

Locality	Approx. Grid Reference	Contacts exposed between	Approx. number of dykes or inclined sheet cutting contact
Corrie Dubh	NM393978	Tb-Ex-Tu	2
Corrie Dubh	NM393977	Ex-Fe	1
Cnapan Breaca	NM391974	Tb-Ex-Tu	4
Dibidil Shore	NM394927	Tb-Ex	3
Dibidil River	NM394930	Le-Tu	5
Beinn nan Stac	NM398938	Ex-Fe	1

Le = Lewisian

Tb = basal Torridonian

Ex = Explosion breccia

Fe = Felsite

Tu = Tuffisite

TABLE 2.3

LOCATION OF CONTACTS BETWEEN EARLIER
ROCKS AND GABBRO OR PERIDOTITE

Locality	Approx Grid Reference	Contact between
Cnapan Breaca	NM394977	Fe-Ga
Meal Breac	NM385980	Fe-Ga
Bealach-an-Fuhrain	NM378949	Fe-Ga
Harris Bay	NM340950	Gr-Ga+Pe
Ard Nev	NM348978	Gr-Pe
Monadh Dubh	NM356997	Gr-Ga
Sandy Corrie	NM365945	Le-Ga

Le = Lewisian

Fe = Felsite

Gr = Granophyre

Ga = Gabbro

Pe = Peridotite

CHAPTER THREE

CLASSIFICATION

Introduction

The classification of the basic and intermediate Rhum minor intrusions is presented in the first part of this chapter. The second part of the chapter is an appraisal of the transitional nature of the Rhum dolerites and gabbros between typical alkaline and tholeiite magma types. The unusual geochemistry of the Rhum minor intrusions presented several difficulties with respect to generally accepted classifications (eg. the Skye lavas nomenclature; Thompson et al., 1972) invalidating the use of strictly defined terms (eg. Hawaiite) to describe the Rhum minor intrusions as discussed in the text.

I. The classification of the minor intrusions of Rhum

Classifying a suite of igneous rocks serves two main purposes. Firstly it subdivides the suite into manageable classes or groups which can be geochemically and petrographically categorised. This categorisation allows for intergroup comparison which may subsequently lead to petrogenetic interpretation. Secondly labelling of the groups with an approved nomenclature aids comparison with similar rock types from other areas.

Four categories of minor intrusion were recognised in the field. The histogram (Fig. 3.1) shows there is a broad range of compositions from ultrabasic to intermediate. This diagram allows appraisal of the range in silica composition in the suite and confirms the separation of some of the types recognised in the field. However, subsequent laboratory investigation of the geochemistry and petrography has revealed distinct sub-groups within the broad field categories, hence a more detailed classification is required.

The problems of classifying a suite of igneous rocks have been discussed by the authors of several petrologic texts (eg. Carmichael et al., 1973 p.29; Hatch et al., 1975 p.185) the principal difficulty being the location of arbitrary boundaries between successively more differentiated rock types within the suite. Although rigid use of these arbitrary boundaries allows for strict comparison with other authors the transitional nature and unusual chemistry encountered in the Rhum suite (discussed later) did not allow application of a standard nomenclature. Thus an alternative approach was adopted which involved the grouping together of petrographically and/or geochemically similar specimens. A brief description of the geochemical and petrographic characteristics of the types of minor intrusion encountered

on Rhum is presented in the subsequent sections.

1)   Dolerites

The dolerite specimens were resolved into 12 groups using geochemical and petrographic criteria. The former chiefly involved the major oxide (principally SiO_2, MgO, CaO, Na_2O and K_2O) and trace element abundances and the normative mineralogies (chiefly the Difference Index (Thornton and Tuttle, 1960) the abundance of normative hypersthene, nepheline and quartz and finally the pro-portion of anorthite in the normative plagioclase). The main petrographic criteria used were the presence or absence of characteristic phenocryst phases and the degree of differentiation of the groundmass. Groups 1 to 7 are basic in composition and include the picritic and big feldspar dolerites, groups 8 to 12 are intermediate in character.

A brief outline of the characteristic geochemical and petrographic features of these groups is presented below.

Group 1 D.I 6-19

These picritic dolerites all contain olivine and chrome spinel phenocrysts. The main geochemical characteristics are high MgO (10.0 - 31.0 wt %) and low SiO_2 (41.0 - 46.0 wt %) and Al_2O_3 (8.0-15.0 ct %). They are petrographically alkalic in affinity as they contain

groundmass olivine but do not generally possess normative nepheline.

Group 2 D.I. 13-20

The majority of this group are aphyric and are characterised by unusually high MgO (10.0-15.0 wt %) Ni (140-425 ppm) and Cr (375-900 ppm) abundances for aphyric rocks. SiO_2 (44.0-47.0 wt %) total alkalis (1.3-2.5 wt %) TiO_2 (1.0-2.0 wt %) and Ba (20-180 ppm) are low. The group is hypersthene normative but also displays alkalic traits, they can be viewed as high-MgO transitional basalts.

Group 3 D.I. 18-25

This group is geochemically transitional between groups 2 and 4 in that the ranges of the major oxides (especially MgO, Na_2O and K_2O) and trace elements (especially Ni and Cr) generally lie between the group 2 and group 4 values. All the specimens are hypersthene normative but the presence of groundmass olivine in some specimens reveals alkalic traits. Taken as a whole the group is transitionally tholeiite in character.

Group 4 D.I. 20-30

This is the largest of the dolerite groups and is petrographically and geochemically diverse. Rocks in the group typically possess SiO_2 in the range 46.0-48.0 wt % and contain less MgO but more Na_2O, K_2O, TiO_2 and P_2O_5

than the group 2 dolerite. Ni values in the range 58-170 ppm are lower than in group 2 but Cr can reach the 600 ppm level. Some high total iron, and CaO variants are found in this group characterised by Fe_2O_3 and CaO values above 13.5 wt % and 12.5 wt % respectively. Members of the group can be hypersthene or nepheline normative thus the group is completely transitional in character.

Group 5   D.I. 15-19

This small group of exceptionally fresh dolerites is geochemically distinct from the other dolerite groups. Members of this group are characterised by higher Al_2O_3 and lower total alkalis TiO_2, Zr, Y and Sr than other Rhum dolerites and closely resemble the low alkali, high CaO olivine tholeiite magmas of Skye (Esson et al., 1975; Matty et al., 1977).

Group 6   D.I. 26-31

Members of this group are only found cutting the lavas of Western Rhum. They possess slightly higher Al_2O_3 (14.0-16.0 wt %) and much lower MgO contents (5.5-8.0 wt %) than the dolerites in other groups. They are predominantly hypersthene normative and can be viewed as low MgO transitional tholeiites.

Group 7 D.I. 18-24

This group is characterised by abundant large
(1-4mm) tabular plagioclase phenocrysts and consequently
possesses high Al_2O_3 and CaO contents ranging from 15.5-
19.0 wt % and 12.5-15.0 wt % respectively.

Group 8 D.I. 20-40

Specimens in this group have SiO_2 contents ranging
from 49.0 to 53.0 wt %; the Na_2O, K_2O, TiO_2, P_2O_5, Ba,
Sr, Nb, Zr and Y values are generally higher than those
encountered in the group 4 dolerites but compositional
overlap between the 2 groups is considerable. Some
members of the group have Fe_2O_3 contents greater than
13.0 wt %. The term tholeiitic basaltic andesite
adequately describes the degree of differentiation.

Group 9 D.I. 36-47

Specimens in this small group are characterised by
silica contents greater than 54.4 wt %. Their fraction-
ated nature is also revealed by the MgO, CaO, Ni and Cr
contents which are lower than those in group 8. The
group's tholeiitic nature is revealed by the presence
of normative quartz and the low total alkalis. They
show only moderate iron enrichment (0.60-0.71) attribut-
able to their normal Fe_2O_3 (8.5-11.0 wt %) but high MgO

(4.5-7.0 wt %) contents when compared with other

tholeiitic rocks of similar SiO_2 content.

Group 10   D.I. 30-36

Although the silica content is similar to the

group 4 dolerites (46 -47 wt %) the Na_2O, K_2O, Ba, Zr

and Sr contents are appreciably higher. This group

is alkaline and their differentiation indices and

normative anorthite contents fall within the ranges of

the Skye hawaiites (Thompson et al., 1972). Their MgO

contents are much higher than those encountered on Skye

(7.0-11.0 wt % as opposed to 2.5-5.5 wt %) thus they

can be termed high MgO hawaiites.

Group 11 D.I. 41-52

The SiO_2 content is similar to that found in the

group 9 rocks however comparisons between the groups

show the group 11 specimens have higher Fe_2O_3, Na_2O, K_2O,

P_2O_5, Ba and Sr contents and lower Ni and Cr values.

Group 11 is not quartz normative and has fairly high

total alkali abundances giving them a distinctly alkaline

character. They are more differentiated than the group

10 dolerites as the SiO_2 Ba and Zr contents are

appreciably higher. Their differentiation indices and

normative anorthite contents are similar to those found

in the Skye mugearites (Thompson _et al_., 1972) but the MgO content in the Rhum specimens is higher (5.0-6.0 wt % as opposed to 2.5-4.5 wt %).

Group 12 D.I. 65-66

This group comprises only 2 specimens but they are sufficiently petrographically and geochemically distinct to merit a separate group. The group 12 rocks are characterised by high Al_2O_3, Na_2O, K_2O, P_2O_5, Ba, Zr, Nb, Y, Sr and Rb contents, the K_2O, Na_2O, Ba and Nb levels in particular being much higher than in the remainder of the suite. Their high differentiation index and low normative anorthite content is analogous to the values exhibited by the Skye benmorites (Thompson _et al_., _op.cit_) however the MgO content is once again much higher in the Rhum specimens.

2)   Gabbros

Two main geochemical classes of gabbro plugs have been distinguished, a high MgO class and a low MgO class. The latter class has been further subdivided into three types, a large group of transitional gabbros, a few quartz gabbros and one differentiate of ferrodiorite composition.

High MgO Gabbros D.I. 16-25

This group is characterised by high MgO, CaO, Ni

and Cr levels and low Na_2O, K_2O and TiO_2. Although similar to the high MgO dolerite groups 2-4, none of the gabbro falls exactly within the ranges of any of the dolerite groups. The group as a whole is transitionally tholeiitic with some nepheline normative members.

Low MgO Gabbros

a) Transitional gabbros

The gabbros are characterised by high CaO (9.4-13.3 wt %) and Sr (204-592 ppm) values and fairly high total alkali and TiO_2 contents. They can be either mildly nepheline or mildly hypersthene normative and thus are completely transitional.

b) Quartz gabbros D.I. 28-29

These all possess normative quartz and two contain modal interstitial quartz testifying to their more differentiated nature. They contain more SiO_2, Na_2O, K_2O, Ba, Zr, Y, Nb and Rb than the previous low MgO gabbro type and less MgO, CaO, Ni, Cr and Sr. They are tholeiitic in character.

c) Ferrodiorite D.I. 58

The ferrodiorite contains moderately abundant interstitial quartz. It possesses high SiO_2, Na_2O, K_2O, Nb, Zr and Y. MgO and Sr, Ni and Cr are present in extremely low quantities. It shows moderate iron

enrichment (0.82) which along with the modal quartz
testifies to its tholeiitic nature.

The acid dykes and peridotite plugs are petro-
graphically and geochemically distinct from the
dolerites and gabbros. The peridohtes exhibit limited
geochemical variation and geochemical subdivision is
unwarranted. The geochemical variation within the acid
rocks is discussed in Chapter 7 (p.249).

II. Appraisal of the transitional nature of the
    Rhum Suite

It is generally recognised that there are three
dominant basalt magma types these being tholeiitic
basalt, alkali olivine basalt and the calc-alkali
basalt type (Wilkinson 1967, Irvine and Baragar, 1971;
Floyd and Winchester, 1975). The first two magma types
are particularly well documented and embrace basalt
magmas from different tectonic settings, the latter
(referred to as High Alumina basalt by Wilkinson, 1967)
is found in association with calc-alkali differentiates.

The petrological study of basaltic suites over
the past fifty years has clearly established the
differences between typical tholeiitic and alkali
olivine basalts (see reviews by Wilkinson, 1967;
Middlemost, 1975) however the recognition of basalt
magmas with properties intermediate between typical
alkali and tholeiitic basalts (eg. Green, 1970; Bass,

1972; Gass et al., 1973) has obscured the clear cut
distinction between these basalt types.

When plotted onto the standard diagrams (Figs. 3.2
to 3.4) the Rhum dolerites clearly straddle the alkali
basalt - tholeiite basalt discriminant line indicating
a transitional nature. Whilst transitional basalts are
clearly present the abundance of what may be termed
"true alkaline" and "true tholeiitic" basalts is
difficult to establish. Reference to the trace element
data further confuses the issue; Winchester and Floyd
(1975) consider that the Nb/Y ratio is a good indicator
of the alkalic or tholeiitic nature of a basaltic rock.
These authors (op.cit,p.335) suggest that alkaline
basalts and alkaline differentiates possess Nb/Y ratios
greater than 0.67 which would exclude even the extreme
alkali affinity differentiates in the Rhum suite Table
3.1.

It is petrogenetically important to assess whether
a bimodal or unimodal basalt population is represented
in the Rhum suite as magma mixing in a bimodal population
could account for the transitional types. Previous
discussion of the Tilley-Muir diagram (Fig. 3.4) by
Cox (1972) shows it is unsuitable for this type of
interpretation.

In order to overcome the difficulties of projection

and to make use of all the analytical data available,
it was decided to investigate the geochemical distinction
between alkaline and tholeiitic basalts using Discriminant
Function Analysis.

Discriminant Function Analysis is a multivariate
statistical technique which linearly combines discrimin-
ating variables (in this case the analysed major oxide
and trace element abundances) to make the classes under-
going analysis (in this case the basaltic magma types)
as statistically distinct as possible. The variables are
first combined into linear discriminant functions (Ap.3.3),
the validity of the functions can also be tested with
classification functions (see Appendix 3.2). These
reclassify the cases of known class type into the classes
as defined by the discriminant functions, a high success
rate in reclassification indicates that there is a
statistical difference between the classes under
discussion. The classification functions can also operate
on cases of unknown class; statistics are available
which show the probability of an unknown case belonging
to any of the analysed classes and also its proximity to
that class centroid or mean (Appendix 3.2). These
features are extremely useful as they give a good
indication of the validity of the supposed class of
an unknown case.

a) Data acquisition

A literature search was undertaken to acquire analyses of alkaline, tholeiitic and calc-alkali basalts. The data sources for the basalts used in the discriminant analyses and the mean values for each basalt class are listed in Appendix 3.1. The alkali and tholeiitic classes include representative analyses from both continental and oceanic environments, the latter included ocean floor basalts. The term basalt in this investigation was defined as analyses with SiO_2 values ranging 45-52 wt % (cf. Floyd and Winchester, 1975). An alternative scheme adopted by Pearce (1976, p.17) defining basalts as analyses with CaO + MgO ranging 12-20 (wt %) was deemed inappropriate as this would have pre-cluded many of the Rhum dolerites under investigation. Any basaltic suites referred to as transitional between typical alkali and tholeiitic basalts were referred to a separate class and their transitional nature was tested as part of the investigation. All the cases contained the major oxides. Many included some trace element data however several had no trace element analyses. This lack of trace element data has been encountered by other workers on compilations of basaltic analyses (eg. Floyd and Winchester, 1975), sufficient numbers of each variable were included in the compilation to give a representative

data set for each basalt class.

b) Results

The results presented in Table 3.2 and Fig. 3.5
show that the three main basalt classes under investi-
gation are statistically distinct in terms of both major
or major plus trace elements. The discriminant functions
which separate these basalt classes are presented in
Appendix 3.3. This investigation confirms that there
are real and distinct chemical differences between the
alkali, tholeiite and calc-alkali classes and the
classifications proposed by the authors listed in
Appendix 3.1 were valid.The vast majority of the Rhum
minor intrusion suite classify (as expected) as either
tholeiite or alkali basalts.

A function was then derived to discriminate between
only the alkali and tholeiitic basalt class. The function
is listed in Appendix 3.3 and the classification results
are presented in Table 3.3 the high success rate on
reclassification once again confirms that the classes
are statistically separate.

The derivation of the value known as the discriminant
score is described in Appendix 3.2. It is obtained by
multiplying the standardised variable for each case by
the values for each variable listed in the discriminant
function, the score can have either a positive or

negative value or can be zero.

The frequency of the discriminant scores based on world-wide occurrences for both the alkali and tholeiite basalt classes, is presented in Fig. 3.6 along with the discriminant scores of some documented basalts believed to be transitional between alkali and tholeiite basalts. The Rhum dolerites, gabbros and lavas are each shown separately. A positive discriminant score indicates a basalt of tholeiitic affinity and a negative score a basalt of alkalic affinity. A discriminant score close to zero indicates that the rock is transitional between the alkali and tholeiite magma types. The alkali and tholeiite basalt classes show a clear bimodal distribution with a distinct paucity of cases with discriminant scores -0.35 to +0.35. Conversely the basalts believed to be transitional by the authors in Appendix 3.1 have a uni-modal distribution as do the Rhum dolerites. The modal discriminant score of both these populations lie in the range -0.35 to + 0.35 thus the existence of truly trans-itional basalt magmas on Rhum and elsewhere is confirmed. The Rhum gabbros and the Rhum lavas also span the range from thoroughly alkaline through transitional types to thoroughly tholeiitic basalts.

Additional data on basaltic compositions from the Mull, Ardnamurchan and Blackstones Bank Tertiary centres and the basalts of the Small Isles is presented in

Fig. 3.7. The basalts from the Small Isles once again show a broad range of compositions with a distinct peak in the transitional region. The abundant basalt data from Skye have been separated into the three different magma types defined by Matt_e_y et al., 1977. The Skye Main Lava Series show a bimodal distribution with peaks at -1.55 and +0.75 probably reflecting the distribution of the nepheline normative and hypersthene normative basalt types within the Skye Main Lava Series (Thompson et al., 1972). There is a distinct lack of basalts with zero to -0.35 discriminant scores in the Skye Main Lava Series. The Fairy Bridge magma type (Matt_e_y et al., 1977) appears to be thoroughly transitional and the low Alkali Tholeiite magma type spans the range transitional to thoroughly tholeiitic as expected. The data from the Tertiary centres of Ardnamurchan, Mull and the Blackstones span the range transitional alkali to tholeiite, the Mull lavas tend to be more alkaline and the Ardnamurchan cone sheets and the Blackstone Bank gabbros are generally more tholeiitic.

In conclusion the validity of the alkaline, tholeiitic and calc-alkaline basalt classes on a world wide scale has been confirmed. However, the existence of basaltic compositions thoroughly transitional between the alkali and tholeiitic magma types has been convincingly

demonstrated on Rhum, in the Hebrides and elsewhere in
the world.
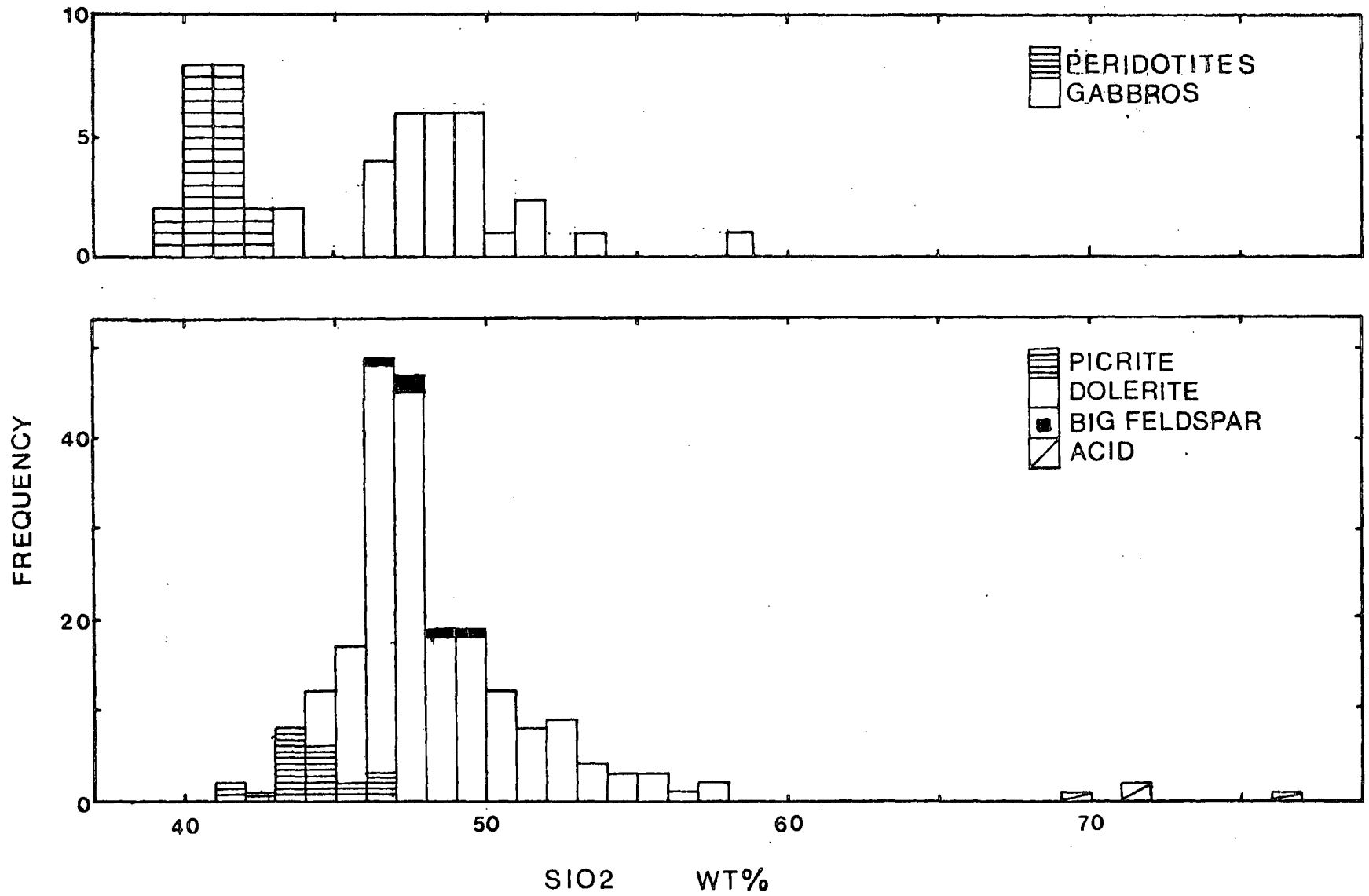
Fig 3.1 SiO2 frequency in the Rhum minor intrusion suite
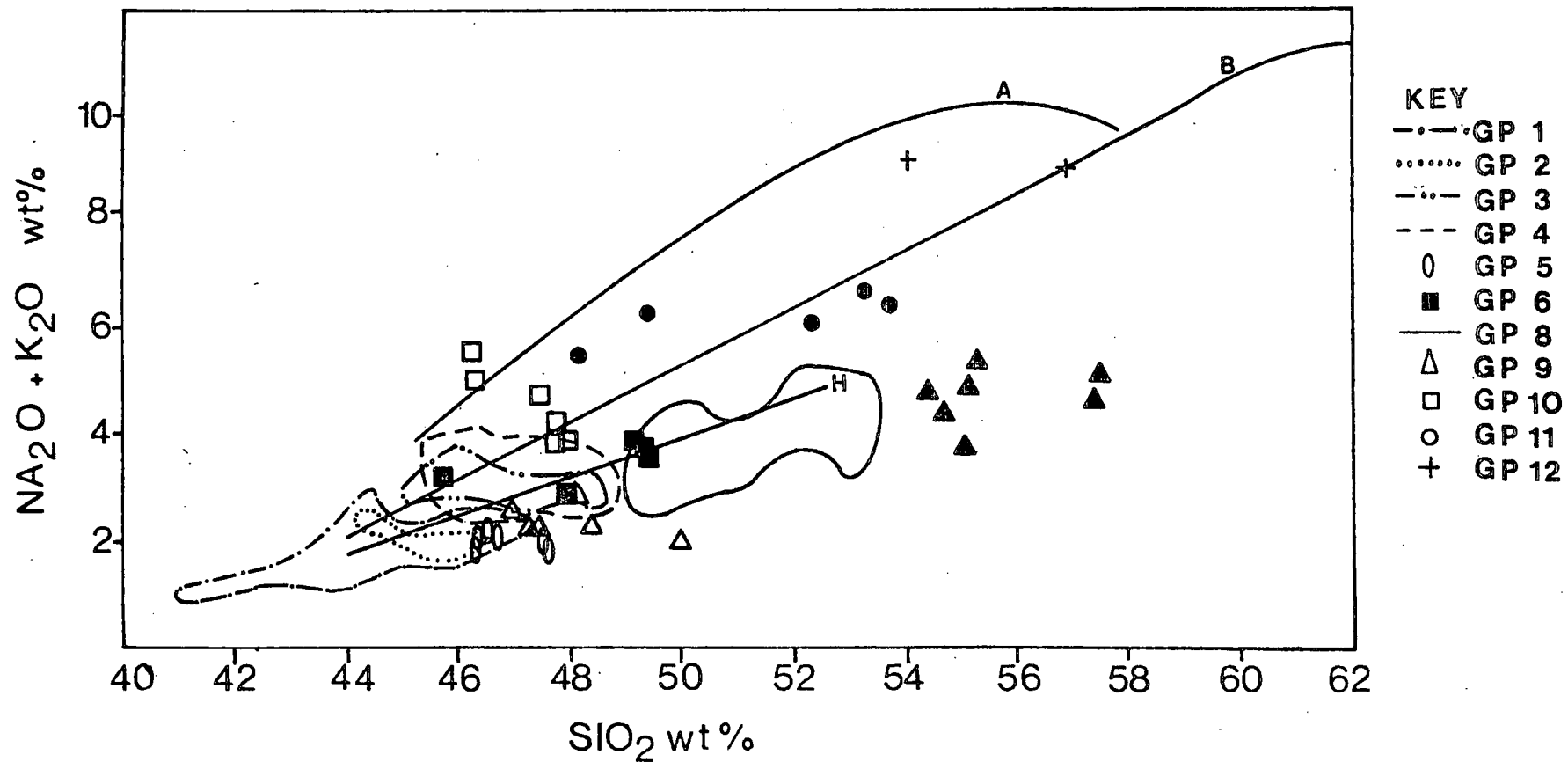
Fig.3.2 SiO$_2$ v. Na$_2$O + K$_2$O variation in the Rhum dolerites, lines A and B refer to the trend of the Skye Main Lava Series, line H is the discriminant line between Hawaiian alkali and tholeiite basalts (all taken from Thompson et al., 1972, Fig.6).

Fig.3.3 Irvine Baragar (1972) projection. The solid line discriminates between the alkalic (AL) and tholeiitic (TH) fields.

OL' = ol+3/4opx

NE' = ne+3/5ab

Q' = qz+2/5ab+1/4opx.
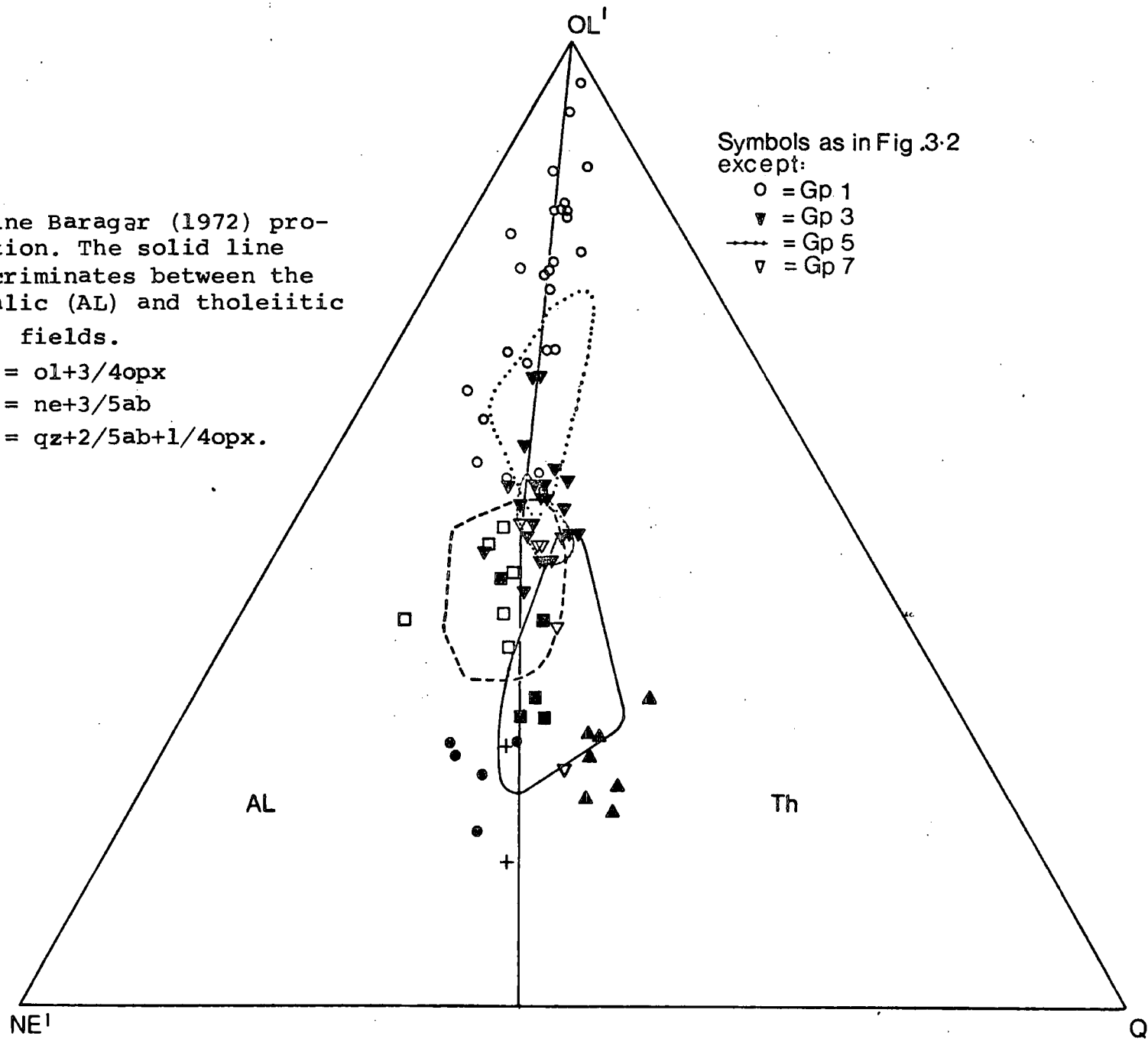
Symbols as in Fig .3·2 except:

o = Gp 1

▼ = Gp 3

—▬— = Gp 5

▽ = Gp 7

OL'

NE'

Q'

AL

Th

84
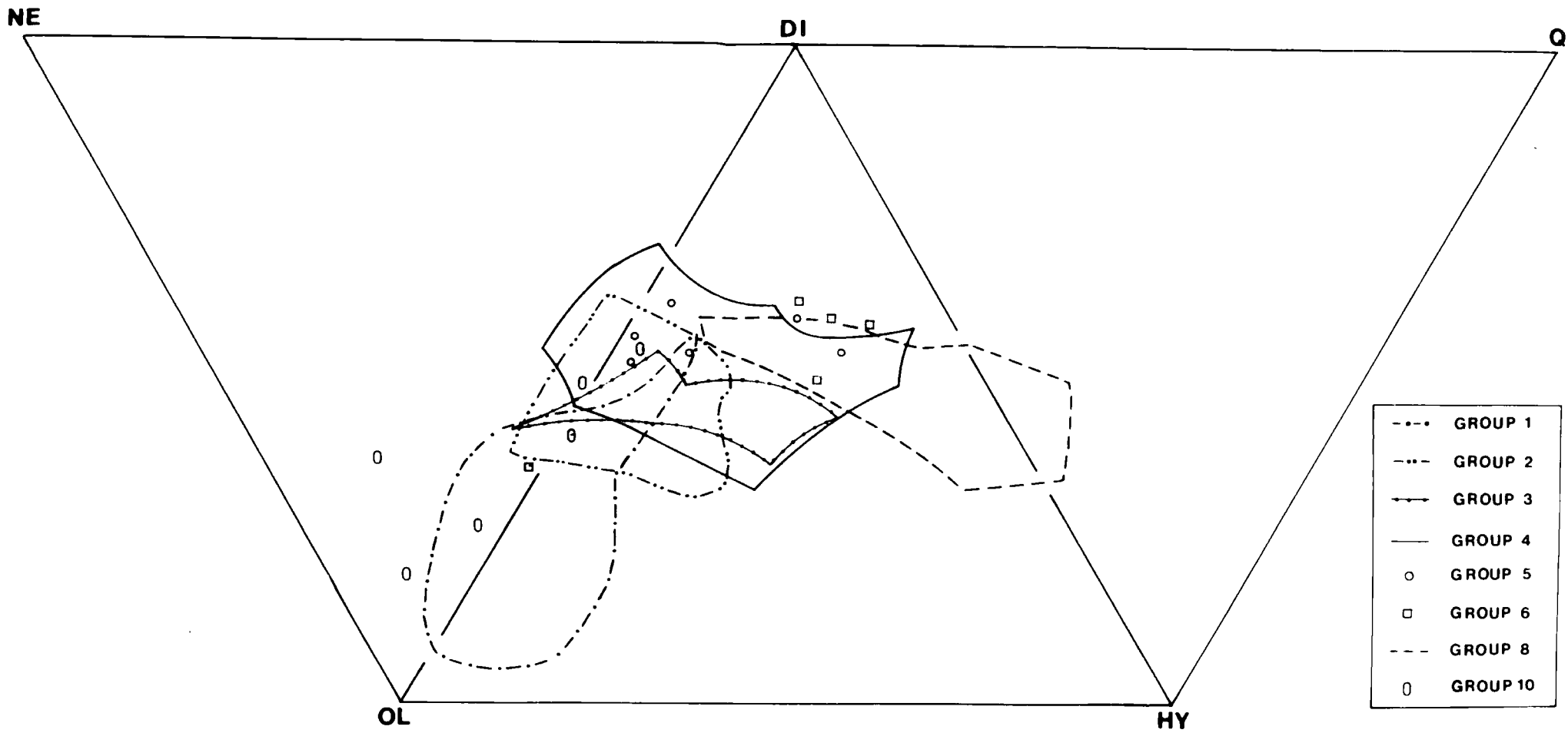
FIG 3.4   Tilley–Muir diagram of the Rhum dolerites

Legend:

- –·–· GROUP 1
- –··– GROUP 2
- ▸–▸– GROUP 3
- ——— GROUP 4
- o GROUP 5
- ▫ GROUP 6
- – – – GROUP 8
- 0 GROUP 10

Triangle vertices: NE, DI, Q (top); OL, HY (bottom)
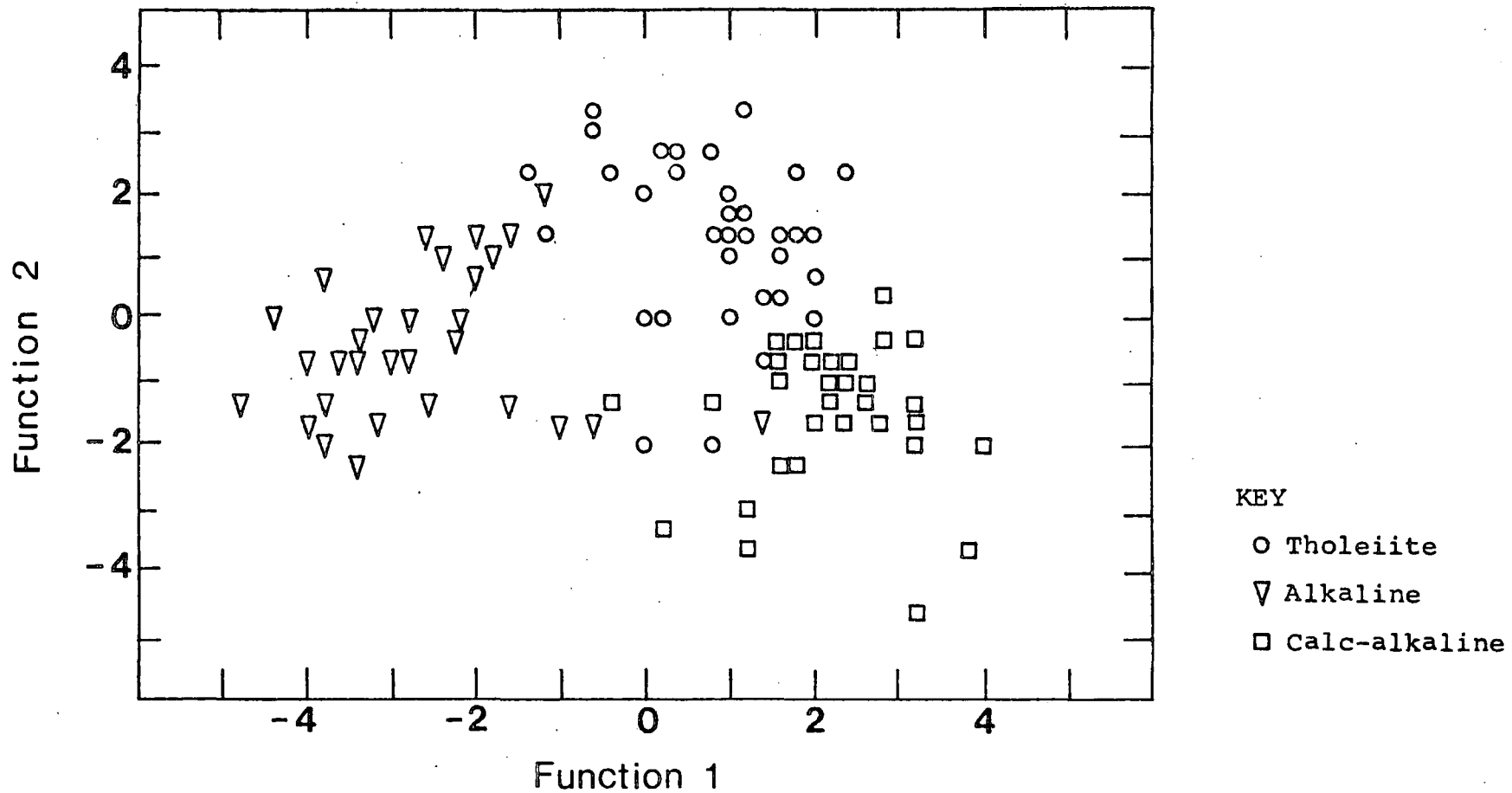
Fig. 3.5 Distribution of tholeiite, alkaline and calc-
alkaline basalts, with respect to the 2 dis-
criminant functions as discussed in text.
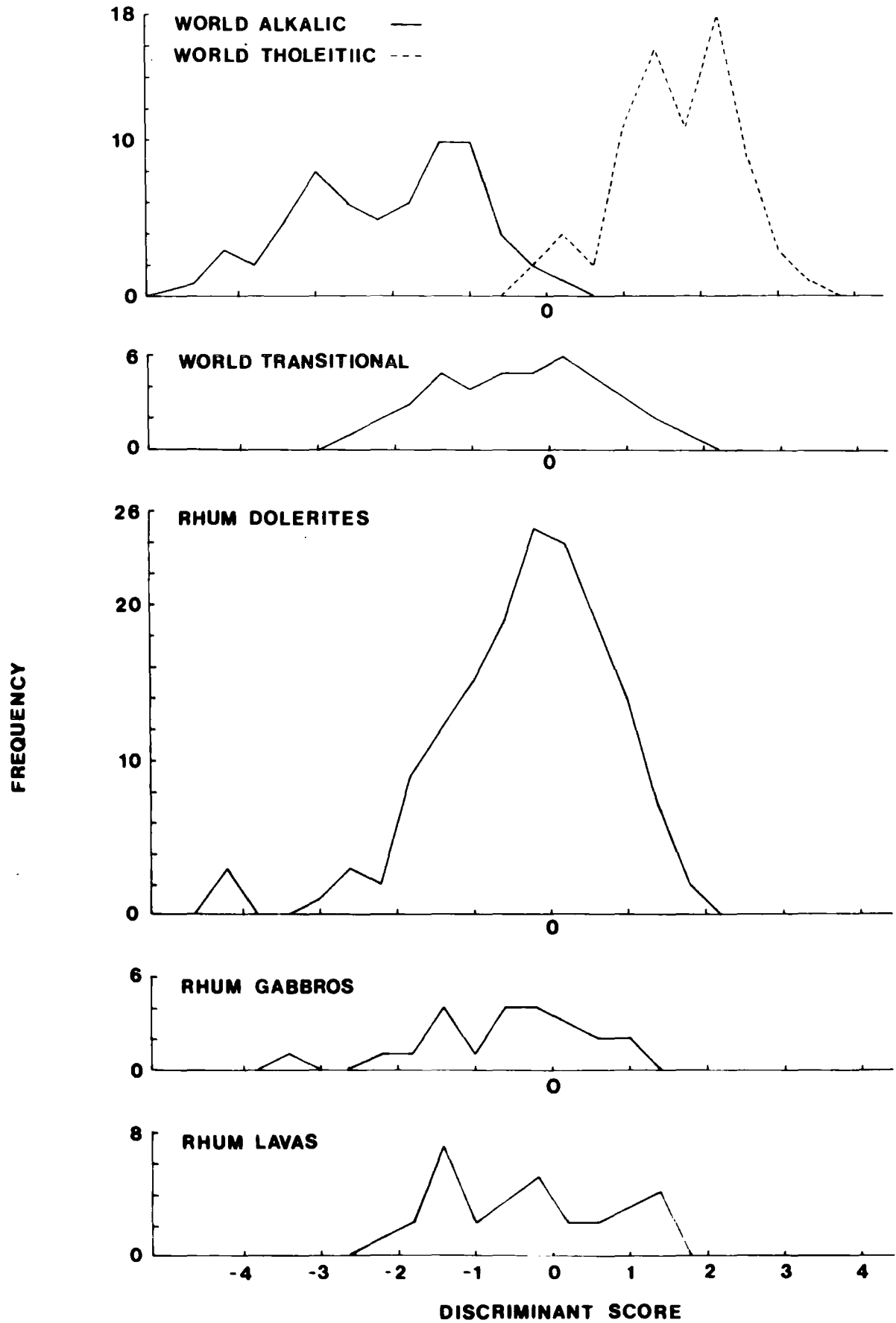
FIG 3.6 Frequency distribution of the discriminant scores of worldwide
alkali,tholeiite and transitional basalts and Rhum magmas.

Fig. 3.7 Frequency of the discriminant scores in
some Hebridean basalts. For data sources
see appendix 3.1.
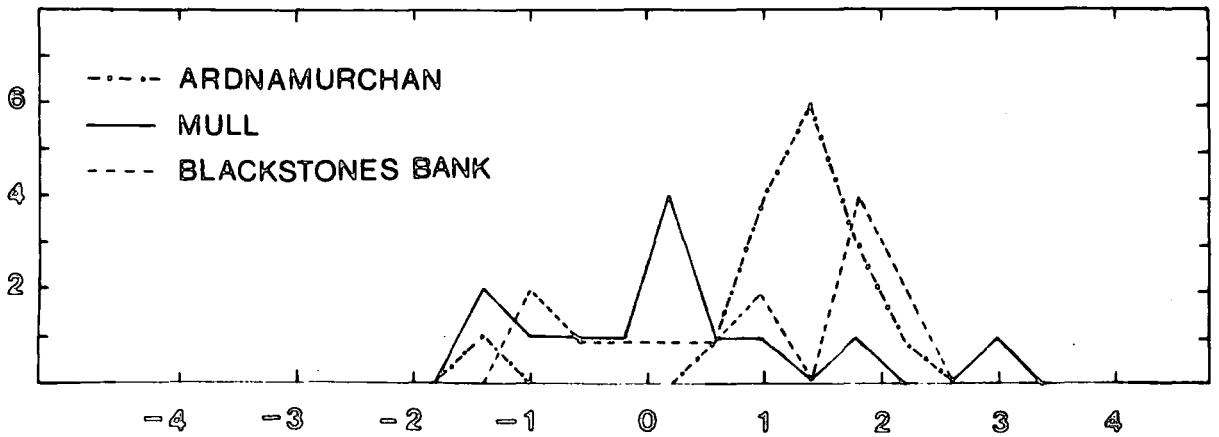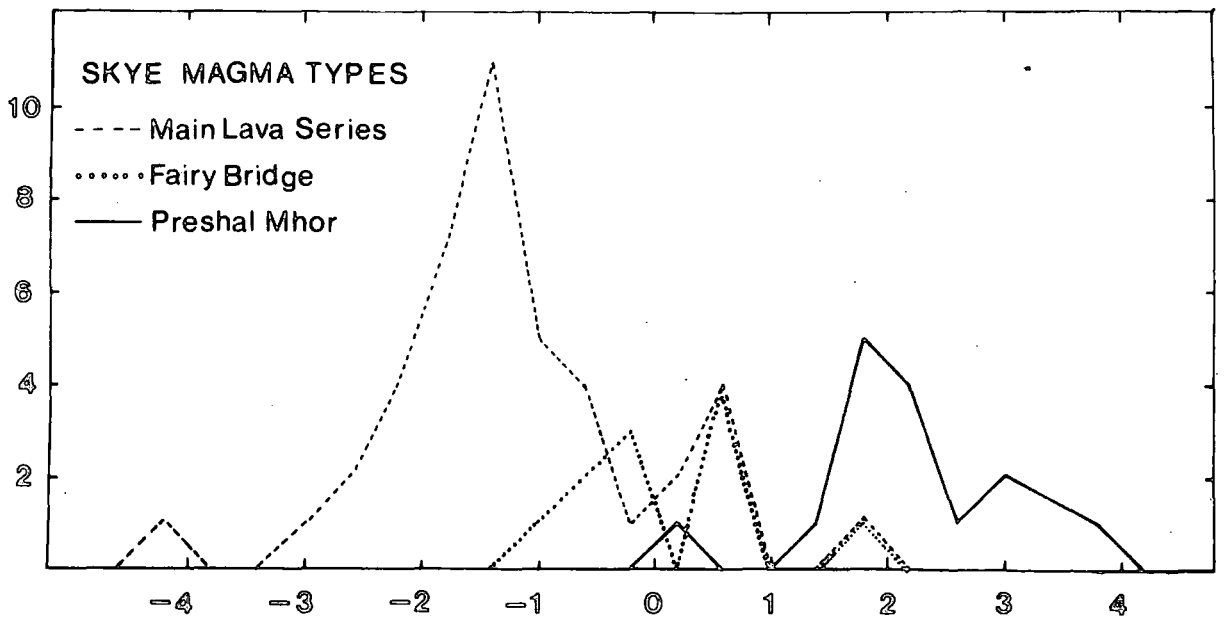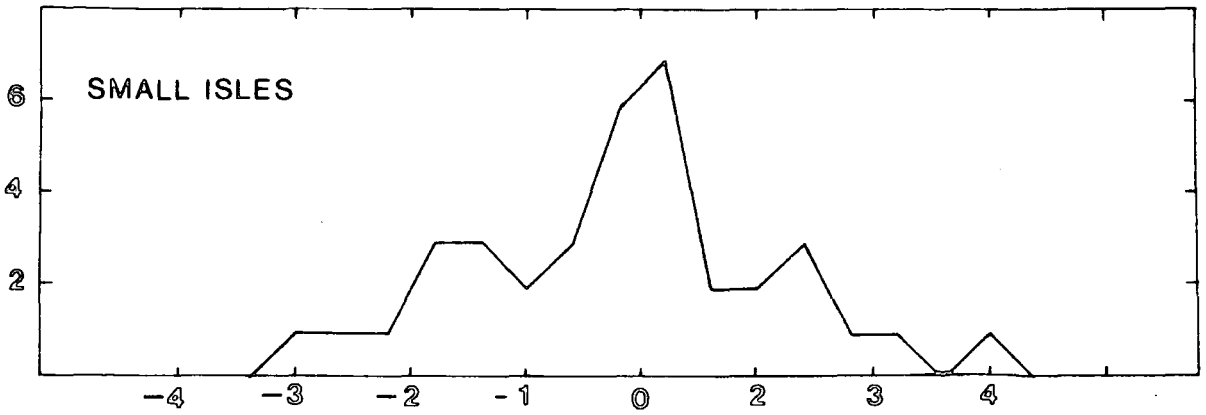
Group	Mean	Maximum	Minimum
1	0.2404	0.5000	0.0909
2	0.2356	0.3125	0.1429
3	0.2231	0.2632	0.1429
4	0.1886	0.3043	0.1071
5	0.1389	0.1667	0.1200
6	0.1653	0.1795	0.1481
7	0.2000	0.2727	0.1429
8	0.2294	0.6154	0.1000
9	0.2535	0.3043	0.1818
10	0.2990	0.3929	0.1905
11	0.3012	0.3667	0.2222
12	0.5305	0.5610	0.5000

Table 3.1   The range of Nb/Y ratios of the
            Rhum dolerite groups.

TABLE 3.2

CLASSIFICATION STATISTICS FOR THE THOLEIITE ALKALINE AND
CALCALKALINE MAGMA TYPES

Major and trace elements

Actual Class	No. of cases	Predicted Class Membership		
		1	2	3
Class 1 Tholeiite	78	74 94.9%	1 1.3%	3 3.8%
Class 2 Alkali	62	3 4.8%	58 93.5%	1 1.6%
Class 3 Calc-alkali	51	1 2.0%	0 0.0%	50 98.8%
Rhum dolerites	156	84 53.8%	68 43.6%	4 2.6%
Rhum gabbros	24	12 50%	12 50%	0 0.0%

Major elements

Actual Class	No. of cases	Predicted Class Membership		
		1	2	3
Class 1 Tholeiite	78	73 93.6%	2 2.6%	3 3.8%
Class 2 Alkali	62	3 4.8%	57 91.9%	2 3.2%
Class 3 Calc-alkali	51	6 11.8%	4 7.8%	41 80.4%
Rhum dolerites	156	84 53.8%	72 46.2%	0 0.0%
Rhum gabbros	24	10 41.7%	14 58.3%	0 0.0%

92

TABLE 3.3

CLASSIFICATION STATISTICS FOR THE THOLEIITE
AND ALKALINE MAGMA TYPES

Major and trace elements

Actual Class	No of cases	Predicted Class Membership	
		1	2
Class 1 Tholeiite	78	76 97.4%	2 2.6%
Class 2 Alkali	62	3 4.8%	59 95.2%
Rhum dolerites	156	85 54.5%	71 45.5%
Rhum gabbros	24	10 41.7%	14 58.3%

Major elements

Actual Class	No of cases	Predicted Class Membership	
		1	2
Class 1	78	75 96.2%	3 3.8%
Class 2	62	3 4.8%	59 95.2%
Rhum dolerites	156	85 54.5%	71 45.5%
Rhum gabbros	24	10 41.7%	14 58.3%

CHAPTER FOUR

PETROGRAPHY

Introduction

This chapter describes the variable petrography of
the Rhum dolerites and includes a more detailed
description of the petrographical features used in the
classification. The gabbro and peridotite plugs and the
acid dykes are also described and a small section is
devoted to the xenoliths in the dolerite dykes. The
mineralogy and mineral chemistry is described in
Chapter 6.

Particular attention was paid to petrographic
features which offer insight into petrogenetic processes;
this includes the presence of different phenocryst
assemblages, the relationships of the groundmass minerals
and the development of unusual textures.

Several of the dolerites are amygdaloidal; chlorite
and calcite are by far the most abundant vesicles but
epidote, quartz, amphibole and zeolites can also
contribute. One of the thick conformable sheets (77243)
has a unique occurrence of amygdaloidal hydrogarnet.

Group One

Olivine and to a lesser extent spinel are ubiquitous
phenocryst phases; the group is petrographically variable

as the phenocryst abundance varies from specimen to specimen. Three main petrographic types are represented in the group, two are characterised by the presence of pale brown groundmass clinopyroxene; the other by additional chestnut brown, strongly pleochroic amphibole. The picritic rocks are often fresh; the general lack of alteration facilitates comparisons of individual specimens and enables recognition of subtle differences between the different petrographic types.

Type 1

These specimens possess variable quantities of phenocrystic olivine (Fo84-Fo88) and chrome-spinel, the former can be fresh (53A76, Plate 4.1) or altered (69A76). The spinel occurs as phenocrysts either enclosed by olivine or independently. They are usually opaque but red-brown transluscent varieties are also present. The titanium-rich aluminous groundmass clinopyroxenes are deep brown in colour and are strongly pleochroic, they are generally interstitial to the elongate, mildly zoned (An55-An78) plagioclase laths and the abundant altered groundmass olivine. The plagioclase crystals are generally equi-dimensional but sparse larger laths may be microphenocrysts. Most sections contain minor quantities of a green pleochroic amphibole which partially rims some of the clinopyroxenes, as well as occurring as an independent groundmass phase.

One section (56A76) exhibits a sharp but unchilled contact between a normal picrite and a more leucocratic facies. The latter contains abundant lilac-brown elongate clinopyroxene laths, altered feldspar and abundant amygdaloidal calcite. There is also abundant emerald green, strongly pleochroic amphibole which both mantles some of the clinopyroxenes and also occurs independently. Opaque oxides are abundant in this leucrocratic facies, the majority are granular but some occur as very elongate fibrous crystals which are possibly ilmenite. In addition quartz and minor green and brown amphibole contribute to the vesicle infill and both phenocrystic and groundmass olivine are absent. This atypical facies is probably due to crystallisation from a volatile-rich differentiated liquid.

Three members of this type were collected from the olivine rich portions of picrite dykes. One fresh specimen (52A76) contains abundant olivine phenocrysts upto 6mm in diameter. The brown groundmass pyroxenes and the mildly zoned plagioclase often interfinger in variolitic growth structures; (Plate 4.2), as with other specimens of this type green amphibole is also present. 77179 is similar but there is less phenocrystic olivine, and the variolitic texture is poorly developed.

Type 2

Although they are similar in many respects to
Type 1, individual specimens generally have a much
greater range in olivine phenocryst size (0.3-2.5 mm),
finer grained groundmass minerals and less groundmass
olivine. The olivine phenocrysts (Fo84-Fo88) are usually
granular anhedral or subhedral crystals but skeletal
hopper shapes (terminology from Donaldson 1976) are also
found in some specimens (eg. 77052, 77095). A weak
variolitic groundmass texture is found in some specimens
(eg. 77052, 77101). The latter has suffered mild thermal
metamorphism and a peculiar dendritic texture formed by
exsolution of opaque minerals has developed in the olivine
phenocrysts. Plagioclase microphenocrysts have also been
observed in some specimens.

Type 3

These specimens have variable quantities of
phenocrystic olivine and spinel, the latter is always
opaque. They possess olivine (which is usually fresh),
very pale brown coloured clinopyroxenes, plagioclase
and spinel as groundmass minerals. In addition they all
contain a chestnut brown, strongly pleochroic amphibole
(kaersutite) in variable abundance. This amphibole
partially and wholly rims clinopyroxene and can also
be seen replacing the latter. In the freshest section
(77236) it occurs as sub-ophitic plates enclosing all

the other minerals. The remaining specimens exhibit re-crystallisation textures of the groundmass minerals which vary in degree from specimen to specimen. In addition the clinopyroxene and to a lesser extent the olivine phenocrysts can show considerable exsolution of opaque oxides. Although it can be seen replacing clino-pyroxene the amphibole appears to be a late stage primary magmatic mineral as it can develop ophitic relationships to other minerals and it has been recrystallised along with the other major phases in some of the specimens.

One final specimen (77024) deserves special mention as it is petrographically unusual. It contains abundant phenocrystic olivine (Fo76) and chrome spinel, the former varying in morphology from elongate chain olivines (Plate 4.3) through hopper olivines to granular varieties (terminology from Donaldson, 1976). The groundmass is extremely fine-grained and consists of granular aggregates of blackened olivine (Fo75), clinopyroxene and plagioclase (An40-An66), with subordinate opaques. The petrological significance of this dyke is discussed in Chapter 6 (p.173).

Group Two

Several of the members of this group have no phenocrysts, others contain very sparse phenocrysts of altered olivine and titanomagnetite or plagioclase (An60-An82), others contain all three of the phenocryst phases

(Table 4.1). The typical group two specimens are aphyric and possess neutral coloured subophitic aluminous clinopyroxenes, zoned elongate plagioclase (An43-An74), abundant altered groundmass olivine and titanomagnetite opaque oxides. Several specimens (eg. 77039, 93A76) exhibit variolitic groundmass textures (Plate 4.4), composed of fans of radiating plagioclase (terminology following Lofgren 1974, p.249) with interstitial clino-pyroxene, olivine and opaque oxide. Several of the plagioclase crystals in these variolites are hollow cored, (eg. 77240). Most of the variolites contain sparse granular olivine phenocrysts (eg. 77039) but hopper olivines have also been located (77019).

One coarse-grained specimen (39A76) is atypical as it possesses a pale brown (as opposed to neutral coloured) ophitic clinopyroxene and fibrous opaques in rounded areas which may be amygdale infills. Although phenocrystic plagioclase is sparse it is found in certain specimens. 65A76 and 70A76 contain plagioclase microphenocrysts in glomerophyric aggregates and as single crystals. These phenocrysts appear to be in equilibrium with the ground-mass. Both 77214 and 77245 carry phenocrystic plagio-clase in addition to subordinate altered olivine; once again the plagioclase appears to be in equilibrium with the groundmass but there are suggestions of reaction rims

around several of the plagioclase crystals in the former.
In addition 77214 contains rare, lighter coloured clino-
pyroxene plates in optical continuity with the enclosing
subophitic groundmass pyroxenes which may be micro-
phenocrysts.

Group Three

The group three specimens are petrographically
variable but 4 main types can be distinguished by their
phenocryst content (Table 4.1).

(i) Aphyric. The aphyric varieties typically possess a
neutral coloured interstitial feathery edged Ca-augite,
elongate mildly zoned plagioclase (An50-An67), many of
which have hollow cores. Both granular and skeletal
needle-like titanomagnetite crystals are present, the
granular groundmass olivine is invariably altered. An
extremely fine-grained chilled facies can be seen in
77080 showing these dykes do not have variolitic chills.
Only one true variolite is present in group 3 (77346)
which closely resembles the variolites in group two but
lacks the sparse olivine phenocrysts.

(ii) Plagioclase-olivine phyric. Phenocrystic olivine is
subordinate in quantity to phenocrystic plagioclase in
the plagioclase-olivine phyric specimens. The former is
always altered and some contain included chrome-spinels,

reaction rims have developed around the plagioclase phenocrysts in one of the specimens (77251). The calcic augites are neutral in colour and vary from granular to subophitic, the sub-parallel plagioclase needles in 77191 give it a distinctive flow aligned groundmass texture.

(iii) Plagioclase-clinopyroxene-olivine phyric. Aluminous clinopyroxene phenocrysts occur in aggregates with either plagioclase (An82) or with both plagioclase and olivine whereas the latter two can occur as independent pheno-crysts. Texturally these aggregates resemble xenolithic accumulations although reaction rims with the groundmass are not always present. One specimen (77082) contains a single plate of phenocrystic clinopyroxene in addition to abundant phenocrysts of plagioclase and altered olivine. Although it is difficult to be certain, it seems that the aggregates of clinopyroxene in these rocks are xenolithic (perhaps cognate in origin) and the pyroxene is not a true phenocryst phase.

(iv) Plagioclase phyric. The fourth main type resembles the aphyric rocks but are characterised by the presence of sparse phenocrystic plagioclase.

Group Four

Three main petrographic types can be recognised in Group Four. These are aphyric, plagioclase phyric and

plagioclase-olivine phyric. Although clinopyroxene, plagioclase and opaque oxides are ubiquitous groundmass phases in group four, olivine can be absent.

(i) Aphyric. The aphyric specimens have a variable petrography, clinopyroxene varies from a neutral coloured non-pleochroic variety to a deep brown titaniferous augite. Compositional zoning is marked in some specimens (eg. 77035, 77012, 95A76) by a diffuse pale brown rim to otherwise neutral coloured pyroxene. The clinopyroxene which is a calcic augite in composition, has a variable habit, the majority is interstitial but ophitic and granular pyroxenes have also been found (eg. 77176 and 95A76 respectively) there is no consistent relationship between clinopyroxene colour and habit. Plagioclase (An40-An43)* generally occurs as small rather elongate laths but pools of interstitial plagioclase are also present; some specimens (eg. 41A76, 77086) contain some moderately skeletal plagioclase crystals. Olivine is always granular in habit and is pseudomorphed by chlorite, talc etc when present. The opaque oxides (titanomagnetites) can be found as elongate rods (eg. 41A76) but the majority are anhedral grains.

(ii) Plagioclase phyric. Plagioclase phenocrysts occur as single crystals and in glomeroporphyritic aggregates;

*Based on very limited analytical data.
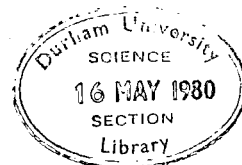
they show mild zoning. Finger print textured reaction
rims have developed around plagioclase phenocrysts in
several specimens. The groundmass relationships are
variable, several specimens have a differentiated aspect
similar to the group eight specimens (see p.107) whereas
others are typically basaltic. There is no consistent
relationship between the clinopyroxene colour (which is
generally neutral but can be pale brown) and habit (which
is typically either interstitial or granular but can be sub-
ophitic) in these plagioclase phyric specimens.

(iii) Plagioclase-olivine phyric. Phenocrystic plagioclase
can also occur with subordinate altered olivine, the
latter may carry included opaque phenocrysts, the opaque
phenocrysts can also occur as independent crystals. Deep
brown interstitial groundmass clinopyroxene is found in
77073 and the groundmass in 77015 (which carries rare
phenocrystic olivine) is mildly differentiated; however,
these specimens are atypical. The majority of the
plagioclase-olivine phyric specimens possess neutral or
very pale brown calcic augite;(which is generally inter-
stitial), mildly zoned plagioclase laths and moderately
abundant granular titanomagnetite.

(iv) Plagioclase-opaque oxide phyric. Some specimens
possess plagioclase and opaque phenocrysts without
associated olivine. The latter can occur either as

inclusions in the plagioclase or as independent
phenocrysts and are rare (sometimes only two per thin
section). The lack of phenocrystic titanomagnetite
suggests that the group four magmas had a low oxygen
fugacity which inhibited the formation of phenocrystic
titanomagnetite.

(v) Plagioclase-clinopyroxene phyric. Phenocrystic
clinopyroxene (generally a calcic augite) always occurs
in association with plagioclase. Although it can occur
in glomerophyric aggregates (47A76 cf. group three) the
majority occurs as single crystals and appears to be a
true phenocryst phase, two specimens (77032, 77351) carry
neutral coloured pyroxene whereas 77348 carries a pale
brown slightly pleochroic variety. In all three specimens
the groundmass pyroxene is similar in colour to the
phenocrystic pyroxene.

The high iron variants noted in Chapter 3 could not
be distinguished from the remainder of group four, they
are generally either aphyric or mildly plagioclase phyric.

Group Five

These specimens all contain calcic plagioclase and
magnesian olivine microphenocrysts either as single
crystals or in aggregates up to 4mm long. The plagioclase
is unzoned and occurs as tabular laths which appear to be

in equilibrium with the groundmass. The olivine is generally fresh and usually occurs as spherical grains although elongate tabular olivine phenocrysts can be seen in 77323. The groundmass is distinctive as the neutral to very pale brown coloured clinopyroxenes are ophitic with individual crystals up to 3mm long, this ophitic texture is preserved in the finegrained chilled specimens (eg. 77056), although it is only weakly developed in one of the coarser specimens (77323). The groundmass plagioclase occurs mainly as needles embedded in the pyroxenes but some is interstitial. The groundmass olivine is generally fresh and is granular in habit, the opaque minerals occur as ragged anhedral interstitial grains.

Group Six

Three petrographic types are developed in group six. Specimens SR182, SR159 and SR282 are similar, they possess sparse, poorly formed, strongly zoned plagioclase microphenocrysts in a matrix of grey coloured subophitic augite, elongate mildly zoned plagioclase laths, sparse altered olivine, interstitial opaques and devitrified interstitial glass. One aphyric specimen (SR211) is distinctive as it contains a deep lilac, moderately pleochroic interstitial clinopyroxene along with fresh granular olivine, elongate plagioclase and granular

opaques. The final specimen (SR141) is atypical as it
is the only post-lava dyke to have suffered serious
alteration. It carries altered olivine phenocrysts in
a groundmass of acicular plagioclase (often with hollow
cores), interstitial pale brown slightly pleochroic
clinopyroxene and small granular opaques.

Group Seven

All these specimens contain variable amounts of
large (up to 6mm diameter) well formed sub-equant
plagioclase phenocrysts; one specimen contains a single
olivine phenocryst. The plagioclase phenocrysts are
slightly zoned (An83-An88) and show no signs of reaction
with the groundmass, they occur as either single crystals
or as 2-4 crystal aggregates. The groundmass typically
consists of a neutral coloured ophitic calcic augite
enclosing acicular plagioclase (An38-An41) and some of
the granular opaques. Some of the specimens were collected
from areas adjacent to later basic intrusions and show
mild recrystallisation of the groundmass minerals. Two
specimens are atypical, 77014 contains fewer plagioclase
phenocrysts and the clinopyroxene is interstitial rather
than ophitic. The groundmass in 12A76 is coarser than
usual for the group; the sub-ophitic aluminous calcic
augite being pale brown in colour as opposed to neutral.
The only analysed pyroxenes in group seven are from

12A76 as this was the only specimen with a sufficiently coarse groundmass.

Group Eight

Four main petrographic types are encountered in group eight (see table 4.1). Despite the variation in phenocryst content many of the specimens have petrographically similar groundmass textures. The groundmass generally contains abundant plagioclase (An26-An68) as laths and in interstitial pools this imparts a leucocratic appearance, granular neutral or straw coloured non-pleochroic augite is subordinate in abundance to plagioclase as are the opaque titanomagnetites. Specimens with groundmass textures as described above are referred to as differentiated (as opposed to basaltic) in this account.

Several of the group eight specimens are characterised by the presence of brown devitrified glass, some specimens are virtually hyalocrystalline (eg. 77078) with plagioclase microlites whereas in others the glass is interstitial to plagioclase and intersertal clinopyroxene. A peculiar angular mesh of extremely fine acicular opaques is developed in the interstitial glass and in some of the hyalocrystalline specimens (Plate 4.5). Several of the glassy specimens contain variolitic plagioclase either as fans as described in group two or as extremely well developed bow-tie structures (Plate 4.6). The

variolitic plagioclase often nucleates at both ends of
the elongate plagioclase microlites (Plate 4.7). Plagio-
clase is the principal phenocryst phase in these glassy
specimens and occurs as extremely well formed sparse
crystals.

The aphyric and plagioclase phyric specimens are
similar as both types have a differentiated groundmass,
rare plagioclase microphenocrysts are encountered in the
former but are more abundant in the latter. These micro-
phenocrysts have poor crystal forms and often appear to
be in disequilibrium with the groundmass, some of the
aphyric specimens have basaltic textures and can carry
sparse altered groundmass olivine.

Plagioclase-clinopyroxene phyric and plagioclase-
clinopyroxene-olivine phyric specimens are generally
similar as they both possess a differentiated groundmass
texture. The olivine is always altered to a green
psuedomorph and is virtually absent in some specimens.
The plagioclase (An44-An80) occurs as altered poorly
formed crystals and the calcic augite is always a neutral
coloured granular variety, the phenocrysts can occur as
single crystals or in aggregates. The majority of these
rocks have a low phenocryst abundance but some specimens
possess up to 50% phenocrysts (eg. 77040).

Some of the plagioclase-clinopyroxene phyric

specimens have a peculiar feathery lobate edged neutral coloured clinopyroxene (Plate 4.8) which can be in association with skeletal plagioclase and elongate rod like opaque oxides. Elongate rod opaques also occur in otherwise typical groundmass textures (eg. 75A76).

Group Nine

The phenocryst phases in these rocks are plagioclase clinopyroxene and altered olivine with subordinate titanomagnetite microphenocrysts. The plagioclase is generally more abundant than either olivine and clino-pyroxene and the latter is subordinate to olivine in the plagioclase-olivine-clinopyroxene-opaque phyric rocks. Both the clinopyroxene and plagioclase often develop reaction rims with the adjacent groundmass and in some specimens (eg. 29A76) seem to have been partially re-sorbed. The latter feature is also evident in the corroded margins of the titanomagnetite micro-phenocrysts (29A76, 76A76, 77209). The groundmass in these phyric rocks is generally leucocratic and very fine grained and the mafic minerals are generally altered. 55A76 is unusual as it carries altered, olive green mildly pleo-chroic amphibole phenocrysts in addition to the plagio-clase (An45-An54) and clinopyroxene phenocrysts. The fresh groundmass in 55A76 contains abundant plagioclase

($\sim$ An47) and subordinate green amphibole, neutral granular augite, granular opaques and interstitial quartz. One of the aphyric specimens is hyalocrystalline with a faint acicular variolitic texture, the other has developed a stronger variolitic texture but differs from the basaltic variolites as in its more sodic plagioclase composition.

Group Ten

The majority of these specimens are plagioclase-olivine-chrome-spinel phyric, the phenocrystic magnesian olivine varies from fresh to altered and the tabular plagioclase laths (An63-An70) are generally in slight disequilibrium with the groundmass. Some contain included opaque phenocrysts which can also occur as independent phenocrysts (eg. 77137). The groundmass clinopyroxene is generally a deep brown pleochroic aluminous titanaugite and occurs interstitially to plagioclase, K-feldspar, olivine and opaque oxides. In addition two specimens (77137, 77184) contain a tan coloured mildly pleochroic primary amphibole, the groundmass of these two specimens is very similar to one of the aphyric specimens (32A76)

Group Eleven

These specimens contain only sparse amounts of the phenocryst phases (oligoclase feldspar and calcic augite)

which are usually less than 1mm diameter. As with groups
nine and ten the plagioclase and clinopyroxene pheno-
crysts often show signs of disequilibrium with the
adjacent groundmass but this is obscured by the generally
altered nature of the specimens. Phenocrystic olivine
where present is always altered and some specimens
(77279, 77347) carry ilmenite or titanomagnetite micro-
phenocrysts. The groundmass is always leucocratic with
abundant plagioclase, the mafic minerals are generally
altered and the opaque minerals are usually granular.
The group as a whole is petrographically homogeneous.

Group Twelve

Both the specimens are very similar, they are
leucrocratic with abundant K-feldspar and some plagio-
clase feldspar laths, the parallelism of these imparts
a trachytic texture. The clinopyroxene and brown
hornblende are altered although very rare blue-green
pleochroic amphiboles are fresh. The opaque minerals
(probably titanomagnetite) are small and granular;
apatite needles are fairly abundant as inclusions in
the feldspar crystals. Amygdales infilled with calcite
and chlorite testify to the presence of volatiles in the
original magma.

Gabbros

High MgO gabbros

The dominant phase assemblage in most of the gabbros is olivine-clinopyroxene-plagioclase-opaque oxide, however some carry additional hypersthene. The olivine in the former is always altered although one specimen has occasional fresher crystals which exhibit pervasive opaque exsolution along cleavages. The clinopyroxenes are generally sub-ophitic although some specimens exhibit interstitial (77031) and granular (77252) textures, they range from colourless to a very pale brown. The plagioclase varies from tabular plates to rather elongate laths and can show extensive alteration. Some specimens (eg. 77256, 77288) have primary green pleochroic amphibole,which generally mantles earlier pyroxene;the opaque minerals are usually interstitial. Sphene and apatite are minor phases in some specimens (eg. 77031, 77256) and secondary epidote is common.

The hypersthene gabbros generally carry olivine which can be fresh (77104) or altered (77033) but the olivine is absent in 77292. The pale pink pleochroic hypersthene is generally subordinate to clinopyroxene but is abundant in 77290. The hypersthene is occasionally jacketed by the later Ca-rich clinopyroxene in 77033

Low MgO gabbros

The most distinctive petrographic features in
these specimens is the abundance of sphene, epidote and
apatite (eg. 77098, 77267), the presence of analcite
and other zeolites (eg. 77067, 77270) and the presence
of brown and green amphiboles which can show spectacular
zonation from their colourless clinopyroxene cores
through brown amphibole to green amphibole (eg. 77270,
Plate 4.9). The gabbros show varying degrees of
alteration of the colourless or brown tinted clino-
pyroxene which can be locally pervasive. The pyroxene
and opaque oxides are generally interstitial to the
strongly zoned somewhat altered plagioclase. The
opaque oxides can develop a distinctive skeletal habit
(Plate 4.10).

The quartz gabbros are petrographically variable,
but all possess colourless clinopyroxene, granular or
interstitial opaques and interstitial quartz. 77102
is characterised by the presence of pink pleochroic
hypersthene and strongly zoned plagioclase. In contrast
77103 possesses a green pleochroic amphibole which
mantles the earlier pyroxene, this specimen also has
interstitial sphene and epidote. The amphibole in 77274
is brown pleochroic and can be seen both rimming and
replacing the clinopyroxene along cleavages. Both 77103

and 77274 have turbid orthoclase feldspar which is intergrown with the quartz in the former.

The ferrodiorite (77264) is similar to 77274 but is much more leucrocratic, the clinopyroxene is distinctly granular with occasional fresh areas. The plagioclase is zoned to alkali feldspar and interstitial quartz is moderately abundant.

Peridotites

The peridotite plugs are usually composed of a homogeneous, feldspathic peridotite consisting of abundant olivine with subordinate chrome-spinel, plagioclase and clinopyroxene. Primary chestnut brown pleochroic amphibole and brown pleochroic biotite are minor phases in some specimens (eg. 77086, 77183) and a green pleochroic amphibole may also be present (eg.77259). The olivine is typically fresh occurring as rounded to tabular grains (1-4mm diameter) in a matrix of slightly zoned plagioclase and a colourless to pale brown clinopyroxene. The latter is virtually absent from some specimens (eg. 77051, 77290).

The olivine grain morphology is variable, a few specimens possess almost spherical olivine crystals (eg. 77357) whilst others contain lobate skeletal crystals up to 7mm diameter (eg. 77089). Although the peridotite

plugs do not possess chilled margins, specimens from the marginal facies can be finer grained than those from the centre of the plug (see Plate 4.11).

The chrome-spinels vary in size from specimen to specimen ranging 0.02 to 0.5mm diameter, they occur as inclusions in the olivines and as independent phases. The clinopyroxene and plagioclase always occur interstitially, the clinopyroxene generally postdating the latter. The inferred order of crystallisation thus being:

Chrome spinel-olivine-plagioclase-clinopyroxene $\pm$

mica and hornblende

Although the plugs are generally petrographically homogeneous xenoliths of dunite (77285) are abundant in the feldspathic peridotite plug north of Minishal (77284) (see p.115) and a skeletal olivine textured xenolith (77054) has been located in 77055.

Acid dykes

These specimens are petrographically variable and are best described separately. The felsitic glass (77159) contains feldspar, opaque oxides and quartz phenocrysts in decreasing order of abundance. The former have developed fingerprint textures probably attributable to reheating by the adjacent gabbros, which would also account for the blackening of the glass   Specimen 77180

is a quartz sanidine spherulite which was described

by Harker (1908, p.140) although sanidine was not

included in the original account   The quartz phenocrysts

can be deeply embayed although subhedral crystals are

also found   The groundmass is texturally variable with

quartz-feldspar spherulites developed amidst aggregates

of 0.05-0.1mm diameter quartz and feldspar crystals

The pitchstone (77239) was also described by Harker

(op cit. p.177) it carries rare quartz opaque and ortho-

clase phenocrysts in an altered brown glass matrix   The

latter contains abundant slightly flow aligned feldspar

crystallites   The final acid dyke (77241) carries moder-

ately abundant plagioclase phenocrysts which are usually

altered to epidote and clay minerals, the groundmass glass

is devitrified to quartz-feldspar aggregates (cf 77180)

with occasional indications of spherulitic structure.

Xenoliths

Although xenoliths are not abundant in the dolerite

minor intrusions several different types have been

encountered. Small bodies of feldspathic Lewisian gneiss

have been located in the inclined sheets in the Allt Slugan

a Choilich   These have suffered varying ammounts of partial

melting and strong reaction rims can develop around the

fingerprint-textured feldspars   Localised production of

acid magma is indicated by the presence of devitrified acid glass in one of the specimens (30A76). The dolerite immediately adjacent to these xenoliths is always chilled to a tachylite facies   One specimen in the same stream section contains a pure calcic plagioclase xenolith (78A76b) which has developed slight reaction rims to the adjacent unchilled dolerite.

Other dolerites contain gabbroic xenoliths, the majority of these appear to be cognate as they are texturally similar despite their coarser size, an exception being the one-pyroxene gabbro nodule in the differentiated groundmass of 77112. The petrography of the xenoliths in the peridotite plugs has been discussed previously (p 114).
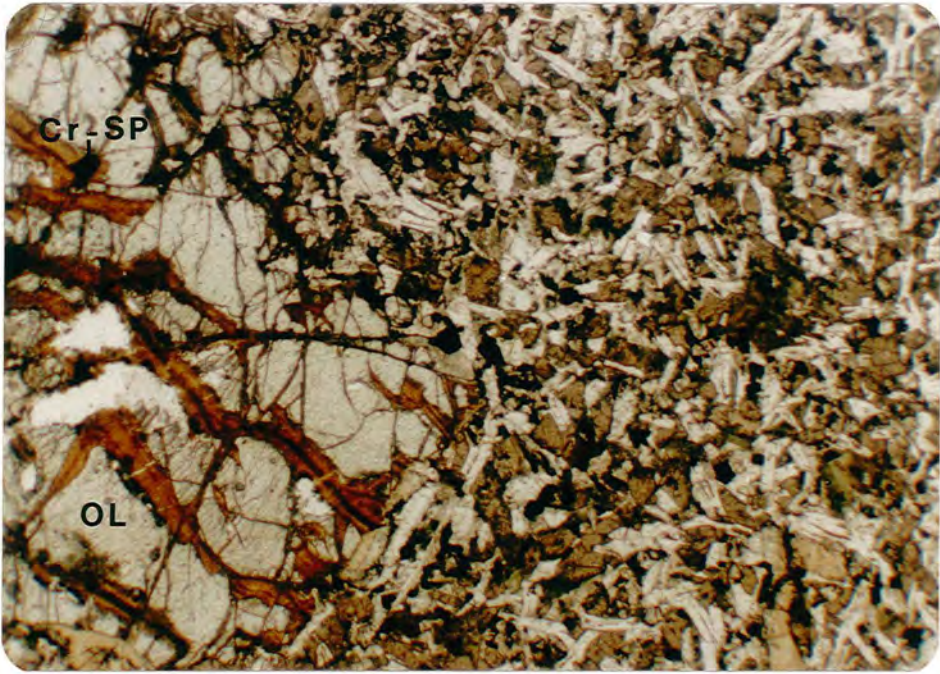
Plate 4.1. 53A76, Olivine phyric group 1 picrite.
Note large granular olivine with included Cr-spinel
and deep brown groundmass clinopyroxene. X20.P.P.

Plate 4.2. 52A76, Group 1. Olivine and Cr-spinel
phenocrysts in a groundmass of variolitic textured
plagioclase and clinopyroxene, note altered ground-
mass olivine. X20. P.P.
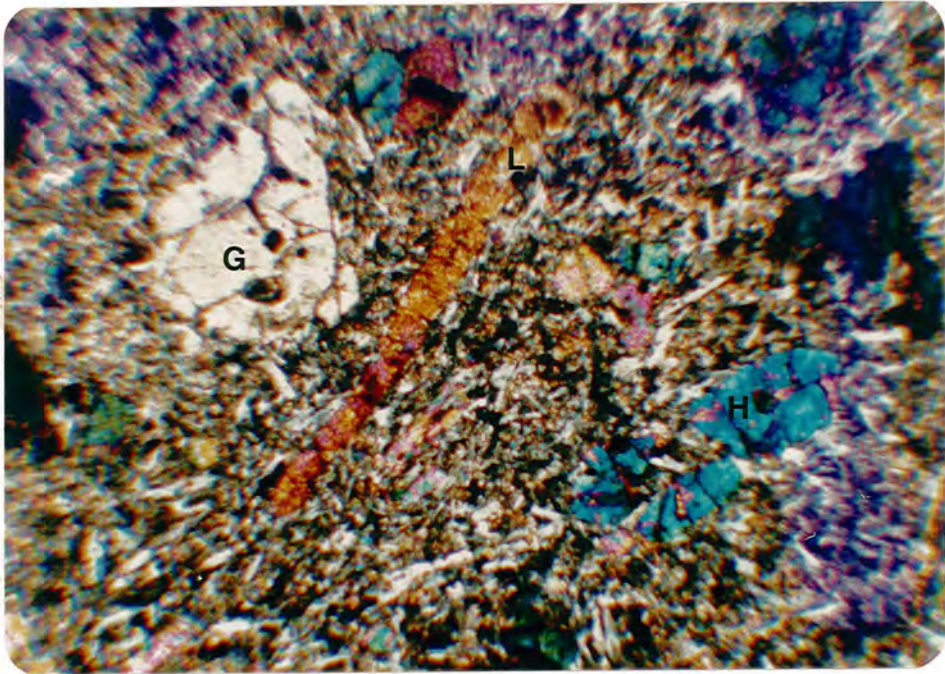
Plate 4.3. 77024, Group 1. Olivine phenocrysts in
a fine grained groundmass of olivine, clinopyroxene
plagioclase and Cr-spinel. G, H and L refer to
granular, hopper and lattice textured olivine crystals
respectively. X50. X.P.
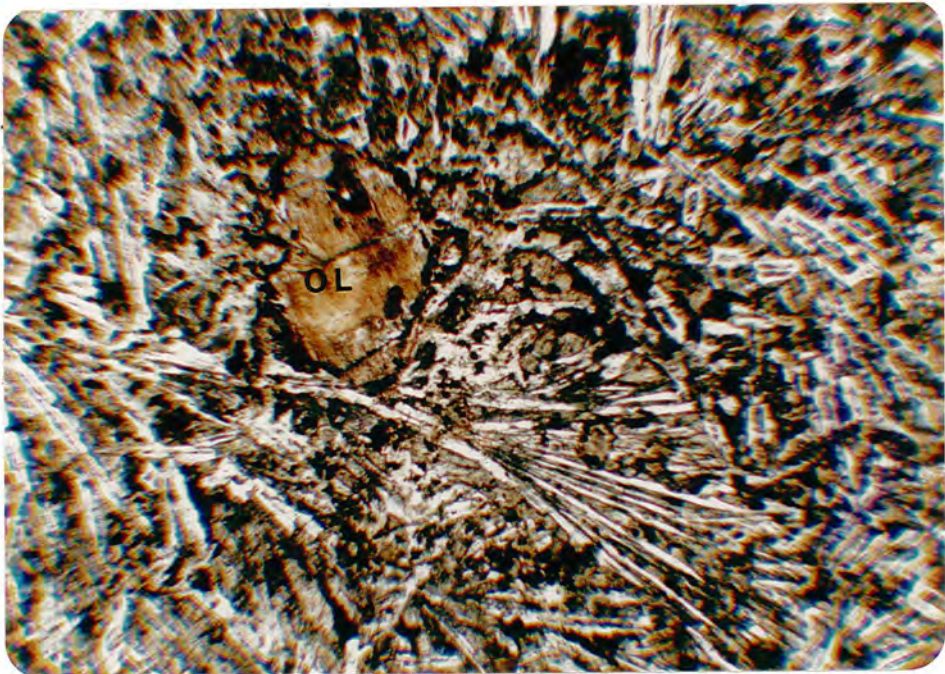
Plate 4.4. 77039, Group 2. Rare altered olivine
microphenocrysts with included Cr-spinel in a
groundmass of variolitic plagioclase (note hollow
cores) with clinopyroxene and opaque oxides.
X45. P.P.
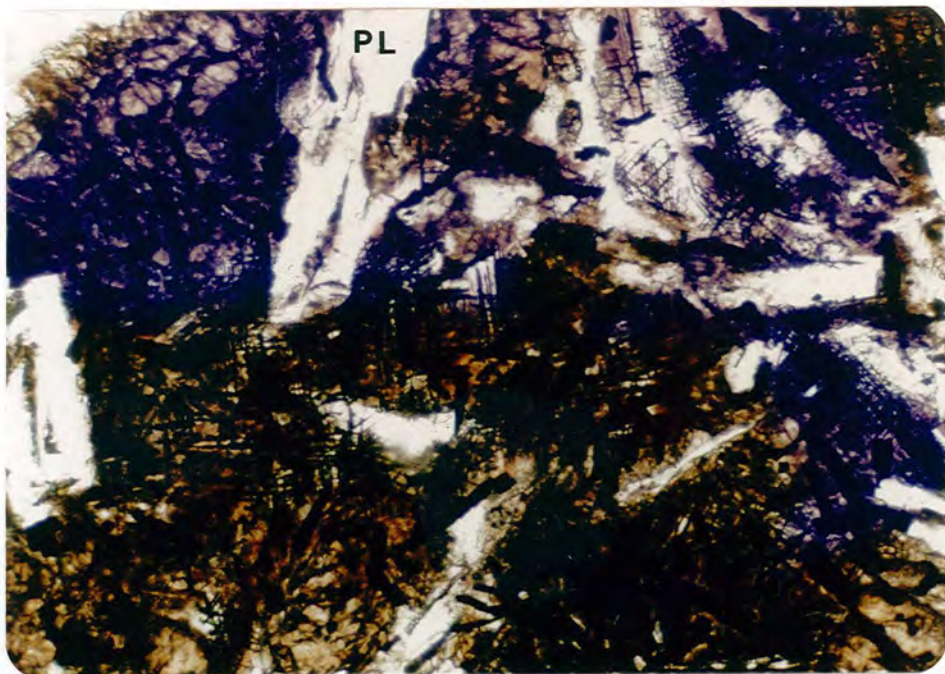
Plate 4.5. 23A76, Group 8. Large opaque rods
(ilmenite?) and fine angular meshes of opaque
in deep brown clinopyroxene and occasionally in
plagioclase. X50. P.P.
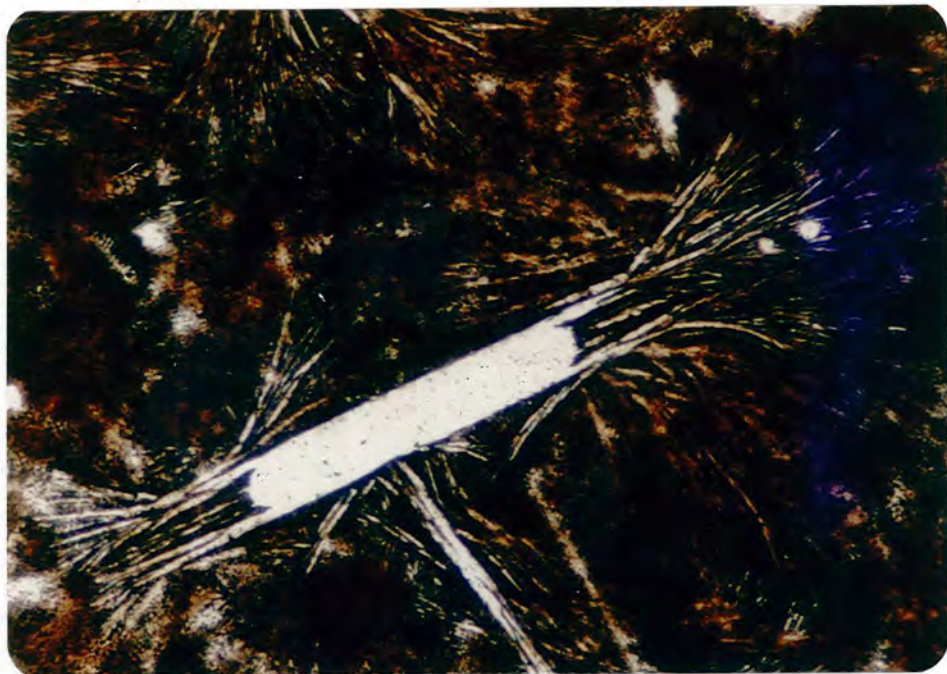
Plate 4.6. 20A76, Group 8. Bow-tie variolitic
plagioclase in altered brown glass matrix. X100.
P.P.
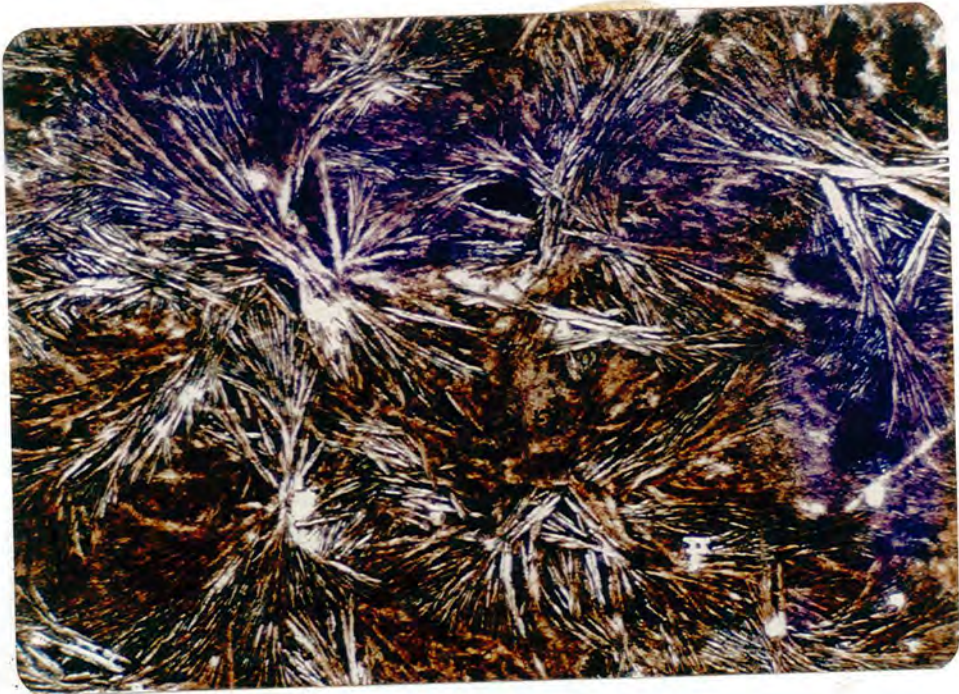
Plate 4.7. 20A76, Group 8. Elongate plagioclase
microlite in dark brown glass, note how groundmass
plagioclase variolites have nucleated on the ends
of the plagioclase microphenocryst. X150. P.P.
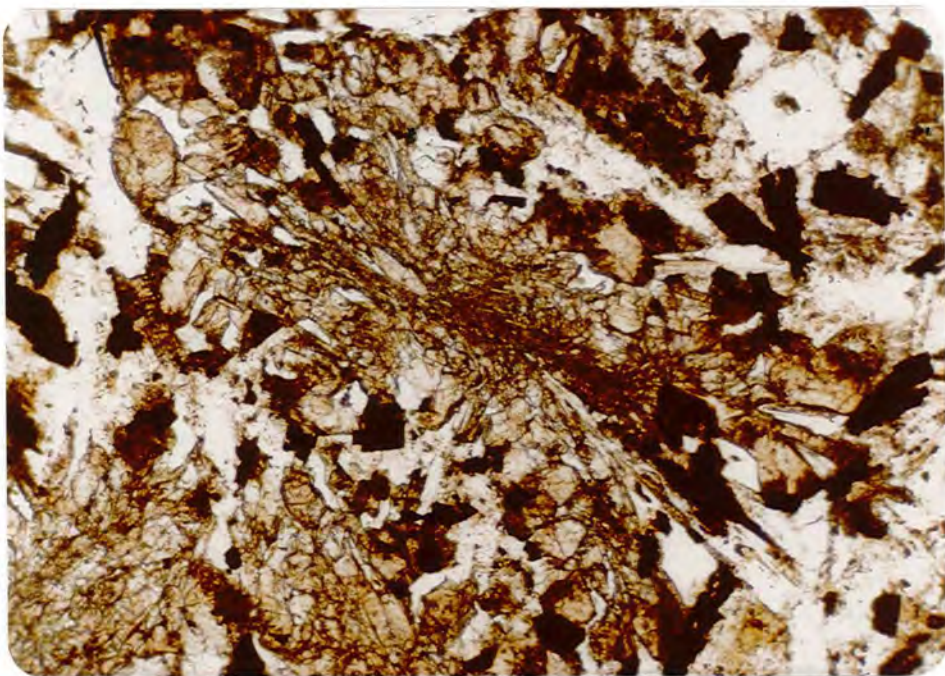
Plate 4.8. 46A76, Group 2. Lobate edged groundmass
clinopyroxene in a plagioclase-opaque oxide matrix.
Note euhedral plagioclase micro-phenocryst in top
right hand corner. This clinopyroxene texture is
more typical of the group 8 rocks but was more easily
photographed in this group 2 specimen. X50. P.P.
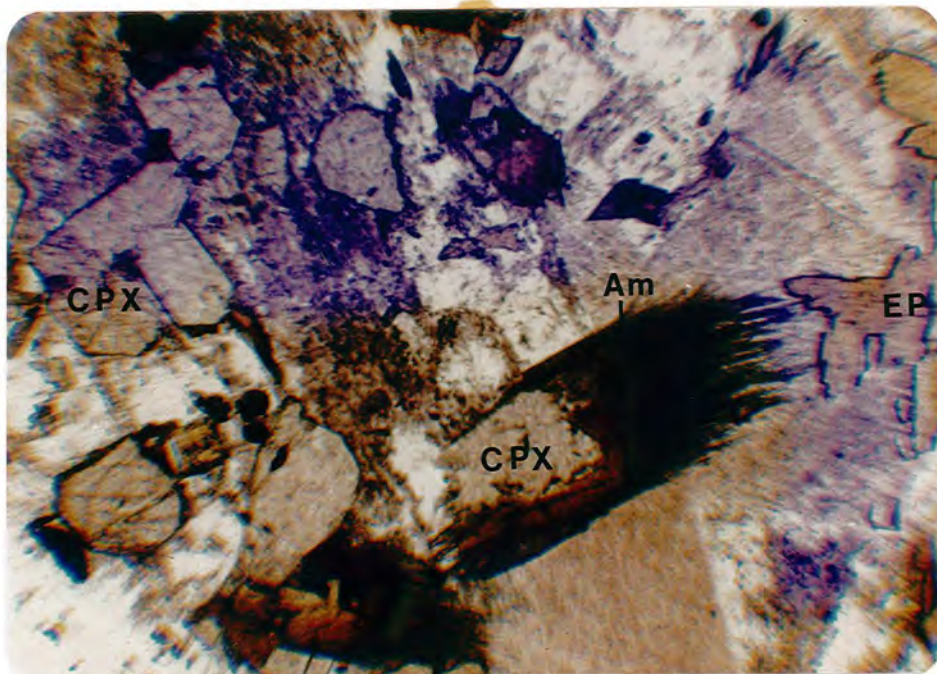
Plate 4.9a. 77250, Gabbro. Granular clinopyroxene
some with brown and green amphibole overgrowths in
a matrix of light brown altered feldspar with
accessory epidote and opaque oxides. X50. P.P.
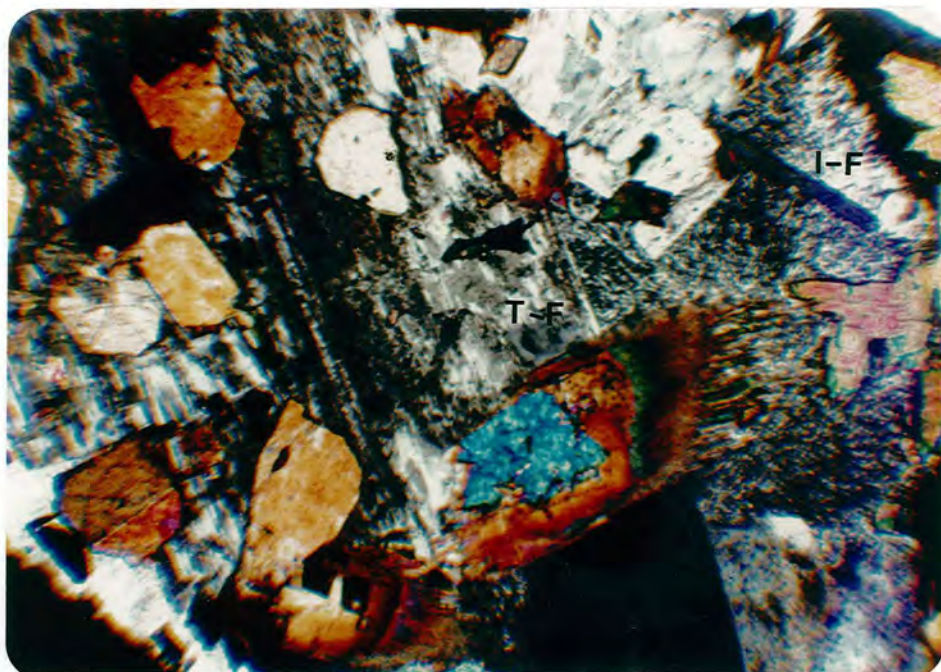
Plate 4.9b. As above. Note the systematic optical
variation in the amphibole jacketing the clino-
pyroxenes. Note also the two generations of (i) large
tabular feldspar (T-F) and (ii) interstitial feldspar
(I-F) brought out by crossed polars. X50. X.P.
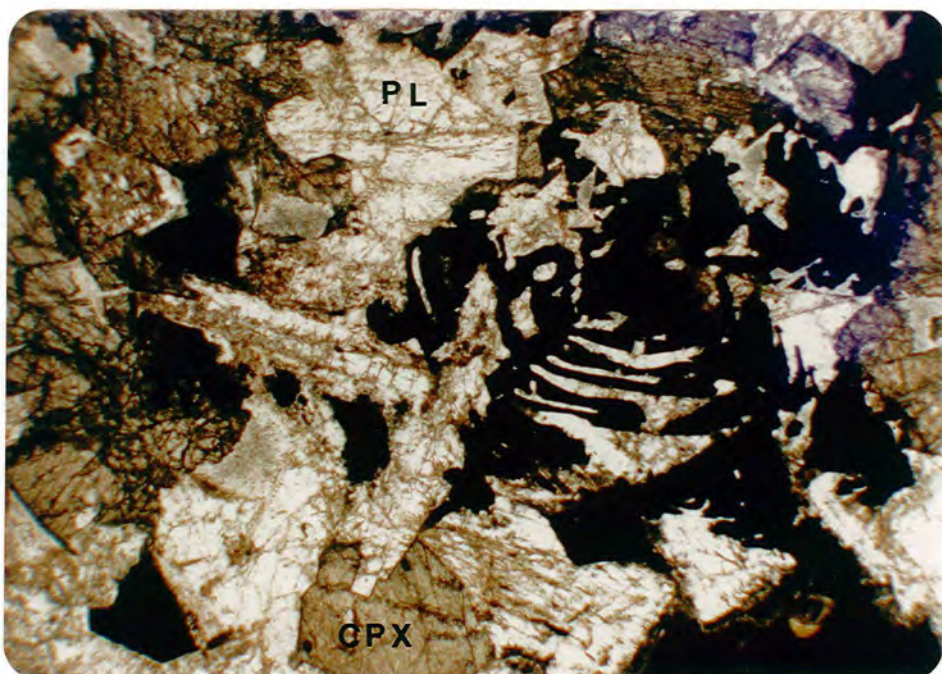
Plate 4.10. 77100, Gabbro. Skeletal textured
opaque oxides in a granular clinopyroxene -
plagioclase matrix. X15. P.P.
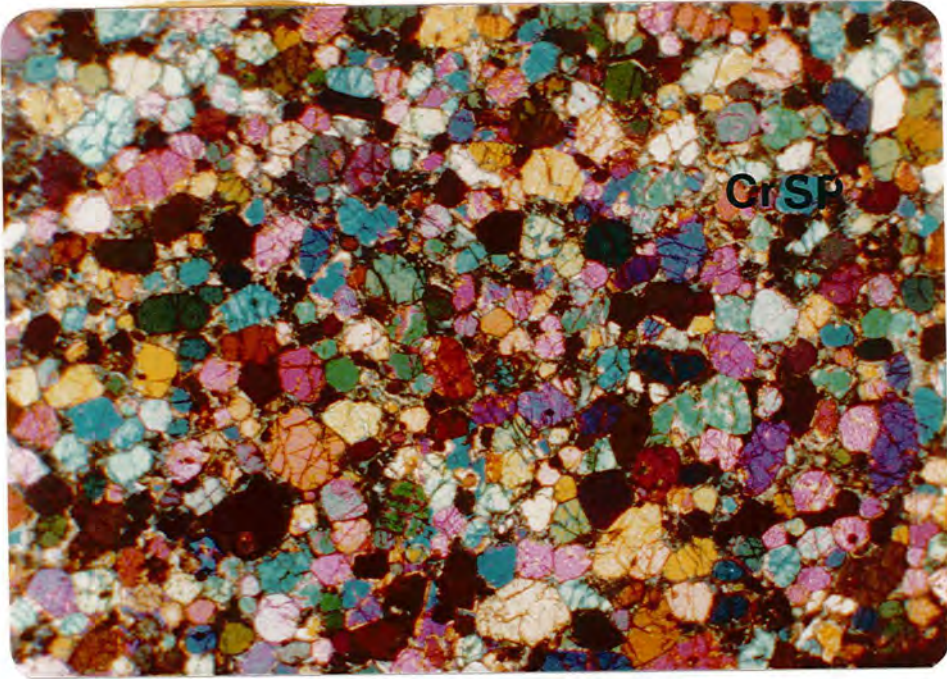
Plate 4.11a. 77357. Peridotite plug chilled margin.
Round granular olivine in extremely sparse plagio-
clase - clinopyroxene matrix. Note the two trans-
luscent red-brown Cr-spinels in the top right hand
corner. X15. X.P.
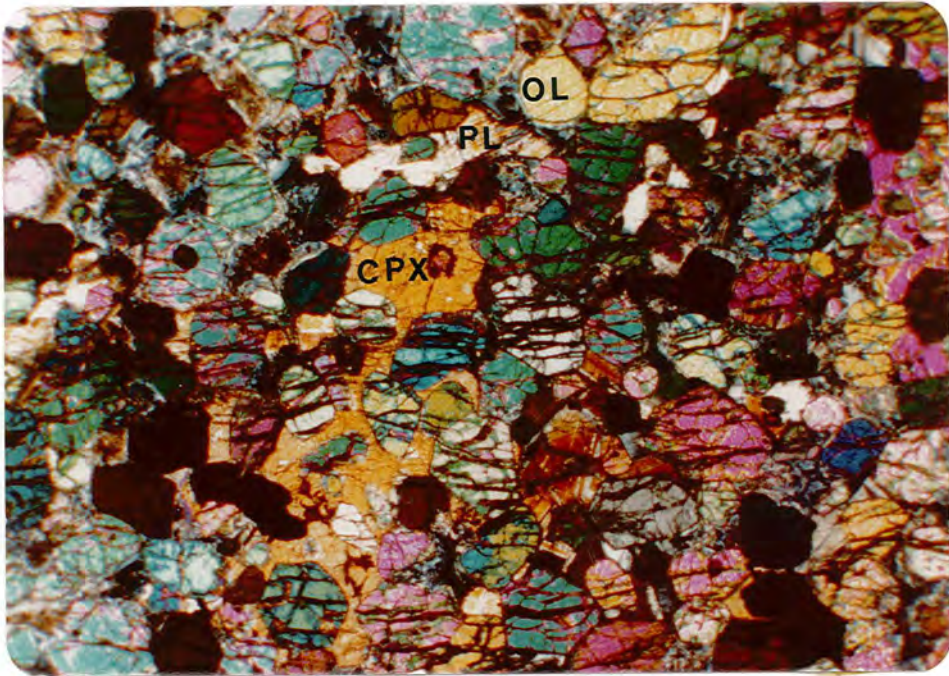
Plate 4.11b. 77358. Peridotite plug core, granular
olivine and Cr-spinel (transluscent to opaque) in
poiki litic clinopyroxene and plagioclase matrix.
Contrast grainsize and other textural variation
with 4.11a. X15. X.P.

Phenocryst Assemblage	GP 1	GP 2	GP 3	GP 4	GP 5	GP 6	GP 7	GP 8	GP 9	GP 10	GP 11	GP 12
A		7	8	31		1		13	3	2	1	2
$Ol\pm Op$	28	8	1	1		1						
Pl		3	2	12		3	5	8				
$Pl-Ol\pm Op$		2	3	12	6					4		
$Pl-Cpx\pm Op$			3	4				16	2		1	
Pl-Op				5								
$Pl-Ol-Cpx\pm Op$				2				7	3		3	

Table 4.1. Phenocrystic assemblages in the Rhum dolerite groups, the figure refers to the number of specimens with that phenocryst assemblage. NB.many of the specimens have less than 5% total phenocryst abundance, it is only the presence of phases which is recorded here.

A = Aphyric   Ol = Olivine   Op = Opaque   Pl = Plagioclase
Cpx = Clinopyroxene

CHAPTER FIVE

THE MAGMATIC SEQUENCE ON RHUM

Introduction

Analysis of the cross-cutting relationships within
and between the dolerite groups allows a more detailed
description of the sequence of minor intrusions on Rhum
than that presented in Chapter 2 (Table 2.1).The gabbroic
plugs and some gabbros associated with the layered peri-
dotites are also considered and a magmatic sequence which
also includes the lavas of western Rhum is presented
(Fig. 5.2).

a) Dolerites

The proportion of the dolerite groups 1-12 encountered
in each of the major dolerite intervals that were defined
in Chapter 2 is presented in Fig. 5.1. The relationships
illustrated here are discussed along with other relevant
observations in the text. As stated in Chapter 3 (p. 82)
the collection is considered sufficiently representative
of the proportions of the dolerite types on Rhum to allow
qualitative discussion of their distribution.

The most comprehensive information on cross-cutting
relationships comes from the felsite slabs in Stony
Corrie, Dibidil (Fig. 2.6) but conclusions based on this
are limited because the dolerite groups 1, 2, 9 and 11

are poorly represented and no group 3 or 10 dykes were found.

(i) Group 1 (28 specimens)

Group 1 magmas are represented in the stratigraphic intervals B-D (Fig. 5.1) but are not found cutting the lavas. They are particularly abundant in the Torridonian outside the Main Ring Fault (which may reflect a sample bias from the picritic dykes in the Allt Slugan a Choilich) but more significantly, are the most abundant dolerite type found cutting the peridotites and gabbros. A cross cutting relationship has been located between two group 1 specimens (77235 and 77236) which indicates that at least two ages of picrites are present within the peridotites. They are known to cut several group 8 dykes and a single group 9 dyke but are themselves cut by the Kilmory thick conformable sheets (group 8) and possibly by a single group 3 dyke SE of Papadil. Although the picrites are abundant in the peridotites the former are also cut by the peridotites on Minishal (Chapter 2, p. 36). To summarise, the picritic dykes appear to have been intruded fairly late in the magmatic sequence on Rhum but do span a considerable time interval.

(ii) Group 2 (20 specimens)

As with group 1, these dykes are represented in the stratigraphic intervals B-D in Fig. 5.1 and thus probably

span a considerable time interval. The cross-cutting relationship between 77212 and 77214 on Dibidil shore (NM 395927) confirms there are at least two group 2 intrusive events. They are cut by group 4b[*] dykes and cut an early gabbro (77033 NM385986) and a group 8 dyke in Stony Corrie Dibidil. Their age relative to other dolerite groups is not known. The specimens from Dibidil shore are not crushed or sheared suggesting they postdate the Main Ring Fault but one specimen (46A76) appears to be truncated by the Main Ring Fault immediately south of the dam on the Allt Slugan a Choilich (NM393983). On balance they are possibly fairly young in age but not as young as the picrites.

(iii) Group 3 (17 specimens)

Only one group 3 dolerite is found in the peridotite stratigraphic interval (Fig. 5.1) and this specimen comes from the gabbro marginal to peridotite at Papadil, which is believed to be older than the peridotites (Chapter 1, p. 8). Since the group 3 dolerites have not been found cutting the layered peridotite sequence, it seems likely that they pre-date the emplacement of the peridotites. They are known to be cut by group 4 dykes and one intrusion cuts the big feldspar dyke (group 7) on Meal Breac (NM 384981) whilst another probably cuts a picrite dyke (group 1) near Papadil. The majority of the

*Group 4b refers to the high iron group 4 variants (Chapter 3, p.69)

specimens from outside the Main Ring Fault are from the inclined sheets in the Allt Slugan a Choilich which are believed to be fairly early in the minor intrusion sequence on Rhum. As with the preceding groups, they probably span a considerable interval but in view of their lack within the peridotites may be earlier than the group 1 and 2 magmas.

(iv) Group 4 (64 specimens)

This group is the most abundant dolerite group on Rhum and many cross-cutting relationships both between intrusions from this group and with intrusions from other groups have been observed. They are the dominant dolerite type in both the Torridonian outside the Main Ring Fault and in the sequence Lewisian to Granophyre within the Main Ring Fault but are relatively scarce amongst dolerites cutting the peridotites (Fig. 5.1, B-D). They show complex within-group crosscutting relationships in Stony Corrie, Dibidil where at least three separate injections of group 4 magmas have occurred and many other within-group crosscutting relationships have been encountered elsewhere on the island (e.g. Harris Bay, Dibidil Shore).

Members of this group cut a group 2 and a group 3 dyke but the reverse relationship has not been encountered, and a group 4 thin conformable sheet is cut by a peridotite plug (NG 349014). Several group 8 dykes are cut by group 4

dykes, but the latter are cut by the Papadil thick conformable sheets (group 8) and other group 8 dykes. A group 4 thin conformable sheet is cut by a group 7 dyke west of Sgoarishal (NG 348017) and a group 4 dyke on Dibidil shore is cut by a group 9 dyke (NM 395927).

The high total iron (group 4b) dykes are cut by other group 4 dykes in Stony Corrie but cut another group 4 dyke on Minishal. Three group 4b dykes are cut by group 2, 8 and 9 dykes respectively whilst another dyke which must be young in age cuts the peridotite plug west of Loch Beauty (NG 358012). Thus the group 4b dykes span a considerable time interval and are included amongst the youngest known group 4 dykes.

The average analyses of ten group 4 dykes inferred to be young in the sequence and of eight group 4 dykes cut by younger group 4 dykes is presented in Table 5.1. Although the two average analyses are broadly similar with respect to the major oxides, consideration of the trace element data suggests that the younger dykes are slightly more differentiated, as the younger dykes are depleted in Ni and Cr and are enriched in Zr, Y and Rb, relative to the average values of the older dykes.

(v) Group 5 (6 specimens)

It is clear from Fig. 5.1 that group 5 dykes are best represented in the lavas but they are also present in

the granophyres and in the Torridonian outside the Main

Ring Fault. Of the 2 specimens not cutting the lavas, the

dyke from the granophyre cuts a group 4 and a group 8 dyke

and the dyke from the Torridonian cuts a peridotite plug,

confirming the very young age implied by their presence

in the lavas.

(vi) Group 6 (5 specimens)

These dykes are only found cutting the lavas (Fig. 5.1)

and along with group 5 are the youngest known Tertiary rocks

on Rhum. As with group 5 no within-group crosscutting

relationships have been observed and they may represent

a relatively short but discrete chronological interval.

(vii) Group 7 (5 specimens)

The age relationships of the group 7 dykes were

discussed in Chapter 2. They are not found in the

peridotites (Fig. 5.1) and are known to be truncated at

the contacts between peridotite and older rocks (Chapter 2,

p. 37). Only limited cross cutting relationships with

other dolerite groups are known. They cut a group 4 dyke

and a Papadil thick conformable sheet (group 8) and are

themselves cut by a group 3 dyke. Their petrographic

uniformity suggests that they represent a fairly discrete

chronological interval postdating the Main Ring Fault

(Chapter 2, p. 37) and thick conformable sheets but pre-

dating the emplacement of the layered peridotites.

(viii) Group 8 (45 specimens)

The group 8 specimens have the greatest known time span of any of the dolerite groups on Rhum. A group 8 episode of intrusion produced the dolerites with liquid-liquid contacts with felsite in Stony Corrie (Chapter 2, p. 34) the oldest known dykes on Rhum and they are also encountered cutting the layered peridotites (Fig. 5.1). Several of the thin conformable sheets and the inclined sheets belong to group 8 as do the relatively young Kilmory and Papadil thick conformable sheets. The former have distinctive geochemical and petrographic character-istics and similar dolerites are not encountered within the Main Ring Fault. However, the Papadil thick conform-able sheet dolerites may have geochemically similar but petrographically disimilar analogs within the Main Ring Fault.

The general early age of the group 8 dolerites in Stony Corrie is confirmed by the consistent cross cutting by later group 4 dykes, a relationship also observed elsewhere on Rhum, e.g. between 77316 and 95A76 (group 4) in the Allt Slugan a Choilich (NM 395988) and between 77325 and 77324 (group 4) in the granophyre west of Harris Bay (NM 355955). They are also known to be cut by picritic dykes in the Allt Slugan a Choilich (NM 394987) and in Corrie Dubh (NM 394981). As previously mentioned the

Papadil thick conformable sheets cut group 4 dykes (77174

and 77175) but are themselves cut by a group 7 dyke.

Thus the group 8 magmas were available from very

early in the history of the complex and were still

available after the emplacement of the layered peridotites,

furthermore they are found in all the different structural

types of dolerite encountered in the field viz. thick

and thin conformable sheets inclined sheets and as dykes.

(ix) Group 9 (8 specimens)

The group 9 dykes appear to be absent from the

peridotites (Fig. 5.1) but are found cutting older rocks

on both sides of the Main Ring Fault. Their age relation-

ships with other groups are uncertain as few cross-cutting

relationships were recorded. One specimen (77209) from

Dibidil shore cuts older group 4 dykes but other specimens

are cut by group 4 dykes. Another specimen is probably

cut by a group 1 dyke in the Allt Slugan a Choilich and

the age relations of the dykes in Stony Corrie are unknown.

In view of their absence from the peridotites the group 9

dykes may predate the emplacement of the peridotites but

their age relationships are obscure.

(x) Group 10 (6 specimens)

In contrast, the group 10 dykes are found cutting

the peridotites and associated gabbros. The two specimens

are from the Papadil Gabbro and are hornfelsed and thus

are probably pre-peridotite sensu stricto but one specimen
definitely cuts fresh marginal gabbro on Monadh Mhiltich
(NM 997357). One specimen cuts a dyke which probably
belongs to group 4 (from petrography) but their age
relationships to other dolerite groups are not known.

(xi) Group 11 (5 specimens)

All but one of these dykes are found cutting the
peridotites, the other which cuts the sequence Lewisian
to granophyre cuts a group 8 dyke. No group 11 specimens
have been located in the Torridonian outside the Main Ring
Fault. As the majority of these group 11 dykes are post
peridotite the group as a whole is judged to be young in
age.

(xii) Group 12 (2 specimens)

Both these intrusions are petrographically fresh;
one cuts the eastern Papadil gabbro - Torridonian contact
(NM 365917) it is believed to be younger than the peri-
dotites in this area because it is not affected by the
thermal metamorphism which affects the other older dolerites
(eg. group 3 and group 10). Their age relations relative
to other dolerite groups are not known.

b) Gabbros

Three of the gabbros under consideration are known
to be early in the history of the complex. Two of these

intrusions are high MgO gabbros (Chapter 3, p. 72) but one is a quartz gabbro. The latter is similar but more differentiated than the group 8 intrusions known to be early from their field relationships in Stony Corrie (Dibidil) (see Table 5.1). The analyses of the high MgO gabbros is also presented in Table 5.1 showing that CaO and MgO rich magmas were also available at an early stage in the evolution of the Rhum central complex.

The precise stage that the younger gabbros were emplaced relative to the dolerite groups cannot be determined from the evidence available at the present time. A late age was inferred from the field relationships discussed in Chapter 2 but there are exceptions (e.g. the altered gabbro plug at NM 378999, which is cut by three later dykes). Thus the late gabbros were probably emplaced over a considerable period of time.

c) Peridotites

Although a relatively young age was inferred for those peridotite plugs which resemble the matrix-banded tongues in the Northern Margin Complex (see Chapter 2, p. 48), the age of petrographically dissimilar plugs (e.g. the deeply weathered peridotite plug on the northside of Kinloch Glen) have not been unequivocally determined. In view of their probable petrogenetic link with the layered peri-

dotites (discussed later, p. 260) the proposed age of these plugs relative to the dolerite magmas of Rhum becomes increasingly important. The evidence presented in Chapter 2, with the qualifications outlined above, all point to a relatively young age for the majority of the peridotite plugs. A chronological sequence of the dolerite groups, the gabbro and peridotite plugs and the acid dykes on Rhum based on the relative age relationships as discussed in this chapter and in Chapter 2, is presented in Fig. 5.2. The acid rocks, peridotites and lavas act as stratigraphic markers and form the basis of the stratigraphy of the magmas which produced the Rhum minor intrusion suite.

The large estimated time gap between the lavas and the layered peridotites is based on the existence of rocks from the Rhum central complex in the conglomerates beneath the Rhum lavas. The estimated time gap between the layered peridotites and the acid rocks is based on the need for multiple dyke injection postdating the acid rocks and predating the peridotites. Although the peridotite tongues are believed to predate the layered peridotites (Dunham,1965b) they are cut by very few dykes hence the small interval between the two on Fig. 5.3. The age gap between the early folding (Dunham & Emeleus, 1967, p.395) and the emplacement of the acid rocks cannot be estimated and may be considerably less than the interval indicated

here.

Two important points are raised by Fig. 5.2; one is the suggestion that the group 5 and 6 magmas postdate the evolution of the remainder of the Rhum dolerites, the significance of this is discussed later (Chapter 7 , p.225); secondly, the alkaline differentiates (groups 10 to 12) appear to have been intruded later than the majority of the dolerite magmas.

To test whether the basic magmas in the Rhum dolerites become more alkaline with time the dolerite groups 2, 3 and 4 were plotted on Fig. 5.3 using the division into dykes cutting (1) the Torridonian outside the Main Ring Fault, and (2) the sequence Lewisian to granophyre and (3) the layered peridotites. The discriminant score derived in Chapter 3 was used as a measure of alkalinity. The dolerites both sides of the Main Ring Fault in Fig. 5.3 span a similar range although the dykes cutting the peridotites do tend to be more alkaline. The distribution of the individual dolerite groups is shown in Fig. 5.4. Here,within each group, the dykes cutting the Torridonian outside the Main Ring Fault and the sequence Lewisian to granophyre within the Main Ring Fault cover similar ranges but the dykes cutting the peridotites tend to be trans- itionally alkalic.

Although the alkalic nature of dykes cutting the

peridotites in Figures 5.3 and 5.4 suggests that the
younger Rhum dolerites do become more alkaline with time, this
assertion must be tempered by the knowledge that:

(1) Group 8 dolerites of tholeiitic affinity cut the
    peridotites,

(2) Gabbros with tholeiitic affinities cut the layered
    peridotites (specimens 33A76, 77163, 77328, 77383)
    thus basic tholeiitic magmas were also available
    sometime after the emplacement of the peridotites.

(3) The abundant group 4 dolerites show no trend towards
    alkalinity from known cross-cutting relationships.
    (This can be shown by plotting the individual dis-
    criminant scores (an indicator of alkalinity) of the
    group 4 dolerites that were used in the compilation
    of the average analyses of the "young" and "old"
    dolerites in Table 5.1). Reference to Fig. 5.5
    shows that the early and late dolerites span a similar
    range of transitional alkaline and transitional
    tholeiitic compositions. The sample sizes are,
    unfortunately, too small to interpret the relative
    distribution of the peaks.

In conclusion differentiates of tholeiitic affinity
were available throughout the history of the complex
whereas alkalic differentiates are only present in the
later stages. The specimens from the dolerite dykes

cutting the peridotites are consistently alkalic in affinity thus there appears to be a trend towards alkalinity with time in the Rhum minor intrusions. The significance of the tholeiitic groups 5 and 6 dykes cutting the lavas is discussed in Chapter 7 (p. 225).

The similarity in the span of transitional compositions in groups 2, 3 and 4 (Fig. 5.4) in dykes cutting the Torridonian outside the Main Ring Fault and the sequence Lewisian-granophyre within the fault suggests that magmas of essentially similar chemistry were available both sides of the Main Ring Fault although for much of this time the dykes in the Torridonian at the present erosion level will have been emplaced at structurally higher levels than their counterparts across the Main Ring Fault. The predominance of thoroughly transitional magmas (O to -0.35 discriminant score) in the group 4 rocks within the Main Ring Fault (Fig. 5.5) may possibly reflect their deeper seated nature (ie. proximity to parental magma truly transitional in composition) than the group 4 magmas emplaced at higher levels outside the Main Ring Fault.

Fig. 5.1 Frequency distribution of the dolerite
groups between the major country rock
stratigraphic intervals defined in
Chapter 2.

A = Dykes cutting the Rhum Lavas

B = Dykes cutting the Torridonian
outside the Main Ring Fault

C = Dykes cutting the layered
peridotites and marginal gabbros

D = Dykes cutting the sequence
Lewisian to Granophyre within
the Main Ring Fault

Dolerite Group
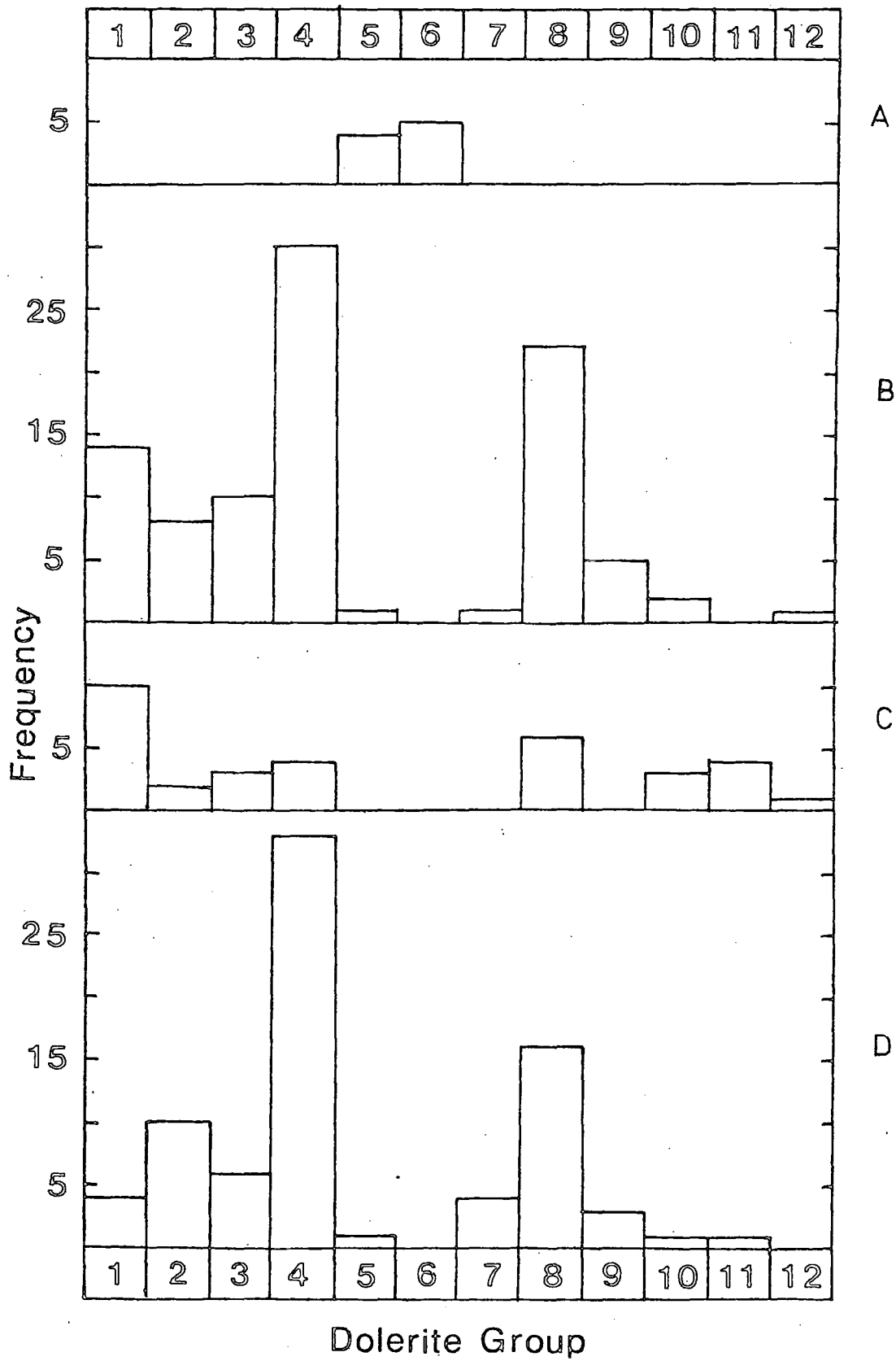
Fig. 5.2 Schematic age relationships of the Rhum
minor intrusion suite with respect to
the major country rock stratigraphic
intervals. Dotted lines indicate areas
of uncertainty.

Key to stratigraphic intervals.

L   =   The Rhum Lavas
LU =   The layered ultrabasic rocks
PT =   The peridotite tongues
AC =   The plutonic acid rocks
EF =   The early folding

Key to minor intrusion suite

1-12 = Rhum dolerite groups
EG =   Early gabbros
LG =   Late gabbros
A   =   Acid dykes
P   =   Peridotite tongues
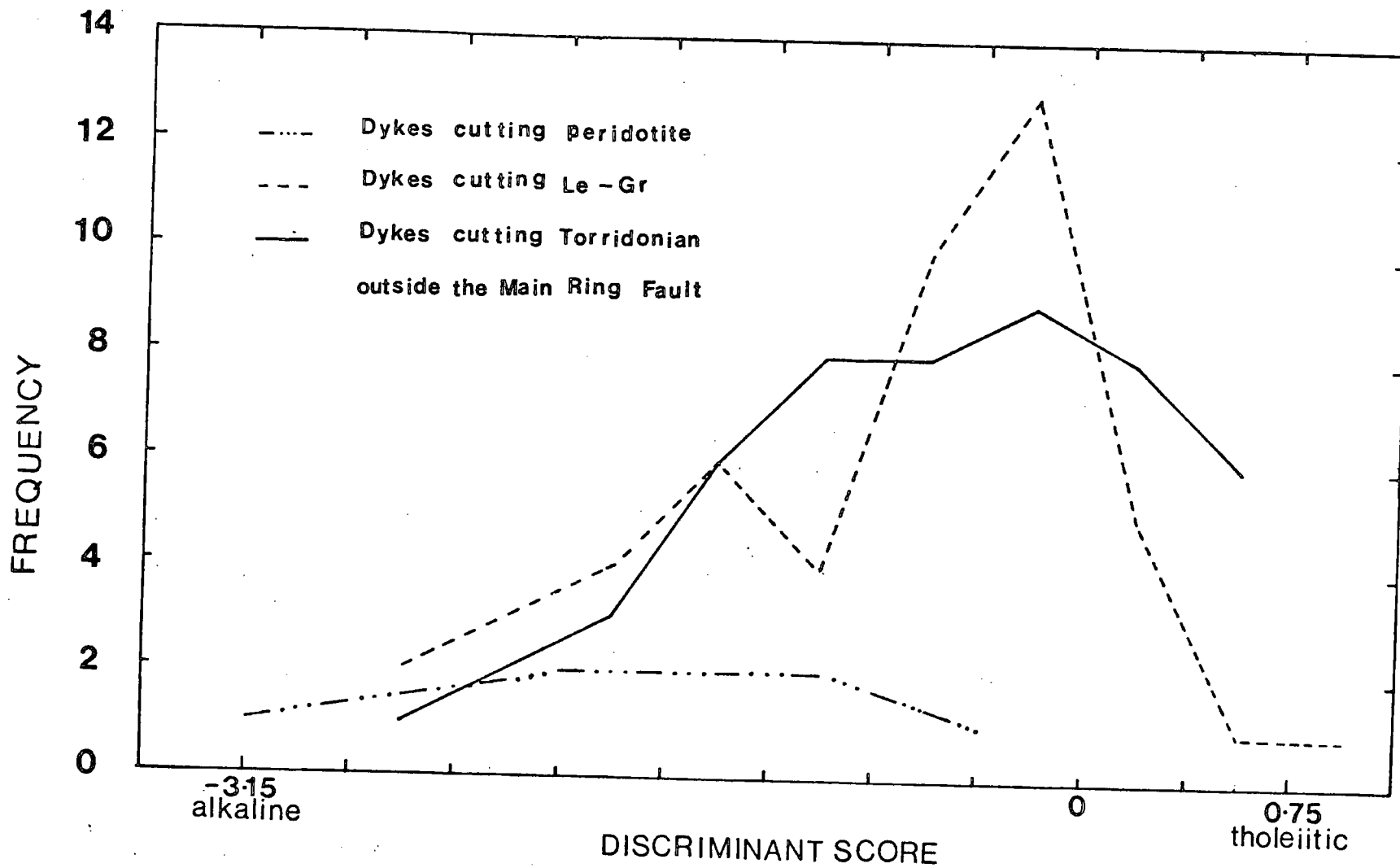
Fig. 5.3 Discriminant score of dykes cutting the three
principal country rock stratigraphic intervals.
(Le-Gr = dykes cutting the sequence Lewisian
gneiss to granophyre).
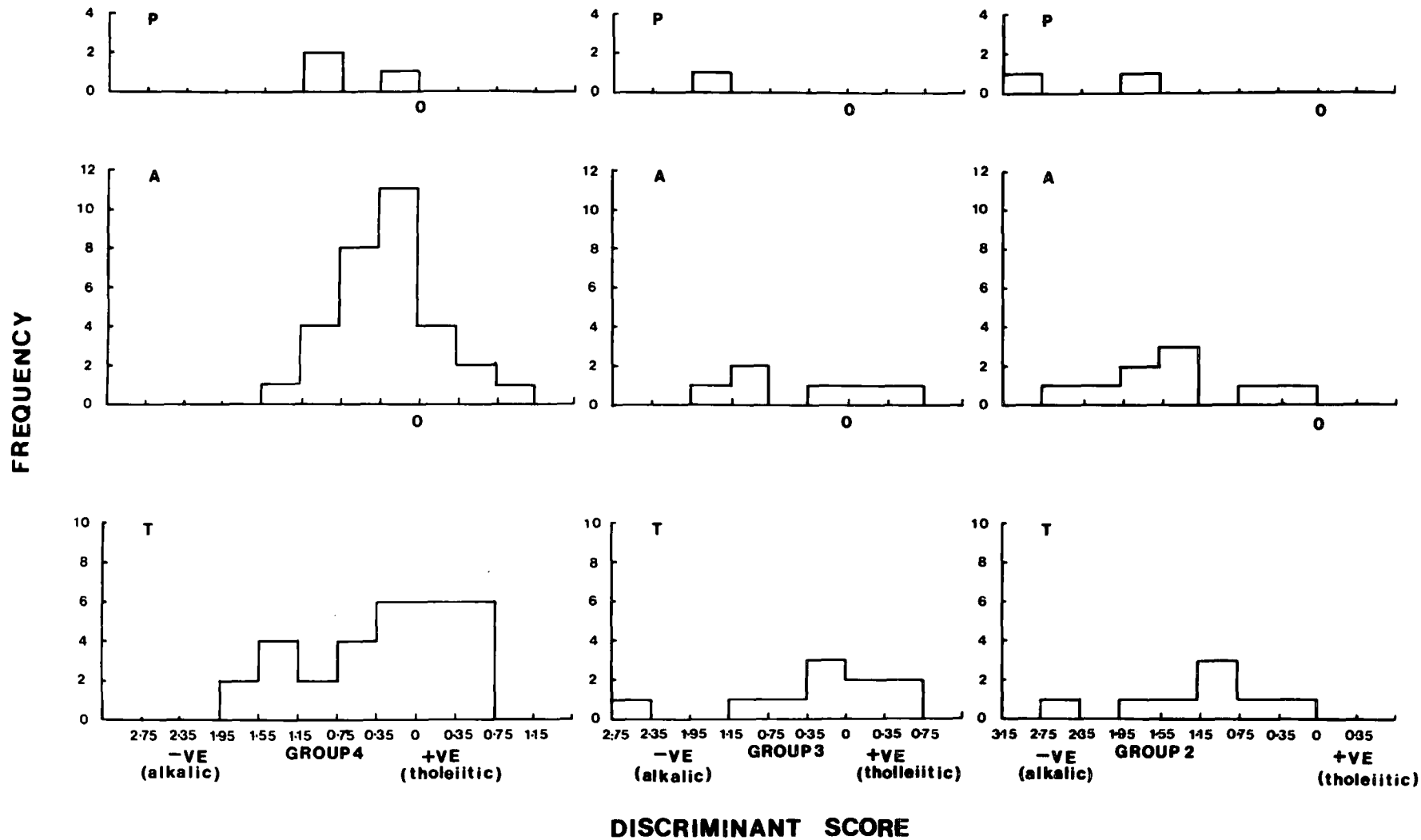
FIG 5.4 Discriminant score of dykes cutting the Torridonian strata outside the Main Ring Fault and the acid and the layered ultrabasic rocks within this fault,(T,A and P respectively).
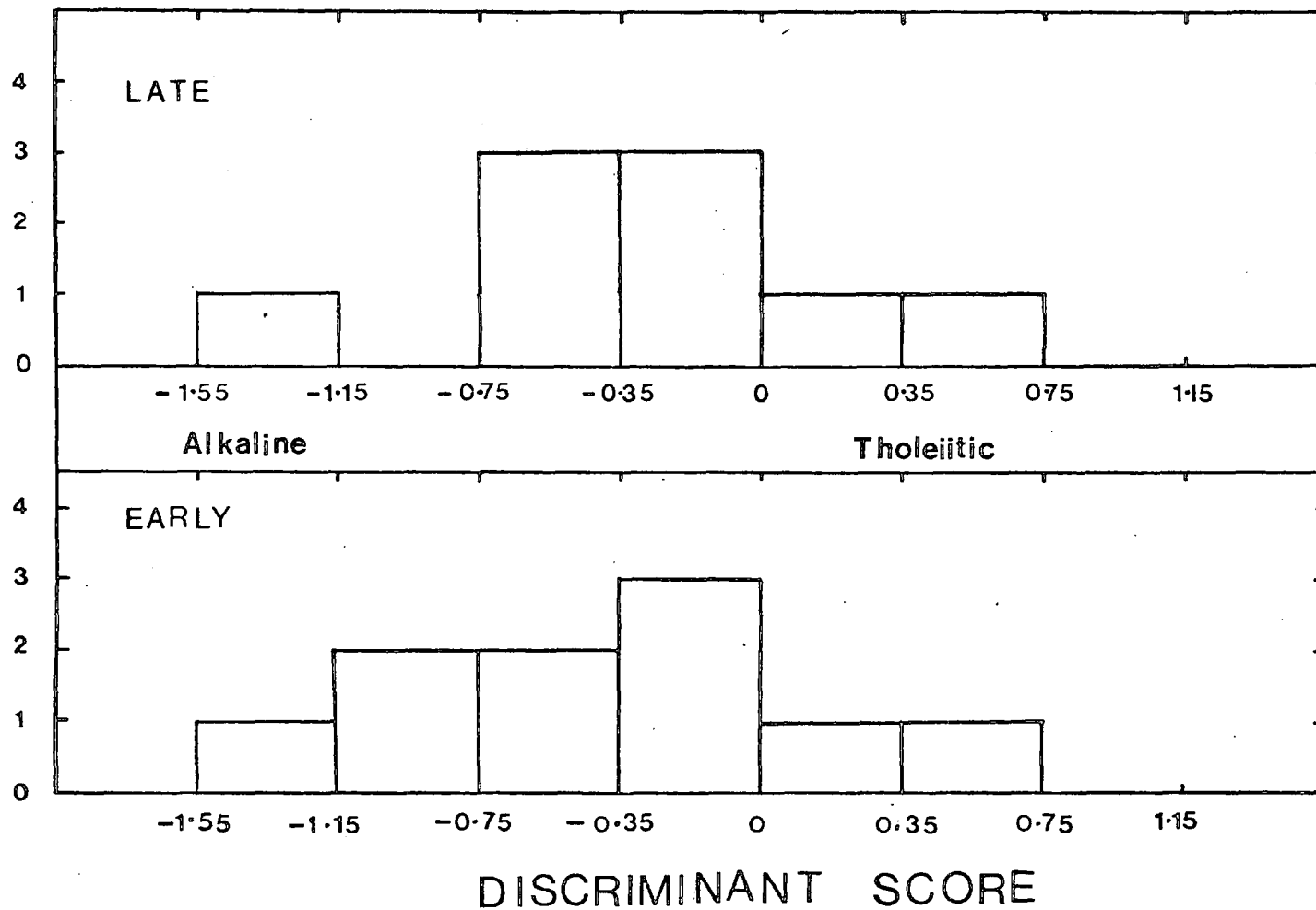
FIG 5.5   Discriminant score of group 4 dykes judged to be early and late in the sequence of intrusion.

	A	B	C	D	E	F
SPEC	–	–	77033	77292	77103	–
SiO_2	47.23	47.35	49.24	48.98	51.42	49.91
Al_2O_3	14.50	14.10	14.39	15.74	13.84	13.11
Fe_2O_3*	12.50	13.37	10.02	11.47	13.02	15.08
MgO	8.98	9.20	11.22	9.74	5.72	6.17
CaO	11.83	10.81	12.14	9.99	9.03	8.98
Na_2O	2.78	2.43	2.02	2.49	3.38	3.25
K_2O	0.21	0.56	0.10	0.16	1.01	0.67
TiO_2	1.65	1.76	0.62	1.17	2.17	2.26
MnO	0.19	0.19	0.16	0.17	0.21	0.22
P_2O_5	0.18	0.19	0.10	0.09	0.20	0.24
Total	100.05	99.86	100.01	100.00	100.00	99.89
Ni	119	94	95	41	32	29
Cr	337	233	337	158	25	88
Ba	103	145	72	117	272	277
Nb	4	4	2	2	6	4
Zr	109	129	16	33	182	163
Y	20	28	9	10	33	31
Sr	169	290	277	323	190	248
Rb	13	19	2	3	25	31
Zn	106	104	64	76	107	137

wt % applies to the upper block; ppm applies to the lower block (Ni through Zn).

Table 5.1   Geochemical comparison of different
aged dolerites and gabbros.

A   Average of 10 older group 4 dolerites

B   Average of 9 younger group 4 dolerites

C, D, E   Early gabbros within the Main Ring Fault.

F   Average of 4 early group 8 dolerites

*Total iron as Fe_2O_3

CHAPTER   SIX

MINERALOGY AND MINERAL CHEMISTRY

Introduction

The mineral chemistry obtained by electron micro-
probe analysis is presented in this chapter, and the
various interpretations which can be put upon this data
are discussed. The analytical technique is described in
Appendix 6.1 and the complete mineral analyses are
presented in Appendix 6.2. Iron was determined as FeO
and is presented as such in the pyroxene, plagioclase,
olivine and amphibole analyses. The Fe_2O_3 contents of
the spinels and ilmenites were calculated by assuming
stoichiometry of these phases as described by Carmichael
(1967).

The compositional variation in the pyroxenes and
spinels is considered to be the product of complex inter-
actions between various petrogenetic processes and con-
sequently requires detailed discussion. The amphibole
(kaersutite) analyses from the type 3 picrites are
presented in Appendix 6.2 but are not considered
further.

PYROXENES

Introduction

The pyroxene lattice can incorporate virtually all the major and minor components of an igneous melt under suitable circumstances. This flexibility, coupled with their common occurrence in igneous rocks offers valuable insight into magmatic processes. Pyroxene chemistry is fundamentally controlled by the host magma chemistry, however, the ultimate composition is affected by several other factors (e.g. the temperature, pressure and rate of crystallisation) and these factors must be taken into account in any interpretation concerning the host magma composition.

a) Dolerites

The individual analyses of pyroxenes in the Rhum dolerite suite have been plotted in the conventional pyroxene quadrilateral (Fig. 6.1), the relevant portions of the tholeiitic Skaergaard trend (Brown, 1957) and the mildly alkaline Shiant Isles pyroxene trend (Gibb, 1973) are included for comparison. The pyroxene from groups 1, 2, 3, 7 and 10 are calcic augites or salites in the classification of Deer et al. (1966), the group 4 pyroxenes are calcic augites and the group 8, 9 and 11 pyroxenes are augites. The group 1, 2 and 4 pyroxenes exhibit a slight decrease in Ca with iron enrichment however this feature is not apparent in the

more limited data for the remaining groups. The pyroxene

suite as a whole is characterised by very limited iron

enrichment, indeed the principal variation within the

pyroxenes in Fig. 6.1 is in the Ca content. This

contrasts markedly with the predominance of Mg^{2+} - Fe^{2+}

variation over Ca^{2+} variation in most pyroxene suites,

see for example Gibb (1973 ,Fig.4). Note, however,

that the zoning from core to margins detected in some

pyroxene grains involves iron enrichment with little

variation in the Ca content.

The variation of Al, Ti, Cr, Na and Mn with iron

enrichment is presented in Figs. 6.2 and 6.3. Al and

Ti generally increase with iron enrichment, especially

in the group 1 pyroxenes. This is also a feature of the

Na variation. In contrast, Cr exhibits a negative

correlation with iron enrichment. The data for Mn is

more ambiguous, the pyroxenes from the basic dolerites

(groups 1 to 7) show no correlation of Mn with Fe content

and the higher Mn content of some of the pyroxenes from

the intermediate rocks exist over a range of Fe contents.

This variation in Mn is possibly attributable to the

presence or absence of coexisting opaque oxides during

pyroxene crystallisation.

The variation of Al against Ti for the groundmass

pyroxenes and the phenocryst pyroxenes is shown in Figs.

6.4 and 6.5 respectively. A general increase of Ti with

Al is a feature of both diagrams. Ti generally sub-
stitutes in a ratio of approximately 1:5 for the
majority of pyroxenes but several of the group 10
pyroxenes in Fig. 6.4 and the group 11 pyroxenes in
Fig. 6.5 are Ti enriched for a given Al content when
compared with the remainder of the pyroxenes in the
suite. The variation of Al and Na with Si content for
the groundmass pyroxenes is shown in Figs. 6.6 and 6.7
respectively. Fig. 6.6 shows that Al is present in
excess of the amount required to satisfy the silica
deficiency in the tetrahedral (z) site thus some of
the Al must be located in the octahedral (y) site.
In addition Fig. 6.7 shows that Na increases with
decreasing Si, which implies there is a positive
correlation between Na and Al.

The relative proportions of Al in tetrahedral and
octahedral co-ordination in both the groundmass and the
phenocryst pyroxenes are presented in Figs. 6.8 and 6.9
respectively. The assignment of Al to Al^{iv} and Al^{vi} was
made on the basis of 6 oxygens by allotting sufficient Al
to make up the Si deficiency (Al^{iv}) to 2 and allotting
the remaining Al to Al^{vi}. Unfortunately this procedure
relies on the accurate determination of Si and some of
the scatter on Figs. 6.8 and 6.9 is undoubtedly due to
some inaccuracy in the Si determinations. However, this

is judged not to have affected the overall relationships
in these diagrams. It is clear from Figs. 6.8 and 6.9
that although much of the Al is in tetrahedral co-ordination
a considerable amount is in octahedral co-ordination; the
significance of this relationship is discussed below.

Discussion

The principal features of the clinopyroxenes in
the Rhum dolerite suite are the limited iron enrichment
developed in these pyroxenes and, secondly, the high Ca,
Al and Ti contents of many of the pyroxenes. The
variation in pyroxene chemistry is due to simple or
coupled substitution of elements into the pyroxene lattice.
These coupled substitutions are necessary to preserve
the charge balance if for example Al^{3+} substitutes for
Si^{2+} in the tetrahedral site.

Limited substitution of Fe^{2+} for Mg^{2+} in the y site
is partly attributable to cooling rate in that the rapidly
chilled lava suites of tholeiitic and alkalic basalt
associations generally exhibit much more limited $Fe^{2+} - Mg^{2+}$
substitution in their pyroxenes, than the pyroxenes in
slowly cooled tholeiitic and alkalic intrusions (Carmichael
et al., 1973). The high MgO content of many of the Rhum
dolerites and the high MgO levels in the intermediate
rocks when compared with intermediate rocks from other
basaltic suites is probably another contributing factor

(ie. the activity of Mg was high in the Rhum melts). It should be noted however that pyroxene analyses are not available from the few dolerites with Fe_2O_3* greater than 15.0 wt%, these would probably extend the known range of Fe^{2+} - Mg^{2+} substitution in the Rhum pyroxenes.

The Al_2O_3 content of the Rhum pyroxenes ranges from 1.5 to 9.0 wt% and is highest in the group 1 pyroxenes (Fig. 6.2). The Al content of pyroxenes is believed to be a function of Si activity and Al activity in the melt, temperature and pressure (Le Bas 1962, Brown 1967, Campbell and Borley 1974, Deer et al. 1979).

The negative correlation of Si and Al and the positive correlation of Al and Ti can be explained by the substitution of Al into the pyroxene lattice via the Ca Ti Al_2O_6 molecule (Yagi and Onuma, 1967), however this would result in a Ti/Al ratio of 1:2 whereas the Rhum pyroxenes have a Ti/Al ratio of approximately 1: 5, This suggests that there was also extensive substitution of Ca-Tschermaks molecule Ca Al_2 SiO_6. The distribution of Al into Al^{iv} and Al^{vi} sites is known to be in part pressure related, higher pressures favouring entry into the Al^{vi} site (Aoki and Shiba 1973). Although many of the groundmass pyroxenes fall in the field of igneous rocks in Fig. 6.8, many fall into the field of higher pressure pyroxenes, but since these groundmass pyroxenes crystallised at low

*Total iron as Fe_2O_3

pressures entry of Al as Al^{vi} is not solely a function of pressure. Several of the pyroxene phenocrysts in Fig. 6.9 also fall in the fields of high pressure pyroxenes and thus may possibly be the results of higher pressure crystallisation. These phenocrysts contain less Al than the groundmass pyroxenes and this is consistent with the low Al contents of pyroxenes believed to be high pressure relicts in the Dippin Sill, southern Arran (Gibb and Henderson, 1978).

In a low pressure environment, the activity of the various melt components is believed to control pyroxene chemistry. Carmichael et al., 1970 showed that low Si activity in the melt will favour formation of aluminous clinopyroxene rather than plagioclase by the equation:

$$\frac{aCaAl_2Si_2O_8}{aCaAl_2SiO_6 \cdot aSiO_2} = K$$
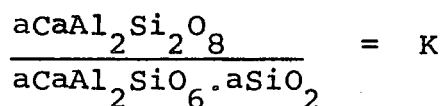
thus explaining the observations of Le Bas (1962) who found an increase in the Al contents of pyroxenes with increasing SiO_2 undersaturation of the host magmas. This reaction explains the special case in which Al^{3+} is distributed equally between the y and z sites. However, Campbell and Borley (1974) suggest that the general equation takes the form

$$\tfrac{1}{2}Y_2O_3 + \tfrac{1}{2}Al_2O_3 + Mg_2SiO_6 = (MY)AlSiO_6 + SiO_2 + MO$$

or

$$ZO_2 + Al_2O_3 + 2Mg_2Si_2O_6 = (M_3Z)Al_2Si_2O_{12} + 2SiO_2 + MO$$
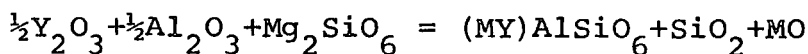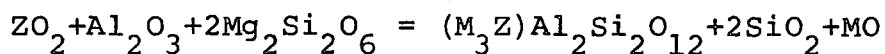
where $Y = Al^{3+}$, Cr^{3+} or Fe^{3+}, $Z = Ti^{4+}$, and $M = Fe^{2+}$, Ca^{2+} or Mg^{2+}.

These reactions show that an increase in aAl_2O_3 and a decrease in $aSiO_2$ in the melt will favour formation of aluminous clinopyroxene and that the Al^{3+} content of the pyroxene is also dependent on the behaviour of the octahedrally co-ordinated cations providing the charge balance. The correlation of Na with Al in Fig. 6.7 suggests that some of the Al in the Rhum clinopyroxenes may have been incorporated as jadeite, however some of the Fe probably existed as Fe^{3+} thus the Na may well be present as acmite.

Le Bas (1962) showed there was a positive correlation of the Ti and Al content of pyroxenes and suggested that the Ti content was a function of the presence of Al^{3+} in the z site. This view was supported by Barberi et al. (1971) who suggested that the low activity of SiO_2 in the melt was the dominant control over the Ti content of a pyroxene. This argument was based on the knowledge that entry of Al^{3+} into the z site favours Ti^{4+} entry into the Y site (Verhoogen 1962) and that substitution of Ca-Tschermaks molecule (ie. Al^{3+} into the z site) is favoured

by low $aSiO_2$. Conversely Gibb (1973) cast Ti in the dominant role and suggested that the Al^{3+} is incorporated into the pyroxene lattice to balance the high Ti^{4+} content of the pyroxene induced by the high $aTiO_2$ in the melt. These authors have also emphasised the role of co-crystallising phases on pyroxene chemistry. Barberi et al. (1971) suggested that crystallisation of plagioclase prior to pyroxene would deplete the Ca-Tschermaks molecule content of the melt and thus would reduce the Al_2O_3 content of the pyroxenes. Gibb (1973) argues that the onset of titanomagnetite crystallisation in the Shiant Isles sill reduced the activity of Ti in the melt thus giving rise to lower Ti and Al levels in the contemporaneous pyroxenes. It should be stressed at this point that Gibbs'(1973) study of pyroxene compositional variation within a closed system environment is ideally suited to the investigation of the effect of co-crystallising phases on pyroxene composition which is not always possible in studies of pyroxene chemistry in suites (like the Rhum minor intrusions) which are derived from different parent compositions at different stages of differentiation.

Rapid cooling rates are also known to facilitate the incorporation of Al and Ti into the pyroxene lattice. High Al and Ti levels have been reported in studies of lunar pyroxenes (up to 9.4 wt% and 8.5 wt% respectively,

Brown et al. 1973). These compositions were attributed to metastable incorporation of the $CaTiAl_2O_6$ molecule during the quench crystallisation of some mare basalts by Brown et al. (op.cit.).

The aluminous group 1 pyroxenes may well be a product of metastable incorporation of Al and Ti as these picrites will have possessed high liquidus temperatures and several have a variolitic groundmass. Variolitic supercooling textures are also a feature of many of the other dolerite groups (see Chapter 4). Thus incorporation of Al and Ti during rapid crystallisation may well have played a part in controlling the groundmass pyroxene chemistry in many of the Rhum dolerites.

The activity of Si and Al are not believed to have played a major role in the genesis of the Rhum dolerite pyroxenes as envisaged by Le Bas (1962) and Barberi et al. (1971) respectively, as early formation of plagioclase did not adversely affect the entry of Al into the clinopyroxene. Aluminous pyroxenes occur in rocks where plagioclase was obviously the earlier phase, e.g. the plagioclase phenocrysts in the group 7 dolerites and the sparse plagioclase microphenocrysts in some of the group 1 dolerites. Chrome-spinel is the dominant opaque phase in groups 1 and 10 thus the activity of Ti is likely to have been higher in these magmas than in those where

titanomagnetite is an important phase. Thus the effect
of Ti activity in the magma on pyroxene chemistry as
envisaged by Gibb (1973) may well have played a role in
determining the compositions of the group 1 and 10 pyroxenes
and other pyroxenes in the suite. In conclusion the high
activity of Mg and to a lesser extent Ti, in the melt
coupled with rapid cooling are believed to be the main
controls over the limited iron enrichment and the
aluminous nature of the Rhum groundmass pyroxenes.
Whilst the pyroxene phenocrysts do plot in the higher
pressure field of Aoki and Shiba (1973), their low Al
and Ti contents suggest that the entry of Al into the
octahedral site is more likely to be a function of the
combined activities of Si, Ti and Al rather than pressure.

Pyroxenes as indicators of host magma composition

There have been several attempts to relate the
chemical compositions of igneous clinopyroxenes to host
magma composition. Le Bas (1962) showed there was an
increase in the proportions of Ti and Al in pyroxenes
from tholeiitic, alkaline and peralkaline hosts respectively
and Coombs (1963) suggested that CIPW norms obtained from
clinopyroxene analyses could be used in much the same way
as whole rock norms to investigate the parent magma type.
More recently, Nisbett and Pearce (1977) utilised
Discriminant Function Analysis to investigate clinopyroxene

composition as a function of their host basalts tectonic setting and concluded that pyroxene chemistry could be used as indicators of tectonic environment.

In contrast the Ti and Al contents of clinopyroxenes have been shown to be unreliable indicators of host magma composition. Gibb (1973), for example, states that the aluminous clinopyroxenes from the mildly alkaline Shiant Islands sill fall in the peralkaline field in the SiO_2-Al_2O_3 diagram of Le Bas (1962) as do many of the Rhum pyroxenes; similarly, Beddoe-Stephens (1977) has shown this diagram to have limited application in calc-alkaline suites. In addition Barberi et al. (1971) have shown that pyroxene with compositions typical of tholeiitic suites can develop from mildly alkaline parents fractionating under low and falling oxygen fugacity. The analysed groundmass pyroxenes in the Rhum dolerites have been plotted on Fig. 6.10, the discriminant scores were calculated using the eigenvectors in Nisbett and Pearce (1977, Table 2) and the discriminant boundaries are redrawn from Nisbett and Pearce (op. cit., Fig.1). The Rhum dolerites are known to be transitional between truly alkaline and truly tholeiitic compositions, the dolerites lie in a "within plate" environment and consequently would be expected to straddle the Within Plate Tholeiite (WPT) and Within Plate Alkaline (WPA) discriminant line. Less than half of the

pyroxenes in Fig. 6.10 lie in the WPA field, most of

the remainder plot in the Volcanic Arc Basalt (VAB) and

Ocean Floor Basalt (OFB) field and only two lie in the

WPT field.   This discrepancy is probably due to the low

Fe and Mn content of the Rhum pyroxenes, as VAB pyroxenes

generally contain less of these constituents than WPT

pyroxenes (Nisbett and Pearce, 1977).

Whilst the host magma composition must exert a

fundamental control over pyroxene chemistry the other

controls discussed earlier in this chapter can cause the

pyroxene composition to deviate significantly from the

expected composition.   Consequently it is suggested that

interpretation of host magma composition and tectonic

environment on pyroxene composition alone as argued by

Nisbett and Pearce (1977) should be approached cautiously.

b) Gabbros and Peridotites

The limited pyroxene data for (i) a high MgO gabbro

(77292), (ii) a low MgO gabbro (77067) and (iii) one of

the peridotite plugs (77.268) is presented in Fig. 6.11.

The pyroxenes from the peridotite plug and the low MgO

gabbro classify as diopsides and salites respectively

in the classification of Deer et al. (1966).   Two types

of pyroxene are found in the high MgO gabbro, monoclinic

augites and enstatitic orthopyroxenes, these high MgO

gabbros are the only rocks in the Rhum minor intrusion suite to possess a 2-pyroxene mineral assemblage. This reflects both their hosts' tholeiitic composition and a slow cooling rate as rapid cooling can produce metastable subcalcic augite in tholeiitic lavas (Kuno 1955 in Deer et al. 1979).

The calcic augites plot in a similar position to some of the group 7 pyroxenes in Fig. 6.1 but are characterised by lower Al_2O_3 and TiO_2 contents (approximately 3.0 and 0.7 wt% as opposed to 1.5 and 5.5 wt% respectively). As with other pyroxenes in the Rhum dolerite suite they are characterised by a low iron content.

The diopsides from the peridotite plug are composition-ally dissimilar to other pyroxenes in the Rhum dolerite suite but compare favourably with pyroxenes from the Rhum layered series. Inspection of the pyroxene analyses in Table 6.1 reveals that the pyroxenes from the peridotite plugs are virtually identical to the two average analyses quoted by Dunham and Wadsworth (1978), except that CaO is slightly higher and Cr_2O_3 significantly lower in the latter.

OPAQUE OXIDES

The opaque oxides in the Rhum minor intrusion suite exhibit a wide chemical variation ranging from Cr-spinels

("chromites") to Fe-Ti spinels ("magnetites") and ilmenites.
Two broad categories can be recognised: Cr-bearing spinels
where Cr is present above trace amounts and Fe-Ti oxides
with only minor Cr content. The majority of the analyses
are from fresh minerals and give totals between approx-
imately 98.5% and 100.5%, the Cr bearing spinels in the
group 2 and 10 rocks are altered and consequently give
lower totals, However, they help illustrate important
relationships and have been included on Fig. 6.12.

Chrome bearing spinels

Cr-rich spinels are abundant in the group 1 rocks
and the peridotite plugs, the majority contain $Al > Cr$
and are Fe-rich and thus classify as picotite (Deer et al.,1966)
(some however, do contain $Fe < Mg$) whilst others contain $Al >$
Cr and classify as magnesio-chromite (Deer et al., op.cit.).
The remaining Cr-spinels, including those from 77024, contain
less Cr + Al than the former and show substantial subs-
titution of Fe^{3+} into the octahedral site.

The variation of the trivalent cations Al^{3+}, Cr^{3+}
and Fe^{3+} is presented in Fig. 6.12. The Cr-spinels from
the type 1 picrites (Chapter 4, p.94) contain more Cr
than the type 2 picrites but less Cr than the spinels
from the peridotite plug, the latter contain slightly
more Fe^{3+} than the former but the Fe^{3+} contents of all
these spinels is consistently low. In contrast, the Cr-

spinels from the group 10 specimen (77184) and the group 1 specimen (77024) contain appreciable Fe^{3+}, there is a consistent decrease in Al^{3+} with increasing Fe^{3+} in all these specimens. The altered spinels in the group 10 rock (32A76) have Fe^{3+} as the dominant trivalent ion, the group 2 spinel phenocrysts (from 77039) are more variable. One contains minor Fe^{3+} and lies in the field of the picrite type 1 and type 2 spinels. The other contains abundant Fe^{3+} and resembles the fresher Fe-Ti groundmass opaque oxides in this and other group 2 specimens.

The chemical variation in Cr-spinels in basaltic liquids can result from primary variation in the composition of liquidus phase and from secondary processes involving either later reaction with the host liquid or subsolidus reaction with adjacent phases or both (Henderson and Suddaby 1971, Henderson 1975, Ridley et al. 1974, Ridley 1977, Dunham and Wadsworth 1978). These secondary processes can make it virtually impossible to elucidate primary variation in spinels unless the phase is included in a co-crystallising or slightly later crystallising phase which effectively prevents reaction between the spinel phase and the melt. However, even when a spinel is included in a silicate phase subsolidus reaction with the enclosing phase may alter the primary spinel composition.

Several of the spinels in the type 1 and type 2

picrites, and all the spinels from the peridotite plug,

were totally enclosed by olivine, The limited chemical

variation within these spinel types strongly suggests

that their compositions are essentially primary, the

spinels from the type 1 picrites containing more Cr^{3+}

than those in the type 2 picrites. The spinels from

85A76 are similar however, to those from the remaining doleri-

tes, these were not protected by an enclosing silicate

phase and thus may have reacted with the melt.

The extreme compositional variation exhibited by the

spinel phenocrysts in 77039 almost certainly is the result

of a two stage process.

Primary variation

The controls over primary compositional variation

in Cr-spinels have been discussed by Hill and Roeder

(1974) and Ridley (1977). Variations in the activities

of the various Cr-spinel components in the melt give

rise to the variations in liquidus spinel compositions,

the availability and activity of Cr in the melt is of

critical importance. Cr^{3+} has a low solubility in

basaltic liquids ($\sim$250 ppm at a $\log_{10} fO_2$ of -8, Hill

and Roeder 1974) and a high octahedral site preference energy.

(Burns 1970, In: Hill and Roeder 1974) consequently

Cr^{3+} will readily enter a spinel phase and thus promotes

spinel crystallisation. Variations in the initial Cr

contents of basaltic melts (which reflects the temperature

and pressure conditions in the zone of partial melting and

the mineralogy of the source material) will affect the

Cr/Al ratio of the liquidus spinels. The activity of Al

in the melt must also play a role, however Ridley (1977)

has noted that the high Al_2O_3 magmas do not necessarily

contain spinels with a high Al/Cr ratio suggesting the

activity of Al may not be of critical importance in

determining the Cr/Al ratio of the liquidus spinel.

The oxygen fugacity of the melt will determine the

Fe^{3+} content of the spinels. Hill and Roeder (1974) show

that high oxygen fugacities favour incorporation of Fe^{3+}

into spinels mainly at the expense of Cr^{3+}, thus spinels

with high Fe^{3+}/Cr^{3+} ratios probably crystallised under

moderate to high ($\log_{10} fO_2 \ 10^{-5}$ to $\log_{10} fO_2 \ 10^{-1}$)

oxygen fugacities. This effect is mainly due to the

abundance of Fe^{3+} ions in melts with high oxygen fugacities.

These ions coalesce to produce much greater quantities of

the spinel phase than is produced at lower oxygen

fugacities. Consequently this causes the Cr content of

the magma to be dispersed amongst a large volume of spinel

crystals with a consequent reduction in Cr content of the

individual crystals. In addition, Hill and Roeder (op. cit.

Fig. 7) have shown that substition of Fe^{3+} and Ti^{4+} with

a concomittant decrease in Al and Cr occurs with
decreasing temperature. The entry of Mg^{2+} and Fe^{2+} into
the tetrahedral site is also largely temperature dependent
(Hill and Roeder, op.cit., Fig.7) but will also reflect
the activities of Mg^{2+} and Fe^{2+} in the melt.

Liquidus spinel compositions are also affected by
the co-crystallisation of pyroxene which stabilises Cr^{3+}
in its octahedral sites. The reaction relationship
between pyroxenes and spinel postulated by Irvine (1967)
has been demonstrated experimentally by Hill and Roeder
(op. cit.) and accounts for the break in spinel crystall-
isation between early chromites and later titaniferous
magnetites observed in several stratiform intrusions
(Irvine 1967).

As stated earlier the compositions of the spinels
from the type 1 and type 2 picrites and the peridotite
plug are considered to be primary. In addition, the spinels
from the Western and Eastern layered series were all
included in olivines (Dunham and Wadsworth, 1978) and
their compositional variation was considered to reflect
primary liquidus variation; similarly the Cr-rich end
members of the Al and Fe reaction trends (Henderson 1975)
and the most aluminous spinel in SR157* (Ridley, 1977)
were also protected from reaction with the melt and are
primary compositions.

* Specimen SR157 is from the Rhum Lavas.

The spinels have been plotted into Fig. 6.13. The boundaries differentiate the fields of spinels from stratiform and alpine peridotites. The majority of the layered series peridotites lie as expected in the field of stratifrom chromites. However, the spinels with higher Mg contents (ie. higher temperature) have Cr/Al ratios more typical of alpine peridotites. On this diagram the Rhum minor intrusion spinels lie in the field of alpine peridotites and the Al-rich Rhum lava spinel with a Cr/Cr+Al ratio of 1:1 lies well into the alpine peridotite field; note once again the similarity of the spinels from the peridotite plug to the layered series peridotites.

The differences between chromites from alpine peridotites and spinels which have crystallised from basaltic liquids in stratiform intrusion have been discussed by Irvine (1967), Pinsent (1974) and Greenbaum (1977). The former have low Fe^{2+} contents and an extremely wide range of Cr/Cr+Al ratios whereas the latter have higher Cr contents, much more restricted Cr/Cr+Al ratios and have a much larger range of Fe^{2+} values. In addition stratiform chromites generally have a greater range in Fe^{3+} content. In his study of the Blue River Alpine body Pinsent (1974) showed that there were distinct compositional differences between the

spinels in the dunites and the spinels in the peridotites.
The former are characterised by $Cr/Cr+Al > 0.575$ and have
$Mg/Mg+Fe^{2+} < 0.60$ whereas the latter have higher Al and
lower Fe^{2+} contents. Pinsent believed that the Cr-rich
spinels in the dunites had crystallised from a basaltic
liquid and states categorically that the spinels in the
peridotites are too Al and Mg enriched to be derived from
a basalt magma under comparable P-T conditions. He
attributed the high Al content of the latter principally
to the P-T controlled metamorphic reaction

Al enstatite + olivine = Al spinel + enstatite
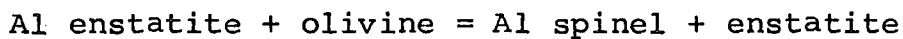
but stated that reaction between the spinels and inter-
stitial liquid (cf. Henderson 1975) may possibly have
played a role.

Thus, it appears that spinels crystallised from basaltic
liquids at low pressure are characterised by $Cr/Cr+Al$ ratios
> 0.575 and higher Fe^{2+} contents than spinels which have
equilibrated at higher pressures and thus emphasises the
pressure dependence of the Al/Cr ratio.

Secondary variation

The compositional variation resulting from complex
reactions with the host basaltic liquid (an alkali basalt
from Muck and an olivine basalt from Rhum) has been
described in detail by Ridley (1977). The trend developed

by variations in the Al, Cr and Fe^{3+} contents in a single

specimen from the Rhum lavas (SR157)   is presented

in Fig. 6.12. The principal features of the reaction

relationships described by Ridley (1977) are similar for

both specimens, these being (i) a substantial increase in

the Cr/Al ratio, this was mainly attributed to the

peritectic reaction

   Aluminous chromite + melt $\rightarrow$ plagioclase + chromite
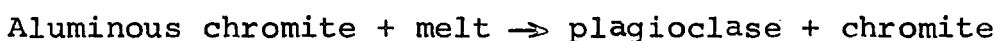
(ii) a gradual increase in the Fe^{3+} content by the

substitution of Al^{3+} for Fe^{3+}. The Fe^{3+} does not replace

the Cr^{3+} because the latter has a much higher octahedral site

preference energy (see p. 163) and is a stable component

of the spinel lattice.

(iii) A gradual increase in the Ti^{4+} content which probably

reflects the coupled substitution $Fe^{2+}-Ti^{4+}$ for $Al^{3+}-Cr^{3+}$.

   In contrast compositional variation attributable to

subsolidus reactions of spinel in the form

   Plagioclase + olivine + chromite $\rightarrow$ Al-enriched

                              chromite + liquid
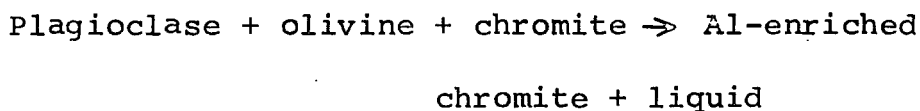
has been described by Henderson (1975) and these "Al

enrichment trends" in the Rhum layered series chromites

are presented in Fig. 6.12. In addition Henderson (1975)

recognised an "Fe^{3+}-enrichment trend" (see Fig. 6.12) which

he attributed to reaction of cumulus chromite with inter-

cumulus liquid over a large temperature range. This

interpretation is consistent with the variation in spinel
composition with falling temperature in the data of Hill
and Roeder (1974) as discussed earlier (p.165).

Discussion

The spinels from the type 1 and type 2 picrite and
the aluminous spinel from the Rhum lavas undoubtedly
crystallised from a mafic liquid yet they lie outside
the field of stratiform spinels in Fig. 6.13. One possible
explanation of this anomalous behaviour is that these
spinels crystallised at greater pressures than the spinels
in stratiform intrusions. The variation of spinel
compositions as a function of pressure has not yet been
studied. However, Hill and Roeder (1974) suggest that
the solubility of Cr will increase with increasing pressure.
This increase in the solubility of Cr will probably result
in a lower Cr/Cr+Al ratio in spinels crystallising at
higher pressure providing the oxygen fugacity of the melt
(which controls the activity of Fe^{3+}) is low. A high
pressure origin has also been proposed for aluminous spinel
phenocrysts in ocean floor basalts (Ridley et al. 1974).
Interpretation of the differences between the spinels from the
type 1 and type 2 picrites and the Rhum lavas is speculative
but one possibility is that the host magma of the latter
contained less Cr than the picritic magmas.

It could be argued that these low Cr/Cr+Al ratios in the spinels from the picrites and the Rhum lavas are a result of reaction with the melt, but Ridley (1977) demonstrated that reactions of this type will increase the Cr/Cr+Al ratio but will also increase the Fe^{3+}, Fe^{2+} and Ti^{4+} contents and the latter are low in these spinels. The subsolidus reactions described by Henderson (1975) do increase the Cr/Cr+Al ratio without altering the Fe^{3+} content but subsolidus reactions are likely to have been minimal in these rapidly cooled bodies.

The primary compositions of spinels in the layered series peridotites have been shown to vary sympathetically with cryptic variation exhibited by the other phases in the layered peridotites (Dunham and Wadsworth 1978). The compositional variation of the layered peridotite spinels in Figs. 6.12 and 6.13 is probably a function of their temperature dependence and related changes in the activities and solubility of Cr, Al and Fe^{3+} in the melt. Note, however, the high Fe^{3+} and Fe^{2+} contents of two of these spinels in Fig. 6.11 and 6.12 suggesting that these spinels were not totally enclosed by olivine in three dimensions.

The similarity of the spinels in the peridotite plugs when compared with the layered series peridotites suggests that they may have a common origin. The dissimilarity of these spinels with those from the picrites

and in the Rhum lava specimen SR157 indicates that these

picrites and this Rhum lava are not suitable parent

magmas for the Rhum layered intrusion.

The origin of the spinel compositions in 77024, 77039,

77184 and 32A76 are problematic as only limited data is

available. The similarity of one of the spinel phenocrysts

in 77039 to the spinels from the type 1 picrites was noted

previously. This contrasts with the other Fe^{3+}, Ti^{4+} rich

spinel in 77039, this variation is probably attributable to

the reaction relationships described by Ridley (1977) or

may reflect the presence of two generations of spinel

phenocryst in this rock. The variation in the spinel

chemistry in 32A76 is probably a result of the reaction

of a Cr-bearing spinel with the melt. The spinels from

77184 and 77024 subparallel the spinel reaction trend

defined by Ridley (1977). The former have more Fe^{3+} than

the spinels from the picrites and the peridotic plug which

may be a function of higher initial Fe^{3+} with subsequent

incorporation of more Fe^{3+} by reaction with the melt.

Iron-titanium oxides

Iron-titanium oxides are ubiquitous minerals in the

Rhum minor intrusions other than the group 1 picrites.

They occur as discrete grains of exsolved ilmenite and

magnetite suggesting that they originally crystallised

as homogeneous titanomagnetites which have re-equilibrated
at lower temperatures. Their small size and the presence
of very fine exsolution lamellae has led to severe
analytical problems. Several of the analyses in Appendix
6.2 contain appreciable SiO_2 (up to $\sim$ 3.0 wt%) which may
be due to the incorporation of small quantities of
silicate phases adjacent to the iron titanium oxides.
In addition several of the analyses do not give totals
within an acceptable range (98.5-100.5%) when recalculated
on a stoichiometric basis. Both these features are
considered to be due to slight movements of the electron
beam during analysis which has resulted in poor quality
data. Because of these difficuties only limited chemical
data on minerals of this composition have been obtained
during this study. These confirm in a qualitative manner
the composition of the opaque minerals in the Rhum minor
intrusions but are not of a sufficiently high standard to
merit quantitative treatment.

OLIVINES

Fresh olivine is only found in the group 1 picrites
and the peridotite plugs, consequently only limited chemical
data are available. The majority of these analyses are of
phenocrysts as most of the groundmass olivines in group 1
are either altered or extremely small making them

unsuitable for analysis. The NiO, CaO and MnO contents

of the analysed olivines have been plotted against Fo

content in Fig. 6.14. The most striking feature of this

plot is the bimodal distribution of the Fo content of

the olivines, those from 77024 range Fo74-Fo77.5 the

remainder range from Fo84 - Fo88.5.

The olivines in the type 1 and type 2 picrites,

85A76 and the peridotite plugs occur as large granular

crystals in a matrix of plagioclase, clinopyroxene and

opaque oxides, an exception being the single groundmass

olivine in a type 2 picrite. The latter contains less

magnesium than the olivine phenocrysts in this specimen,

this reflects the temperature dependence of the Mg content

of olivines. The olivines from the peridotite plug show

limited variation in Mg content ($\sim$ Fo85) and all but one

of the type 1 and type 2 phenocryst olivines exhibit a

limited compositional range (Fo86-Fo88.5). These compo-

sitions are typical of high temperature olivine phenocrysts

in basaltic melts.

In contrast the olivine phenocrysts in 77024 occur

in various morphologies ranging from lattice and chain

olivines, through hopper olivines to granular olivines

(see Chapter 4, p. 97). Similar textures have been

described by Donaldson (1976) who showed that olivine

morphology in picritic and basalt magmas varies

systematically with either the degree of supercooling of the melt prior to olivine nucleation or the rate of cooling of the melt or both. High degrees of supercooling and rapid cooling rates favour formation of the lattice and chain olivines and progressively lower degrees of supercooling and lower rates of crystallisation produce branched olivines, hopper olivines and granular olivines respectively (Donaldson 1976, Fig.8). The limited compositional range of the olivine phenocrysts of 77024 in Fig. 6.14 contrasts with the large variation in the morphology of the olivine phenocrysts in this rock. Any petrogenetic interpretation of the chemistry and olivine textures in 77024 must take into account the following features.

(i)   The presence of a fine-grained chilled margin containing abundant elongate olivine crystals.

(ii) The coexistence of a wide range of olivine morphologies in the central facies of the dyke.

(iii) The limited compositional range (Fo74.8-Fo76.3) exhibited by all but one of the olivine phenocrysts in this dyke.

(iv) The high MgO content ($\sim$ 15.5 wt%) of the whole rock analysis.

The elongate olivines will have been extremely fragile, however, although some of these crystals are bent the

vast majority have not been snapped or broken. This

suggests that these olivines crystallised more or less

in situ. It could be argued that the MgO content of

this rock is due to enrichment by the addition of

cumulus olivine. However, the granular olivines are

very similar in composition to more skeletal varieties

an exception being a single granular olivine with a

higher Fo content (Fo77.5 as opposed to Fo76.3). This

similarity in olivine composition. suggests all these

olivines are produced by isothermal crystallisation of

a supercooled MgO rich liquid. The olivine morphology

may also reflect rapid cooling rates and this is

supported by the presence of elongate chain and lattice

olivines in the chilled margin, but the absence of

extreme textures,(e.g. swallow-tail olivines, Donaldson

1976, Fig.8) suggests that the enclosing country rock

(peridotite) was still at relatively high temperatures

(ie. the chilled margin reflects the temperature

difference between the MgO-rich liquid ($\sim$ 12 00 $^{\circ}$C*) and

consolidated peridotite ($\sim$ 900°C)).

To summarise, injection of a supercooled MgO-rich

liquid into hot consolidated peridotite resulted in the

in situ development of elongate lattice and chain olivines,

subsequent rapid, virtually isothermal crystallisation,

*estimate based on the liquidus temperatures quoted by
 Donaldson (1976).

produced branched, hopper and granular olivines respectively, as the degree of supercooling approached zero.

Having rapidly attained equilibrium, heat losses to the enclosing peridotite resulted in the magma following a "more normal" crystallisation path with the development of a fine-grained groundmass composed of slightly lower temperature phases.

The olivines with Fo contents greater than Fo84 in Fig. 6.14 generally have NiO contents ranging from 0.3 - 0.45 wt%, no systematic depletion in NiO with decreasing Fo content can be discerned in these samples. However, the olivines in 77024 have significantly lower NiO (0.15-0.20 wt%). This decrease in NiO with decreasing Fo content is a typical feature of olivine compositions (Simkin and Smith, 1970). Sato (1977) has shown that the majority of mantle olivines contain 0.35-0.45 wt% NiO, the high NiO contents (0.3-0.4 wt%) of the olivines with Fo contents greater than 84.0 is probably due to a high Ni content in their host magmas. The CaO content of the olivines in Fig. 6.15 varies between 0.15 and 0.65 wt%, the majority of the olivines contain 0.3-0.4 wt% CaO. The CaO content of magmatic olivines is thought to decrease with increasing pressure (Simkin and Smith 1970). A more recent work by Ferguson (1978) related

the CaO content of olivines to the Ca activity in the melt and the dependence of the CaO contents of olivine on the CaO content of the host magma has been shown experimentally by Watson (1979a). Ferguson (1978) also suggested that the lower CaO content of olivines in hypabyssal rocks, when compared with their extrusive counterparts, was reflected in the ability of CaO to diffuse out of the olivine lattice in the slower cooling environment.

The MnO content of the forsteritic olivines varies between 0.15 and 0.25 wt% and increases to approximately 0.60 wt% in the more iron-rich compositions. These are similar to the values reported by Simkin and Smith (1970) who also observed an increase in MnO with increasing iron content.

The olivines in the Rhum layered series vary between Fo78 and Fo88.5. In addition, they contain 0.17 to 0.40 wt% NiO (Dunham and Wadsworth 1978) and thus their compositions compare favourably with the olivines in the Rhum minor intrusions (excluding those in 77024). The layered series olivines contain less CaO (0.02-0.20 wt%, Dunham and Wadsworth 1978) than the olivines in the Rhum minor intrusions, the lower content of the former may reflect the slower cooling rate of their plutonic environment.

FELDSPARS

Chemical data for the feldspar minerals is only available for some of the dolerite groups in the Rhum minor intrusion suite, the limited data for the group 4 plagioclase is embodied in Appendix 6.2 but is not discussed here. The dominant feldspar mineral is plagioclase but K-feldspars are found in the alkaline differentiates.

The variation of the plagioclase data in the picritic group 1 rocks and the basic group 2 and 3 rocks is presented in Fig. 6.15. There is a wide variation in plagioclase composition (An80-An40) in the group 1 and 2 rocks. The sparse data for the group 3 rocks indicate a more differentiated composition (An70-An45). The overlap in compositions between the phenocrysts and groundmass compositions in group 2 is also worthy of note as it emphasises the compositional variability within each of the dolerite groups.

The compositional heterogeneity of the feldspar phenocrysts (An84-An88) is a feature of the group 7 plagioclases in Fig. 6.16, as is the separation of these phenocrysts from the more sodic groundmass (An40). A wide range of compositions are found in the group 8 rocks (Fig. 6.17) the phenocrysts range from surprisingly calcic compositions (these rocks are intermediate);

however the groundmass plagioclases zone to An30.

The group 10 rocks exhibit an extremely wide range of feldspar compositions from calcic phenocrysts in 77090 to coexisting albite and orthoclase in the groundmass of 32A76 (Fig. 6.17). A less extreme range from sodic plagioclase (An36) to orthoclase is encountered in group 11 and the groundmass K-feldspars in the group 12 specimen (77132) exhibit only minor variation.

Key to symbols on Fig. 6.1.

O Group 1	() Group 7
▲ Group 2	⊕ Group 8
-⊙- Group 3	□ Group 9
▼ Group 4	▨ Group 10
+ Group 6	⊕ Group 11
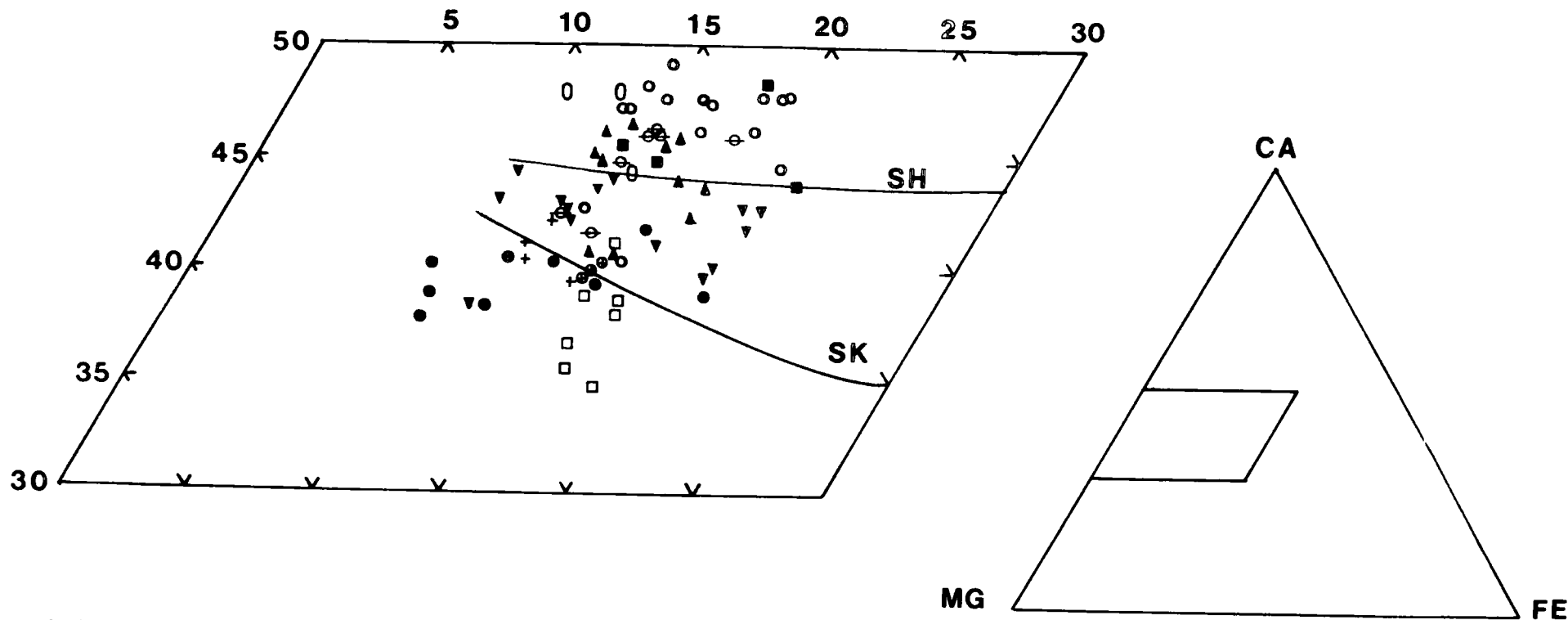
Fig. 6.1 Clinopyroxenes in the Rhum dolerite suite, lines SH and SK are the approximate trends developed by the Shiant Isles sill clinopyroxenes (Gibb 1973) and the Skaergaard intrusion calcic augites (Brown 1957) respectively. See adjacent page for key to symbols.

Fig. 6.2 Al, Ti, Cr in the Rhum dolerite clinopyroxenes
plotted against Fe/Fe+Mg (all on the basis of
6 oxygens). Symbols as for Fig. 6.1 except
ϕ = Group 11.
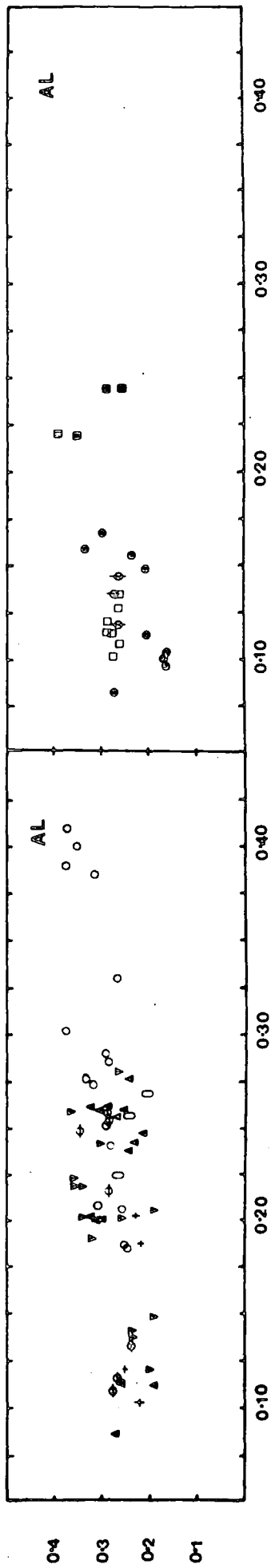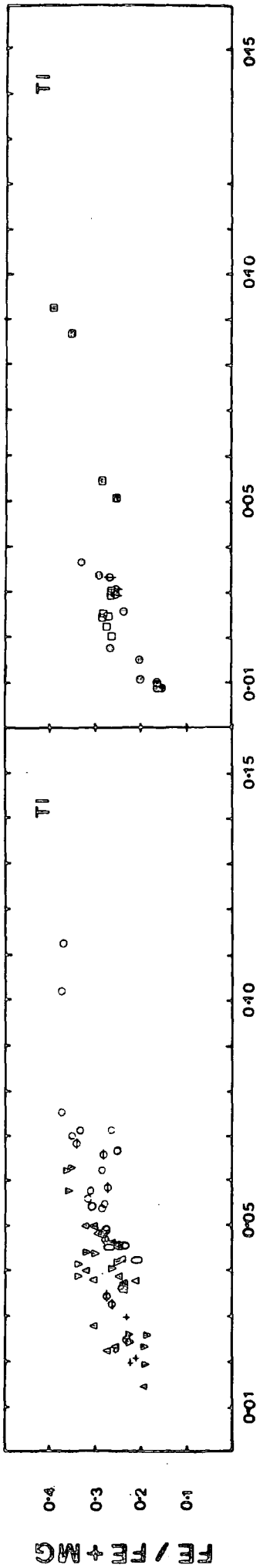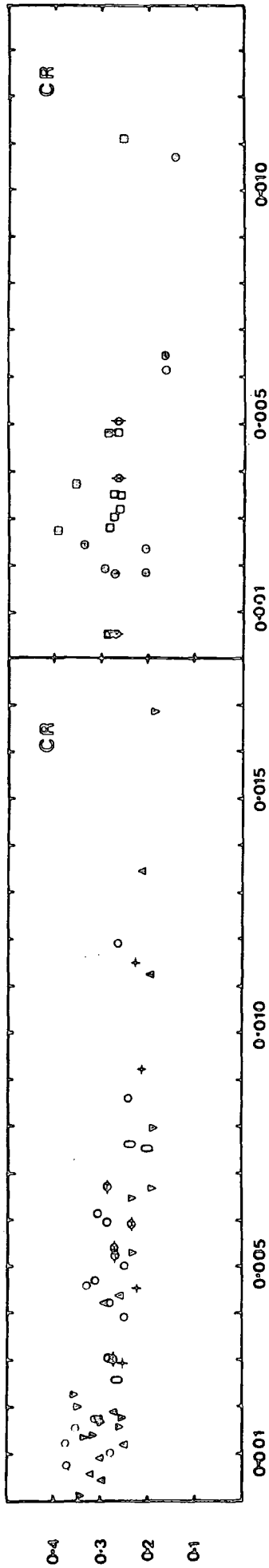
Fig. 6.3 Na and Mn in the Rhum dolerite clinopyroxenes
plotted against Fe/Fe+Mg (all on the basis of
6 oxygens). Symbols as for Fig. 6.1 except
ϕ = Group 11.
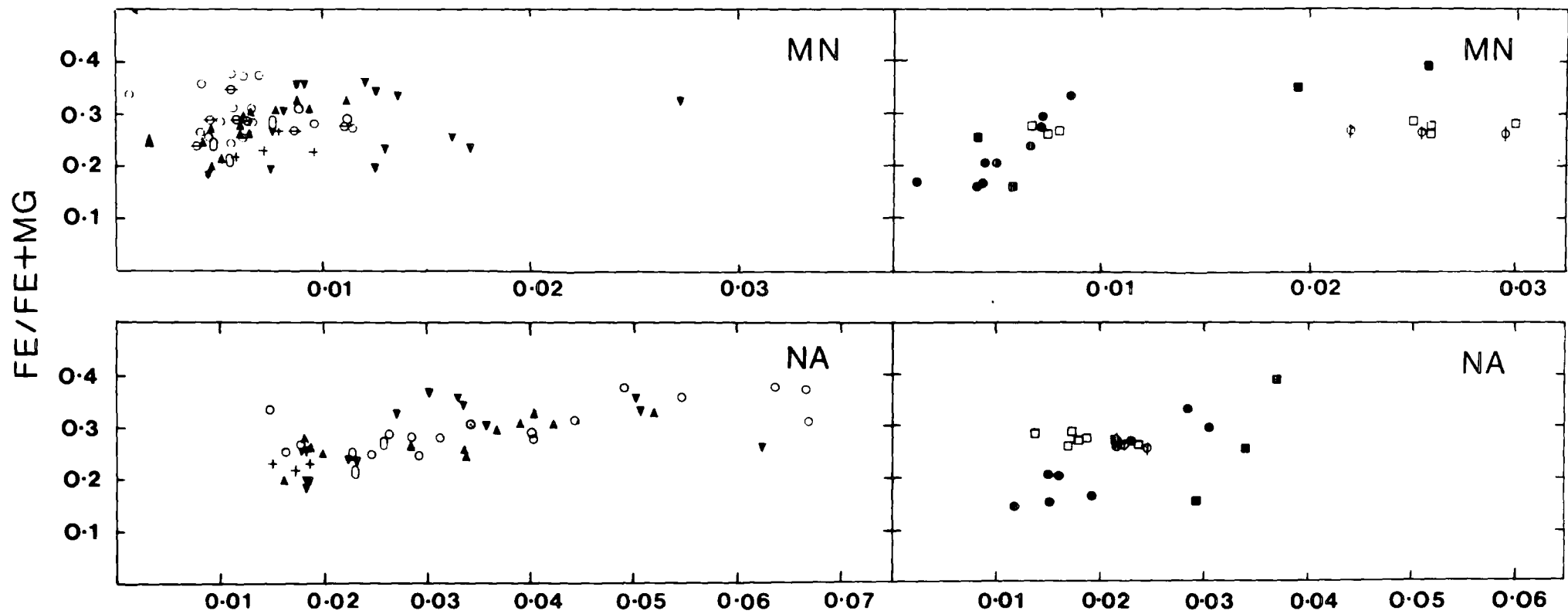
Fig. 6.4 Al v. Ti in the dolerite groundmass pyroxenes,
ratios are the proportion of Ti substituted
relative to Al (all on the basis of 6 oxygens).

Key to symbols in Figs. 6.4 - 6.10

▨	Group 1	⊕	Group 8
▽	Group 2	⊸⊛	Group 9
▢	Group 3	▨	Group 10
△	Group 4	⊸▨⊢	Group 11
0	Group 7		
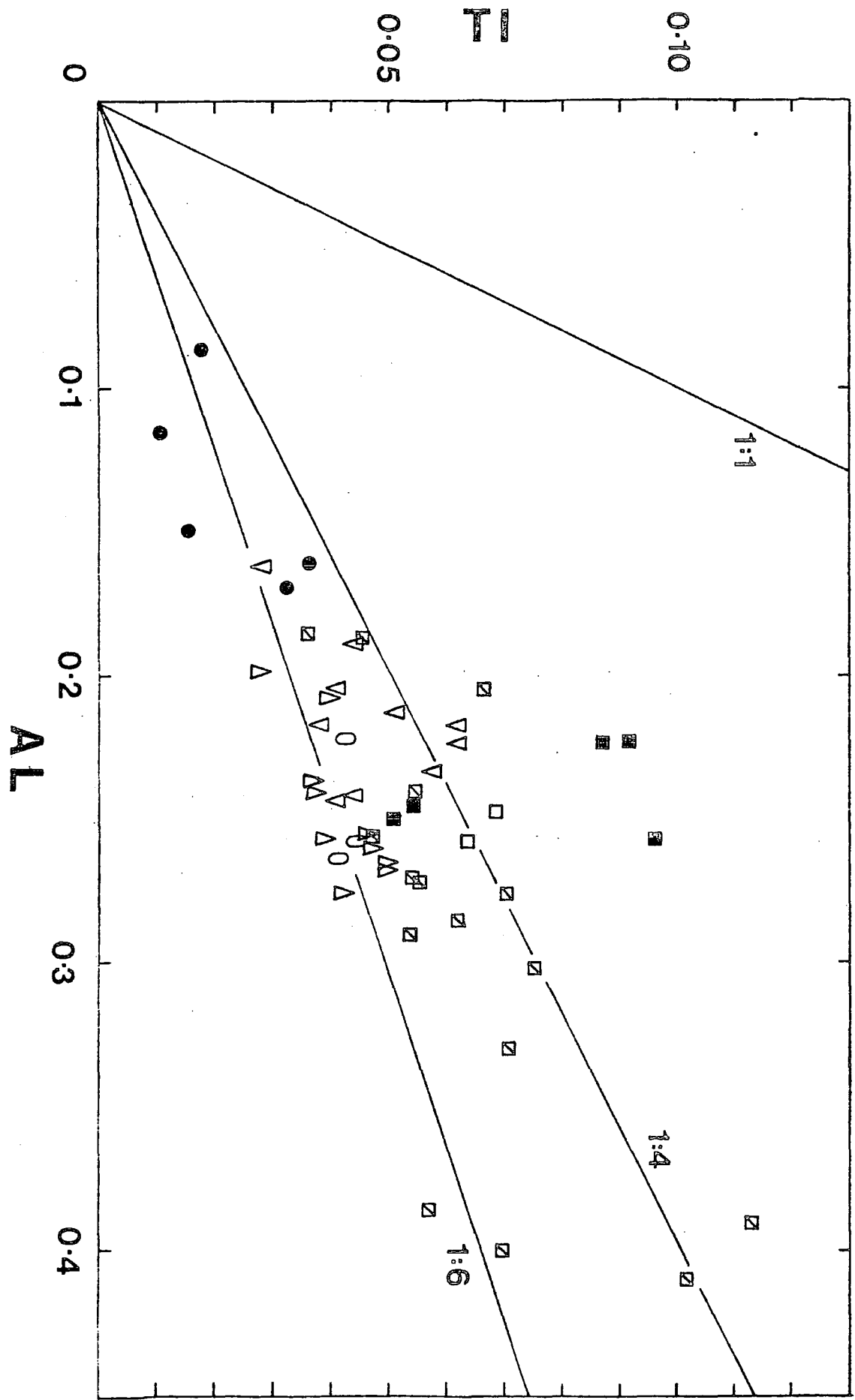
Fig. 6.5 Al v. Ti in the dolerite clinopyroxene phenocrysts,
ratios are the proportion of Ti substituted relative
to Al (all on a basis of 6 oxygens). Key to symbols
on p.186.
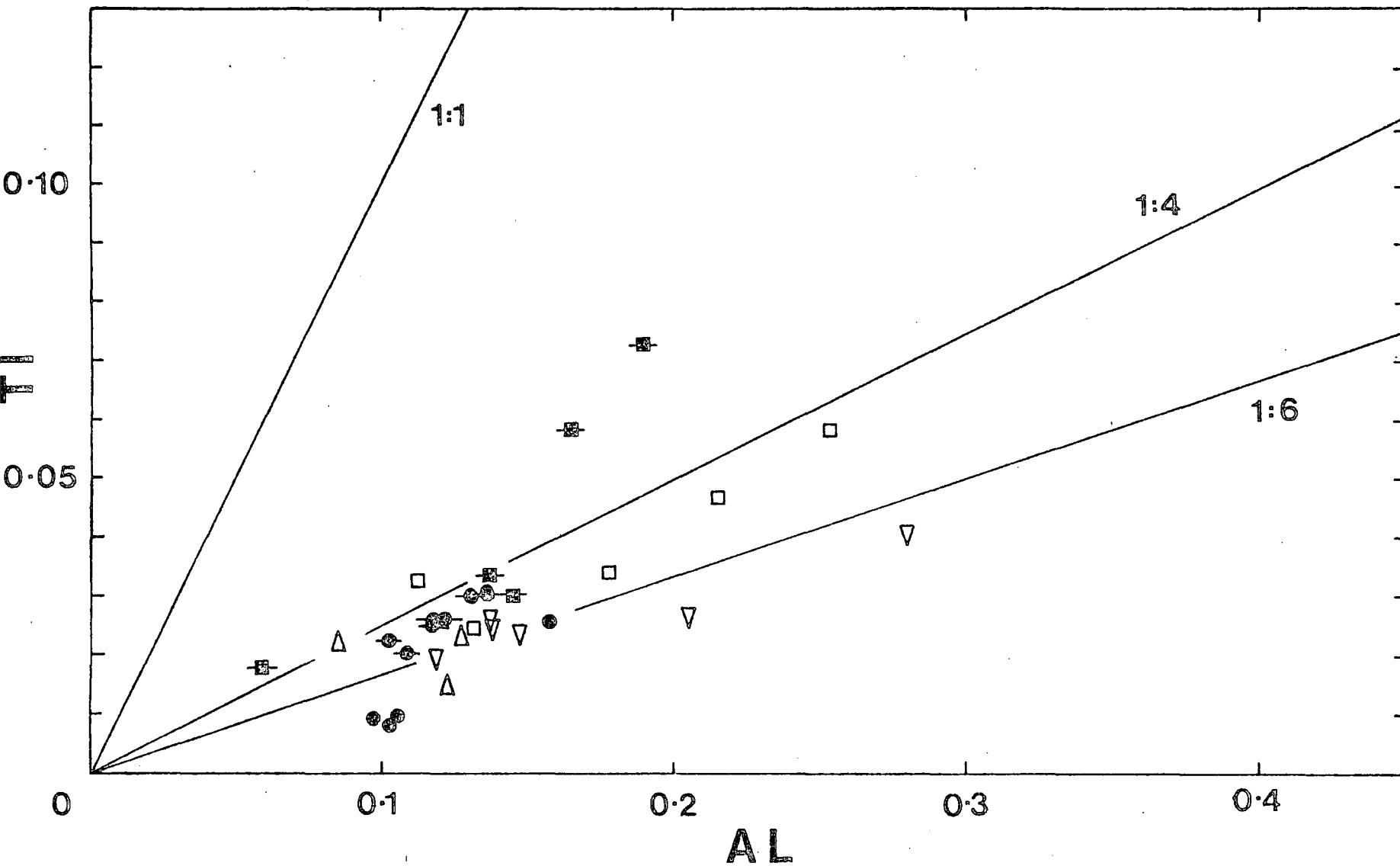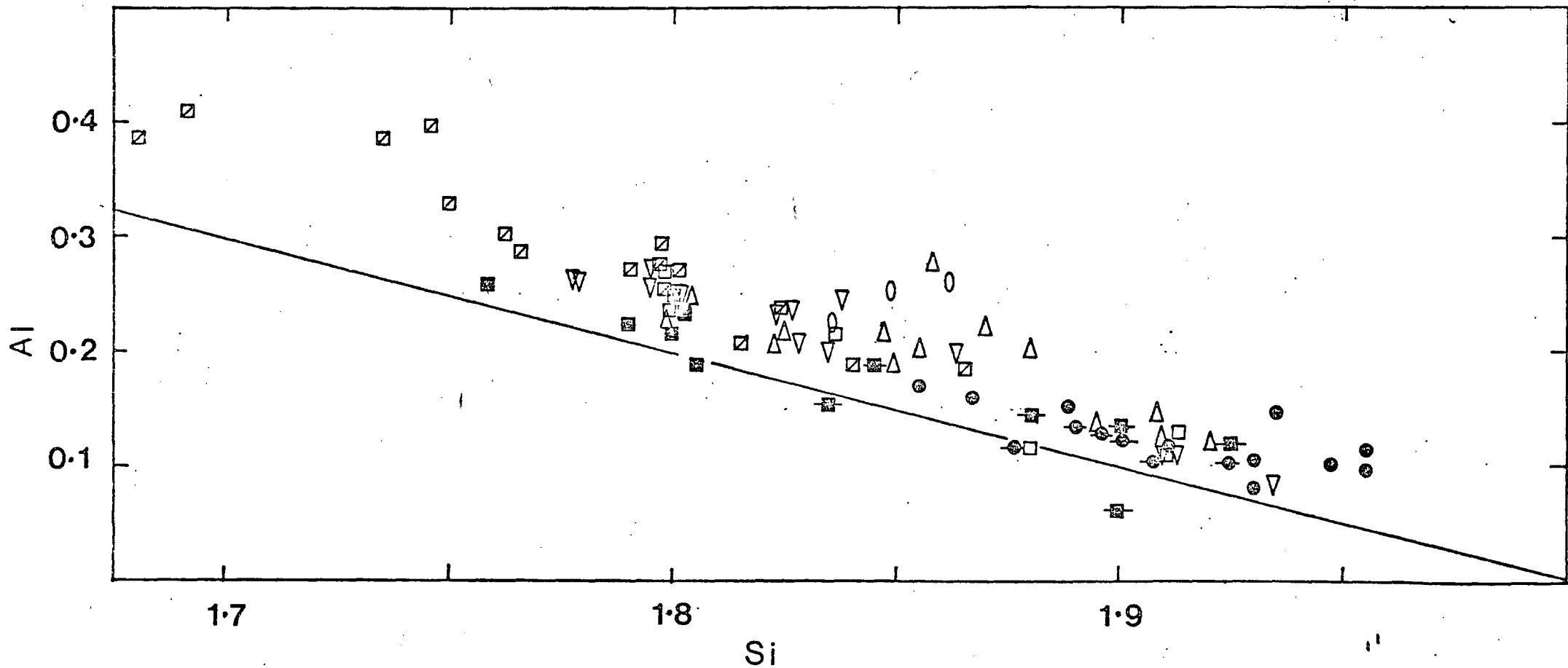
Fig 6.6 Si v Al in the dolerite clinopyroxenes (on a basis of 6 oxygens). The solid line indicates the amount of Al required to fill the Z site. Key to symbols on p 186.
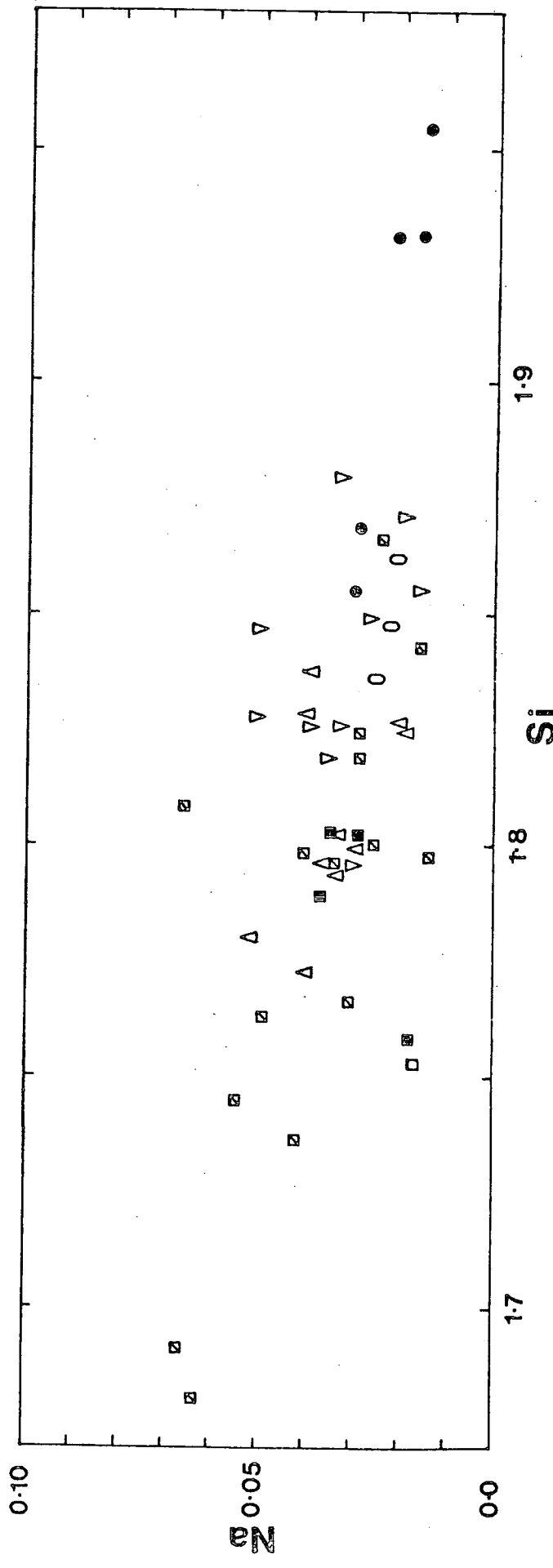
Fig 6.7 Si v Na in the dolerite groundmass pyroxenes. Symbols as in Fig 6.4. (on a basis of six oxygens).

Fig. 6.8 Al^{IV} v. Al^{VI} in the dolerite groundmass pyroxenes. The fields of pyroxene in igneous rocks and in basalts with granulites and inclusions are taken from Aoki and Shiba (1973, Fig. 3). Key to symbols on p.186.
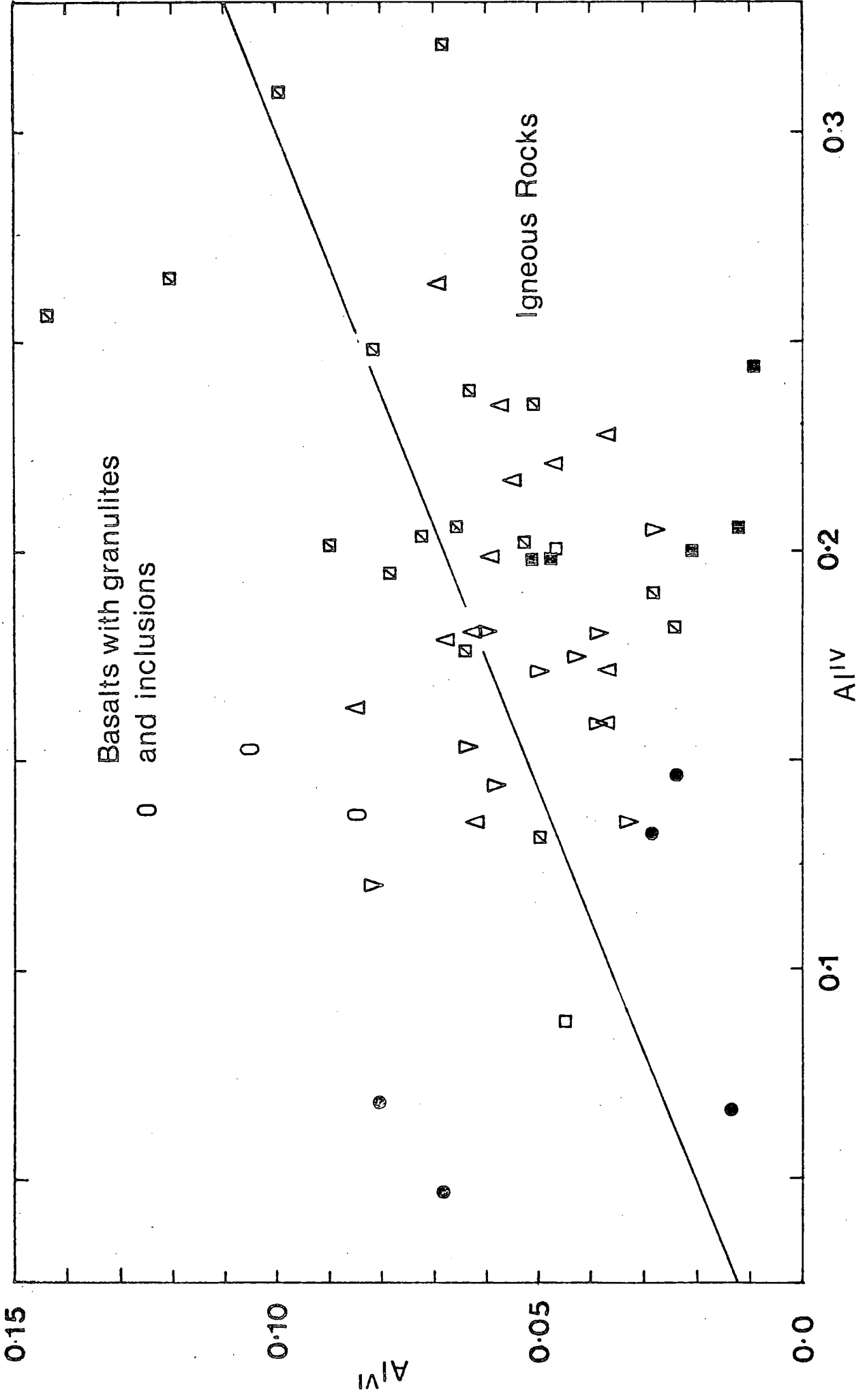
Fig. 6.9 Al^{IV} v. Al^{VI} in the dolerite phenocryst pyroxenes.
The fields of pyroxenes in igneous rocks and in
basalts with granulites and inclusions are taken
from Aoki and Shiba (1973, Fig.3). Key to symbols
on p.186.
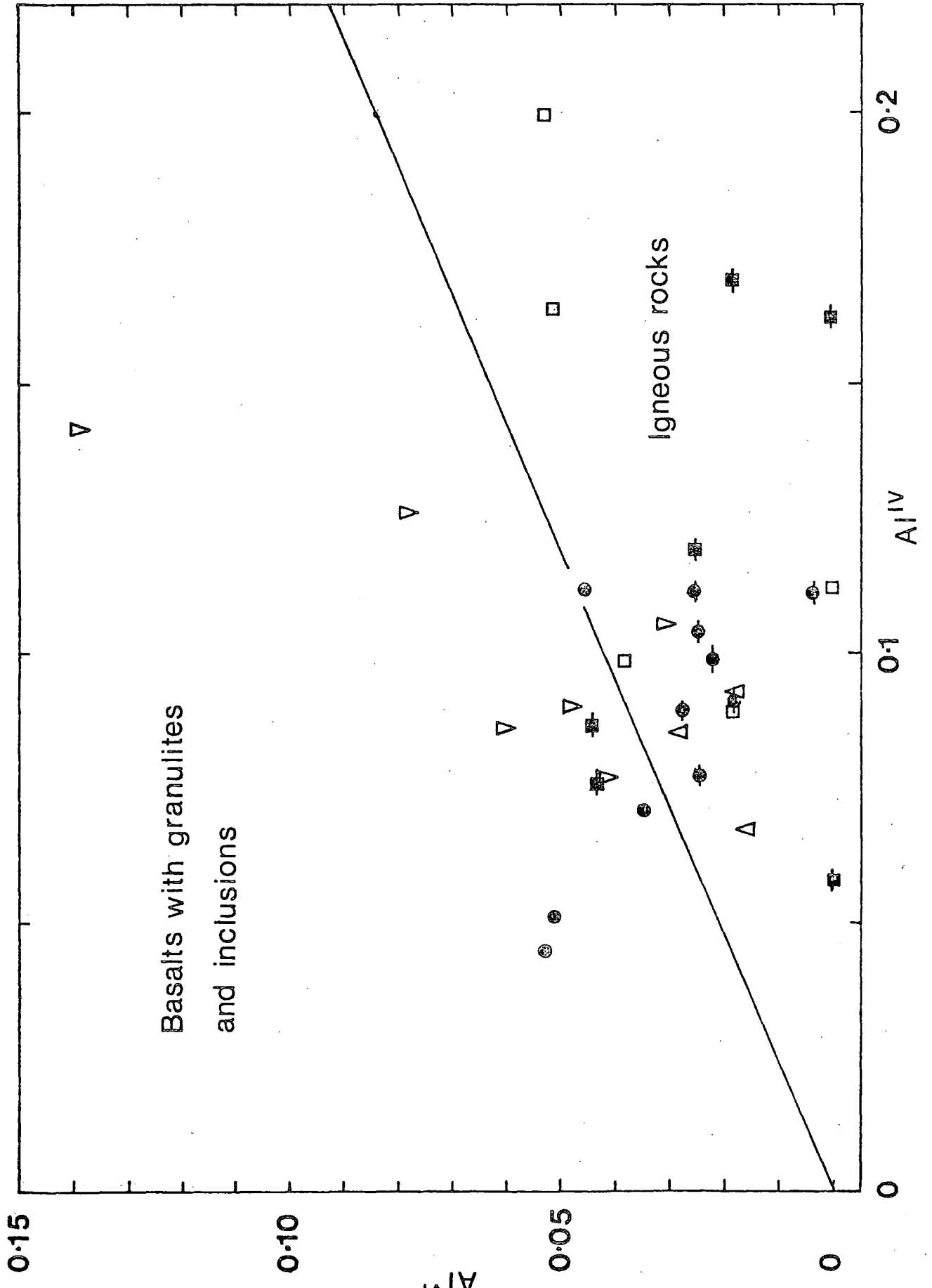
Fig. 6.10 Tectonic discriminant analysis of the
Rhum dolerite pyroxenes. The fields
for Within Plate Alkaline (WPA),
Within Plate Tholeiite (WPT), Volcanic
Arc Basalt (VAB) and Ocean Floor Basalt
(OFB) are taken from Nisbett and Pearce
(1977, Fig.1). The discriminant scores
on Functions 1 and 2 were obtained using
the functions listed in Nisbett and Pearce
(op.cit., Table 2). Key to symbols on
p.186.
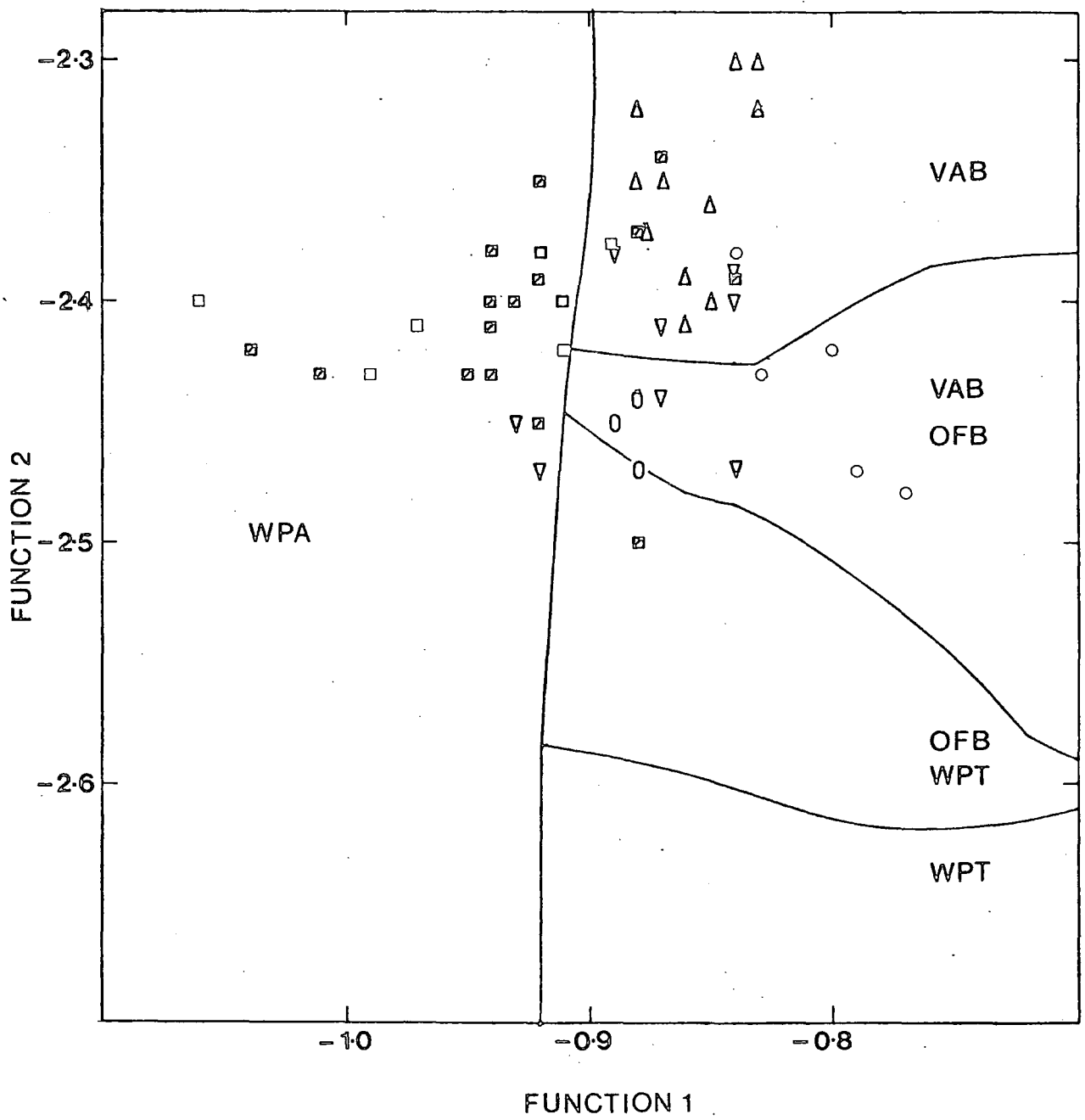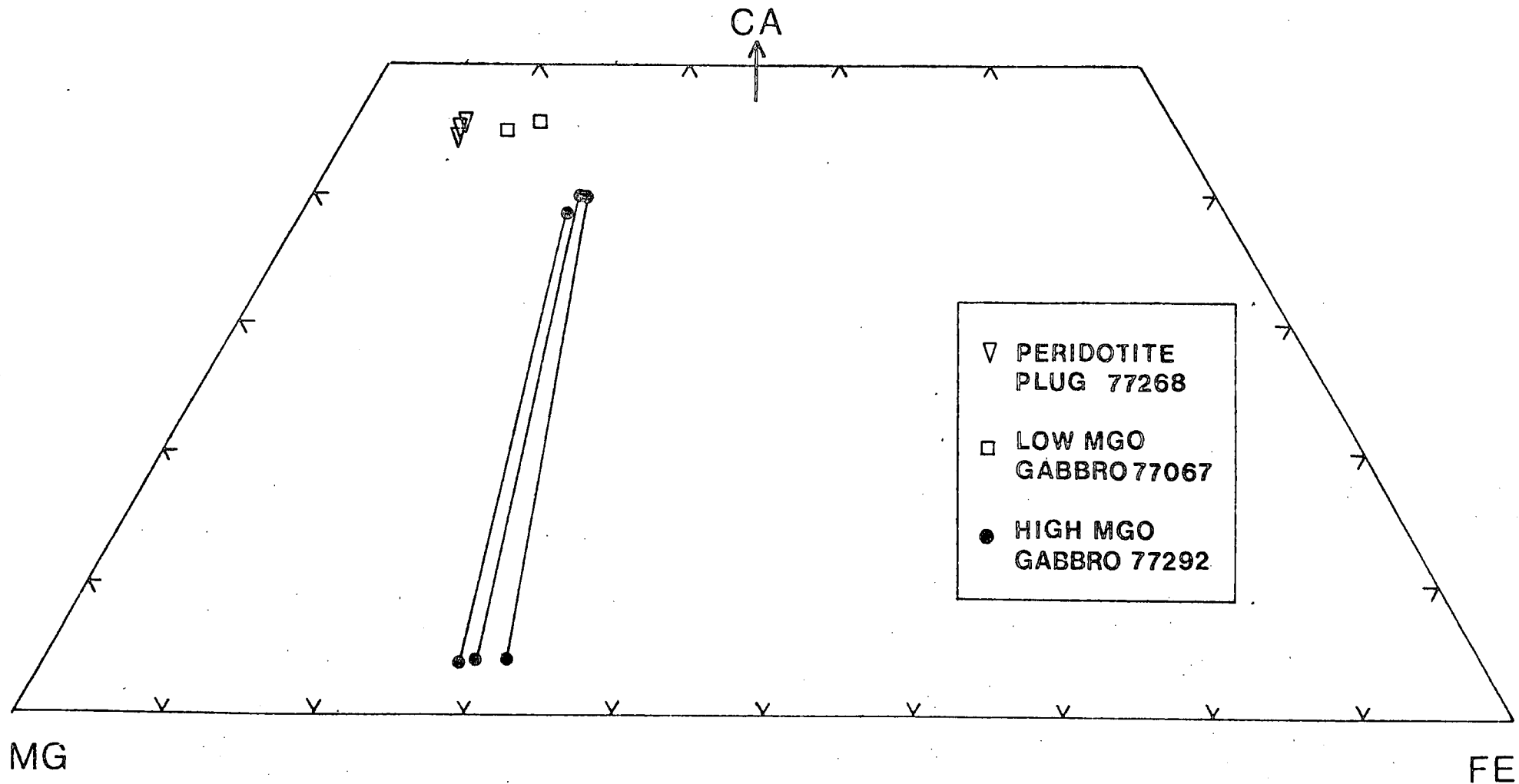
Fig. 6.11 Ca-Mg-Fe variation in pyroxenes from gabbro and peridotite plugs, tie lines join co-existing pyroxenes.

Fig. 6.12 Al-Cr-Fe variation in Rhum Cr-spinels.

Key to symbols

□ Type 1 Picrite (Gp.1)   ◨ 77039 (Gp.2)

□ Type 2 Picrite   "   + 77184 (Gp.10)

O 85A76 (Gp.1)   "   ☀ 32A76 (Gp.10)

⊖ 77024 (Gp.1)   "

▽ 77268 (Peridotite plug)

○ Rhum layered peridotite spinels (Dunham
   and Wadsworth, 1978, Tables IV and V).

U12——U12 Trend of variation exhibited by
          layered peridotite spinels of the base
U8——U8 of units 8 and 12 (Henderson,1975,Fig.11).

SR157—O—O— Spinel variation in the Rhum Lava specimen
            SR157, Ridley 1971, Table 2; circles mark
            individual data points and the arrow
            indicates the direction of zoning from core
            to margin.
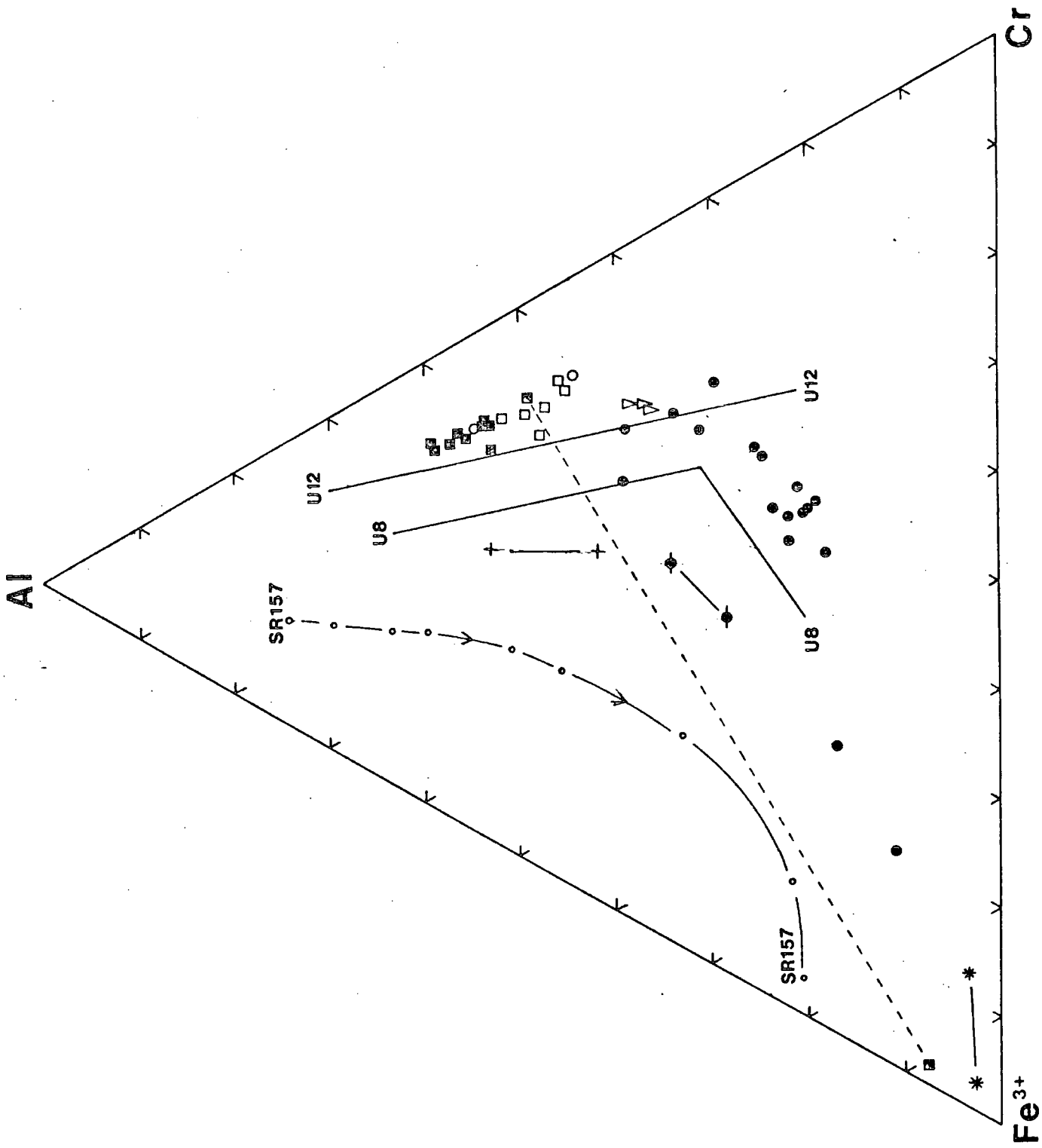
Fig. 6.13 Mg/Mg+Fe v. Cr/Cr+Al variation in Rhum
Cr-spinels. The fields of spinels in
stratiform intrusions and in alpine
peridotites are taken from Greenbaum
(1977, Fig.15). Symbols as in Fig. 6.12.
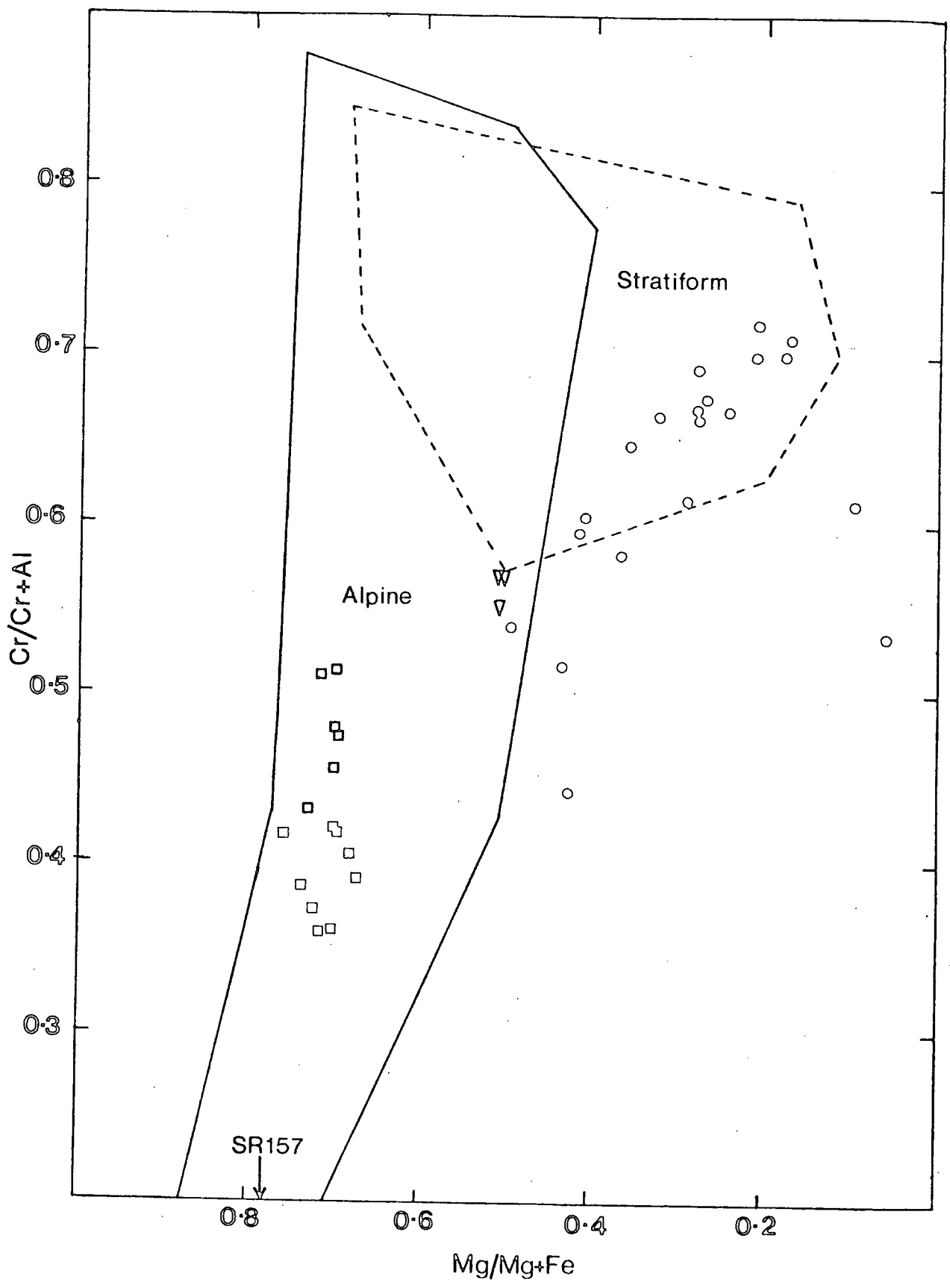
Fig. 6.16 NiO, CaO and MnO variation plotted against Mg/Mg+Fe
variation in Rhum minor intrusion olivines. Open
symbols are phenocrysts, closed symbols groundmass.

Key to symbols

   O Type 1 picrite (Group 1)   △ 77024 (Group 1)

   □ Type 2 picrite (Group 1)   O 85A76 (Group 1)

   ▽ 77268 (Peridotite plug)
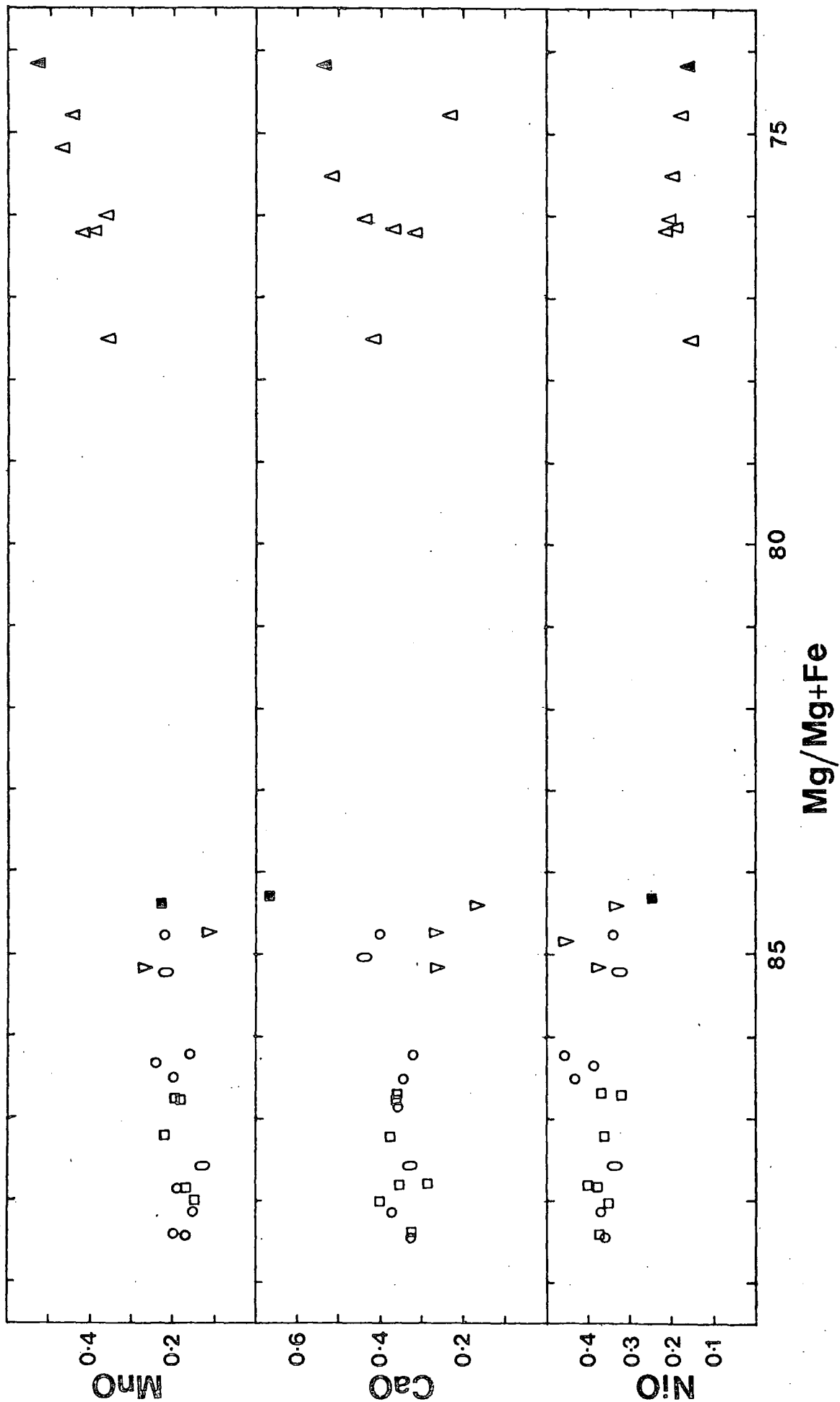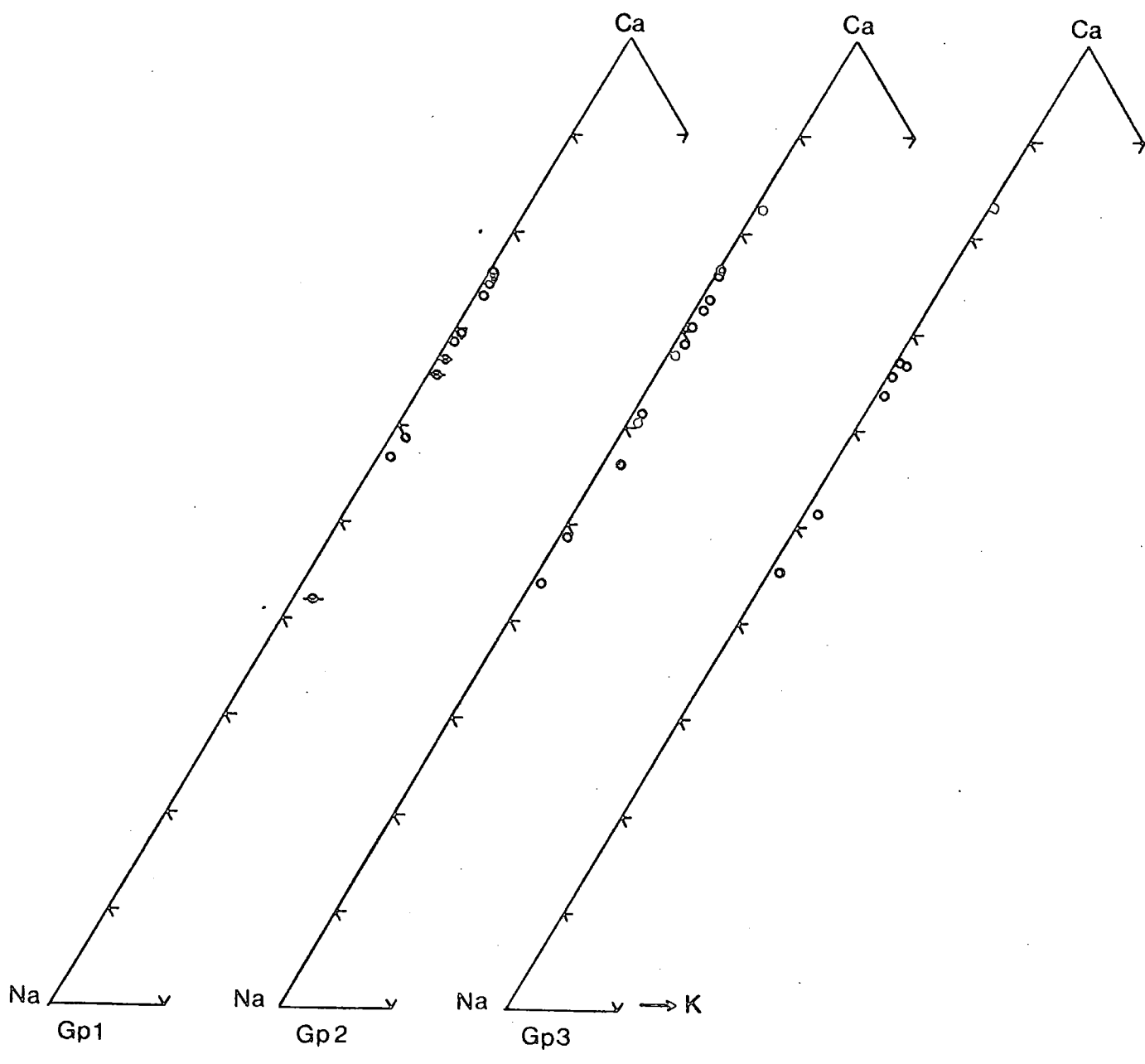
Fig. 6.15 Plagioclase variations in dolerite
groups 1-3. Closed symbols phenocrysts,
open symbols groundmass.
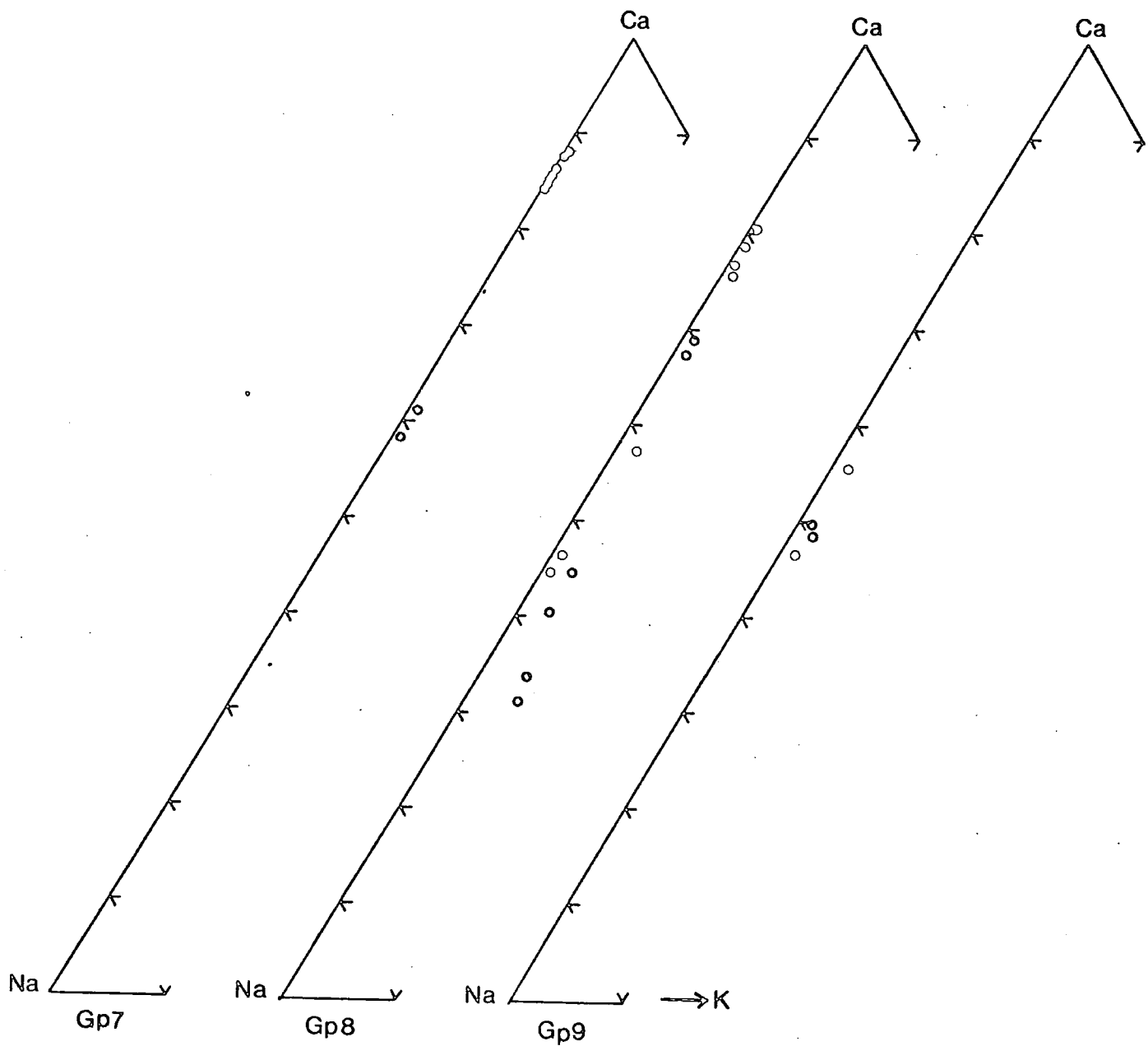
Fig. 6.16 Plagioclase variations in dolerite
groups 7-9, closed symbols phenocrysts.
open symbols groundmass.

FIG 6.17 FELDSPARS

○ GP 10 32A76, 77090
□ GP 11 77023 77279
△ GP 12 77132
Closed symbol = Phenocryst
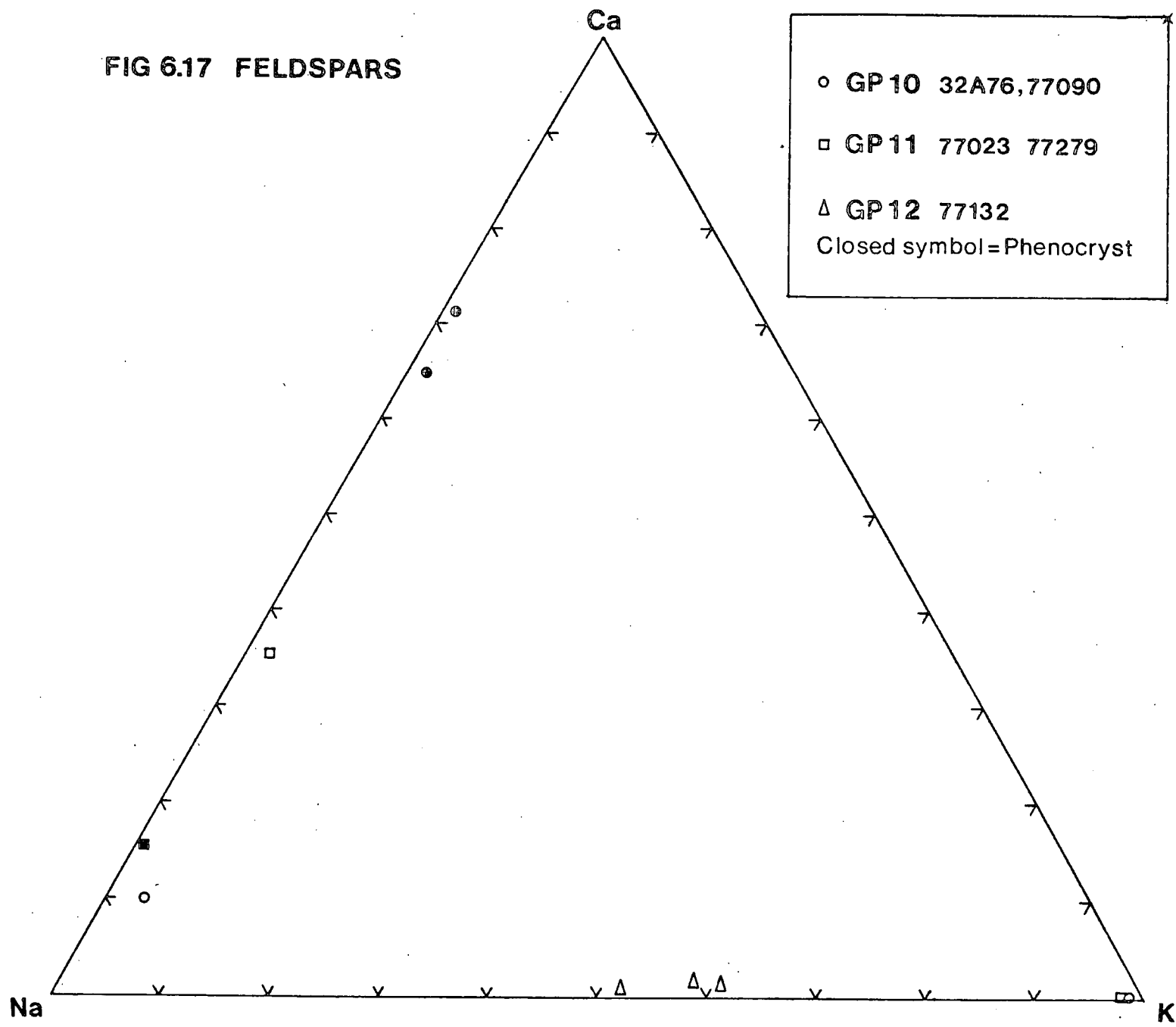
	1	2	3	4	5
Specimen	7726804	7726805	7726806	9698	DB
SiO_2	50.36	50.98	51.34	51.46	51.78
TiO_2	0.56	0.55	0.56	0.50	0.30
Al_2O_3	4.02	3.77	3.71	3.17	3.12
Cr_2O_3	1.40	1.32	1.29	0.61	0.68
FeO	4.40	4.45	4.50	5.48	4.14
MnO	0.28	0.17	0.17	–	–
MgO	16.34	16.09	16.39	15.63	16.63
CaO	21.40	21.38	21.69	23.09	23.00
Na_2O	0.27	0.33	0.30	–	–
wt % NiO	0.07	0.09	0.04	–	–
Total	98.89	99.12	99.99	99.94	99.65
Fe	7.22	7.35	7.36	8.71	6.55
Mg	47.78	47.37	47.79	44.27	46.86
Ca	45.00	45.27	44.84	47.02	46.60
Mg No	86.88	86.56	86.65	83.56	87.74

Table 6.1 Pyroxenes in the peridotite plugs and in the
layered series peridotites.

Numbers 1 to 3 Pyroxenes from peridotite plug
(this study)

Numbers 4 and 5 Average analyses of selected
cumulus pyroxenes from the Western Layered Series
(Dunham and Wadsworth 1978 Table V1)

Mg No = Mg/Mg + Fe

CHAPTER SEVEN

GEOCHEMICAL VARIATION AND PETROGENESIS

Introduction

This chapter deals with the geochemical variation exhibited by the Rhum minor intrusion suite and considers the various factors which have produced this compositional variation. A brief assessment of the effects of alteration on the geochemistry of the suite is presented in the first section. The subsequent sections consider in detail the geochemistry of the ultrabasic, basic, intermediate and acid rocks respectively and a petrogenetic synthesis is presented in section five.

The analytical procedures used to determine the major oxide and trace element abundances are described in Appendix 7.1 and the analyses of all the minor intrusions are presented in Appendix 7.2. In order to reduce overcrowding on the variation diagrams presented in this chapter, a representative set of the freshest aphyric analyses was selected for each group, these analyses are denoted with an asterisk in Appendix 7.2.

I. An assessment of the affects of alteration

Most geochemical studies of igneous rocks are based on the underlying assumption that the major oxide

and trace element abundances observed in the analysed

rock are equivalent to the abundance of these oxides

and elements in the original magma; however, petrographic

studies reveal that most terrestrial igneous rocks have

undergone varying amounts of post-solidification changes

(alteration).

In order to discuss magmatic effects, it is necessary

to first assess and then minimise the effects of alter-

ation. This problem may be tackled in several ways.

The most obvious solution is to use extremely fresh

material for analysis. However, this may not always be

possible as this extremely fresh material may not be

sufficiently representative of the chemical variation

exhibited by the igneous rock suite.

Various procedures have been recommended to reduce

alteration effects. Irvine and Baragar (1971) recognised

that the H_2O, CO_2 and O_2 content of most analyses were

unlikely to represent those of the original magma and

recommended that analyses should be normalised to 100%

volatile free. It has also been recognised that oxid-

ation of a rock during alteration will cause the Fe_2O_3/

FeO ratio to deviate significantly from the magmatic

ratio (Irvine and Baragar 1971, Thompson, et al.,

1972, Brooks 1976, Clarke and O'Hara 1979). The

Fe_2O_3/FeO ratio of a rock is of considerable importance

in determining the proportions of Ne or Hy in C.I.P.W.
normative calculations. The Fe_2O_3/FeO ratio is also
critical in the calculations involving the FeO and MgO
distribution coefficients between olivine and magma and
thus merits attention. The problem is best illustrated
by focusing attention on a single analysis and determining
the various Fe_2O_3 and FeO values recommended by the various
authors. The procedures adopted are as follows:

(i) Wt% Fe_2O_3 = wt% TiO_2 + 1.5 (Irvine and Baragar 1971).

(ii) Wt% Fe_2O_3 = 1.5 if Na_2O + K_2O < 4.0 wt% (Thompson,
et al., 1972).

(iii) Fe_2O_3/FeO = 0.15 (Brooks 1976).

(iv) Fe_2O_3/Fe_2O_3 + FeO = 1.5 (Clarke and O'Hara 1979).

The results are expressed in Table 7.1. Estimated values
for Fe_2O_3 range between 1.45 and 2.88 and the Fe_2O_3/FeO
ratios vary between 0.150 and 0.344. On the basis of
these calculations the consensus of opinion would
estimate Fe_2O_3/FeO ratios of 0.15 to 0.18 in basic magmas.

At an early stage in this study, a Fe_2O_3/Fe O ratio
of 0.25 was adopted on the basis of the discussion of
iron oxidation states in Johannesson (1975, p.136) and
this value was used in the subsequent normative calculations.
The evidence presented above would suggest that a lower
Fe_2O_3/FeO value would have been more acceptable. This
would have the effect of moving the hypersthene normative

specimens in Fig. 3.2 and Fig. 3.3 towards the critical

plane of silica under saturation and moving the nepheline

normative specimens away from this plane giving the suite

a slightly more alkaline character. It does not, however,

effect the conclusions in Chapter 3 concerning the trans-

itional nature of the suite as the Discriminant Function

Analysis procedure operated on total iron in a single

oxidation state (Appendix 3.2).

The Fe_2O_3/FeO ratio is also important in assessing

the molar concentration of FeO (XFeO) for use in

calculations involving the distribution coefficient (Kd)

of XFeO and XMgO between olivine and magma in the form

$$Kd = \frac{X^{FeO}_{Ol}}{X^{MgO}_{Ol}} . \frac{X^{MgO}_{liq}}{X^{FeO}_{liq}}$$

The theoretical composition of the liquidus olivines in

equilibrium with 54A76 have been calculated using the

estimated XFeO derived in Table 7.1 and a Kd value of

0.30 (Roeder and Emslie 1970) the results are presented

in Table 7.1 and reveal olivine compositions ranging

Fo90.14-Fo91.33, thus illustrating the dependance of the

calculated olivine composition on the assumed Fe_2O_3/FeO

ratio.

The main conclusions that can be made from this survey

are, firstly, there is at present no agreement on the precise Fe_2O_3/FeO ratio applicable to basic magmas, and secondly that conclusions based upon assumed or estimated Fe_2O_3/FeO ratios (eg. the transitional nature of the Rhum Suite based on normative parameters) should be be independently checked by alternative procedures when possible.

Normalisation of an analysis to 100% volatile free with a fixed Fe_2O_3/FeO ratio actually alters the values quoted in an original rock analysis in an   attempt to reduce the effects of alteration when discussing magmatic processes. A complimentary approach is to assess the mobility of a major oxide or trace element during an alteration process, thus giving an indication of its reliability as a petrologic tool.

Several different types of alteration process have been recognised. They can operate simultaneously or independently and each process induces a different geo-chemical effect. The three main types are:

   (i) Weathering

  (ii) Hydrothermal alteration caused by the circulation

       of groundwater in convection systems around

       magma chambers.

 (iii) Zeolitisation attributed to circulation of

       alkaline solutions in basaltic lava piles.

The effects of weathering on the geochemistry of the rocks

presented in this study were reduced to a minimum
during the sample preparation (Appendix 7.1) as
considerable efforts were made to use unweathered
material. Amygdaloidal zeolites are not common in the
Rhum dolerites but interstitial zeolites are locally
abundant in several of the low MgO gabbros. This
suggests that zeolitisation has not had a profound
effect on the chemistry of the dolerites but may be
more important in the low MgO gabbros.

The diagnostic petrographic features of hydro-
thermal alteration have been outlined by Morrison (1978)
who recognised three stages:

1) Alteration of olivine to serpentine, chlorite and
   iron oxides.

2) Albitisation of plagioclase with patchy development
   of calcite and epidote and re-equilibration of the
   titanomagnetite to Fe-Ti oxides and sphene.

3) Total re-equilibration of the igneous mineralogy to
   a quartz-chlorite-albite-amphibole-sphene-epidote
   assemblage.

Although many of the Rhum minor intrusions have suffered
breakdown of olivine to serpentine-chlorite mixtures
(see Chapter 4)   development of albitised plagioclase,
sphene and epidote is not common. None of the specimens

have suffered total re-equilibration of their igneous

mineralogy.

The composition of the basalt suffering alteration

is important as this affects the location of certain

elements within the rock matrix (Humphris et al., 1978).

The siliceous interstitial glass in tholeiite basalts

is metastable and is susceptible to change during zeo-

litisation or hydrothermal alteration. Consequently,

element mobility in tholeiitic basalts is greater than

element mobility in transitional and alkaline basalts

(Humphris et al., 1978, Morrison, 1978).

Studies of element mobility in subaerial and sub-

marine basalts has shown that TiO_2, P_2O_5, Nb, Zr and Y

are immobile in basalts which have suffered moderate

hydrothermal alteration and/or zeolitisation and are

only slightly mobile in extreme cases (Pearce and Cann

1971, 1973; Hermann et al., 1974; Smith and Smith 1976,

Ridley et al., 1974, Floyd and Winchester, 1975; Wood

et al., 1976; Morrison, 1978). In addition Al_2O_3 and Cr

are also considered to be stable under alteration

(Pearce and Flower, 1976; Humphris and Thompson, 1978).

SiO_2, MgO, CaO, FeO, Fe_2O_3, K_2O, Sr, Ba and Rb

have been shown to mobile (Smith and Smith 1976, Ridley

et al., 1974; Wood et al., 1976; Humphris and Thompson, 1978;

Humphris et al., 1978; Morrison, 1978). However, the degree

of mobility is dependent on several factors (eg. basalt composition, type of alteration, degree of alteration). Of the cited studies it is the works of Wood et al. (1976), Morrison (1978) and Humphris et al. (1978) which are most relevant to this study as these authors have assessed element mobility under non-spilitic alteration conditions. The conclusions that can be drawn from these studies are that SiO_2, MgO and Rb may have been mobile and that K_2O, Sr and Ba probably were mobile during the hydrothermal alteration of the Rhum minor intrusions. However, it should be borne in mind that the transitional nature of many of these Rhum rocks probably makes them less prone to chemical change than tholeiitic basalts. One effect which has not yet been assessed, but may be relevant to any subsequent studies of element mobility, is that hydrothermal effects are most pervasive in the gabbros, suggesting that the grainsize of a rock may also determine its susceptibility to hydrothermal alteration. Specimens which exhibit features attributable to mild thermal metamorphism (blackening of the feldspars, clinopyroxenes and olivines by exsolved opaque oxides) have not been used to illustrate geochemical variation wher—ever possible.

Summary

The effects of postmagmatic alteration on the geo-chemistry of the Rhum minor intrusions has been minimised by:

(i)   Removing all weathered surfaces from specimens prior to analysis and discarding dolerite specimens in which albitisation of the plagioclase has occurred.

(ii)   Using analyses normalised to 100% volatile free with a fixed Fe_2O_3/FeO oxidation ratio where appropriate (a corollary of the analytical technique employed in this department).

(iii) Cautious interpretation of the variation exhibited by the K_2O, Sr, Rb and Ba data. The large variation exhibited by the SiO_2 and MgO data is judged to reflect large primary variations which have only been slightly effected by secondary processes (ie. the trends developed by the SiO_2 and MgO data are a primary feature in which secondary alteration has produced scatter around the original trend).

II. Basic and Ultrabasic rocks

Introduction

This section describes the geochemical variation exhibited by the dolerite groups 1 to 7 and attention is also focussed on the gabbroic rocks, although only the geochemistry of the high MgO gabbros is considered in detail. The group 7 rocks contain abundant plagioclase phenocrysts and consequently do not approximate liquid compositions and   have not been represented on the variation diagrams. The group 1 picrites exhibit various quantities of modal phenocrystic olivine (ranging 1-50%). However, the specimens with abundant phenocrystic olivine have been included on several of the diagrams as they highlight certain geochemical features. The MgO content of rocks believed to have occurred as ultrabasic liquids on Rhum is discussed later. (p. 251)

a) Groups 1 to 4

That magnesian olivine has played a considerable but not exclusive part in the geochemical variation of Groups 1, 2 and 3 is clear from Fig. 7.1 in that high MgO rocks show a systematic decrease in MgO with increasing iron enrichment. The olivine control line for the Kilauean 1959 summit eruption is also represented on Fig. 7.1. The various MgO and $Fe_2O_3^*$ contents of the

*total iron as Fe_2O_3

magmas defining this line are attributed solely to the

varying abundance of phenocrystic magnesian olivine (Fo83)

in these lavas (Gunn 1971, Murata and Richter 1966) and

the data points defining this line all fall very close

to it. This would suggest that olivine control is the

only feature contributing to the trends of groups 1, 2

and 3 in Fig. 7.1.

However, reference to Fig. 7.2 reveals that there is

considerable variation in $Fe_2O_3^*$ for a given MgO content.

The Kilauean 1959 olivine control line is also represented

in Fig. 7.2 and once again the points defining this

control line fall very close to it. The spread of the

data points of groups 1 to 3 on Fig. 7.2 suggests that

the geochemical variation of MgO and $Fe_2O_3^*$ in these

rocks is not attributable to olivine fractionation alone.

Three different types of picritic magmas were defined

on petrographical grounds (Chapter 4, p. 94) and this

discrimination is substantiated geochemically. For

example, the three picritic types are characterised

by differing Ni contents for a given MgO value (Fig.7.3)

in addition the Type 1 and Type 2 picrites can be

differentiated by comparison of their Ni/Cr ratios, the

former generally contain more Ni for a given Cr value

(Fig. 7.4). The picrite specimen 77024 does not conform

geochemically, with any of the picrites types (note, for

example, the exceedingly high Ni values in Fig. 7.3)

and thus must be viewed as an independent magma type.

This internal geochemical variation in the group 1

picrites further supports the conclusion that olivine

fractionation alone (or with Cr spinel) cannot account

for the spread of $Fe_2O_3^*$ values in the group 1 magmas.

The variation of the Al_2O_3 and CaO contents of the

dolerite groups 1-4 relative to MgO can be seen in

Fig. 7.5 and Fig. 7.6. In general, the group 1 rocks

show systematic increases in both Al_2O_3 and CaO with

decreasing MgO. A systematic increase in CaO with

decreasing MgO is also a feature of the group 2 rocks

and despite the scatter of the data points a general

increase of Al_2O_3 with decreasing MgO can be discerned

in the group 2 rocks plotted on Fig. 7.5. The Al_2O_3

and CaO contents of groups 3 and 4 show little systematic

variation with MgO, indeed the group 4 rocks exhibit widely

varying Al_2O_3 contents for a given MgO content. However,

close examination of the group 4 data reveals that the

rocks with lower MgO values generally possess lower CaO

contents. The group 3 rocks exhibit greater geochemical

homogeneity than group 4 - this is a clear feature in

Fig. 7.5 and Fig. 7.6 and also in Fig. 7.2. In the

latter variation diagram the group 4 rocks exhibit a

systematic increase in $Fe_2O_3^*$ with decreasing MgO.

Having established the relationships between the

MgO and the $Fe_2O_3^*$, Al_2O_3 and CaO contents of groups 1,

2, 3 and 4 it is useful to characterise their Al_2O_3 and

CaO variation relative to their iron enrichment ($Fe_2O_3^*$/

$Fe_2O_3^*$+ MgO) ratios. The CaO contents of the group 1

rocks show systematic linear increases with increasing

iron enrichment in Fig. 7.7. However, only a general

non-linear increase in Al_2O_3 can be discerned in

Fig. 7.8 emphasising once again that there are several

different magma types represented in group 1. The

group 2, 3 and 4 rocks exhibit a range of CaO and Al_2O_3

values for a given iron enrichment ratio in Fig. 7.7

and Fig. 7.8 respectively. However, viewed as a whole

these basic rocks exhibit a fairly constant range of

CaO and Al_2O_3 contents over a wide range of iron enrich-

ment values (approximately 0.45 to 0.625); with a slight

decrease in the CaO and Al_2O_3 contents when the iron

enrichment ratio exceeds 0.625.

The principal geochemical features described above

can be summarised thus:

(i) The group 1 rocks and the group 2 rocks possess

internal variation in CaO, Al_2O_3 and $Fe_2O_3^*$ which

cannot be explained by olivine fractionation alone.

The group 2 rocks occasionally contain plagioclase macro-

phenocrysts (Chapter 4, Table 4.1) but these are

not encountered in the group 1 rocks. Thus, whilst plagioclase may be responsible for some of the compositional variation in group 2, the CaO and Al_2O_3 variation in group 1 can be explained only by invoking control by the phases plagioclase and/or aluminous clinopyroxene neither of which are found as phenocryst phases in this group. The variation of $Fe_2O_3^*$ values for a given MgO content in Fig. 7.2 can only be attributed to an iron bearing phase other than olivine , possibly pyroxene.

(ii) The group 4 rocks show a systematic decrease in MgO with increasing $Fe_2O_3^*$ which cannot be explained by fractionation of forsteritic olivine (Fig. 7.1 and 7.2), thus it is necessary to invoke control by either a less magnesian olivine or control by MgO in pyroxene. It is difficult to explain the sharp change in slope between the MgO rich groups 1 - 3 , and the group 4 rocks in Fig. 7.1 by change in olivine composition alone; thus, pyroxene control over the group 4 trend appears reasonable. However, the petrographic data presented in Table 4.1 shows clinopyroxene is a rare phenocryst phase in the group 4 rocks and orthopyroxene is absent.

(iii) The group 3 and 4 rocks possess an essentially constant range of CaO and Al_2O_3 values over a wide

range of iron enrichment ratios (Figs. 7.7 and 7.8).
This relationship precludes orthopyroxene control
as this would increase the CaO values with increasing
iron enrichment. Extensive plagioclase fractionation
would cause Al_2O_3 and CaO depletion whilst holding
the iron enrichment ratio constant, thus plagioclase
control can explain some of the variation of CaO
and Al_2O_3 perpendicular to the trend but cannot explain
the trend itself. The CaO and Al_2O_3 depletion in
the group 4 rocks with iron enrichment ratios greater
than 0.625 is possibly attributable to plagioclase
fractionation.

The plot of CaO against the CaO/Al_2O_3 (Fig. 7.9)
shows that the CaO/Al_2O_3 ratio in the group 2, 3 and 4
rocks decreases systematically with decreasing CaO. This
trend results from depletion of both CaO and Al_2O_3 with CaO
being more rapidly depleted than Al_2O_3. This relationship also
precludes extensive calcic plagioclase control over the
Al_2O_3 and CaO levels in these rocks, as plagioclase contains
more Al_2O_3 than CaO. The group 1 picrites also show a
systematic relationship between CaO and Al_2O_3. In this
latter trend CaO depletion relative to Al_2O_3 is less
marked. A range of plagioclase compositions have been
plotted in Fig. 7.9 and indicate that plagioclase can
account for the scatter across the trend but cannot account

for the trend itself.

Fig. 7.10 plots CaO against Al_2O_3 for groups 2 to 4,
despite the scatter a general increase in Al_2O_3 with
decreasing CaO can be discerned. The points X1 and X2
on Fig. 7.10 are the calculated residual liquid compositions
following 25% subtraction of a calcic pyroxene (CaO = 20%,
Al_2O_3 = 2%) and an aluminous calcic pyroxene (CaO = 20%,
Al_2O_3 = 10%) respectively from the high lime liquid X.
The slight Al_2O_3 enrichment with decreasing CaO can thus
be best explained by aluminous clinopyroxene control.
The point X3 is the calculated residual liquid composition
after subtraction of 20% plagioclase (An76) from the high
lime liquid and illustrates that calcic plagioclase alone
cannot control the observed trend. It is possible that
the trend developed in Fig. 7.10 is the result of the
joint influence of both plagioclase and a diopsidic
pyroxene. The general increase in Na_2O, Sr and Ba with
decreasing CaO in the group 2-4 rocks implies that plagio-
clase has not played a significant role in their genesis,
consequently it is suggested that the trend in Fig. 7.10
is largely the result of aluminous clinopyroxene control.
The group 4 rocks with approximately 9-10 wt% CaO and
13.5 wt% Al_2O_3, are Al_2O_3 depleted when compared with
other rocks with similar CaO contents. This suggests
that plagioclase has played a role in the genesis of the
former.

The compositions of diopside and the compositional range of the sparse clinopyroxene phenocrysts occurring in groups 3 and 4 along with the projected trend for groups 2 to 4 have been plotted in the inset of Fig. 7.9. The depletion in CaO suggests that the controlling phase was a Ca-rich clinopyroxene as CaO-poor clinopyroxenes (with CaO approximately 13-14 wt% CaO) would not produce marked CaO depletion. However, the Ca-rich clinopyroxene phenocrysts plotted in Fig. 7.9 and 7.10 contain insufficient Al_2O_3 to produce the observed trends. A suitable clinopyroxene would contain 18-20 wt% CaO and 8-10 wt% Al_2O_3. Pyroxenes with this sort of composition have been recorded in plutonic nodules occurring in alkali basalts (e.g. Binns et al., 1970). The increase in Fe_2O_3* with limited MgO depletion exhibited by the group 4 rocks (Fig. 7.2) indicates that this controlling pyroxene probably had a high MgO/FeO ratio.

Some of the trace element data for groups 1 to 4 is presented in Fig. 7.11 and the major oxides K_2O and TiO_2 are plotted against Zr in Fig. 7.12. The group 1 rocks are characterised by low abundances of Zr, Nb and Ba but Sr can reach the 300ppm level; K_2O and TiO_2 are generally low. The groups 2 to 4 rocks exhibit systematic increases in Nb and Y with increasing Zr, Ba is generally low but increases to the 500ppm level in some of the group 4 rocks.

Sr   and TiO$_2$ shows a somewhat scattered but general

increase with increasing Zr, K$_2$O is generally low in all the

basic rocks. The K$_2$O content of the nepheline-normative

members of group 4 are anomalous in that K$_2$O is generally

lower than in the hypersthene normative specimens, this

is also a feature of the Skye Main Lava series basalts

(Thompson et al. 1972) and a possible explanation is

discussed later.

b) Groups 5 and 6

Introduction

It was suggested in Chapter 5 (p.135) that the Rhum

dolerite groups 5 and 6 (and by inference the Rhum lavas)

postdate the mantle partial melting event which gave rise

to the Rhum Central Complex and its associated minor

intrusion suite. This suggestion is based on five main

lines of evidence which are:

(i) The similarity of groups 5 and 6 to the Preshal

Mhor and the Main Lava Series magma types of Skye

respectively (Mattey et al. 1977, Thompson et al. 1972)

and their dissimilarity to the magma types in the Rhum

Minor Intrusion Suite.

(ii) The dissimilarity of the Rhum lavas and the Rhum

minor intrusion suite.

(iii) The extensive time interval represented by the

conglomerates underlying and interbedded with the Rhum

Lava succession.

(iv) The relative ages of Rhum and Skye deduced from

both geological and geophysical evidence (p. 235).

(v)   The disposition of the group 5 and 6 dykes relative

to the Skye dyke swarm.

Before comparing groups 5 and 6 with the basic

magmas of Skye it is necessary to discuss the term

"magma type" in its Hebridean context.   Three magma

types have been recognised on Skye and have been referred

to as the Skye Main Lava Series magma types, the Fairy

Bridge magma type and the Preshal Mhor magma type (Mattey

et al. 1977).   These authors noted that there was

considerable geochemical variation within each type

but showed that each possessed a distinctive (and there-

fore diagnostic) geochemical fingerprint.   Whilst

recognising the overall geochemical similarity of the

Preshal Mhor magma type to low alkali — high calcium

olivine tholeiite magmas in the Mull dyke swarm, these

authors were deterred from grouping the Mull and Skye

dykes of similar overall chemistry into a single overall

magma type because they considered it possible that the

Mull dykes were not chemically identical to those on Skye.

In a more recent review, Thompson (1978) has further

emphasised this point and states that:

"It may be most satisfactory at present to treat
each geographically-distinct igneous suite as a separate
local magma type and postpone the Province-wide correlation
of these until adequate data are available". It is
evident that, despite their similarities, each of the
Tertiary centres in Northwest Scotland and Northern
Ireland, is in many respects unique, therefore it is
reasonable to suggest (as Mattey et al. 1977 and Thompson
1978 have done) that each centre may possess magma types
unique to that centre; however, there is a current trend
in the research on these Tertiary Central Complexes to
equate any refractory basalt composition with the Preshal
Mhor magma type of Skye (eg. Skelhorn et al. 1979, Gamble
1979). It will be shown later that refractory basalt
magmas do occur on Rhum but cannot be equated with the
Preshal Mhor magma types as defined by Mattey et al. 1977.
It is suggested that research workers follow the philosophy
outlined by Thompson (1978) and treat each centre as an
individual entity rather than invoking the Skye magma
succession as the "norm" (as done by Gamble 1979) and
assess in detail the relationships of the magmas within
each complex before making sweeping comparisons with
other centres.

The chemical analyses of all the group 5 dolerites are presented in Table 7.2 along with an average analysis and the range of the major oxides and trace elements of the Preshal Mhor magma type and the refractory magmas found on Rhum. The diagnostic features of the Preshal Mhor magma type (Mattey et al. 1977) are:

(i)   CaO > 11.00 wt%.

(ii) Low Na_2O, K_2O, TiO_2, P_2O_5, Nb, Zr and Y abundances.

(iii) Distinctive Ti/Y and Zr/Y ratios.

Visual inspection of the analyses reveals that the major oxides and trace element abundances of group 5 dykes all lie with the range of values present in the Preshal Mhor magma type and the values quoted in the group 5 specimens closely resemble the average quoted values of 15 represent- ative Preshal Mhor magma type analyses. An exception to this is the K_2O abundance in the group 5 dolerites which is consistently lower than the average Preshal Mhor magma type value. The diagnostic Ti/Y and Y/Zr ratios of the group 5 specimens also lie within the ranges quoted for the Preshal Mhor magma type. It has been suggested by Sun et al. (1979) that Zr and TiO_2 approximate middle REE

in behaviour and Y approximates heavy REE in behaviour.

These characteristic ratios are thus a function of source

composition and more importantly the depth and degree of

partial melting thus explaining the importance which

Mattey et al. (1977) place on these parameters. Inspection

of the gabbro analyses presented in Table 7.2 reveals

that refractory basalt magmas do occur on Rhum and are

characterised by CaO, Na_2O, K_2O, TiO_2, P_2O_5, Zr and Y

abundances similar to the Preshal Mhor magma type.

However, all but one of these gabbros possess Ti/Zr

ratios outside the diagnostic values for the Preshal Mhor

magma type and all but one have Y/Zr ratios distinctly

lower than those found in the Skye magmas. Thus, the

group 5 dykes are extremely similar, if not identical to

the Preshal Mhor magma type of Skye but are dissimilar to

the Rhum refractory basalt types. When compared with

other dolerites in the Rhum suite, group 5 are character-

ised by higher Al_2O_3 and by much lower MgO and Ni values

than other olivine phyric dolerites.

The group 6 dolerites are chemically heterogeneous,

although three of the specimens are very similar (and

may be sampled from the same dyke, see p. 297). An

average of these has been presented along with other

group 6 dolerites and some Skye Main Lava series analyses

in Table 7.3. One of the specimens (SR211) is slightly

nepheline normative, the remainder are hypersthene
normative.

The group 6 dolerites are only found cutting the
Rhum Lavas. They are geochemically distinct from the
other Rhum dolerites in that all the group 6 dykes have
low MgO, Ni and Cr and higher Na_2O. In addition, SR211
is characterised by much higher Al_2O_3 than usually found
in Rhum basic magmas (cf. group 5); SR141 and the average
analysis of SR159, SR182 and SR282 (analysis 7, Table 7.3)
have distinctly higher K_2O, Ba and Rb than other members
of the Rhum dolerite suite. They compare more favourably
with some of the low MgO gabbros (eg. 77261) but the
latter have suffered fairly extensive hydrothermal
alteration whereas all but one of group 6 (SR141) are
exceedingly fresh.

It is not possible to correlate group 6 with basic
magmas from Skye with the same degree of certainty as
group 5 because only limited trace element data for the
Skye Main Lava Series have been published. However,
inspection of the analysed Skye Main Lava Series
(Thompson et al. 1972) supplemented with analyses supplied
by I. Williamson (unpublished data) has revealed analyses
of the Skye Main Lava Series basalts comparable to the
Rhum group 6 dolerites. The similarity of SR211 and SK291
(Table 7.3) is quite striking and SK932 and SK280 are also

quite similar. Analysis 7 (Table 7.3) compares

favourably with 751218 and SK956. The similarity of

SR141 to 751201B is less convincing in that

Fe_2O_3 in SR141 is slightly higher, TiO_2 is considerably

higher and K_2O is appreciably lower, however the overall

impression is that group 6 compare favourably with the

Skye Main Lava Series and are dissimilar to the remainder

of the Rhum Minor intrusion suite.

The relationships between the Rhum Lavas and the

Rhum minor intrusion suite are discussed more fully in

Chapter 8. The main conclusion that can be drawn from a

comparison of the Rhum lavas and the Rhum minor intrusions

is they are geochemically dissimilar, as the high MgO, CaO,

Ni and Cr fingerprint of the basic minor intrusions cannot

be discerned in the basic lavas.

The conglomerates underlying and interbedded with

the Rhum Lava succession contain abundant examples of

all the rock types represented in the Rhum Central Complex

(Chapter 1, p. 11). The common occurrence of allivalite

clasts confirms that the central complex was unroofed

prior to the eruption of the lavas. Petrographic exam-

ination of some of the dolerite cobbles has shown (as

expected) that specimens of the Rhum dolerite suite also

occur in these conglomerates. Specimen SR140/3 is petro-

graphically identical to some of the petrographically

distinctive big feldspar dolerites (eg. 77047, 77258)
and the mildly plagioclase-clinopyroxene phyric specimen
79012 is petrographically similar to some of the group 8
specimens. These relationships indicate that the cover
over the central complex and its associated minor intrusions
was removed by erosion during the Tertiary, postdating the
emplacement of the layered ultrabasic rocks and predating
the eruption of the lavas.

It is suggested here that the period of time represented
by the layered ultrabasic emplacement-lava eruption interval
was long enough to allow extinction of the Rhum partial
melting event. The actual duration of this time interval
can only be assessed unequivocally by radiometric dating,
however a more qualitative approach can be made by
analogy with the erosion rates encountered in more recent
volcanoes which have been radiometrically dated.

Erosion rates are dependent on two main factors,
firstly lithology and secondly climatic conditions. It is
difficult to estimate the thickness of the strata originally
overlying the Rhum central complex but the presence of
inverted tridymite in some of the partially melted
Torridonian sediments puts an upper limit in the region
of 3.0 Km (depths calculated using the stability field of
tridymite figured in Deer et al. 1966 p.348, with an
upper temperature limit of 1200°C and a rock density of 2.73).

A depth of 2 km was suggested by Dunham (1970, fig. 1, p. 26). This is based on the assumption that the roof of the magma chamber coincides with the Torridonian-Lewisian unconformity. Emeleus (in press) has pointed out that the Lewisian cobbles in the conglomerates do not show the effects of partial melting characteristic of the Rhum Lewisian at the present erosion level. This suggests that a considerable thickness of Lewisian gneisses overlay the central complex and 2 km may be viewed as a minimum value.

The rocks overlying the central complex thus comprised; Lewisian gneiss and Torridonian arkose sediments, in addition the possibility that a lava pile was also present must be taken into account if Brown's (1956) open system fractionation model for the Rhum Magma chamber is valid.

Evaluation of the Tertiary palaeoclimate is intrinsically subjective, however the presence of laterite weathering deposits in the lava successions of Skye (Anderson and Dunham 1966) and Antrim (Emeleus and Preston 1969, p.21) in conjunction with the presence of active water erosion indicated by the river systems envisaged in the Tertiary by Geike (1896) and Emeleus (1973) suggests an environment in which erosion rates will have been high. This conclusion is corroborated by

the presence of felsite boulders up to 2 m diameter in the Rhum conglomerates (Emeleus pers. comm.).

The erosion rates on the Indian Ocean volcanic island of Reunion have been assessed by McDougal (1971) who found them to be rapid, in the order of 680-850 cm/1000 years. In addition he showed that the plutonic rocks (syenites) in the core of the extinct volcano (Piton des Neiges) had been uncovered within the last 0.2 my and probably within the last 0.07 my indicating how quickly a central complex can be unroofed under favourable circumstances.

It is difficult to evaluate whether the erosion rates over the last 0.07 my on Reunion can be applied to the Rhum Tertiary situation. Lateritic boles are present in the lava sequence of Reunion (McDougal, 1971) and in Tertiary lavas of Great Britain, thus there are similarities but Reunion has sub-tropical oceanic island climate whereas Rhum will probably have been more continental. The rainfall on Reunion is likely to have been higher than the Tertiary rainfall on Rhum and as the palaeoclimate suggested for the British Tertiary (Anderson and Dunham, 1966) is analogous to that found in the Northern Mediterranean at the present day. In view of these differences it is probable that any calculations based on the erosion rates of Reunion will give a minimum estimate of the time

interval between the emplacement of the ultrabasic

complex and the eruption of the lavas on Western Rhum.

The calculations pertaining to a depth of cover of

either 1.5 km, 2.0 km and 2.5 km and with erosion rates

of 680 or 850 cm/1000 years are presented in Table 7.4.

The minimum value (0.176 my) calculated from a depth

of cover of 1.5 km and an erosion rate of 850 cm/1000

year is a considerable period of time and would probably

be sufficient for a partial melting event to become

extinct, the actual ultrabasic emplacement-lava eruption

interval is probably greater than the quoted minimum

estimate.

Gravity surveys have revealed considerable positive

Bouguer anomalies over Rhum and Skye which are attributed

to bodies of dense basic rocks approximately 10 km to

20 km diameter respectively which extend to depths of

approximately 15 km (McQuillin and Tuson 1963, Bott and

Tuson 1973). Magnetic surveys have revealed that the

basic rocks underlying Rhum are characterised by a

reversed magnetic anomaly whereas the basic mass under-

lying Skye is reversely magnetised at depth beneath the

Cuillins but is normally magnetised under the Redhills

(Bullerwell, 1972). The relationships indicate that

the Skye centre spans a magnetic reversal whereas Rhum

does not, thus the centres are of different (although

possibly overlapping) age.

It is of course a prerequisite to the hypothesis advocating a Skye source for the group 5 and 6 dolerites that the Skye Tertiary igneous centre (or at least the generation of the Skye Main Lava Series and Preshal Mhor magma types) postdate the Rhum centre. The relative ages of these Skye magma types have been assessed by Mattey et al. (1977) who considered the Preshal Mhor magma type to be generally younger than the Skye Main Lava series magma type.

The evidence concerning the relative ages of the Tertiary centres of Rhum and Skye is sparse and equivocal. A radiometric (K/Ar) age for the Western Granophyre is 58 my (Emeleus pers. comm.), this compares with K-Ar dates 59 my to $\sim$ 55 my and Rb-Sr dates of $52^{+}_{-}3$ and $51^{+}_{-}4$ for the Skye Lavas and the Redhills granophyres respectively (Brown and Musset 1976). These authors consider the young ages (< 55 my) for the Skye lavas are due to resetting by hydrothermal alteration associated with the Redhills granophyres and considered the dates of $59.2^{+}_{-}0.7$ and $59.3^{+}_{-}1.0$ my from lavas outside the O^{18} depleted hydrothermal aureole (Taylor and Forrester 1971) to be more realistic. This would suggest the Skye Lavas are coeval with the Western Granophyre.

Conflicting evidence comes from the interbasaltic

conglomerates located towards the base of the Skye lava
series in southwest Skye. These conglomerates contain
granophyre pebbles which cannot be derived from the Skye
Redhills granophyres as field evidence has shown that
these postdate the lavas. Some of the granophyre pebbles
are petrographically similar to the granophyres in the
Rhum granophyres   (I.T. Williamson pers. comm.). In
view of the presence of granophyre pebbles in the inter-
basaltic conglomerates of Canna which are petrographically
identical to the Western Granophyre of Rhum (Emeleus 1973)
and the sub-marine connection between the lava piles of
Skye and Canna along the Canna Ridge (Binns et al. 1973)
it seems reasonable to suggest that the granophyre pebbles
in the Skye interbasaltic conglomerates are derived from
Rhum.

To summarise, the relative ages of the Rhum and Skye
centres assessed by radiometric methods would suggest that
Rhum and Skye are coeval whereas the bulk of the geological
evidence favours Rhum as the older centre. Evaluation of
radiometric ages is extremely difficult as indicated by
the degree of error on published analyses; in addition,
the resetting of ages by hydrothermal activity must also
be taken into account. In view of these known difficulties of
radiometrically dating the British Tertiary centres it is
perhaps not surprising that these dates conflict with the

geologic evidence. The bulk of the evidence available

at this time suggests that the Rhum and Skye centres are

of different age and that Rhum is the older of the two.

The geometry of the Skye dyke swarm was determined

by Speight (1972) and the distribution of the Skye

magma types within the swarm was investigated by Mattey

et al. (1977). These authors showed that the Skye dyke

swarm at the present erosion level consists predominantly

of the Preshal Mhor magma type with subordinate Skye Main

Lava Series and Fairy Bridge type dykes. Furthermore,

Mattey et al. (1977) found that there was spatial geo-

chemical variation across the swarm with the bulk of the

Preshal Mhor type dykes being located within 6 km of the

central axis of the swarm.

The orientation of the dykes cutting the Rhum lavas

relative to the trend of the Skye dyke swarm is presented

in Fig. 7.13 where it can be seen that the Rhum dykes

generally strike NW-SE and span the strike direction of

the Skye dyke swarm. However, only very limited conclus-

ions may be drawn from this observation as the Rhum sample

population is very small. The Rhum dykes lie approximately

25 km from the centre of the Skye dyke swarm on Sleat and

represent a dilation of approximately 0.66%, thus if they

are members of the Skye dyke swarm they can only be

considered as outliers. Mattey et al. (1977) located dykes

of Preshal Mhor and Skye Main Lava series magma type
up to 18 km and 16 km respectively from the central
axis of the Skye swarm. Their sampling range extended
to only 18 km from the central axis of the swarm thus
the possibility of the Rhum dykes being outliers of
the Skye swarm cannot be rejected on the basis of their
observations alone

Summary

The evidence discussed previously shows that the
group 5 and group 6 dolerites are very similar to the
Preshal Mhor and the Main Lava Series magma types of
Skye. A period of time greater than 0.176 my elapsed
following the emplacement of the layered peridotites
and prior to the eruption of the lavas of western Rhum,
this time interval is judged sufficient to allow
extinction of the Rhum partial melting event. Although
the relative ages of the Rhum and Skye Centres have not
been unequivocally determined the bulk of the evidence
available at this time suggests that Rhum is the older
centre. Although the Rhum dykes cutting the lavas are
displaced 25 km from the centre of the Skye swarm they
represent less than 1% dilation and could be outliers
of the Skye swarm. Their general NW-SE strike direction
is compatible with the regional dyke swarms of both Rhum

and Skye (Speight, 1972) and cannot be cited as evidence in favour of a Skye or Rhum origin.

In conclusion, although there are many uncertainties pertaining to the hypothesis that Rhum group 5 and group 6 dykes are outliers of the Skye regional dyke swarm it is suggested the group 5 and group 6 dykes are genetically related to the Skye partial melting event and not the Rhum partial melting event.

c) Group 7

The outstanding petrographic feature of group 7 is the presence of abundant (up to approximately 50%) subequant plagioclase phenocrysts. The compositions of the plagioclase phenocrysts in the three specimens investigated by microprobe analysis are very similar and only mild zoning (An88-An84) was detected. If these dolerites were the result of in situ crystallisation of an aluminous magma, one would expect the phenocrysts to exhibit substantial zoning; furthermore, the subequant faces suggest that these crystals grew in a low nucleation density environment in which the effect of adjacent crystals on the growing faces was minimal. The large plagioclase phenocrysts contrast markedly with the extremely fine-grained groundmass, thus it is suggested that these dykes are produced by intrusion of a magma carrying

abundant cumulus plagioclase.

The composition of the interstial^ti^ liquid in 77258 was calculated by subtraction of a composition equivalent to the observed modal percentage of plagioclase and the result is presented in Table 7.5. This interstitial liquid is SiO_2 enriched and Al_2O_3 depleted suggesting that some of plagioclase (possibly overgrowths on original cores) is not cumulus. It is difficult to be sure what proportion of the plagioclase in these rocks is non cumulus, however the lack of detected zoning suggest it is not considerable.

One possible source for these cumulus plagioclase crystals is the high level magma chamber associated with the Rhum central complex. However, there is a distinct lack of other phenocryst phases in the group 7 dolerites thus it is unlikely that they are produced by flushing out of the magma chamber floor as one would expect additional phases to be involved. An alternative explanation is that they represent a magma fraction of plagioclase flotation cumulates as this adequately explains the lack of other cumulus phases.

d) Gabbros

The high MgO gabbros contain approximately 10-12 wt% MgO and are consequently MgO depleted when compared with the dolerite groups 1 and 2 (Fig. 7.1, 7.2). They

are characterised by slightly higher Al_2O_3 but similar

CaO contents relative to the group 2 to 4 dolerites in

Fig. 7.5 and Fig. 7.6 respectively. They also possess

lower iron enrichment ratios than the majority of the

group 2-4 dolerites in Fig. 7.7. They generally contain

higher CaO for a given CaO/Al_2O_3 ratio than the group

2-4 dolerites in Fig. 7.9 but follow the trend produced

by the dolerites in this diagram. Similarly they exhibit

a slight increase in Al_2O_3 with decreasing CaO in Fig.

7.10, an exception being the aluminous gabbro specimen

77104.

An important geochemical feature of these high MgO

gabbros is the exceedingly low abundance of the incom-

patible trace elements Zr, Nb, Y and Ba and the incom-

patible major oxides TiO_2 and K_2O. This is a clear

feature of Figs. 7.11 and 7.12 respectively.

The low abundance of the incompatible elements

suggests that these magmas were produced by a high degree

of partial melting. In addition their low Ni content

(41 to 215ppm) suggests that they have also undergone

significant olivine fractionation. The sympathetic

relationship of CaO and Al_2O_3 in Figs. 7.9-7.10 may be

attributable to either differing degrees of partial

melting of mantle material containing aluminous calcic

clinopyroxene and/or fractionation of an aluminous clino-

pyroxene. This is discussed in more detail in section

five (p.262).

The low MgO gabbros are characterised by MgO contents

of less than 9.0 wt%, their differentiated character

when compared with the high MgO gabbros and the dolerite

groups 2 to 4 is clearly visible in several of the

variation diagrams (eg. Fig. 7.1, 7.2, 7.5 and 7.7).

However, their high CaO contents distinguish them from

the intermediate rocks (Figs. 7.6 and 7.7), as do their

Zr, Y and TiO_2 contents (Fig. 7.11 and 7.12). The Ba

and Sr data in Fig. 7.11 must be viewed cautiously as

these gabbros have suffered significant hydrothermal

alteration (p. 215). Their CaO and CaO/Al_2O_3 values are

juxtaposed with the group 2-4 dolerites in Fig. 7.9.

E) Peridotites

An average analysis and the range of compositions

encountered in the peridotite plugs is presented in

Table 7.6. The compositional variation in Fig. 7.14

largely reflects the abundance of modal magnesian olivine.

The scatter around the trends in Fig. 7.14 are attributable

to variations in the proportion of plagioclase and clino-

pyroxene in the groundmass of these peridotites, as

plagioclase is a ubiquitous interstitial phase whereas

clinopyroxene may or may not be absent (Chapter 4, p.113).

A possible source for the magmas which gave rise to the
peridotite plugs is discussed later. (p. 260).

II. Intermediate rocks

Introduction

The differentiates exhibit considerable geochemical
variation. Two main series were recognised in Chapter 3
a series of differentiates with alkalic affinities
(groups 10 to 12) and a series with tholeiitic affinities
(groups 8 and 9), the gabbroic differentiates are also
tholeiitic in affinity. These intermediate rocks generally
display sympathetic variation of their major oxides with
increasing SiO_2 content. Although these features have not
been displayed diagramatically in this account this
relationship should be bourne in mind in assessing other
geochemical features described here.

It is clear from Fig. 7.2 that several of the inter-
mediate rocks continue the $Fe_2O_3^*$ enrichment, MgO depletion
trend characteristic of the group 4 rocks. These rocks
have been plotted onto Fig. 7.1   where it can be
seen they continue the trend developed by the group 4
rocks. The remaining differentiates in Fig. 7.2 follow
an $Fe_2O_3^*$ + MgO depletion trend and consequently must
have/been controlled by either a different phase or phases
than those responsible for the iron enrichment trend or
by similar phase(s) of different composition.

Intermediate rocks of the $Fe_2O_3^*$ + MgO depletion trend.

The variation of MgO against $Fe_2O_3^*/Fe_2O_3^*$ + MgO is

presented in Fig. 7.1 where it can be seen that although

the intermediate rocks possess generally similar iron

enrichment ratios to the basic groups 2 to 4, the

differentiates of tholeiitic affinity generally possess

lower MgO for a given iron enrichment ratio than the

basic rocks and the same is true for the more advanced

alkali differentiates (groups 11 and 12); however,

group 10 fall in the same field as the MgO rich group 4

rocks. Some of the relationships in Fig. 7.2 have already

been described but the fact that the group 10 rocks are MgO

rich and lie within the group 4 field is worthy of note,

as is the scatter of both the alkaline and tholeiitic

differentiates along the $Fe_2O_3^*$ + MgO depletion trend.

These relationships suggest that the intermediate rocks

of this trend are controlled by a pyroxene phase poorer

in MgO than that producing the $Fe_2O_3^*$ enrichment trend.

Some of the $Fe_2O_3^*$ depletion may be due to titanomagnetite

control as there is a slight decrease in TiO_2 with

decreasing $Fe_2O_3^*$ in the intermediate rocks (Fig. 7.15).

The plots of MgO against Al_2O_3 (Fig. 7.5) and CaO

(Fig. 7.6) show that the intermediate rocks generally

possess similar levels of Al_2O_3 to the basic rock groups

2 to 4 and show few signs of Al_2O_3 depletion with

decreasing MgO. The aluminous nature of group 12 in

Fig. 7.5 is worthy of note. In contrast, CaO in both

the alkalic and tholeiitic differentiates shows marked

depletion with decreasing MgO in Fig. 7.6. This

sympathetic relation of MgO and CaO precludes orthopyroxene

control but suggests that a Ca-rich clinopyroxene could

control this trend. The lower CaO levels in the

differentiates are highlighted in the plot of CaO against

iron enrichment ratio (Fig. 7.7).

The relationship of CaO to Al_2O_3 in the intermediate

rocks is presented in plots of CaO against Al_2O_3 (Fig.

7.16) and the ratio CaO/Al_2O_3 (Fig. 7.17). The relation-

ships of the various groups (which reflect different

degrees of differentiation) on Fig. 7.16 are complicated,

as there is much greater variation in the levels of CaO

and Al_2O_3 in the differentiates than was encountered in

the basic groups 2 to 4 (Fig. 7.10).

There is a marked decrease in CaO with a slight

decrease in Al_2O_3 with increasing differentiation in

groups 10 and 11. However, group 12 shows extreme CaO

depletion coupled with Al_2O_3 enrichment. Despite the

variation in Al_2O_3 abundance a general trend of a CaO

depletion for roughly constant Al_2O_3 can be discerned in

the tholeiitic differentiates. Fig. 7.17 shows that

there is a decrease in the CaO/Al_2O_3 ratio of the

differentiates with decreasing CaO suggesting that clino-
pyroxene has played a major part in the decrease of CaO
with differentiation in the intermediate rocks.

The CaO depletion and Al_2O_3 enrichment in group 12
can be accounted for by invoking Ca-rich clinopyroxene
as the only controlling phase. However the Al_2O_3 depletion
with increasing differentiation in groups 10 and 11 and
the constancy of Al_2O_3 with CaO depletion in the tholeiitic
differentiates is best explained by invoking limited
plagioclase control, as one would expect an increase in
Al_2O_3 (cf. group 2 to 4) if clinopyroxene were the only
controlling phase.

These hypotheses can be assessed by referring to the
trace element data presented in Figs.7.11,7.12. Zr is
used as a fractionation index in these plots.

A general feature of these plots is a systematic
linear increase of both Nb and Y in the intermediate
rocks with increasing Zr. There is considerable scatter
of the Sr and Ba data which is probably due in part to
alteration effects. Despite the scatter, Sr generally
shows a slight initial increase with increasing Zr
relative to the basic rocks, then maintains a roughly
constant abundance with increasing Zr. Exceptions to
this are the group 10 rocks with high Sr ($\sim$ 400 ppm)
at the Zr 130 ppm level and the slight increase of Sr

in the group 12 rocks. Ba exhibits similar relationships
to the Sr data in that Ba increases and then maintains
roughly constant values with increasing Zr, however the
high Ba rocks ($\sim$ 500 ppm) at the 125 ppm Zr level are
less well marked and the group 12 rocks are distinctly
separate from the other differentiates. No distinction
between the alkaline and tholeiitic differentiates can
be made using the Nb and Y data, however the tholeiitic
differentiates generally possess lower Sr and Ba for a
given Zr value.

The lines M1 and M2 on Fig.7.11 refer to the trends
developed in the group 1 and group 2 lavas of Mull,
(Beckinsale et al. 1978). Note that the general increase
in the Y and Ba with decreasing Zr is the reverse of the
relationship for the Rhum minor intrusions in the case
of Y, and Ba is not nearly so depleted in the advanced
differentiates of Rhum when compared with Mull.

The extent of plagioclase control over the geo-
chemistry of the alkaline rocks can be assessed from
the Sr and Ba data. The group 10 rocks generally have
high initial Sr and Ba abundances but the group 11 rocks
are Zr enriched (ie. more differentiated) and can be depleted
in Ba and Sr relative to group 10. The group 12 rocks
are greatly enriched in Ba relative to groups 10 and 11
and Sr relative to group 11. The Ba and Sr depletion

with differentiation in groups 10 and 11 can be explained

by plagioclase control, the high levels of Sr and Ba in

group 12 coupled with the high K_2O (Fig. 7.12) and Al_2O_3

abundances precludes extensive plagioclase control during

the evolution of these rocks. The fact that Sr is less

abundant in the group 12 rocks than in the group 10 rocks

suggests that the former are not directly genetically

related to group 10. The sharp increase and then roughly constant

values of Ba and Sr with increasing differentiation in

the tholeiitic intermediate rocks suggests plagioclase

control was important in producing the geochemical

variation in the more differentiated specimens.

III.Acid Rocks

The analyses of the four acid minor intrusions are

presented in Table 7.7 along with an average analysis of

the plutonic acid rocks of Rhum and a differentiated acid

dyke from Eigg. Specimens are somewhat similar to the

acid plutonic rocks,however one of the specimens (77180)

is extremely differentiated and is more similar to one

of the felsite dykes of Eigg (Anal.E6, Table 7.7). The

acid rocks of Rhum and the Small Isles (Ridley, 1973)

have_∧been plotted in Fig. 7.18. The Rhum plutonic rocks lie

in a tightly constrained field, the Rhum acid hypabyssal

rocks are less tightly constrained but do not exhibit

the wide variation of the Small Isles acid volcanics.

The origin of the acid magmas of Rhum were discussed by Dunham and Emeleus (1967) and Dunham (1968) who concluded that they were the result of partial melting of Lewisian gneiss. In a review of the Tertiary acid igneous centres,Meighan (1979) noted that if zircon acted as a refractory phase during partial melting of Lewisian gneiss the resulting acid magmas would contain less Zr than the gneiss. Support for this view comes from the experimental work of Watson (1979b) who has demonstrated the low solubility of Zr in peraluminous melts ($\sim$ 100 ppm). The acid plutonic and acid minor intrusionsof Rhum have higher Zr levels than the Lewisian gneisses of Rhum and northwest Scotland (Meighan 1979, Table 6). These relationships support the contention of Meighan (1979) that the Rhum acid magmas may have been produced by fractional crystallisation of a basic tholeiitic magma.

The paucity of intermediate rocks in the Rhum minor intrusion suite (see Fig. 3.1) would argue against the production of the Rhum acid magmas by fractional crystallisation of a tholeiitic parent. Furthermore, one might expect more than one major episode of acid magmatism if the acid magmas are due to fractional crystallisation of a basaltic parent. The high Zr contents of the Rhum magmas are compatible with an origin by partial melting of Lewisian gneiss, if refractory zircon crystals are

removed along with the acid magma when the magma

serparates from its source.

In conclusion the close temporal association and

general similarity of three of the minor acid intrusions

with the plutonic acid rocks of Rhum suggests they have

a common origin. The fourth acid dyke more favourably

compares with one of the Small Isles felsite dykes

(Ridley 1973). It is located on the southernmost tip

of Rhum (less than 8 km from Eigg) and possibly is

genetically related to the Eigg acid association.

IV. Petrogenesis

a) Ultrabasic magmas and ultrabasic liquids in the

Rhum minor intrusion suite.

The term ultrabasic is applied to igneous rocks

with less than 45 wt% SiO_2 (Williams et al. 1955,

Wyllie 1967). The existence of ultrabasic magmas on

Rhum cannot be in doubt since several of the group 2

dolerites, the vast majority of the group 1 picrites and

all of the feldspathic peridotites in the peridotite

plugs contain less than 45.0 wt% SiO_2. Whether these

compositions ever existed as liquids at high crustal

levels is much more open to debate. The possible presence

of ultrabasic liquids in the upper crust is an extremely

controversial subject. The main arguments both in

favour and against the existence of ultrabasic liquids have recently been reviewed by Clarke and O'Hara (1979) who categorised the two antithetic views.

(i) Bowen (1928) considered that all high magnesian lavas were olivine phyric and that no basaltic liquids with normative olivine greater than 10% can exist in nature. With this interpretation, based on liquid line of descent arguments, low MgO basalts are primary and related high MgO compositions are enriched in early formed olivine.

(ii) However the discovery and interpretation of spinifex textured koma tites as quenched high MgO liquids (eg. Cox 1978) has led to the converse view in which the high MgO liquids are primary and the related low MgO basalts are derived by a process of olivine fractionation. These diametrically opposed views lead to the problem of how can cumulus-olivine enriched compositions be distinguished from a liquid composition. It is generally assumed that aphyric basalts closely approximate liquid compositions as evidenced by the use of aphyric rocks in illustrating liquid lines of descent (eg. Yoder and Tilley 1962; Thompson et al. 1972). This procedure has already been adopted in this study and on this basis the majority of the fine grained essentially non-porphyritic rocks of group 2 are liquids and several

are ultrabasic liquids containing up to 15 wt% MgO (eg.
44A76, 93A76, 77121, 77122). Additionally although the picritic
rock 77024 contains abundant olivine phenocrysts, the
textural variation and limited compositional variation
of the olivine phenocrysts are consistent with the
interpretation that this specimen reflects the isothermal
crystallisation of a supercooled ultrabasic liquid with
15.5 wt% MgO (Chapter 6, p. 173).

The type 1 picrites have MgO contents ranging from
14.8 to 30.9 wt%. One of the specimens (77321) is the
chilled margin of a picrite dyke and contains 9.04 modal
% olivine microphenocrysts. The observed composition of
77321 and the calculated olivine-free liquid represented
by this specimen are presented in Table 7.8 (Anal. 1 and 2).This
procedure estimates the ultrabasic liquids in the type 1
picrites can contain up to approximately 19.5 wt% MgO,
thus implying that the group 1 rocks with MgO greater
than 19.5 wt% are cumulus olivine enriched and rocks
with less than 19.5 wt% have suffered olivine fractionation.
The varying abundance of MgO in these type 1 picrites can
be explained by a flow differentiation process (cf. Gibb
1968) which can produce magmas containing abundant olivine
(MgO enriched compositions) with concomittant MgO
depleted magmas in other parts of the same dyke. In
this process it is considered that an MgO-rich magma
with approximately 10% olivine microphenocrysts was
intruded into a fissure. Rapid chilling at the margins

produced a chilled high MgO rock equivalent to the

liquid composition + 10% olivine microphenocrysts

(77321). The magma within the fissure started to

crystallise large quantities of olivine and subsequent

flow movement of the magma through the fissure caused

the olivine to differentiate into cumulus olivine enriched

portions and olivine depleted portions. The MgO content

of a specimen from a flow differentiated dyke is con-

sequently dependent on two factors:

(i)   The amount of cumulus olivine in the

       specimen

(ii)   The degree of olivine fractionation which

       the interstitial liquid has undergone.

This latter point explains the low MgO content of the

virtually aphyric specimen 54A76 (1.5 modal % olivine

phenocrysts) with 14.89 wt% MgO. This specimen has

suffered olivine removal and is a fractionate of the

original magma. The olivine that crystallised from the

original magma fraction contributed to the cumulus-

enriched portion of the dyke. Specimens like 71A76 with

11.6 modal % olivine phenocrysts and 19.6 wt% MgO

represented fractionated interstitial picritic liquid

plus cumulus olivine. The schematic relationship between

four specimens with varying MgO contents is presented

in Fig. 7.19. Specimens 52A76 and 77321 are from the

same intrusions. However, both 54A76 and 77A76 are

from different dykes.

One difficulty pertaining to this hypothesis is that the observed modal abundance of olivine phenocrysts in the thin sections of the group 1 specimens does not always vary sympathetically with the MgO content. This is exemplified by comparison of 53A76 and 71A76, the former has a higher MgO content (20.73 wt% MgO as opposed to 19.59 wt% MgO) but possesses, less olivine phenocrysts (6.4 modal % as opposed to 11.7 modal %). This may possibly be due to the former having a higher MgO content in the interstitial liquid, (ie. the interstitial liquid in 53A76 has suffered less olivine fractionation than the liquid portion of 71A76) but probably reflects the fact that olivine is unevenly distributed in the samples. This means that the thin sections may not be strictly representative of the chemically analysed material. Fortunately the olivine microphenocrysts in 77321 are evenly distributed throughout the sample thus modal analysis of this specimen will give more reliable results than modal analysis of other type 1 picrite specimens.

The type 2 picrites generally contain less MgO than the type 1 picrites (10.7 to 20.4 wt% as opposed to 14.8 to 30.9 wt%) which suggests that the liquid producing these dykes contained less MgO than that involved in the genesis of the type 1 picrites. This

cannot be demonstrated unequivocally due to the uncertainties in the modal analysis procedure discussed above. However, the presence of olivine phenocrysts in the low MgO specimens (eg. 77093 with 10.71 wt% MgO) and the abundant olivine in the higher MgO specimens (77101 contains 21.5 modal % phenocrystic olivine for a MgO content of 20.36 wt%) is in accordance with this interpretation. Unfortunately none of the type 2 picrite specimens are from the chilled margin of these dykes making it impossible to calculate a liquid composition.

The type 3 picrites also possess a lower range of MgO compositions than the type 1 picrites (12.4 to 25.8 wt%). By analogy with the type 2 picrites the liquids involved in these dykes probably contained less MgO than the calculated MgO content of the type 1 picrite liquids. The presence of abundant kaersutite suggests that these magmas contained substantially more H_2O than the other picrite magmas. In addition, these picrites contain significant quantities of normative nepheline and contrast with the hypersthene normative type 1 and type 2 picrites. The relationship of the type 3 picrites to other members of the Rhum minor intrusions suite is not clear and their origins remain obscure.

Several authors (eg. Mattey <u>et al</u>. 1977, Donaldson

and Brown 1977, Jakobsson <u>et al</u>. 1979) have suggested

that enrichment in cumulus olivine in phyric rocks can be

discerned by comparing the observed core compositions of

the olivine phenocrysts with the calculated composition

of olivines which would be in equilibrium with the whole

rock composition if the latter was indeed a liquid.

These calculations are based on the distribution

coefficient of FeO and MgO between olivine and the host

liquid (see p. 211). The results of the calculations

for the type 1 and type 2 picrites excluding the extremely

olivine rich rocks 52A76 and 77179 but including the

calculated liquid composition of 77321 are presented in

Table 7.9. The calculations are based on an $Fe_2O_3/Fe+Fe_2O_3$

magmatic ratio of 1.5 and a Kd value of 0.30 as recommended

by Clarke and O'Hara (1979).

The observed Fo content of the olivine phenocrysts

in the type 1 and type 2 picrites range Fo88.5 - Fo85 and

Fo88.5 - Fo86 respectively. This suggests that all of

the type 1 picrite compositions and more importantly,

sample 54A76 and the calculated phenocryst free composition

of 77321 which are believed to be ultrabasic liquids in

this study are enriched in cumulus olivine. Similarly

the type 2 picrites with MgO > 13.46 would also be

cumulus enriched by this line of reasoning. It must be

noted however that these calculations are subject to uncertainty in both the estimate of the $Fe^{3+}/Fe^{3+}+Fe^{2+}$ ratio of the magma and also the value of Kd, estimates of the latter vary between 0.26 and 0.39 (Roeder and Emslie 1970; Cawthorn et al. 1973, Sato 1977) with 0.30-0.33 being the generally accepted value (Thompson 1974b, Mattey et al. 1977, Donaldson and Brown 1977). This flexibility allows for an alternative explanation of the discrepancy between the calculated and observed olivine phenocryst compositions. The presence of variolitic groundmass textures in the type 1 and type 2 picrites was noted in Chapter 4 and these were attributed to supercooling. Similarly the unusual olivine textures in 77024 were considered to reflect nucleation and growth in a supercooled ultrabasic liquid. The calculated liquidus olivine composition of 77024 is Fo91.04 and the observed olivine composition is approximately Fo75-Fo76 (Fig. 6.15) thus supercooling causes a considerable reduction in the liquidus olivine composition. Consequently the observed liquidus olivine composition in the type 1 and type 2 picrites may be the result of a small degree of supercooling which produced variolitic textures in the interstitial liquid but did not affect the olivine crystal morphology. The composition of mantle olivines is considered to be between Fo94 and Fo90 (Clarke and

O'Hara 1979). Consequently it is possible that the
calculated liquidus olivine compositions of the Rhum
ultrabasic rocks indicate that they existed as liquids
in equilibrium with mantle olivines. Supporting evidence
for this contention comes from the spinel compositions
in the type 1 and type 2 picrites, the high Al content
of these minerals is considered to reflect crystallisation
at depth prior to emplacement in the upper crust (Chapter
6, p. 167).

A comparison of some ultrabasic rocks in the Rhum
minor intrusions with the picrite dykes of Skye and some
worldwide rocks believed to have existed as high MgO
liquids at high crustal levels is presented in Table 7.8.
An important feature of Table 7.8 are the differences in
the MgO contents of the Rhum rocks (Analyses 1 to 6) and
the two picrite dyke chilled margin compositions from
Skye (Analyses 7 and 8, Gibb 1976). This relationship
is exemplified by the high MgO content of a chilled Rhum
picrite (77321 with $\sim$ 22 wt% MgO) and the Skye dykes
($\sim$ 10-15 wt% MgO) and suggests that the picrite dykes
of Rhum involved a liquid with higher MgO than that
~~involved a liquid with higher MgO than that~~ involved in
the Skye picrites. This is perhaps not surprising as
both the basic and intermediate rocks in the Rhum minor
intrusion suite are MgO enriched when compared with rocks

of analogous differentiation in other Hebridean suites

(see Fig. 8.1).

The remaining analyses in Table 7.8 are from high

MgO lavas with olivine phenocrysts. The lava compositions

are judged to have existed as liquids within the upper

crust and their olivine phenocryst content is believed

to reflect equilibration of the initial liquid composition

to a low pressure environment.

The peridotite plugs are ultrabasic in composition,

and consist of abundant large granular olivines in a

coarse grained matrix of interstitial plagioclase and

clinopyroxene. These textures suggest that these plugs

are not the crystallisation products of extremely MgO

rich liquids but are the result of crystallisation of a

crystal mush, rich in cumulus olivine and spinel. A

possible source for these crystal mushes is the magma

chamber responsible for the layered peridotite rocks of

Rhum and the compositional similarity between the minerals

in one of the plugs (77068) and the minerals in layered

series was noted in Chapter 6. Although many of the

plugs are petrographically very similar to 77068, others

are not. Consequently, the plugs may have tapped a magma

source over a period of time and the limited data on

the mineral chemistry of the plugs should be treated with

caution. It is tentatively suggested that these plugs

represent the flushing of an olivine rich mush from the

high level Rhum magma chamber. A corollary of this

suggestion is that pure olivine rocks (dunites) which

have not yet been observed in the layered peridotites

at the present erosion level (Brown 1956, Wadsworth 1961)

are present at depth, as abundant dunite xenoliths have

been located in one of the peridotite plugs.

b) Assessment of the degree of partial melting.

It is extremely difficult to distinguish between

the effects of progressive partial melting and

fractional crystallisation in the Rhum minor intrusions

with the available data: rare earth element and isotope

analyses on critical compositions would no doubt lead

to less equivocal interpretations. However, the available

evidence suggests that the differentiates are more likely

to be the products of fractional crystallisation (cf. the

Skye lavas, Thompson et al. 1972, Thompson 1974a) than

limited partial melting as proposed for the differentiates

in the Mull lava succession (Beckinsale et al. 1978).

Sun et al. (1979) have suggested that plots of Ti

ppm against the ratio CaO/TiO_2 and Al_2O_3/TiO_2 (Fig. 7.20

and 7.21 respectively) can give an indication of the

degree of partial melting for the primitive members of

a rock suite. The main points to note in Figs. 7.20

and 7.21 are the low Ti content of the high MgO gabbros

and 77024 and the separation of the type 1 and type 2

picrites. The former generally have lower CaO/TiO_2

and Al_2O_3/TiO_2 ratios (ie. higher CaO and Al_2O_3 contents

for a given Ti content).

The trends developed in both Fig. 7.20 and 7.21

are due to increases in the CaO and Al_2O_3 content of the

rocks with decreasing TiO_2. Similar trends in mid-ocean

ridge basalts were attributed to various degrees of

partial melting by Sun _et al_. (1979). In their inter-

pretation the rocks with high TiO_2 contents and low

CaO/TiO_2 and Al_2O_3/TiO_2 ratios were the products of

limited partial melting. At these low melting levels

the bulk of the Ti (which is an incompatible element)

enters the melt but the majority of the CaO and Al_2O_3

is retained in the refractory residue. Increased partial

melting increases the CaO and Al_2O_3 contents of the melt

and reduces the levels of TiO_2 in the melt by dilution.

These relationships indicate that the high MgO gabbros,

77024 and one of the group 2 rocks are the product of

substantial partial melting.

The interpretation of the relationships between the

compositions with lower TiO_2 contents and higher CaO/TiO_2

and Al_2O_3/TiO_2 ratios and the compositions with higher

TiO_2 contents in the remaining rocks is much more

difficult. It was stated earlier that the dominant

control over the CaO and Al_2O_3 contents of the group 1

to 4 rocks was a calcium rich aluminous clinopyroxene.

The trends in Figs. 7.20 and 7.21 could be interpreted

as either the result of progressive partial melting of

a Ca-rich aluminous mantle clinopyroxene or fraction-

ation of this composition from melts with low TiO_2

contents and high CaO/TiO_2 and Al_2O_3/TiO_2 ratios or both.

Another important relationship which comes out of

these diagrams is that the high MgO group 1 and 2 magmas

have variable TiO_2 contents and CaO/TiO_2 Al_2O_3/TiO_2

ratios. Although the concentration of TiO_2 in the group

1 rocks will depend largely on the volume of olivine

phenocrysts in the sample, the presence of olivine will

not affect the CaO/TiO_2 and Al_2O_3/TiO_2 ratio of the

rock. Note for example that the calculated liquid

composition of 77321 after subtraction of 10% olivine

increases the TiO_2 content but does not alter the ratios

in Figs. 7.20 and 7.21. The group 1 and 2 rocks are

MgO rich and probably have not suffered substantial

loss of olivine during ascent. This suggests that the

TiO_2 levels in these rocks approximate the primary TiO_2

contents of the melt which implies that most of group 1

and 2 are the product of smaller degrees of partial

melting than the high MgO gabbros. This interpretation

is consistent with the abundance of the other incompatible elements (Ba, Nb, Zr, Y, Sr, Rb) in these rocks.

It was noted earlier that several of the nepheline normative compositions in the group 4 dolerites contain less K_2O than the hypersthene normative compositions. It is generally accepted that nepheline normative magmas are produced by lower degrees of partial melting than hypersthene normative compositions as this explains the general high abundance of the incompatible elements including K_2O in the former. The anomalous behaviour of K_2O has also been observed in the nepheline and hypersthene normative lavas of Skye (Thompson et al. 1972, Thompson 1974a). These authors suggested that K_2O in the mantle underlying Skye was housed in the K_2O bearing mineral phlogopite making K_2O a compatible, not incompatible, element. In this model small degrees of partial extract small quantities of K_2O from the mantle giving low K_2O nepheline normative basalts. Increased partial melting results in total consumption of the phlogopite giving rise to higher K_2O contents in the hypersthene normative lavas. This interpretation by Thompson and co-workers may also explain the lower K_2O contents of the nepheline normative group 4 rocks on Rhum.

In their studies of the Mull lavas, Beckinsale et al. (1978) found that the intermediate rocks of their

groups 1 and 2 contained less Y and Sr respectively
than the related basalt compositions. They suggested
that these intermediate rocks were the product of limited
partial melting at different levels. In this model the
Y and Sr in groups 1 and 2 were retained by the source
rock (garnet lherzolite and plagioclase lherzolite
respectively) until increased partial melting consumed
the garnet and plagioclase fractions of the lherzolite
source releasing Y and Sr into the melts. The converse
relationship (ie. a general increase in both Y and Sr
on differentiation) is found in the Rhum minor intrusions.
This contrary relationship may be interpreted as either
production of intermediate rocks by limited partial
melting of a spinel lherzolite source (as neither Y
and Sr would be retained) or the Rhum intermediate rocks
were produced by fractional crystallisation.

The presence of intermediate rocks throughout the
sequence of minor intrusion on Rhum (see Fig. 5.2) lends
support to an origin by fractional crystallisation in
that fractionated magmas held within the mantle or lower
crust would be available for intrusion throughout the
history of the complex. In addition, the phases controlling
the chemical trends in the differentiated compositions
(calcic aluminium poor clinopyroxene, olivine and
plagioclase) are all present as low pressure phenocrysts

in these rocks.

c) Relative depths of the petrogenetic processes.

There are two main factors to be taken into account in this discussion. First, the transitional nature of the Rhum minor intrusion suite as demonstrated in Chapter 3 and second, the suggestion made earlier that the majority of the group 1 and 2 rocks are the product of small degrees of partial melting.

The existence of a thermal divide separating nepheline normative and hypersthene normative compositions along the di-fo-an join in the simplified basalt tetrahedron at one atmosphere has been convincingly demonstrated by several experimental petrologists (Yoder and Tilley 1962, O'Hara 1963, Presnall et al. 1978). This divide effectively separates the crystallisation paths of alkaline basalts and olivine tholeiites and prevents the derivation of alkaline basalt from olivine tholeiite (and vice versa) by fractional crystallisation at atmospheric and low pressures.

This divide is known to break down at higher pressures but the precise depth to which it extends is not known. O'Hara (1968) suggested a limiting pressure of 8 kb for this divide but more recent work by Presnall et al. (1978) in the system $CaO-MgO-Al_2O_3-SiO_2$, suggests that it extends

to pressures of only 3 kb. The latter recognised that the effect of Na_2O on their simplified basalt compositions would increase this limiting pressure to approximately 4 kb but did not discuss the effects of iron and TiO_2. These authors also noted that the disposition of the isothermal surfaces along the join di-fo-an would allow derivation of simplified tholeiite basalt compositions from simplified alkali basalt compositions between 3 and 20 kb total pressure.

Recent geophysical work on the continental margin off Northwest Scotland has shown that the Hebridean crust is approximately 27 km thick (Bott et al. 1979). This is considerably less than the 40 km estimate of Thompson (1974a, p.334). The thermal divide discussed above would extend to approximately 18 km ($\sim$ 4 kb) and consequently would not be operative in the lower crust and upper mantle.

The transitional nature of the Small Isles volcanics (Ridley 1970, 1971), the Ardnamurchan cone sheets (Holland and Brown 1971), the Skye lavas (Thompson et al. 1972, Thompson 1974a), the Mull lavas (Beckinsale et al. 1978) and other world wide transitional basalts (eg. southwestern Australia, Green 1970) is believed to reflect derivation below the low pressure thermal divide in the simplified basalt tetrahedron. A similar explanation is proposed

for the transitional nature of the Rhum minor intrusions. Previous discussions on the depth of origin of the transitional Hebridean basalts (Ridley 1971, Holland and Brown 1971, Thompson et al. 1972) have been based on earlier estimates of the depth extent of the di-fo-an thermal divide which necessitate derivation from pressures greater than 8-10 kb (∿ 35-40 km). However, the evidence presented earlier does not necessitate such deep level control over the petrogenetic processes which produced the Rhum minor intrusion suite. Independent evidence from experimental data led Thompson (1974a) to propose a depth origin of 60 km (∿ 17 kb) for the primitive Skye main lava series basalts. In addition, the geochemical arguments of Beckinsale et al. (1978) require derivation of the group 1 Mull lavas from a garnet lherzolite source. A possible depth estimate of 80 km (∿ 25 kb) for the source of these Mull lavas can be made from the stability field of garnet presented by Carmichael et al. (1973, Fig. 13.1). It was shown earlier (p.224) that the dominant control over the CaO and Al_2O_3 variation in the basic Rhum minor intrusions was probably exercised by an aluminous MgO rich, calcic clinopyroxene which is not, however, preserved as phenocrysts in these rocks. The Al_2O_3 content of clinopyroxenes is believed to increase with increasing pressure (Aoki and

Shiba 1973, Thompson 1974b, Wass 1979)(but see p. 157)
and mantle pyroxenes are MgO rich. In addition, the
composition of the Group 1 rocks are believed to have
been equilibrated with mantle olivines. Consequently
it is suggested that the group 1 picrites and the other
basic minor intrusions are derived from a high pressure
source within the upper mantle.

In the absence of experimental data and any
significant geochemical constraints, estimates of the
relative source depths of the basic Rhum minor intrusions
is purely speculative, however the progression towards
alkalinity and the general increase of MgO content
with time as noted in Chapter 8 requires explanation.
The earliest basic rocks on Rhum are incompatible-
depleted gabbros which are considered to be the products
of substantial partial melting. These were then
followed by the voluminous group 4 and group 8 compositions
which account for the bulk of the Rhum minor suite with
the MgO rich group 1 and group 2 magmas entering at a
later stage (Fig. 5.2). O'Hara et al. (1975) have noted
that MgO rich compositions can be produced by limited
partial melting of a garnet-lherzolite source at
approximately 30 kb (95-100 km), this may well explain
the high abundance of incompatibles in the type 1 and
type 2 picrites (especially type 1). It is tentatively

proposed that the progression towards alkalinity and high MgO compositions in the Rhum minor intrusions with time reflects a general increase in the depth of partial melting with a limited degree of partial melting at the deeper levels producing more alkalic melts.

The compositional variation within the basic rocks and the coexistence of nepheline normative and hypersthene normative compositions may reflect simultaneous different degrees partial melting at different levels or cyclic reversals in the degree of partial melting at the same depth, or both. In addition mantle heterogeneity may be a contributing factor.

The majority of the intermediate rocks are believed to be the product of low pressure fractional crystall-isation of basalt magma at depths up to 15 km (the extent of the fo-an-di thermal divide) as this explains the divergence towards extreme alkaline and tholeiitic compositions. The main phases producing the variation will have been olivine, plagioclase, clinopyroxene and to a lesser extent Fe-Ti oxides. Olivine and Cr-spinel may have also fractionated at high level but slow ascent through the mantle and the lower crust would favour olivine and spinel fractionation en route. The extent of possible deeper level fractional crystallisation cannot be accurately gauged from the available data but

the sparse differentiates following the iron enrichment and MgO depletion trend in Fig. 7.2 are probably the product of higher pressure fractional crystallisation. In addition, the high normative olivine contents of the group 10 rocks (15.8% - 25.3%) suggests these magmas could have been in equilibrium with mantle olivine, implying a higher pressure derivation.

The effects of crustal assimilation.

Recent work on the Nd and Sr isotope ratios of some basalts from Eigg, Muck and Skye (Carter et al., 1978) has shown that crustal contamination has played a role in the genesis of these rocks. In view of the 27 km thick crust underlying Rhum, there is a distinct possibility that there has been interaction of mantle derived magmas with salic crustal rocks during the ascent of magma to high crustal levels. The total absence of mantle derived plutonic nodules in the Rhum minor intrusion suite and in the Hebridean basalts in general lend support to this suggestion as the nodules may have been lost by a settling or filtering process during ascent of magmas through the crust. It is very difficult to assess the extent of crustal contamination in the Rhum minor intrusions. The general lack of gneissose xenoliths and xenocrysts (p. 115) in the Rhum rocks suggests that incorporation of crustal

material may have been limited. In addition Carter _et al._ (1978) note that the most contaminated lavas did not have SiO_2 contents commensurate with the bulk assimilation of a corresponding proportion of Lewisian gneiss and suggested that Sr and Nd were extracted from basement rocks preferentially with respect to SiO_2. Whilst the findings of Carter _et al._ (1978) will be of considerable importance in any isotope study of Hebridean igneous rocks including the Rhum minor intrusions, the extent of crustal contamination on the bulk compositions of the Rhum rocks may have been minimal.

Fig. 7.1 MgO v. iron enrichment in the Rhum minor intrusion suite.
          Olivine control line for Kilauea (1959) plotted using data
          in Gunn (1971, Table 1).

          Key to symbols.

◪ Group 1 (Type 1)   ● Group 8

◩ Group 1 (Type 2)   ◆ Group 9

⊟ Group 1 (Type 3)   -◆- Differentiated gabbros

▫ Group 1 (77024)   ▪ Group 10

△ Group 2   ♠ Group 11

□ Group 3   -▪- Group 12

▽ Group 4

+ Low MgO gabbro

φ High MgO gabbro

FIGURE shows a scatter plot with axes:
- Y-axis: MGO WT%, ranging from 0 to 30+
- X-axis: FE2O3*/FE2O3*+MGO, ranging from 0.3 to 0.8

OLIVINE CONTROL LINE
KILAUEA 1959 (FO83)

FIELD OF HIGH FE
DIFFERENTIATES
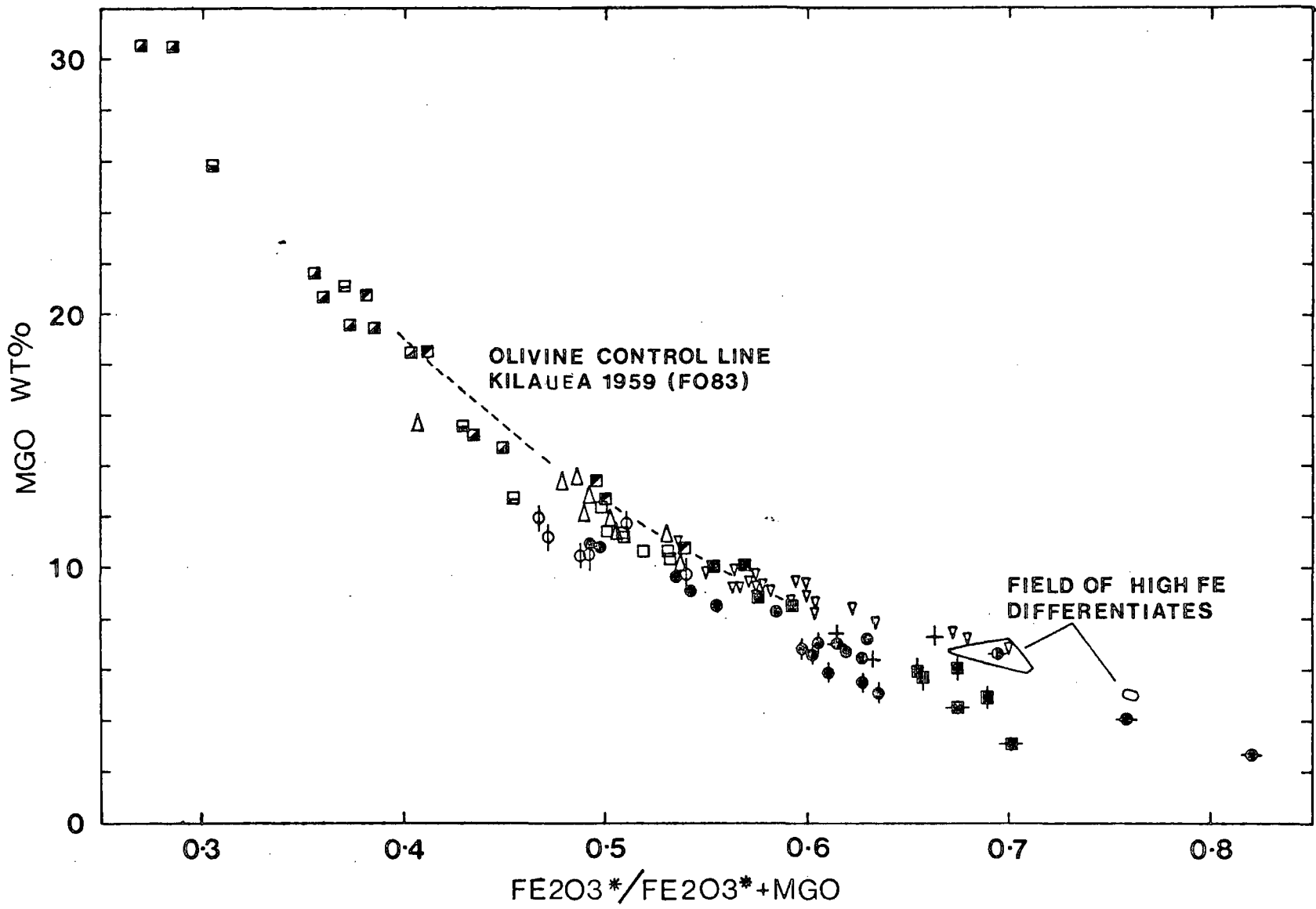
Fig. 7.2 MgO v. Fe_2O_3* variation in the Rhum minor
intrusion suite. Olivine control line for
Kilauea (1959) plotted using data in Gunn
(1971, Table 1).

Symbols as in Fig. 7.1.
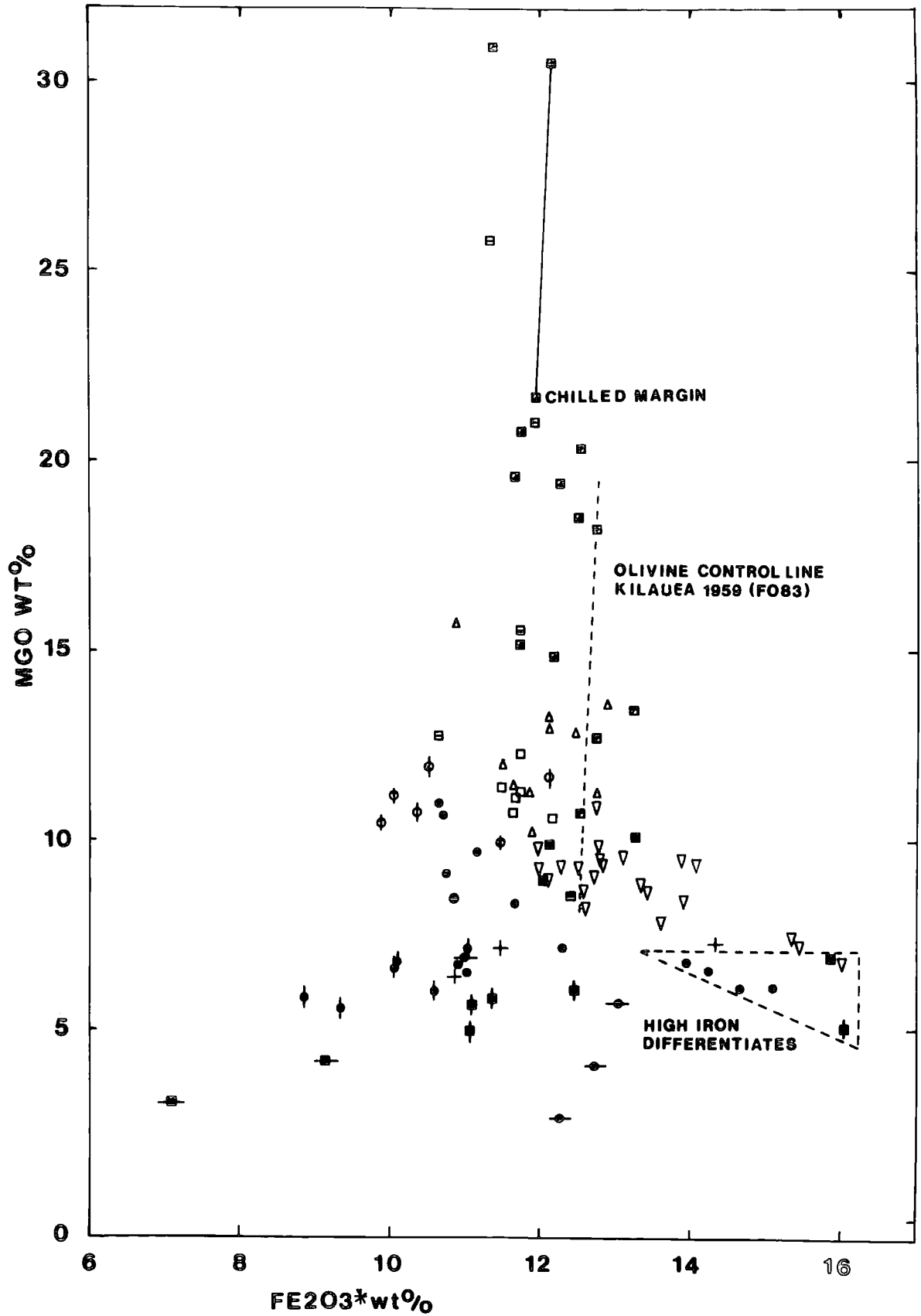
Fig. 7.3 Log Ni v. MgO variation in dolerite groups 1-4.

Symbols as for Fig. 7.1 except:

⌀ = Group 1 type 1

⬚ = Group 1 type 2

⊟ = Group 1 type 3

⊞ = Group 1 (77024)
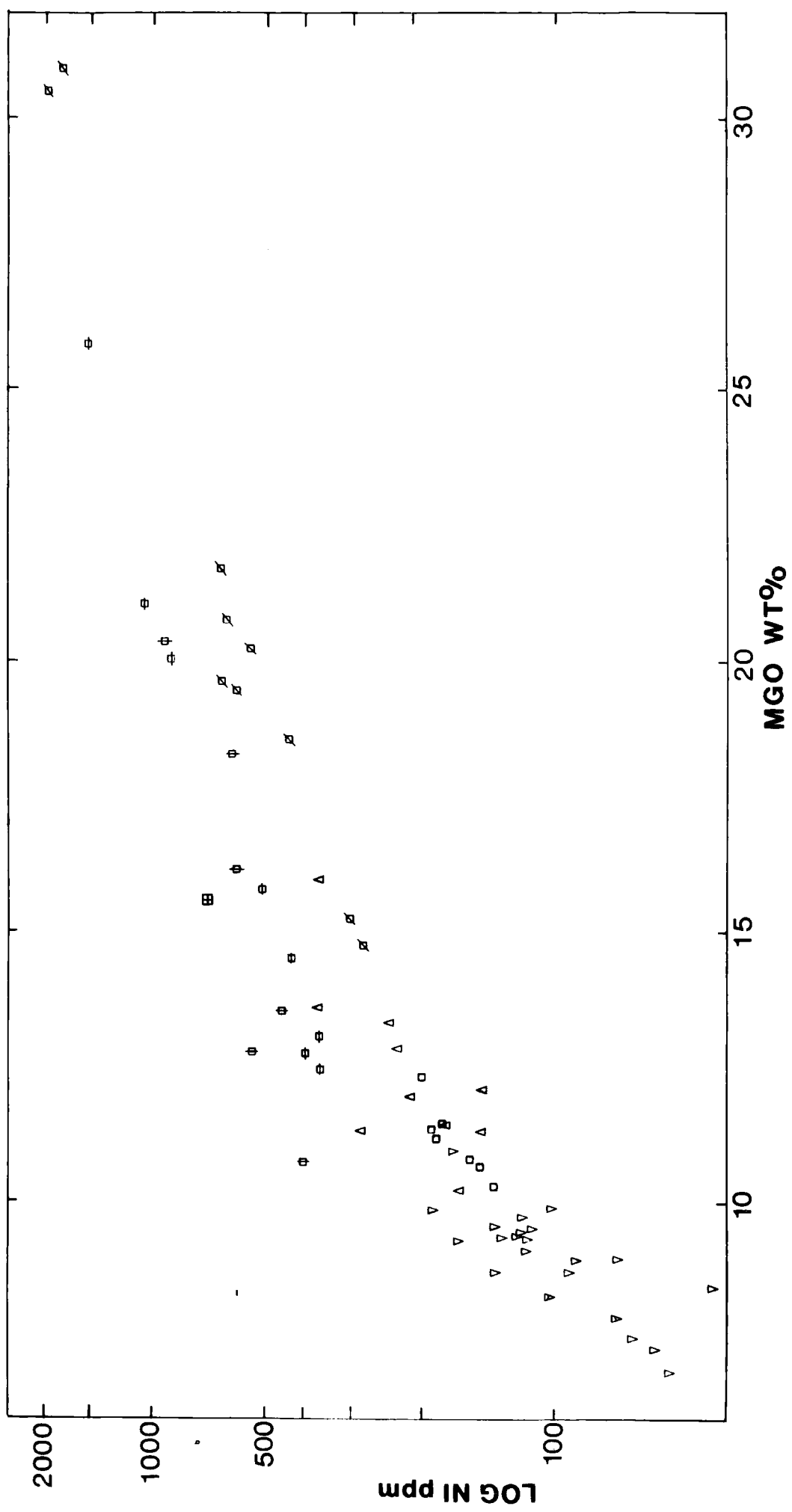
Fig. 7.4 Log Ni v. Log Cr in dolerite groups 1-3.
(Note that this diagram includes <u>all</u> the
picrites listed in appendix 7.2). Symbols
as in Fig. 7.1.

Log Cr ppm X10²

Log Ni ppm X10²
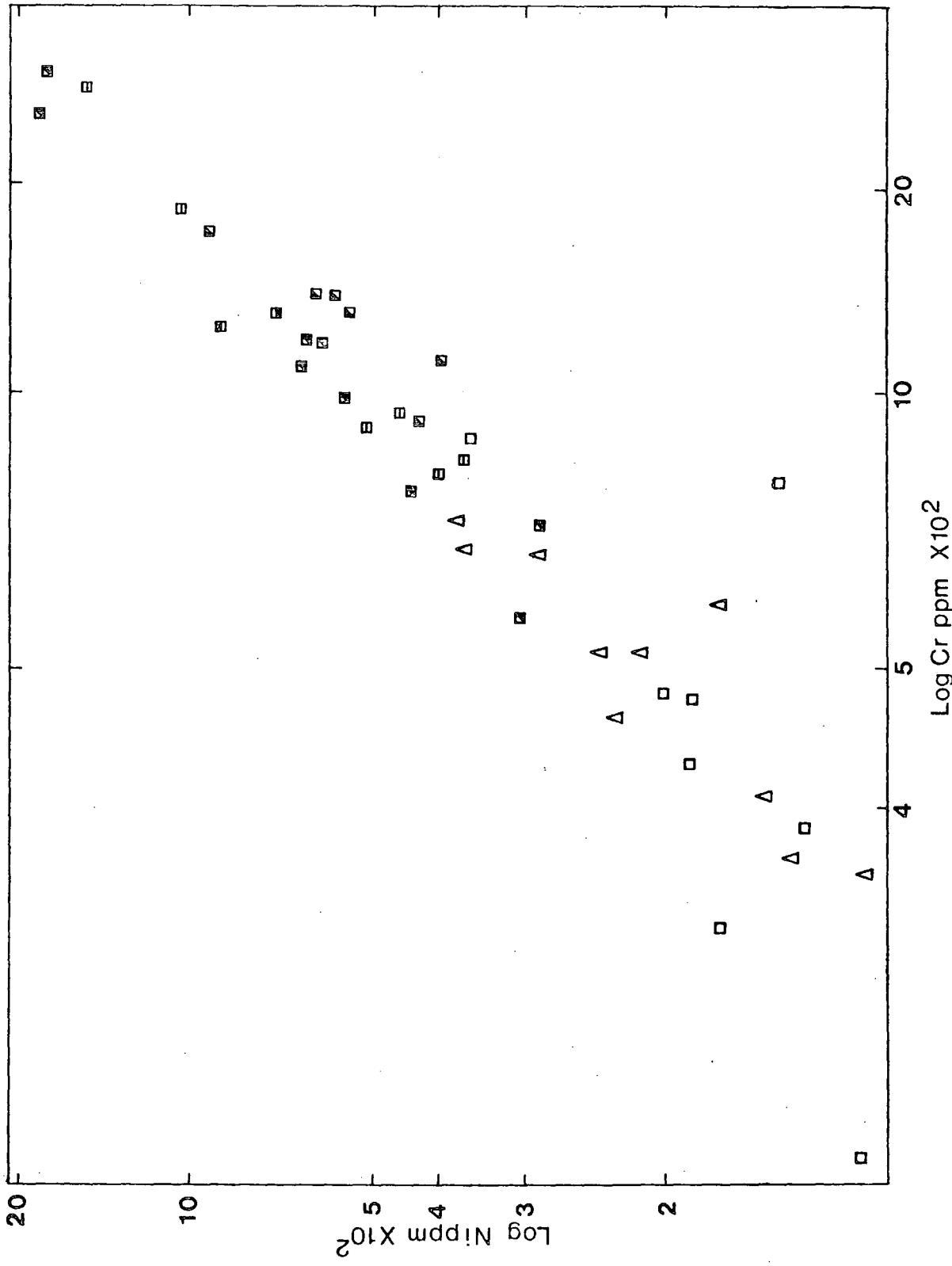
Fig. 7.5 MgO v. Al_2O_3 variation in the Rhum minor intrusion suite. Symbols as in Fig. 7.1 except H = high iron differentiate.
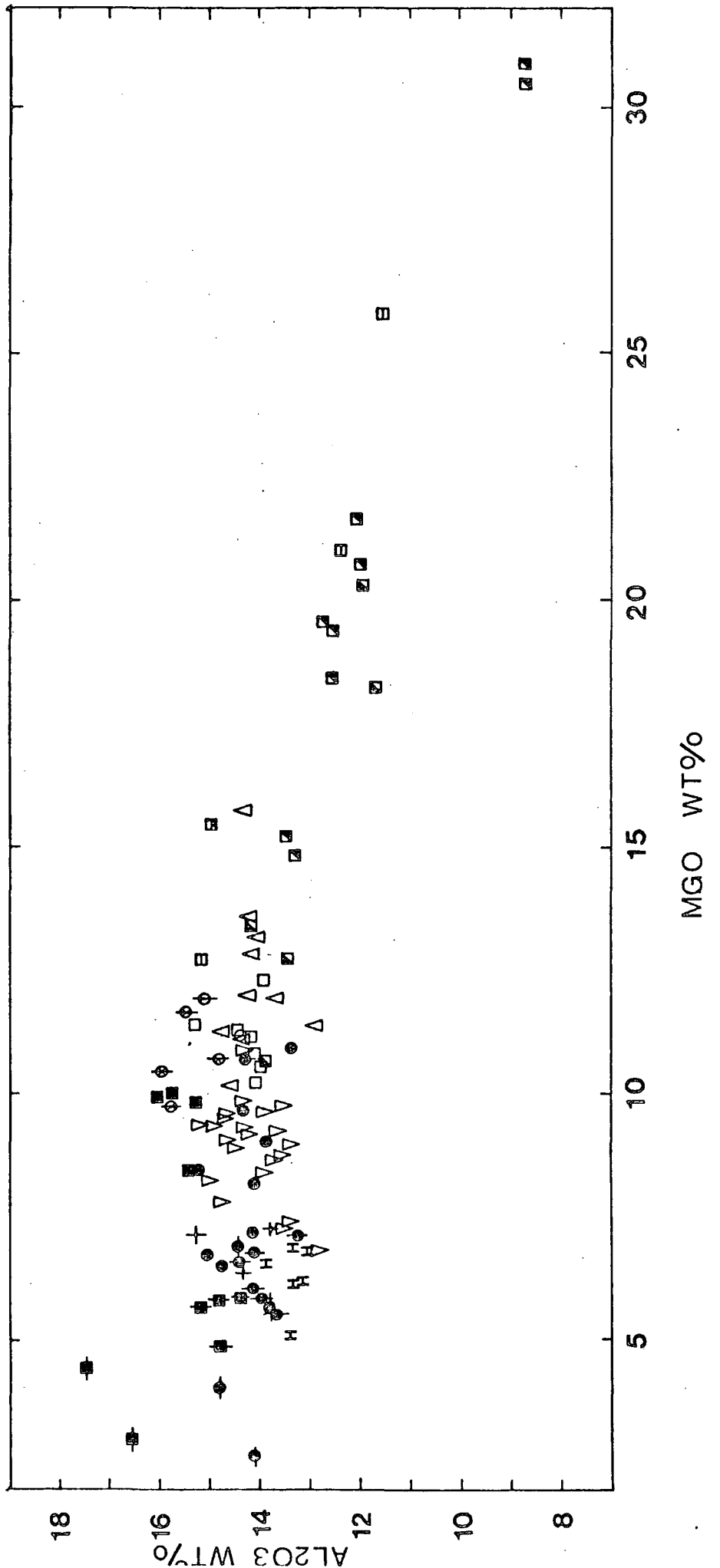
Fig. 7.6 MgO v. CaO variation in the Rhum minor
intrusion suite. Symbols as in Fig. 7.1
except H = high iron differentiates.

Fig. 7.7 CaO v. iron enrichment in the Rhum
minor intrusion suite. Symbols as
in Fig. 7.1 except H = high iron
differentiates.

FE2O3*/FE2O3* + MGO

CaO wt%
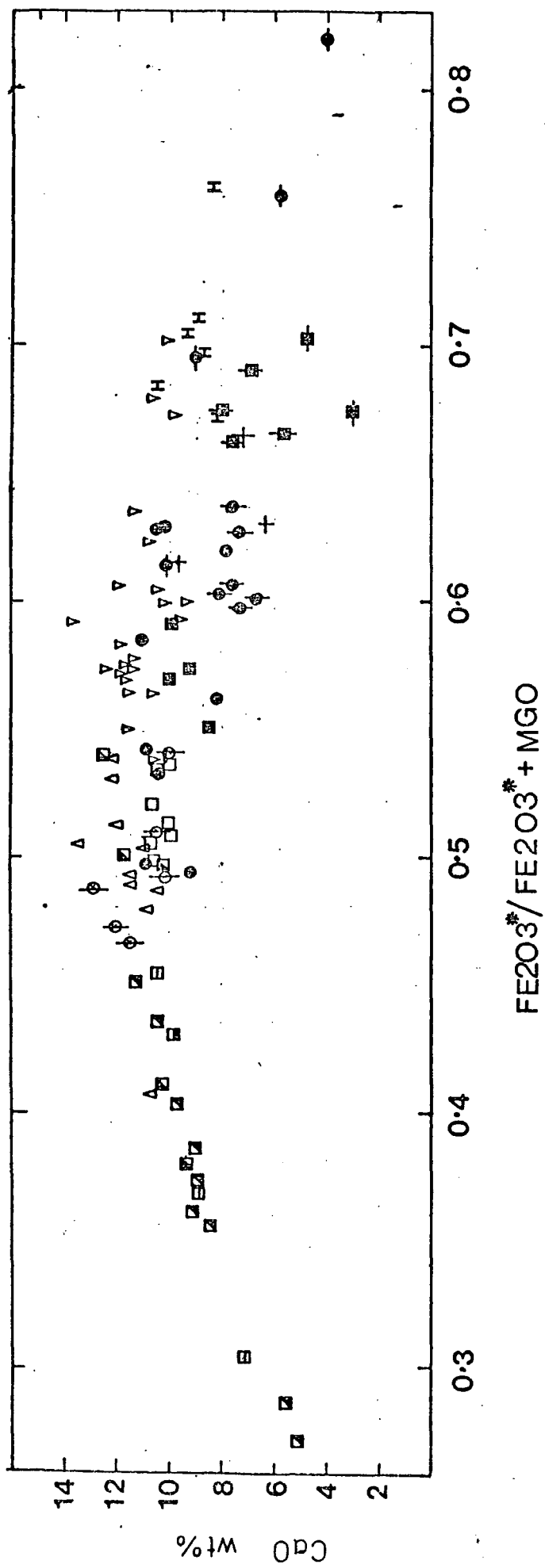
Fig. 7.8 Al_2O_3 v. iron enrichment in the Rhum
minor intrusion suite. Symbols as in
Fig. 7.1 except:

∅ = Group 1 type 1

⏛ = Group 1 type 2

⊟ = Group 1 type 3

■ = Group 1 77024

H = High iron differentiates

$Fe_2O_3^*/Fe_2O_3^*+MgO$

Al_2O_3 wt%
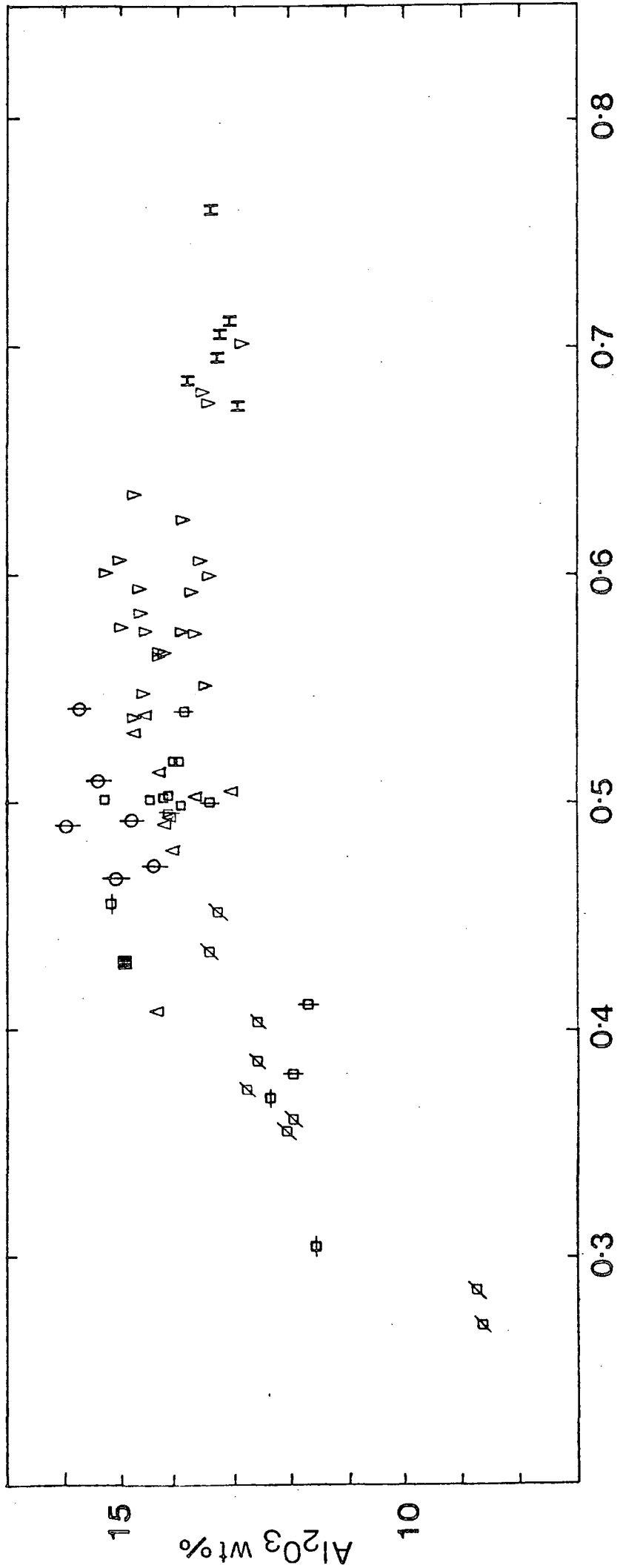
Fig. 7.9 CaO v. CaO/Al$_2$O$_3$ variation in group 1-4
dolerites and gabbros (excluding gabbroic
differentiates). The inset marks the
compositional field of the clinopyroxene
phenocrysts found in these rocks relative
to the trend developed by the gabbros and
the dolerite groups 2-4 in the main diagram.
See text for discussion. Symbols as in
Fig. 7.1.
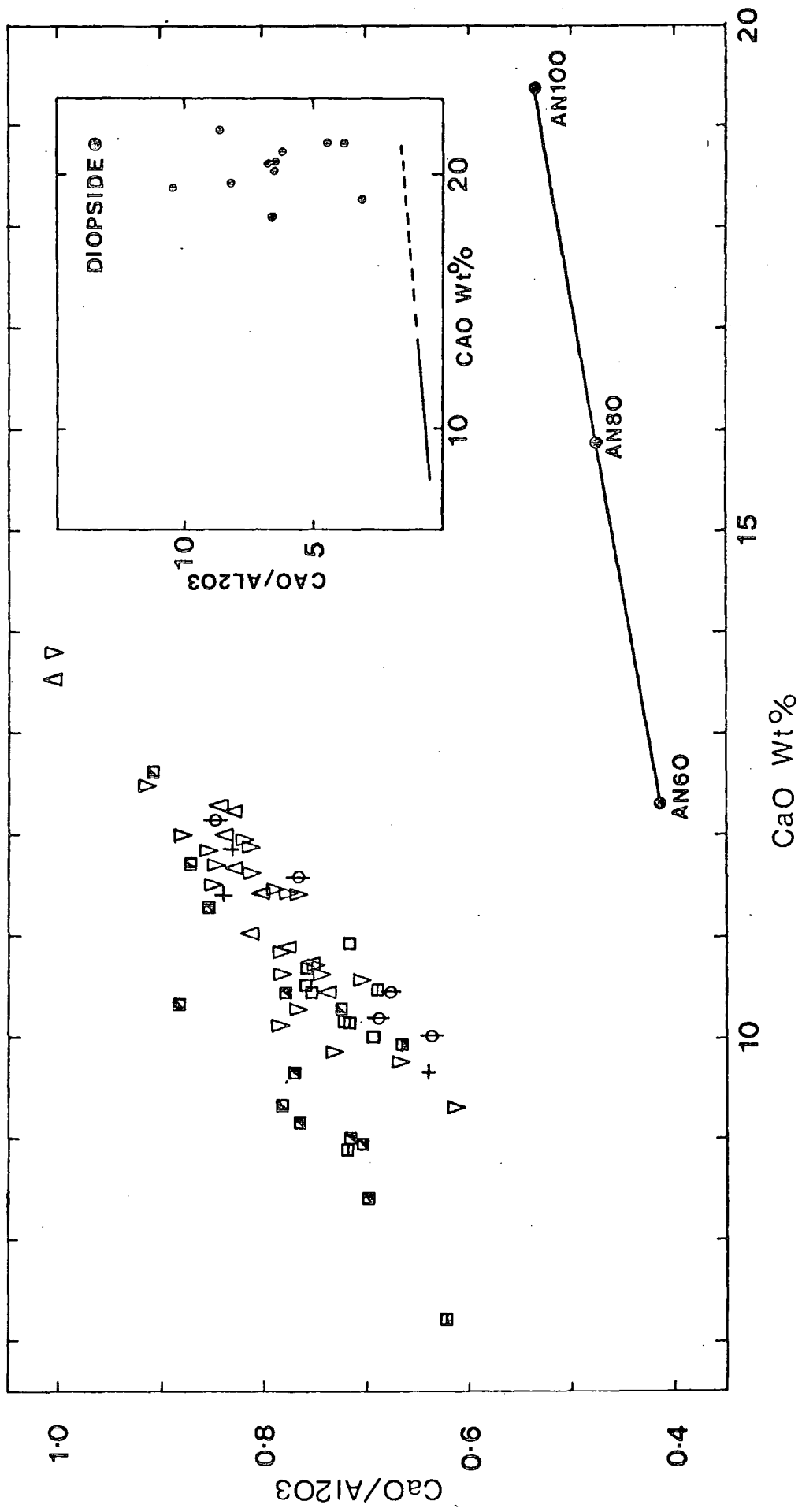
Fig. 7.10 CaO v. Al_2O_3 variation in the dolerite groups 2-4
and the high MgO gabbros. Points X1 and X2 are
the calculated residual liquid compositions following
25% subtraction of a calcic pyroxene (CaO = 20%,
Al_2O_3 = 2%) and an aluminous calcic pyroxene (CaO =
20%, Al_2O_3 = 10%) respectively from the high lime
liquid X. Point X3 is the calculated residual liquid
composition after subtraction of 20% plagioclase
(An76) from the high lime liquid X. (See discussion
on p.223). Symbols as in Fig. 7.1.
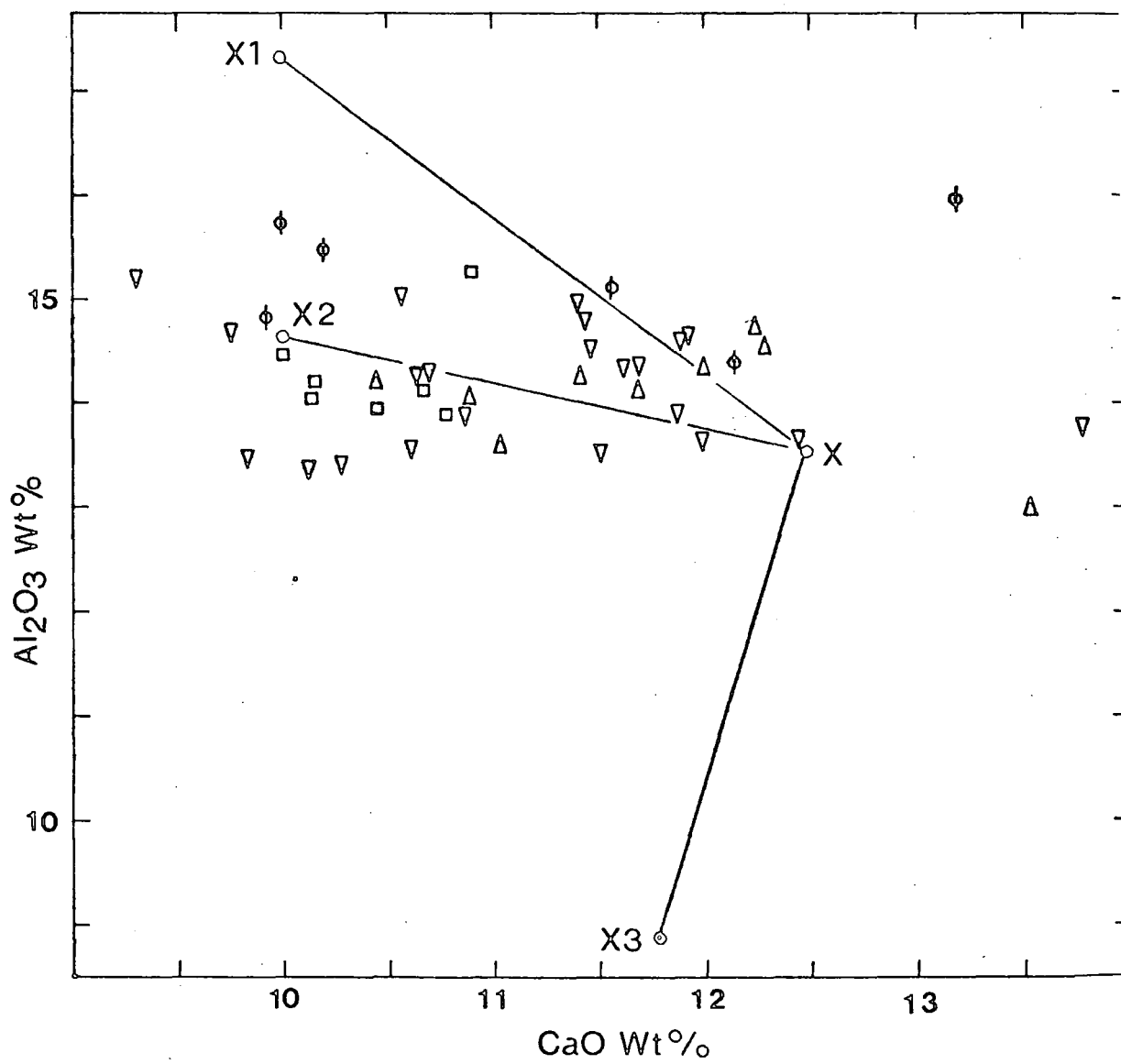
Fig. 7.11 Nb, Y, Sr and Ba v. Zr variation in the Rhum minor intrusion suite. Lines M1 and M2 refer to the trends developed in the Mull lavas (Beckinsale *et al*., 1978, Fig.5). Symbols as in Fig. 7.1 except:
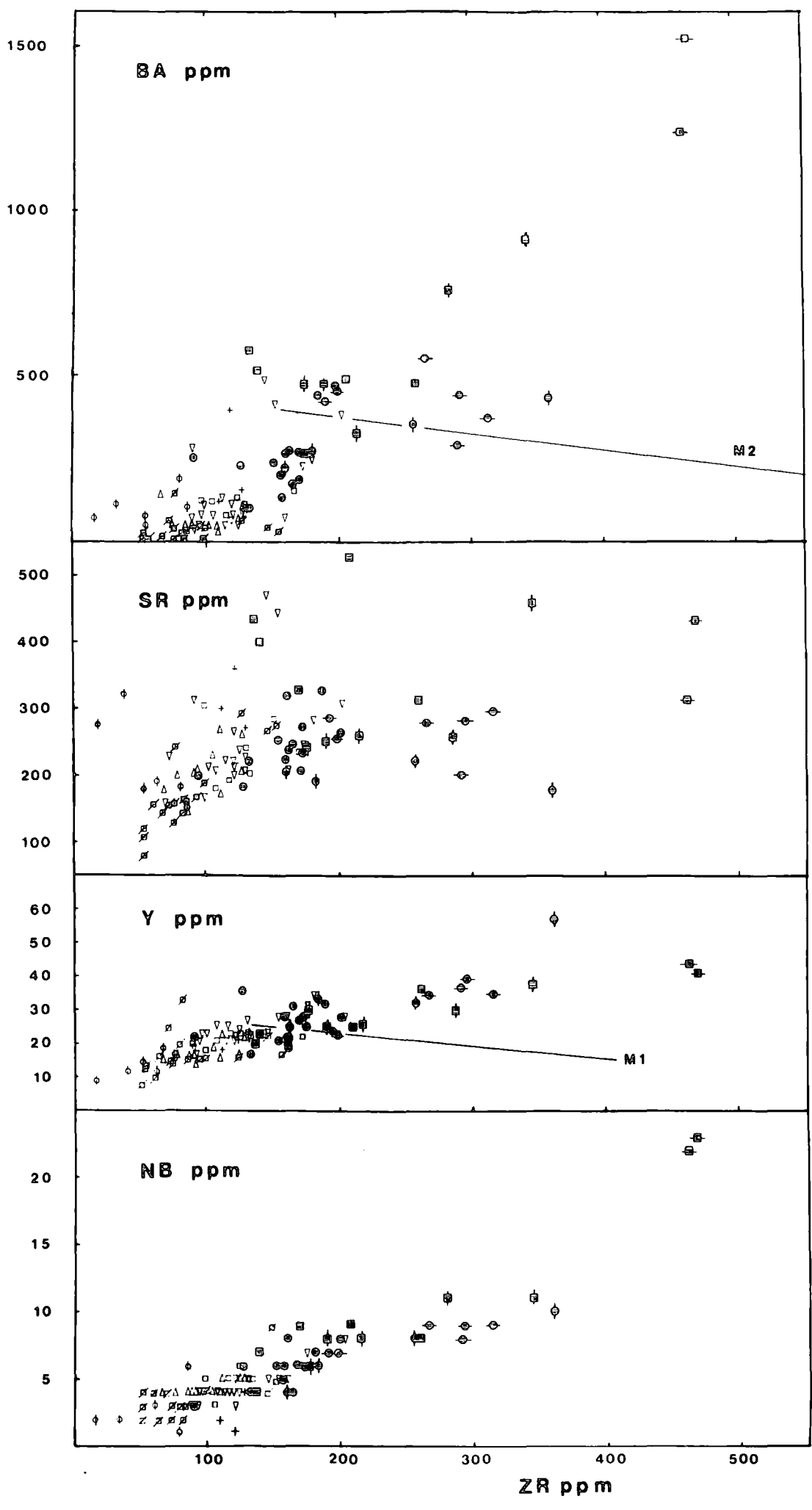
⊠ = all group 1.

Fig. 7.12 TiO_2+K_2O v. Zr variation in the Rhum
minor intrusion suite. Symbols as in
Fig. 7.1 except:

$\not{\emptyset}$= all group 1.
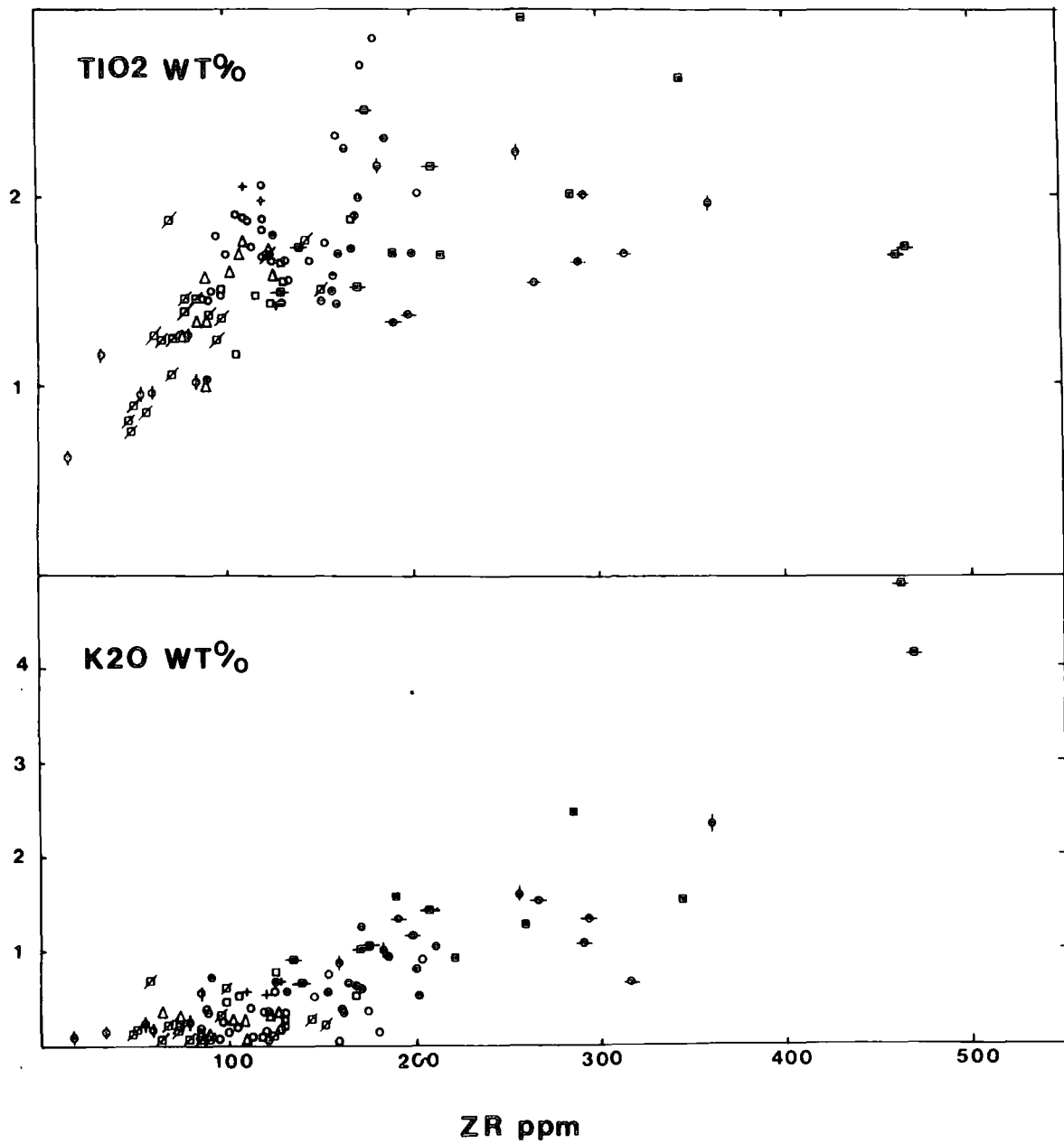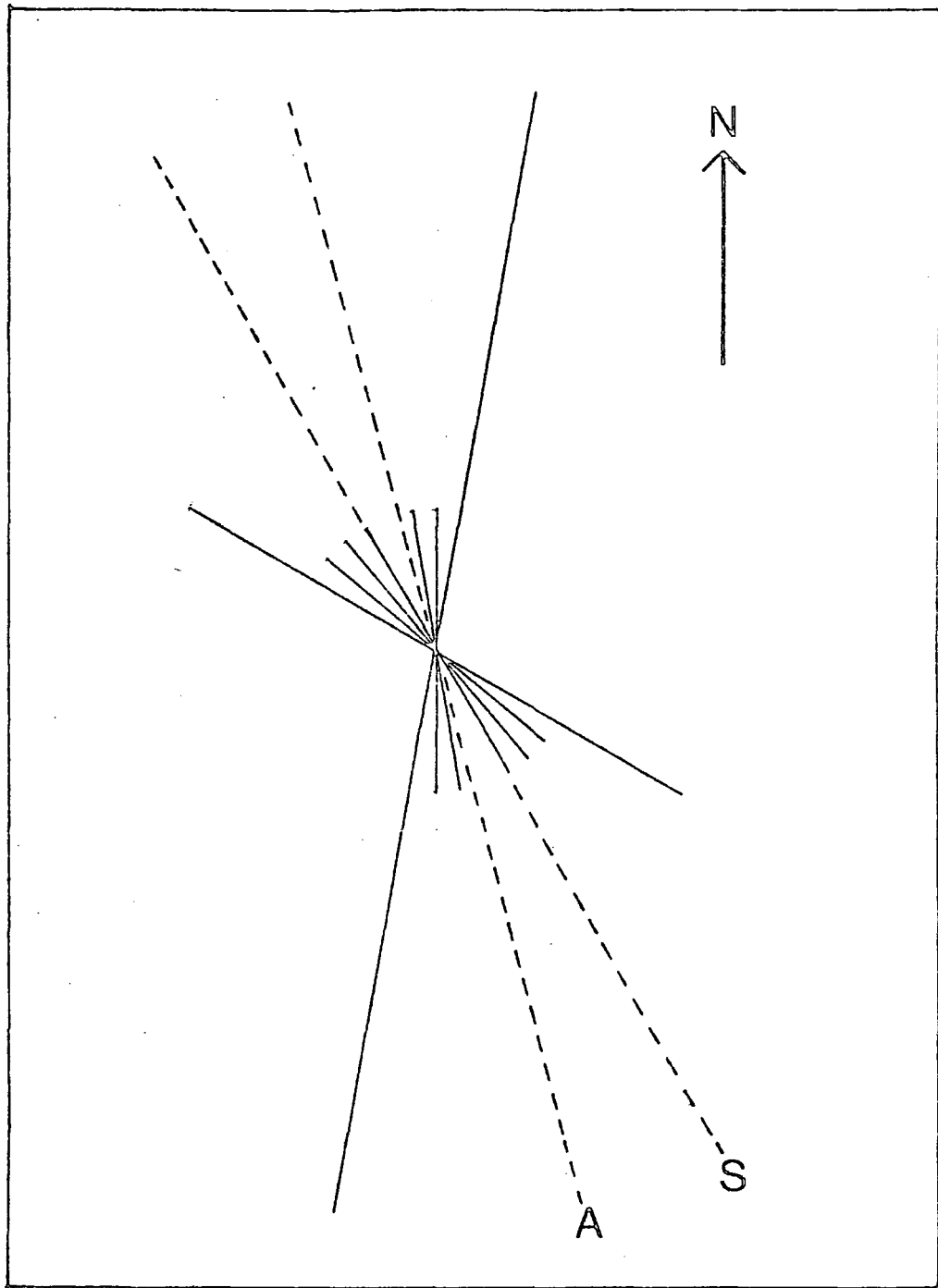
Fig 7·13 Strike orientation of dykes cutting
the Rhum lavas. Lines A and S refer
to the Skye swarm at Arisaig and
Sleat (taken from Mattey et al 1977 fig I)

Fig. 7.14 Major oxide chemical variation in the peridotite plugs. D.l. is the Thornton-Tuttle (1960) Differentiation Index.
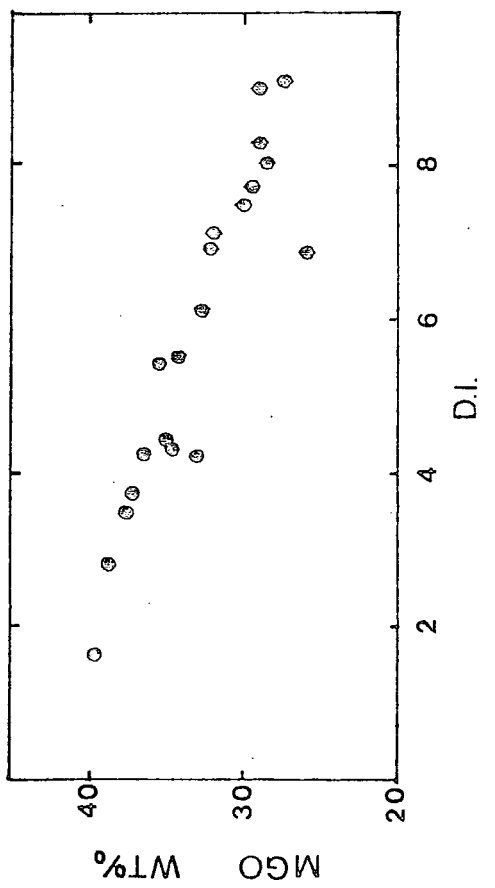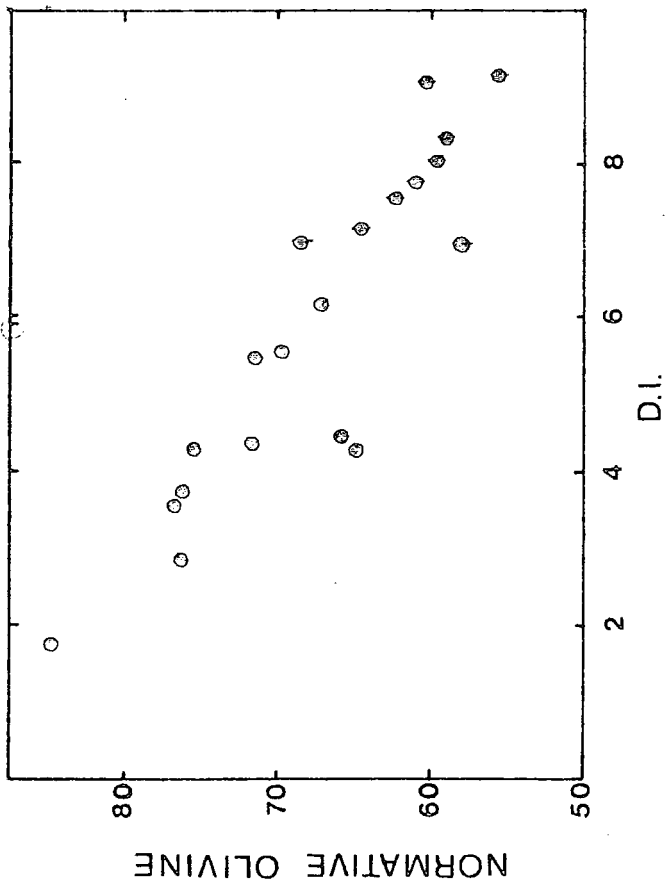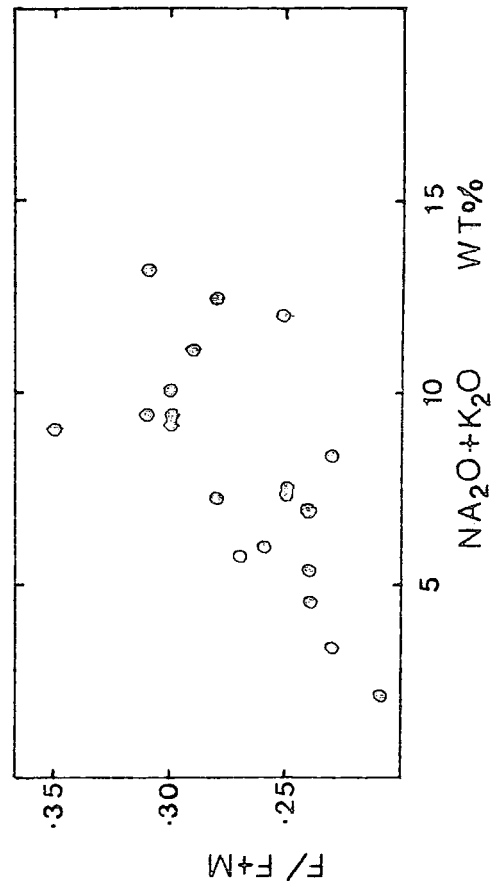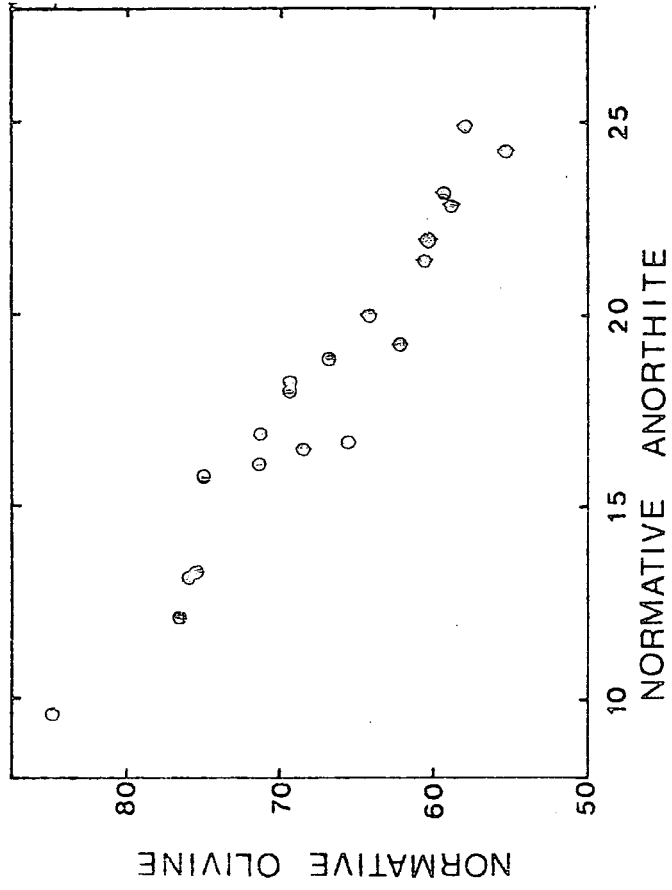
Fig. 7.15 Fe_2O_3* v. TiO_2 variation in the intermediate
minor intrusions. Symbols as for Fig. 7.1.
High iron differentiates not included.
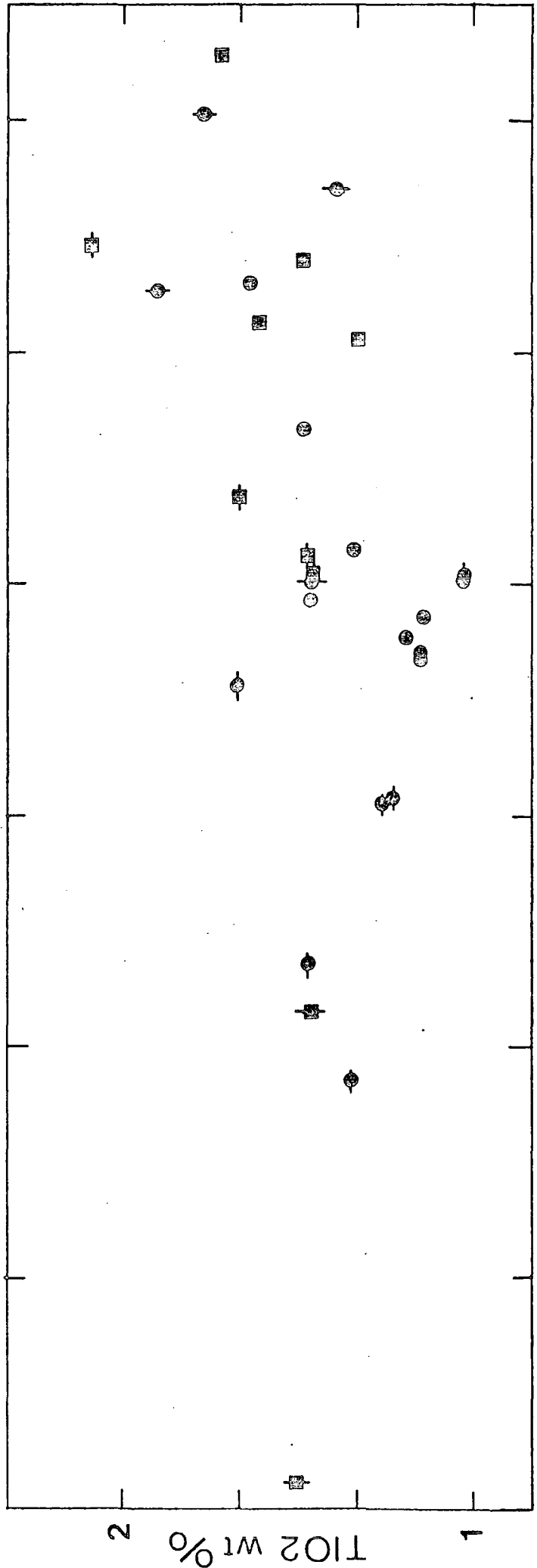
Fig. 7.16 CaO v. Al_2O_3 variation in the intermediate
rocks. Direction of fractionation vectors
for calcic-clinopyroxene (CC) aluminous-
calcic-clinopyroxene (ACC) and plagioclase
(An76) taken from Fig. 7.10. Symbols as in
Fig. 7.1. High iron differentiates not
included.
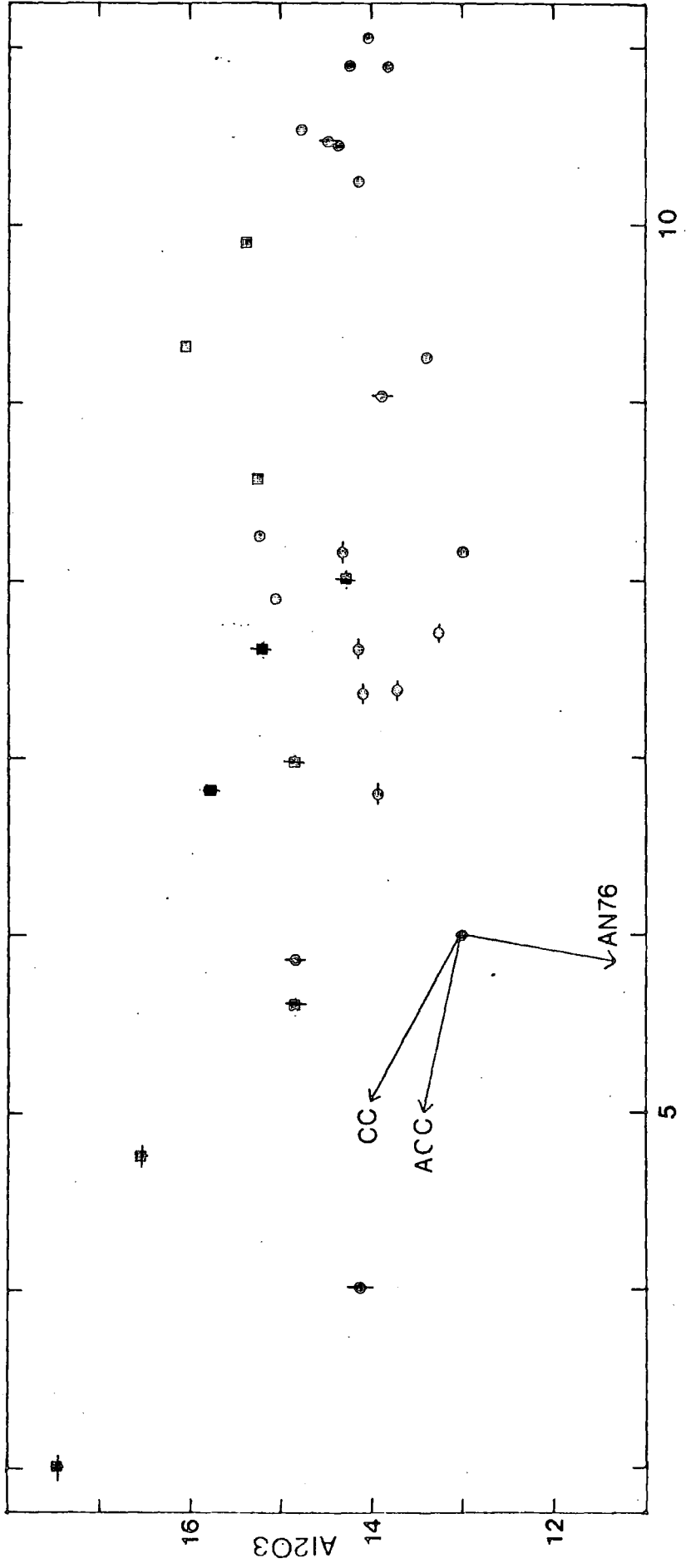
CaO

Fig. 7.17 CaO v. CaO/Al_2O_3 variation in the intermediate
minor intrusions. Solid line refers to a range
of plagioclase compositions (An20-An60). Symbols
as in Fig. 7.1. High iron differentiates not
included.
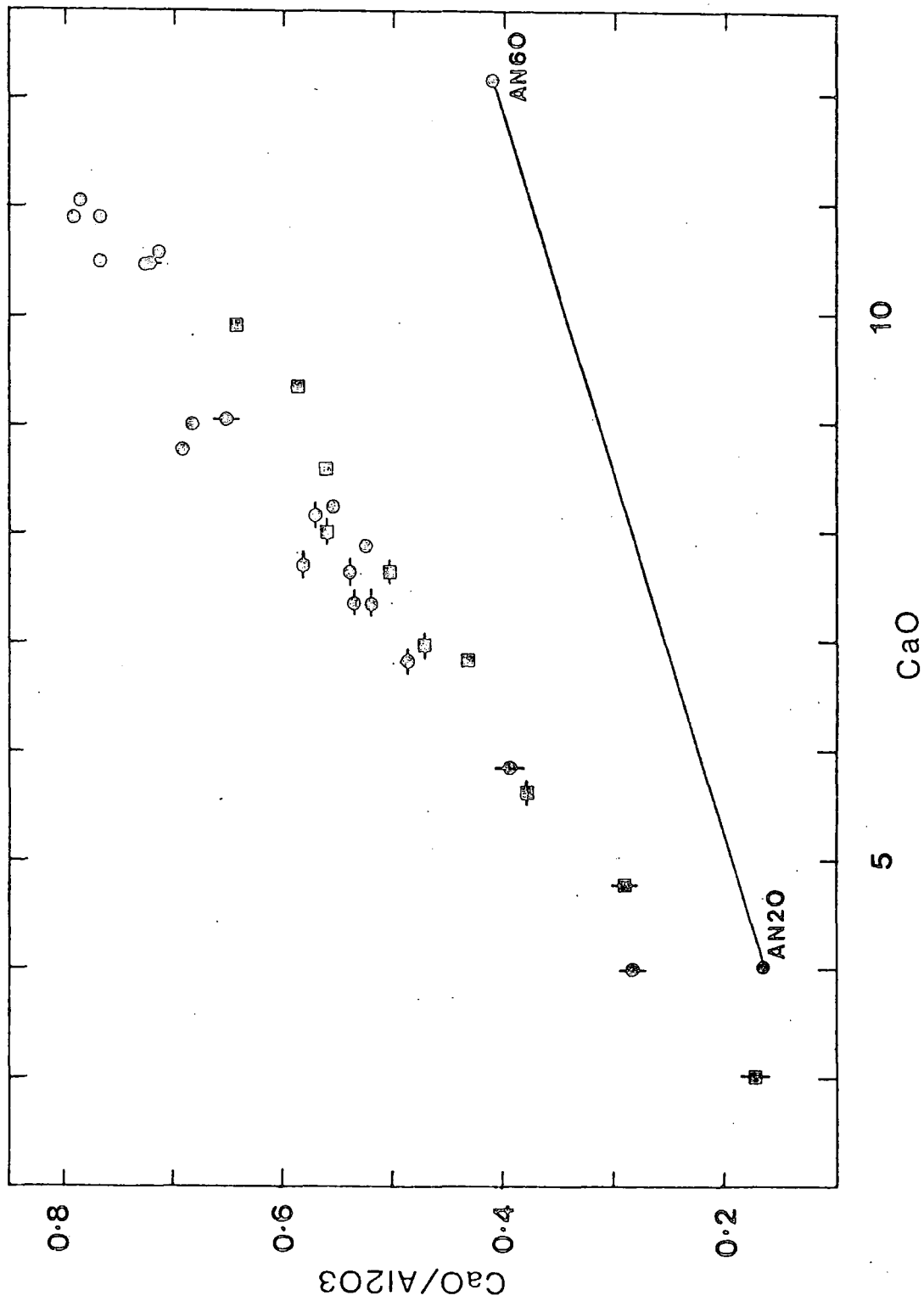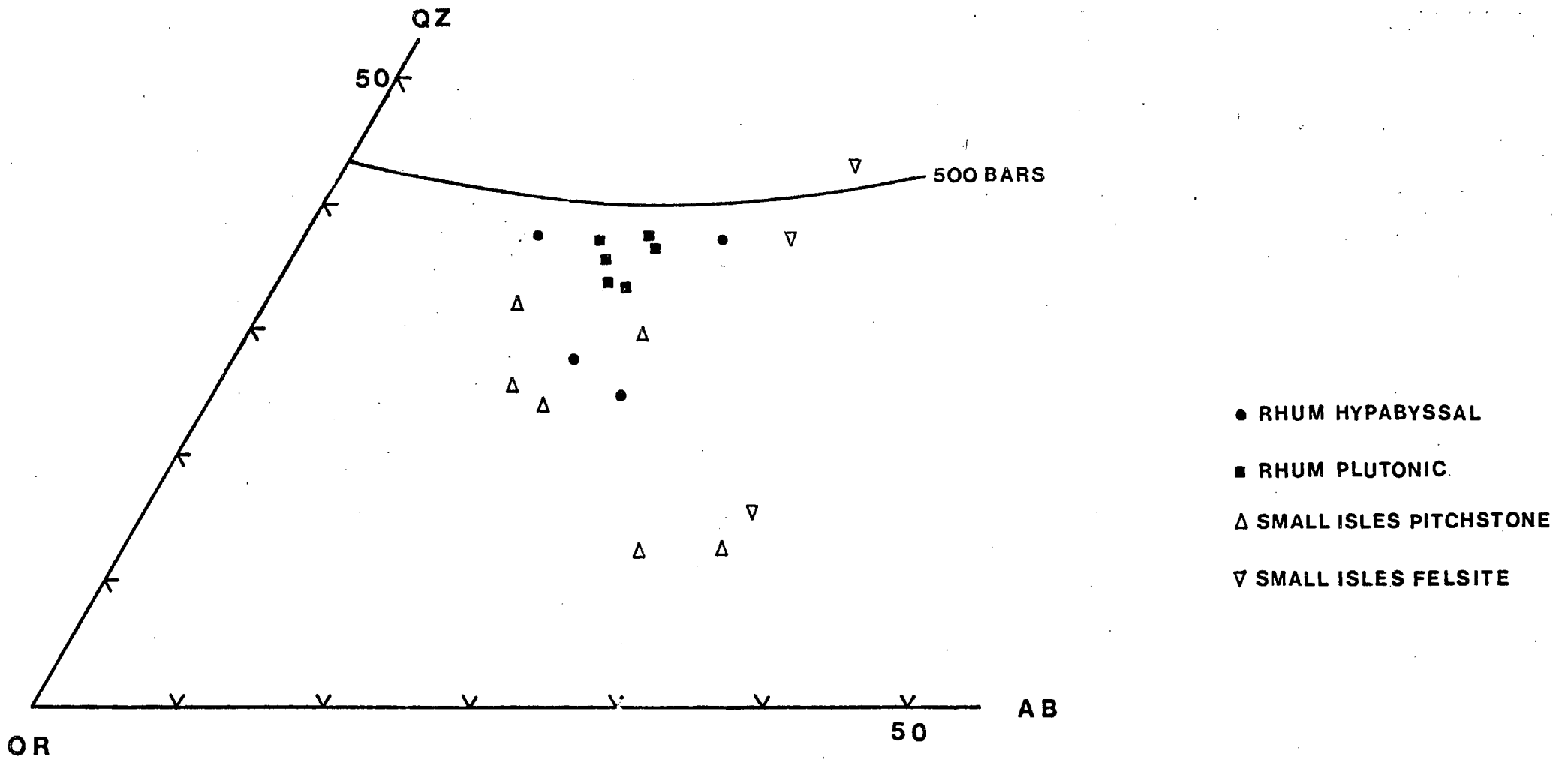
Fig.7.18. Rhum and Small Isle acid rocks projected into the normative system Qz-Or-Ab. The phase boundary feldspar + quartz + liquid at 500 bars is taken from Ridley (1971, Fig.3). Rhum hypabyssal (this study), Rhum plutonic (Dunham 1968, Table 3), Small Isles acid rocks (Ridley 1973, Table 6).

SPEC   MgO wt%

52A76   30·52

54A76   14·84

77321   21·69

77A76   19·42
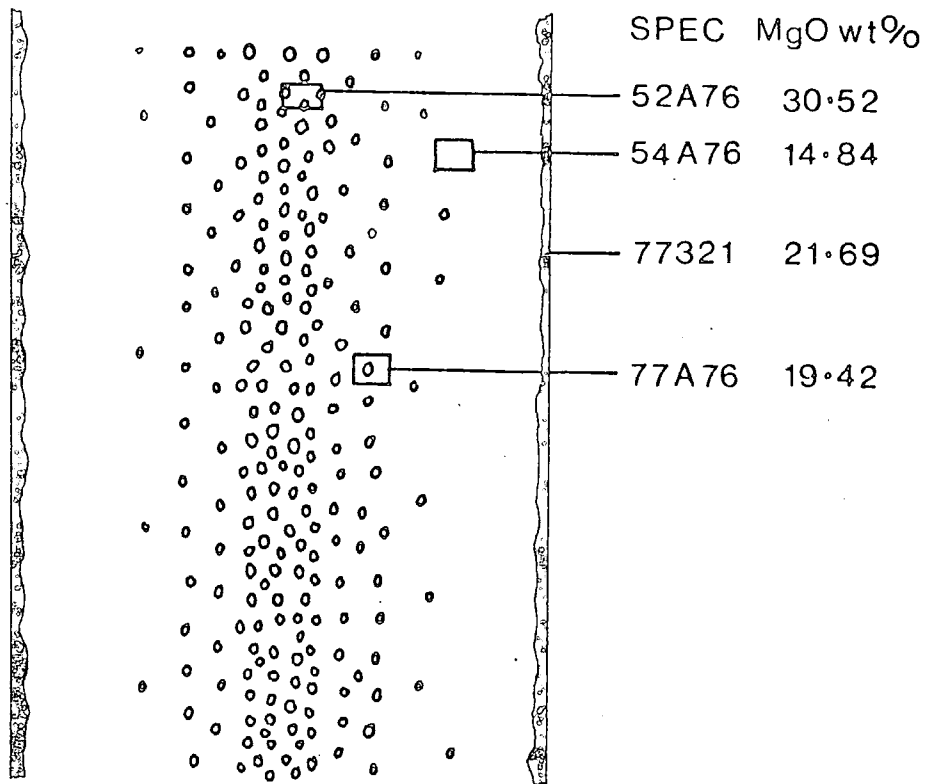
Fig. 7.19 Sketch illustrating the relationship of
          specimens with varying MgO contents in a
          flow differentiated picrite dyke.

Key
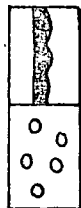
Chilled margin

Olivine phenocrysts

Fig. 7.20 Ti v. CaO/TiO$_2$ variation in the dolerite groups
1-4 and the early (high MgO) gabbros, 77104 not
included. C refers to the calculated liquid
composition of 77321. Symbols as in Fig. 7.1.
The field of mid-ocean-ridge basalts (MORB) is
taken from Sun et al.(1979, Fig.1).
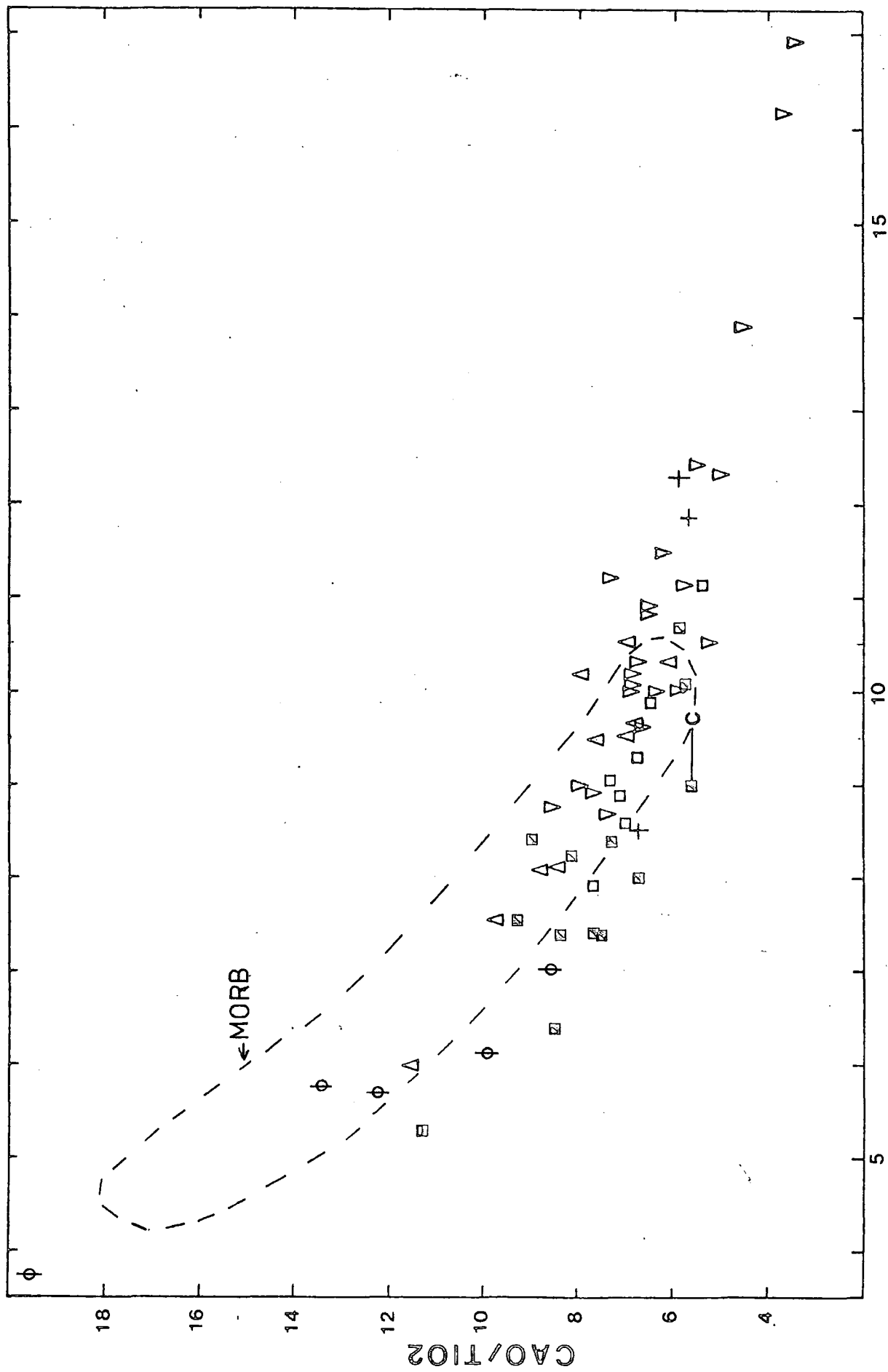
Fig. 7.21 Ti v Al$_2$O$_3$/TiO$_2$ variation in the dolerite
groups 1-4 and the early (high MgO) gabbros,
77104 not included. C refers to the calculated
liquid composition of 77321. Symbols as in
Fig. 7.1. The field of mid-ocean-ridge basalts
(MORB) is taken from Sun et al. (1979, Fig.1).
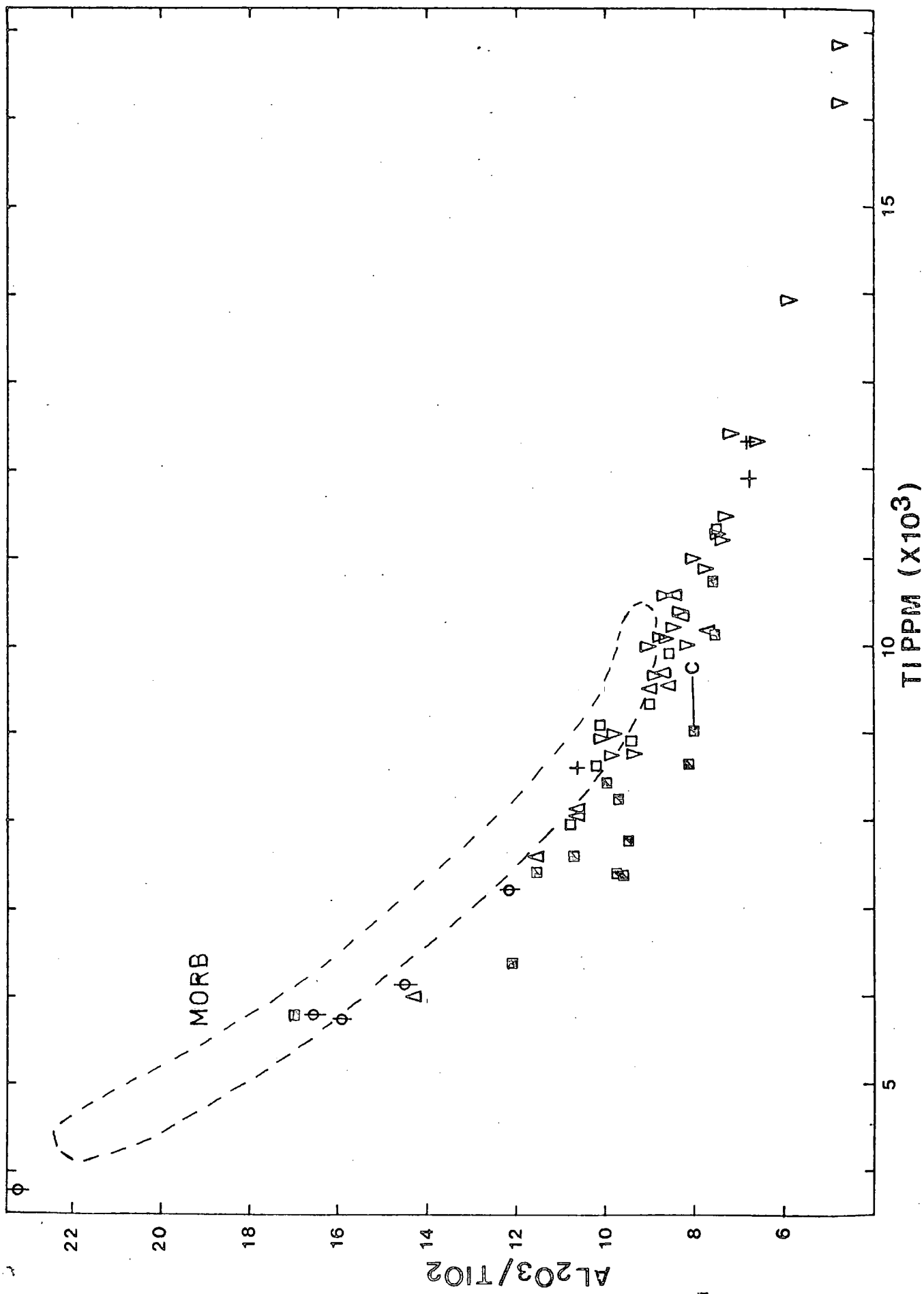
Specimen	Fe$_2$O$_3$*	Total alkalis	TiO$_2$	MgO
54A76	12.19	1.65	1.38	14.84

Method	Fe$_2$O$_3$	FeO	Fe$_2$O$_3$/FeO	Calculated liquidus olivine composition (Fo)
1	2.88	8.38	0.344	91.33
2	1.50	9.62	0.156	90.17
3	1.45	9.66	0.150	90.14
4	1.67	9.46	0.176	90.31

Table 7.1 Calculated Fe$_2$O$_3$ ratios and liquidus olivine compositions in 54A76 to show the affects of the various iron oxidation state procedures advocated by different authors.

Method 1 = Irvine and Baragar (1971)
Method 2 = Thompson et al. (1972)
Method 3 = Brooks (1976)
Method 4 = Clarke and O'Hara (1979)

*Total iron as Fe$_2$O$_3$

		Skye			Group 5 dolerites						High MgO Gabbros					
		1	2	3	4	5	6	7	8	9	10	11	12	13	14	16
	Specimen	Average	Max	Min	77056	77323	SR151	SR229	SR238	SR284	77031	77033	77257	77292	77320	77104
	SiO_2	47.98	46.37	50.03	46.35	46.34	46.57	47.50	46.75	47.61	49.95	49.24	47.15	48.98	46.14	47.42
	Al_2O_3	16.35	13.86	21.34	14.43	15.92	15.78	14.53	16.18	15.05	14.82	14.39	15.12	15.74	15.44	15.94
	Fe_2O_3*	11.66	7.42	15.22	12.73	12.01	12.41	13.28	12.26	12.94	10.37	10.02	10.52	11.47	12.14	9.97
	MgO	8.34	6.28	11.83	9.92	10.02	9.23	8.39	8.96	8.51	10.71	11.22	11.95	9.74	11.68	10.48
	CaO	12.10	10.87	13.57	13.56	12.49	12.58	12.85	12.58	12.68	10.18	12.14	11.57	9.99	10.45	12.95
	Na_2O	2.12	1.71	2.72	1.70	2.01	2.16	1.96	2.04	1.82	2.18	2.02	2.28	2.49	2.36	1.88
	K_2O	0.16	0.04	0.22	0.08	0.05	0.05	0.06	0.05	0.05	0.56	0.10	0.22	0.16	0.23	0.17
	TiO_2	1.02	0.38	1.42	0.97	0.92	0.99	0.16	0.94	1.09	1.02	0.62	0.95	1.17	1.27	0.96
wt %	MnO	0.18	0.10	0.23	0.20	0.18	0.19	0.19	0.19	0.19	0.15	0.16	0.16	0.17	0.16	0.14
	P_2O_5	0.09	0.05	0.14	0.07	0.08	0.08	0.10	0.08	0.10	0.08	0.10	0.10	0.09	0.12	0.09
	Total	100.00			100.01	100.02	100.04	100.02	100.03	100.04	100.02	100.01	100.02	100.00	99.99	100.00
	Ni	—	— (121)	— (203)	163	176	149	90	147	108	157	95	215	41	174	209
	Cr	—	— (381)	— (457)	454	484	441	420	418	430	440	337	833	158	321	785
	Ba	—	— (6)	— (16)	29	24	272	45	170	68	101	72	72	117	97	51
	Nb	5	0 (1)	9 (2)	3	3	3	4	3	3	6	2	0	2	1	3
	Zr	49	20 (30)	83 (46)	43	42	45	56	47	47	86	16	56	33	79	61
	Y	25	8 (16)	37 (25)	21	21	25	24	23	23	17	9	15	10	19	12
	Sr	118	95 (106)	167 (143)	119	90	118	101	98	105	149	277	181	323	184	193
	Rb	1	0 (0)	8 —	2	1	2	2	2	1	14	2	6	3	7	3
ppm	Zn	—	— (67)	— (77)	76	74	85	77	74	na.	56	64	60	76	86	46
	Ti/Zr	121	100	144	135	131	132	124	120	139	71	232	102	212	96	94
	Y/Zr	0.51	0.40	0.66	0.49	0.50	0.56	0.43	0.49	0.49	0.20	0.56	0.27	0.30	0.24	0.20
	Zr/Nb	9.8	6.8	13.8	14.3	14.0	15.0	14.0	15.7	15.7	14.3	8.0	—	16.5	26.3	20.3

Table 7.2 A comparison of the Skye Preshal Mhor magma type with the Rhum group 5 dolerites and the early gabbros.

Analysis 1 Average of 15 representative Preshal Mhor type dykes and lavas (Mattey et al. 1977 Table IIA) water free

Analyses 2 - 3 Compositional range of Preshal Mhor magma type, (Mattey et al. 1977, Esson et al. 1975).
    Trace element data in brackets (I.T. Williamson - unpublished data)

Analyses 4 - 9 Group 5 dolerites (this study)

Analyses 10 - 16 High Mgo gabbros (this study). All but 77104 are either known or inferred to be early in
    the Rhum sequence.

*Total iron as Fe_2O_3 na = not analysed

		1	2	3	4	5	6	7	8	9
	Spec.	SR211	SK291	SK932	SK280	SR141	751210B	A	751218	SK956
	SiO_2	45.76	45.67	44.89	44.81	47.96	47.36	49.44	49.47	48.57
	Al_2O_3	16.98	16.28	16.04	15.48	14.69	15.00	14.19	14.35	15.70
	Fe_2O_3*	14.32	13.85	14.76	13.98	14.25	13.12	14.17	13.23	12.98
	MgO	7.95	8.43	9.97	10.02	7.53	9.72	5.81	6.48	7.00
	CaO	9.70	10.33	9.29	9.91	10.63	11.04	10.50	10.94	10.29
	Na_2O	3.08	2.83	2.81	2.71	2.72	2.02	3.01	2.92	3.02
	K_2O	0.11	0.31	0.22	0.25	0.12	0.39	0.71	0.16	0.59
	TiO_2	1.74	1.73	2.05	1.80	1.76	1.44	1.81	2.10	1.41
	MnO	0.18	0.22	0.21	0.22	0.16	0.17	0.21	0.19	0.22
wt %	P_2O_5	0.19	0.20	0.20	0.19	0.18	0.19	0.22	0.15	0.22
	Total	99.01	99.88	100.44	99.37	100.00	100.45	100.07	99.99	100.00
	Or	0.7	1.9	1.3	1.5	0.7	2.3	4.2	1.0	2.6
	Ab	25.3	22.1	22.0	20.5	23.3	17.2	25.7	25.0	24.0
	An	32.6	31.2	30.7	29.9	27.8	30.9	23.4	25.9	30.8
	Ne	0.6	1.2	1.0	1.6	–				
	Di	12.2	15.8	11.7	15.4	19.9	18.7	23.1	23.0	14.3
	Hy	–	–	–	–	11.7	11.4	10.3	15.5	9.9
	Ol	21.1	20.3	24.8	23.5	8.8	12.8	5.5	1.7	11.5
	Mag	3.9	3.7	4.0	3.8	3.8	3.5	3.8	3.6	3.6
	Ilm	3.3	3.3	3.9	3.5	3.4	2.8	3.5	4.0	2.8
	Ap	0.5	0.5	0.5	0.5	0.5	0.5	0.5	0.4	0.4
	D.I.	26.5	25.1	24.4	23.5	24.0	19.5	30.0	25.9	26.7

Table 7.3 A comparison of selected Skye lavas with Rhum dolerite group 6.

Analyses 1, 5, 7 Group 6 (This study)
Analyses 2 – 4 and 9 Skye Main Lava Series (Thompson et al. 1972)
Analyses 6 and 8 Skye Main Lava Series (I. T. Williamson unpublished data)
*Total iron as Fe_2O_3, all norms calculated with an $Fe_2O_3/Fe_2O_3 + FeO = 0.25$
A = average analysis of SR159 SR182 and SR282

Thickness of overburden	Erosion at 680 cm/1000 y	Erosion at 850 cm/1000 y
1.5 km	0.220 my	0.176 my
2.0 km	0.294 my	0.235 my
2.5 km	0.367 my	0.294 my

Table 7.4 Calculated duration of layered ultrabasic rock – lava eruption interval.

	SPEC 77258	P1 COMPOSITION*	CALCULATED LIQUID
SiO_2	48.40	47.16	49.60
Al_2O3	18.89	33.04	6.04
Fe_2O3	8.38	0.65	15.51
MgO	6.52	0.19	12.28
CaO	14.21	16.97	11.61
Na_2O	1.67	2.58	1.77
K_2O	0.66	0.02	1.25
TiO_2	1.04	0.02	1.98
MnO	0.13	–	0.25
wt % P_2O_5	0.09	–	0.17
equivalent wt % pc	49.9**		

* Average of 7 analyses of group 7 phenocrysts

** Modal percent converted to equivalent wt %

Table 7.5 Calculated interstitial liquid composition in a big feldspar (group 7) dolerite.

	Average	Maximum	Minimum
SiO_2	40.90	42.14	39.30
Al_2O3	7.84	10.81	4.08
$Fe_2O_3{}^*$	12.05	14.43	10.55
MgO	33.13	41.91	26.60
CaO	4.24	6.57	1.95
Na_2O	0.72	1.15	0.18
K_2O	0.10	0.17	0.03
TiO_2	0.48	0.77	0.24
MnO	0.18	0.20	0.16
P_2O_5	0.07	0.10	0.03

wt %

Total   99.71

	Average	Maximum	Minimum
Ni	1915	2535	1233
Cr	2398	4456	2214
Ba	30	91	0
Nb	2	8	0
Zr	30	53	13
Y	6	11	1
Sr	72	147	22
Rb	3	5	0
Zn	74	110	47

ppm

Table 7.6   Average composition and the range of compositional variation in the peridotite plugs.

Table 7.7   Comparison of Rhum plutonic, Rhum hypabyssal
and Eigg hypabyssal acid rocks.

Analyses 1 - 3   Average and range of Rhum pluton:
(Dunham 1968 Table 3)
Analyses 4 - 8 (this study)
Analysis 9   Cleadale felsite dyke (Ridley 1973 T:

+(includes 1.8% Acmite)

		1	2	3	4	5	6	8	9
		Average	Max	Min	77159	77239	77241	77180	E6
	SiO_2	70.74	72.54	69.39	69.52	71.68	69.36	76.13	75.76
	Al_2O_3	12.69	13.82	12.00	13.49	13.03	13.78	12.69	9.44
	Fe_2O_3*	5.04	5.43	3.50	4.86	4.91	5.22	2.45	3.16
	MgO	0.79	1.14	0.32	1.18	0.36	0.84	0.07	0.36
	CaO	1.74	2.33	0.97	2.03	2.70	1.15	0.07	0.71
	Na_2O	4.12	4.28	3.92	4.73	4.41	4.72	3.83	3.21
	K_2O	3.21	3.68	2.68	3.18	2.15	3.99	4.56	5.19
	TiO_2	0.66	0.81	0.42	0.74	0.59	0.71	0.22	0.15
	MnO	0.15	0.36	0.06	0.09	0.10	0.08	0.04	0.05
wt %	P_2O_5	0.13	0.20	0.03	0.19	0.05	0.11	0.02	0.08
	Total	99.27			100.01	99.98	100.16	100.08	98.11
	Ba	1176	1317	1033	896	847	–	161	–
	Nb	–	–	–	14	20	19	24	–
	Zr	324	411	266	349	704	664	524	–
	Y	–	–	–	36	74	59	40	–
	Sr	221	249	197	188	367	130	17	43
	Rb	93	99	59	88	181	115	166	116
ppm	Zn	–	–	–	108	115	–	107	–
	Qz	29.78			22.8	30.2	21.0	35.1	38.9[+]
	Cor	0.38			–	–	–	1.4	–
	Or	19.12			18.9	12.8	23.7	27.0	31.4
	Ab	34.68			40.2	37.5	40.1	32.4	20.1
	An	5.97			6.2	9.4	4.7	0.2	2.7
	Dl	1.38			2.2	3.1	0.3	2.8	4.7
	Hy	2.20			6.6	4.4	7.2	–	–
	Mt	4.03			1.3	1.3	1.4	0.7	0.3
	11	1.30			1.4	1.1	1.4	0.4	0.2
	ap	0.3			0.5	0.1	0.3	–	–

319

TABLE 7.8

COMPARISON OF RHUM HIGH MgO LIQUIDS WITH OTHER HEBRIDEAN AND WORLDWIDE HIGH MgO COMPOSITIONS
Analyses 1-6 (this study); Analyses 7-8 (Gibb 1976, Table 1); Analyses 9-10 (Clarke 1970, Table 1)
Analyses 11-12 (Jakobsson et al. 1979)

	1	2	3	4	5	6	7	8	9	10	11	12
Spec	77321	77321L	77024	44A76	54A76	93A76					RE78	RE149
SiO_2	42.66	42.38	44.51	45.69	45.09	46.62	45.64	46.54	45.6	44.4	46.21	46.21
Al_2O_3	12.06	12.90	14.96	14.31	13.30	12.94	13.11	14.77	10.8	10.2	13.69	13.00
Fe_2O_3*	11.93	12.87	11.72	10.86	12.18	12.03	11.95	11.36	11.4	12.1	9.32	10.08
MgO	21.69	19.60	15.55	15.73	14.84	14.89	14.58	9.86	19.7	18.6	18.15	18.78
CaO	8.41	8.97	9.93	10.75	11.29	9.85	10.72	12.06	9.2	9.7	10.99	10.79
Na_2O	1.16	1.24	2.18	1.08	1.56	1.65	1.39	1.53	1.04	1.37	1.32	1.16
K_2O	0.20	0.22	0.05	0.35	0.09	0.30	0.13	0.14	0.08	0.13	0.01	0.05
TiO_2	1.50	1.60	0.88	1.00	1.37	1.41	0.78	1.17	0.76	1.18	0.41	0.50
MnO	0.16	0.17	0.17	0.14	0.17	0.18	0.16	0.19	0.18	0.17	0.15	0.16
P_2O_5	0.23	0.25	0.08	0.09	0.15	0.13	0.08	0.07	0.09	0.14	0.02	0.05
Total	100.00	100.00	100.03	100.00	100.04	100.00	98.54	97.69	98.85	97.99	100.27	100.78
Or	1.2	1.3	0.3	2.1	0.5	1.8	0.8	0.9	0.5	0.8	0.1	0.3
Ab	9.9	10.0	14.9	9.2	13.3	14.1	12.1	13.4	9.0	12.0	11.2	9.8
An	27.4	29.2	33.0	33.5	29.3	27.3	29.9	34.1	25.1	22.0	31.6	30.1
Di	10.5	11.2[1]	12.3[2]	15.8	21.1	17.0	19.4	22.0	16.7	21.3	18.4	18.4
Hy	1.0	[1]	[2]	10.8	2.8	12.5	10.8	15.8	15.9	5.6	5.3	7.6
Ol	43.4	40.9	32.8	23.6	26.7	21.1	22.8	8.2	28.1	32.4	30.1	30.0
Mt	3.2	3.5	3.1	2.9	3.3	3.2	3.3	3.1	3.1	3.3	2.5	2.7
Il	2.9	3.1	1.6	1.9	2.6	2.7	1.5	2.3	1.5	2.3	0.8	1.0
Ap	0.5	0.6	0.2	0.2	0.4	0.3	0.2	0.2	0.2	0.3	0.0	0.1
D.I.	11.1	11.6	16.9	11.3	13.9	15.9	12.8	14.2	9.5	12.7	11.3	10.1
Modal % ol pc	9.1‡	0.0	‡	A	1.45	A	~20	A	-	-	22.6	26.8

+[1] includes 0.3%Ne; +[2] includes 1.8%Ne; *Total iron as Fe_2O_3; ‡ Olivine phyric but see Chapter 6; ‡ modal%
converted to equivalent wt% to calculate 77321L; All norms calculated water free with an $Fe_2O_3/FeO+Fe_2O_3$ ratio
of 0.25. A = aphyric.

Type 1 Picrite				Type 2 Picrite			
Specimen	Modal % olivine phenocrysts	MgO wt%	Calculated liquids olivine composition (Fo)	Specimen	Modal % olivine phenocyrsts	MgO wt %	Calculated liquids olivine composition (Fo)
53A76	6.4	20.73	93.13	77052	15.8	16.14	90.65
54A76	1.45	14.84	90.31	77093	n.d.	10.71	86.76
69A76	n.d.	18.47	91.88	77095	n.d.	12.74	88.44
71A76	n.d.	19.59	92.15	77101	21.9	20.36	92.55
77A76	n.d.	19.42	92.40	77107	n.d.	18.24	91.64
77077	10.2	15.19	90.86	77224	n.d.	13.46	88.60
77321	9.4	21.69	93.29				
77321L[+]	0	19.60	91.09				
7734L	6.3	15.74	90.62				

Observed range of olivine phenocryst
compositions Fo 84.9 - Fo 88.8

Observed range of olivine phenocryst
compositions Fo 86.9 - Fo 88.8

Table 7.9   Calculated liquidus olivine compositions in the type 1 and type 2 picrites; see text
for discussion of modal data and interpretation.

[+]calculated olivine phenocryst free composition.   n.d. = not determined.

CHAPTER   EIGHT

THE PROBLEM OF THE RHUM LAYERED SERIES PARENT MAGMA
    AND THE RELATIONSHIP TO OTHER HEBRIDEAN SUITES

Introduction

This chapter is split into two sections. Part
one deals with the enigmatic question of the composition
of the magma parental to the Rhum layered peridotites.
The various hypotheses pertaining to this composition
are discussed in detail and an alternative hypothesis
is presented. The second section compares the Rhum
dolerite and Rhum lava suites and the relationship of
the former to some other Hebridean basaltic suites is
mentioned in brief.

I. THE PROBLEM OF THE RHUM LAYERED SERIES PARENT MAGMA
Introduction

The layered ultrabasic rocks of Rhum consist of a
subhorizontal alternation of olivine-rich (feldspathic
peridotite) and plagioclase-rich (allivalite) layers that
were originally thought to represent a succession of
sill-like injections of peridotite and allivalite
magma (Harker 1908), but are now interpreted as a
cumulate sequence dominated by a large scale alternation
of olivine-chrome spinel cumulates and olivine plagioclase $^{+}_{-}$
clinopyroxene cumulates, (Wager and Brown 1968). Each

peridotite layer and the overlying allivalite layer
are thought to be the complementary products of a single
major episode of crystal accumulation and are referred
to as units. Fifteen units have been recognised in
the 750m sequence forming the twin peaks of Askival and
Hallival in eastern Rhum (Brown 1956). These units vary
between 15m and 150m in thickness and the peridotite
member is generally considerably thicker than the
allivalite. By contrast in Southwest Rhum, only three
complete units (B,C,D) varying between 300m and 500m in
thickness have been recognised in the 1400m succession
of Southwest Rhum (Wadsworth 1961). These are underlain
by harrisites and cumulates believed to represent the
top of another unit (A). The intervening ground between
the two documented areas is presently undergoing detailed
research (J. McClurg pers. comm.).

The ultrabasic rocks are thought to represent the
uplifted central portion of the high density mass known
to underlie Rhum (McQuillin & Tuson, 1963). The absence
of a definite chilled margin has lead to various hypotheses
concerning the composition of the magma responsible for
the ultrabasic rocks. As stated earlier Brown (1956),
Wadsworth (1961) and Wager and Brown (1968) convincingly
demonstrated that the majority of these peridotites were
the product of crystal settling and related processes.

Any hypothesis concerning the parent magma composition
must take into account the abundant constraints which
these and subsequent studies (Donaldson et al. 1973,
Donaldson 1975, Henderson and Gejbels 1977,Dunham and Wadsworth,
1978) place on the parent magma composition.

There are four current hypotheses concerning this
parent magma and the proposed compositions pertaining
to three of these hypotheses are presented in Table 8.1.
Having established that the concept of cumulus phases
and intercumulus liquids were relevant to the Rhum
pluton, Brown (1956) noted the extensive zoning of
the interstitial minerals in a specimen from unit 3 and
suggested that the interstitial liquid in this ortho-
cumulate rock approximated the primary unmodified parent
composition. He estimated the composition of this liquid
by subtracting the proportion of the chemistry equivalent
to the cumulus phases (50%) from the whole rock analysis
(Analysis 1, Table 8.1).

An alternative hydrous felspathic peridotite parent
magma was proposed by Donaldson et al. (1973) and later
discussed in more detail by Donaldson (1975). These
authors showed that magmas of this composition were
available in the peridotite breccias of western Rhum
and were responsible for the production of the poikilo-
macro-spherulitic feldspars up to 1m diameter which are
best developed in the Dornabac breccia. These feldspars

(composition An80) were considered to reflect rapid growth under conditions of low nucleation density. No zoning was detected between the nucleus and ray extremity and the absence of an overlying liquid precluded an interpretation of these unzoned feldspars as adcumulus growth phenomena. In his later paper Donaldson (1975) emphasised that the unzoned, calcic compositions of the more normal textured plagioclase in other breccias on Rhum could not be explained by the adcumulus growth hypothesis as the matrix liquids were intruded into semi-consolidated peridotite and were consequently not in contact with overlying liquid. In addition he noticed that the calcic anorthosite-gabbro veins which extend from the breccias into the adjacent peridotites were the filter pressed residual liquids from the breccia matrices. These veins contain at least 10% more normative anorthite than basalt and must have been derived from a relatively mafic parent. The Eastern Layered Series peridotites contain a very small proportion of late stage primary hydrous phases and this argues against a hydrous parent. Donaldson (1977) has since restated his opinions and now considers a calcic parent akin to the Preshal Mhor magma type and the eucritic dykes of Skye to be a suitable parent. A hydrous feldspathic peridotite magma is considered to be an unlikely parent composition and is not discussed further.

A detailed hypothesis advocating a eucrite parent (Analyses 2 and 3, Table 8.1) which was intruded with olivine and chrome-spinel phenocrysts at a temperature slightly above the plagioclase liquidus was outlined by Gibb (1976). The main justification for this proposal was the abundance of this type of magma in and around the Skye central complex and the suggestion of Gibb (1976) that the Rhum and Skye centres may have been comagmatic.

Finally, there is a growing body of opinion that a refractory magma akin to the Preshal Mhor magma type of Skye (Mattey et al., 1977) may have parental to both the Rhum layered peridotites (Donaldson 1977, Dunham and Wadsworth 1978) and other Hebridean layered intrusions (Skelhorn et al. 1979, Gamble 1979). There is some confusion in terminology regarding this proposed parent. Dunham and Wadsworth (1978) explicitly state that the low-alkali, high-calcium tholeiite of Esson et al. (1975) (which equals the Preshal Mhor magma type of Mattey et al. 1977) is a likely parent. Similarly Skelhorn et al. (1979) draw attention to the compositional similarity of the chilled margin of the Ben Buie intrusion with the Preshal Mhor magma type. In his account of the anorthosite dykes of northwest Skye, Donaldson (1977) noted the striking similarity of the interstitial liquid in these dykes with Preshal Mhor magma type. However,

in his discussion of the parent magma compositions of the

layered basic and ultrabasic rocks of Skye and Rhum he

considers "high-lime liquids" (in the sense of Drever

and Johnson 1966) to be suitable parents. Despite these

difficulties in terminology it is clear that these

authors (perhaps with the exception of Donaldson 1977)

consider the Preshal Mhor magma type _sensu stricto_ to

be the Rhum parent magma. Finally it should be noted

that both Dunham and Wadsworth (1978) and Gamble (1979)

considered the eucrite parent of Gibb (1976) to be a "high

calcium low alkali tholeiite" (Dunham and Wadsworth op.cit.

p.355, Gamble op.cit. p. 5); however, it will be shown later

that this is clearly not so.

Constraints on the parent magma composition

The most obvious constraint on any parent magma

composition is that it must be capable of crystallising

phases compositionally identical to those found in the

layered peridotites. Whilst this is obviously difficult

to show unequivocally, it is a clear feature of the

reasoning behind both Brown's (1965) and Gibb's (1976)

hypothesis in that these magmas would crystallise the

high temperature minerals Cr-spinel, forsteritic olivine,

calcic plagioclase and diopsidic pyroxene. Minerals of

this composition do occur in the picritic dykes of Skye

(Gibb 1968). The mineralogy of the Preshal Mhor magma type was investigated by Esson et al. (1975) who show that the compositions of the olivine and plagioclase phenocrysts are similar to those in the Rhum layered series and the groundmass pyroxenes are also sufficiently calcic. However, no spinel phenocrysts were observed and the composition of the groundmass spinels is titanomagnetite not Cr-spinel. This discussion is not intended to quibble over minor detail as both Brown (pers. comm. 1976) and Gibb (pers. comm. 1977) presented the analyses quoted in their accounts to illustrate the broad type of magma they were discussing, not the precise parent composition. However, the discrepancy in spinel composition noted above is judged to be significant.

The broad sequence within each unit of olivine Cr-spinel cumulates successively overlayed by olivine-plagioclase and plagioclase-clinopyroxene cumulates infers the following order of low pressure crystallisation:

Olivine - plagioclase - clinopyroxene

In addition, the presence of several discrete Cr-spinel layers at the base of several units (Brown 1956) indicates Cr-spinel preceeded olivine. The sequence of crystallisation $Ol \rightarrow Pl \rightarrow Cpx$ in compositions 1 to 3 (Table 8.1) has been confirmed experimentally at atmospheric pressure by Forster (1978) who also showed spinel preceeded olivine in

compositions 1 and 3. It must be noted however that
the melted compositions were Cr free and the crystall-
isation behaviour of spinel in these charges is
consequently not strictly comparable with Cr-bearing
compositions. The melting relationships of two Preshal
Mhor type basalts was investigated at atmospheric pressure
by Esson et al. (1975) who showed that plagioclase was
the liquidus phase, closely followed by olivine then
clinopyroxene then magnetite. The Rhum magma chamber
was emplaced at very high crustal levels (the overburden
was estimated to be 1.5 to 2.5 km thick in Chapter 7, p.233).
This slight increase in pressure is unlikely to reverse
the order of crystallisation determined at atmospheric
pressure by Esson et al. (op.cit.). Thus the presence
of plagioclase as the first liquidus phase in the Preshal
Mhor magma type means this basalt does not satisfy a
fundamental requirement of a Rhum layered series parent
magma. Note however that Dunham and Wadsworth (1978)
consider the crystallisation of each unit begins within
the allivalite of the underlying lithological unit (ie.
below the allivalite-peridotite phase change which marks
the junction between the lithological units) which
perhaps surmounts this difficulty.

One of the main points to come out of Brown's (1956)
and Wadsworth's (1961) studies was the distinct lack of
optically detectable cryptic variation within the Rhum

ultrabasic sequence. Subsequent mineralogical

investigations by electron microprobe analysis has

shown there is slight but significant cryptic variation

within each of peridotite units (Dunham and Wadsworth

1978) with the phases in each unit attaining a

temperature minimum some way below the lithological

top of each unit. Brown (1956) considered each unit

to be a product of the accumulation of unzoned high

temperature minerals from a basaltic parent, the absence

of complementary differentiates necessitating an open

system fractionation environment. To explain the lack of

cryptic variation Brown (1956) cited the synthetic

system Di-An-Fo (Osborn and Tait 1952, in Brown op.cit.)

which indicated there would be a small drop in temperature

from the liquidus to the three phase cotectic. However,

more extensive experimental investigation in the system

Di-Fo-An-Ab (Yoder and Tilley 1962) showed that there

would be a considerable drop in temperature to the three

phase cotectic. This work prompted Wager and Brown (1968)

to invoke the process of delayed crystal nucleation in a

supersaturated magma to explain the lack of cryptic

variation. This hypothesis was questioned by Gibb (1976)

who considered in the light of his previous work on

this topic (Gibb, 1974), that supersaturation of

plagioclase was unlikely to occur in a slow cooling

plutonic body the size of the Rhum intrusion. It should

be noted, however, that delayed nucleation of olivine in supercooled liquids has been invoked to explain the peculiar textured olivines (harrisite) in the Rhum intrusion (Donaldson 1974) showing that supercooling is a viable petrogenetic process within the Rhum peridotites. The fall in temperature from the olivine liquidus to the clinopyroxene liquidus in Brown's (1956) proposed parent was shown to be in the order of $100^{\circ}C$ by Forster (1978) which suggests that considerable cryptic variation (greater than that found by Dunham and Wadsworth, 1978) would be expected if a basalt was the parent magma (but see later discussion, p.333).

The fall in temperature from the olivine liquidus to the clinopyroxene liquidus is substantially reduced in Gibb's (1976) hypothesis in that the magma enters the chamber with olivine and Cr-spinel in suspension at a temperature just above the plagioclase liquidus. In this model the Cr-spinel and olivine are precipitated to form the sp-olivine cumulates and the olivines are thought to re-equilibrate to slightly lower temperatures during descent. Crystallisation and settling of plagioclase then clinopyroxene ensues, producing the ol-pl and pl-cpx cumulates. Early experimental work on this type of magma (Gibb 1971) showed that the temperature drop from the entry of plagioclase to the

entry of clinopyroxene was probably small ($\sim 10^{\circ}$C).
However, subsequent work has shown this to be erroneous
and the plagioclase-clinopyroxene temperature interval
is estimated to be in the order of 45°C (Biggar and Gibb, 1976).
Experimental work on Analyses 2 and 3 (Table 8.1) has
shown an even greater plagioclase-clinopyroxene temper-
ature interval of approximately 80° (Forster 1978). The
main conclusior that can be drawn from these experimental
investigations is that the fall in temperature from the
plagioclase liquidus to the clinopyroxene liquidus in
the Skye picrites is not compatible with the limited
cryptic variation encountered in the Rhum layered
peridotites.

An alternative explanation of the lack of cryptic
variation in the Rhum periodites has been advanced by
Usselman and Hodge (1978). These authors believed that
the thermal history of the liquid involved in open system
fractionation could be modelled numerically. They
showed that a limited number of replenishing intervals
and volumes can produce the situation where heat lost
during cooling equals the heat of input on replenishment.
Thermal modelling of the Rhum magma chamber, showed that
the constancy of process producing the individual units
yielded a steady thermal fractionating state with a
limited temperature interval. This has important

repercussions for the proposed Rhum layered series
parents (especially Brown's 1956 basic parent) as the
small fluctuations (less than 10°C) around the olivine-
plagioclase cotectic (Usselman and Hodge 1978, Fig.7) show
that little cryptic variation would be expected in these
phases in passing from unit to unit. Unfortunately
Usselman and Hodge did not show the effect of clinopyroxene
crystallisation on their model as this may upset the
delicate thermal balance attained along the olivine-
plagioclase cotectic, however the prior crystallisation
of spinel before olivine may reflect the rapid cooling
of magma on entry into the open system magma chamber.
These difficulties   withstanding, the thermal model
discussed above does seem to provide a viable explanation
of the limited cryptic variation within each unit and
explains the constancy of composition between successive
units within the peridotite sequence.

One feature of the Rhum ultrabasic rocks is the
complete separation of the Cr-spinel, into distinct
seams at various levels within these rocks. The
calculated settling rates of olivine and Cr-spinel
through a basic magma is presented in Table 8.2. (For
discussion of the methods used in these calculations see
Appendix 8.1). The gross differences between the
settling rate of olivine and Cr-spinel (chiefly a

function of their disparate size) suggest that the latter

would not be capable of forming a separate cumulate

horizon and argue in favour of in situ crystallisation

of all the phases in the magma chamber.   In addition both

Henderson and Gejbels (1977) and J. McClurg (pers. comm.)

have noted the presence of olivine cumulates both over-

lain and underlain (by thin spinel seams which once

again is not compatible with Gibbs (1976) hypothesis.

Another constraint on the parent magma composition

was given by Henderson and Gejbels (1977) who showed the

plagioclase within the Rhum peridotite are characterised

by light REE enrichment, which is strong evidence for a

light REE enriched parent.   In their discussion of this

observation Henderson and Gejbels (op.cit.) considered

this argued in favour of a basaltic parent produced by

limited partial melting and argues against a Preshal

Mhor magma type parent as these have light REE depleted

patterns (Mattey et al. 1977) and are believed to be

products of substantial partial melting (Thompson et al.

1972; Thompson 1974a; Mattey et al.1977; Wood 1979). There

is no REE data concerning the eucritic picrite dykes of

Skye.

Estimates of the volumes of basalt magma (Analysis 1,

Table 8.1) which produced the exposed peridotite sequence

on Rhum have been made by Henderson and Gejbels 1977. Calculations

based on an assumed Ni Kd coefficient of 10 between

olivine and magma (reasonable in view of the data in

Hart and Davis (1979, Fig.5)) and a NiO content of olivine

in the range 0.23-0.25 wt%; indicate large volumes of basalt

magma (2,200 km^3) are required by a basalt parent. This

volume estimate is probably too high as Dunham and Wadsworth

(1978), show the Rhum olivines can possess up to 0.4 wt%

NiO. Nevertheless a large volume of magma is a pre-

requisite of a basalt parent. The high Ni content of the

eucrite parent (Analysis 2 and 3, Table 8.1) drastically

reduce the necessary volume of the parent liquid. The

peridotite sequence in the eastern and western layered

series is known to be approximately 2.2km thick (Dunham

and Wadsworth 1978) but is believed to be underlayed by

15km of high density rocks (McQuillin and Tuson, 1963).

Although the underlying rocks probably contain a proportion

of differentiated material, a basalt parent will require

that enormous volumes of differentiates ($\sim 40x10^3 km^3$)

would have been expelled from the magma chamber, and the

bulk of these rocks must have been removed prior to the

eruption of the lavas of western Rhum (p.233). A high

MgO parent with an attendant low NiO olivine-magma Kd

(between 3 and 6, Hart and Davis 1979, Fig.7) and high

bulk magma Ni content will drastically reduce the volume

requirements of the parent magma.

Donaldson (1974) has shown that olivine textures very similar to those in the harrisitic or crescumulate peridotites of Rhum can be reproduced experimentally in supercooled magmas with low nucleation densities and high normative olivine. It can be argued that these crescumulate olivines are the product of upward growth of olivine from the magma chamber floor in a stagnant basalt magma (Wager et al. 1960) but the evidence presented by Donaldson (1974, 1976) is more convincing, thus a high normative olivine content (20-30%) appears to be a requisite of the Rhum parent magma. High normative olivine is a feature of one of the Skye picrites (Analysis 3, Table 8.1) but Gibb's (1976) model envisaged crystallisation of olivine prior to entry into the magma chamber and cannot explain these crescumulate textured rocks. The Preshal Mhor magma type (Analysis 1, Table 7.2) has a normative olivine content of approximately 15 wt% and does crystallise olivine but the Ni and Cr contents are relatively low. Donaldson (1977) explicitly states that these low trace element abundances support the proposition that these magmas "have fractionated large amounts of olivine and Cr-spinel during ascent from the mantle". Thus it appears that this magma type would be incapable of crystallising the large volumes of olivine encountered in the Rhum peridotites and possibly could not produce

the crescumulate textured olivines.

Finally, any proposed parent will gain credence
if magmas of similar composition are known to exist
on Rhum. The similarity of the proposed basalt parent
to the marginal gabbro of the northeastern margin of
the peridotite sequence was noted by Wager and Brown
(1968) and this study has shown that magmas broadly
similar to the Preshal Mhor magma type were available
at an early stage in the evolution of the complex. In
addition Preshal Mhor type magmas have been located as
dykes cutting the Rhum lavas but these are considered
to postdate the evolution of the Rhum magma chamber (see
detailed discussion in Chapter 7, p.239) and consequently
may not have been available during the formation of the
Rhum layered peridotites. The broad similarities of the
Rhum group picrites with the Skye picrites was noted
in Chapter 7, p. 259, but the latter are different in
detail (especially the lower MgO content) with respect
to the Rhum picrites.

The existence of high MgO liquids on Rhum has been
demonstrated in this study (see Table 7.8 and discussion
in relevant text) and it is suggested that magmas of this
type are the parent magma to the Rhum layered peridotites
as they satisfy the necessary requirements of a Rhum
parent magma discussed above.

These ultrabasic liquids crystallise minerals of the correct type (Cr-spinel, forsteritic olivine etc.) and by analogy with experimental work on rocks of similar composition (Gibb 1971, Forster 1978) will crystallise these minerals in the requisite order. Note however that the compositional dissimilarity of the Cr-spinel compositions in the type 1 and type 2 picrites (and the Rhum lavas) with respect to the primary spinels from the layered peridotites (Fig. 6.13) suggest that the former are not the precise parental magma type. These ultrabasic magmas (with high normative olivine) will be capable of producing crescumulate textured olivines on super-cooling and their high MgO and Ni contents are commensurate with the production of limited volumes of differentiates. One problem which has not been convincingly overcome is the limited cryptic variation within the peridotite units, however, if the thermal model of Usselman and Hodge (1978) is applicable to Rhum then this ultrabasic liquid parent will be as applicable as a basaltic parent. Confirmation of this however requires more detailed experimental and thermal modelling to produce an unequivocal interpretation.

In conclusion the Preshal Mhor magma type is believed to be an unsuitable parent magma for the Rhum layered peridotites. The basalt parent of Brown (1956) and the

eucritic parent with olivine + Cr-spinel in suspension

of Gibb (1976) have certain disadvantages which are

overcome by a high MgO - high CaO ultrabasic parent.

Magmas of the latter composition have been shown to

have existed on Rhum during the Tertiary, consequently

it is suggested that these Rhum magmas are the parent

magma to the Rhum layered peridotites.

II. A COMPARISON OF THE RHUM DOLERITES WITH THE RHUM
    LAVAS AND OTHER HEBRIDEAN SUITES.

The geochemistry of the Rhum lavas has been

presented in the revised Rhum Memoir (Dunham et al.,

in press) and the comparisons made here are consequently

based on as yet unpublished data. Four series of

mineralogically and chemically distinct lava flows of

olivine basalt, hawaiite, basaltic-andesite and icelandite

have been distinguished on Rhum and these are referred

to as the lava groups 2 to 5 respectively (Emeleus 1976,

Dunham et al., in press). Another basalt type geo-

chemically distinct from the former occurs as clasts in

the conglomerates associated with the lavas (Group 1,

Dunham et al., in press). The current investigation of

the petrographic and compositional variation of all the

rock types found as clasts in these conglomerates is

very important, as these conglomerates are the only key

to a better understanding of the geological history of

Rhum in post ultrabasic emplacement and pre-lava times.

Although both the lava and the dolerite suites contain a mixed assemblage of transitional basalts (Chapter 3, Fig. 3.6   ) and basaltic differentiates, comparisons of the dolerite groups with the lava groups of analogous composition has revealed important differences between the two suites. In addition, the dolerite groups 1-3 and the differentiated dolerite groups 11 and 12 have no analogues in the Rhum lava pile.

The tholeiitic lava group 1 basalts are similar in some respects to the more tholeiitic members of the dolerite group 4. However, there are differences in the Al_2O_3, MgO and Na_2O abundances, the Al_2O_3 content of the dykes is somewhat lower and the MgO and Na_2O contents higher than the levels in the lava group 1 basalts. Comparisons of the Al_2O_3 and MgO contents of the lava group 2 basalts and the more alkalic group 4 dolerites, the Hawaiites of lava group 3 and dolerite group 10 and the basaltic andesites of lava group 4 and the dolerite group 8 reveal similar discrepancies. The difference in MgO content of the two suites gives lower iron enrichment values for the dolerites (Fig. 8.1).

Although the icelandite lava group 5 and the dolerite group 9 rocks have similar SiO_2 contents they differ greatly in the relative abundances of Al_2O_3, MgO, CaO,

K_2O, TiO_2 and P_2O_5 these being lower (with the exception of MgO and CaO) in the dolerite dykes.

Some of the dolerite specimens were collected from dykes believed to have acted as feeders to overlying lavas (p.27). The geochemical differences outlined above suggest that these dykes did not feed the lavas now preserved _in situ_ or in the conglomerates of western Rhum, but to earlier lavas which were eroded prior to the eruption of the lavas of western Rhum. This emphasises the point made in Chapter 7 (p.232) that there is a considerable erosion interval postdating the emplacement of the dykes and preceeding the eruption of the lavas.

The high levels of MgO in the Rhum dolerite suite when compared with other Hebridean suites has been mentioned in Chapter 3 (p. 79). The well documented magma types of Skye (Thompson _et al_. 1972; Mattey _et al_. 1977) and some average compositions of the tholeiitic Ardnamurchan cone sheets (Holland and Brown, 1971) have been plotted along with the Rhum dolerites and the Rhum lavas in Fig. 8.1. This standard plot is generally used to illustrate the differences between tholeiitic differentiation (Fe-enrichment with limited alkali enrichment) and alkalic differentiation (little Fe-

enrichment for large increases in total alkalis) but
is used here to emphasise the dissimilarity between
the Rhum dolerite suite and the other Hebridean suites.
Note that the group 1 and group 2 lavas of Mull
(Beckinsale et al. 1978) are compositionally similar
to the Skye Main Lavas Series basalts (Beckinsale et al.
1978, p. 421).

Two other points of interest concerning the Rhum
minor intrusion suite in its Hebridean context merit
discussion. The Rhum dolerites are characterised by
fairly low concentrations of the incompatible elements
(Ti, K, P, Nb, Zr and Y) and Morrison (1978) has shown
this is also a feature of the Mull and Skye lavas. This
suggests that the mantle underlying the Hebridean centres
was depleted in incompatible elements prior to the
generation of the Tertiary magmas. This may be a primary
feature of this mantle which accreted with low incom-
patible element concentrations early in the Earth's
history or may reflect thorough leaching of incompatibles
during an earlier regional partial melting event. The
presence of Permo-Carboniferous dykes in the Hebrides
has been noted by Speight (1972) and Permo-Carboniferous
dykes in general are known to be alkalic in composition
(MacGregor, 1948   ). It is possible that the Permo-
Carboniferous partial melting event removed the bulk of

the incompatible elements leaving only an incompatible
depleted residue available for the Tertiary partial
melting event.

The zoning of the Skye lava pile from alkalic
basalt to tholeiitic basalt was considered to reflect
a progressive increase in the degree of partial melting
by Thompson et al. 1972 and Wood 1979. Similar zoning
of lava piles in Iceland and Troodos led Gibson et al.
(1976) to propose this was/general feature of basalts
from extensional tectonic environments. The Rhum minor
intrusion suite however shows the reverse situation in
that the earliest known igneous rocks on Rhum are
incompatible-depleted tholeiitic gabbros ($\simeq$ Preshal
Mhor tholeiite of Skye) and there is a progression
towards more alkalic (and more magnesian) compositions
with decreasing age. In view of the known differences
in the sequence of intrusion of analogous rocks on
Rhum and Skye (the generalised sequence lavas - basic
and ultrabasic intrusives - granophyre on Skye is the
reverse of the Rhum sequence), it is perhaps not sur-
prising that the trends of basic magma composition
associated with the centres are so dissimilar.

Fig. 8.1 $Fe_2O_3*/Fe_2O_3* + MgO$ v. $Na_2O + K_2O$ variation in some Hebridean suites.

Key to symbols

- o   Rhum dolerite suite (this study)

- ○   Average composition of Rhum Lava groups (Emeleus in Dunham et al. (in press).

- ⌀   Skye Preshal Mhor magma type (Mattey et al., 1977, Table IA).

- □   Skye Fairy Bridge Magma type (Mattey et al., 1977, Table V).

- □   Skye Main Lava Series magma type (Thompson et al., 1972, Table 1).

- Δ   Average composition of Ardnamurchan cone sheets (Holland and Brown, 1971, Table 1).

NA2O+K2O WT%

FE2O3/ FE2O3+MGO X10²
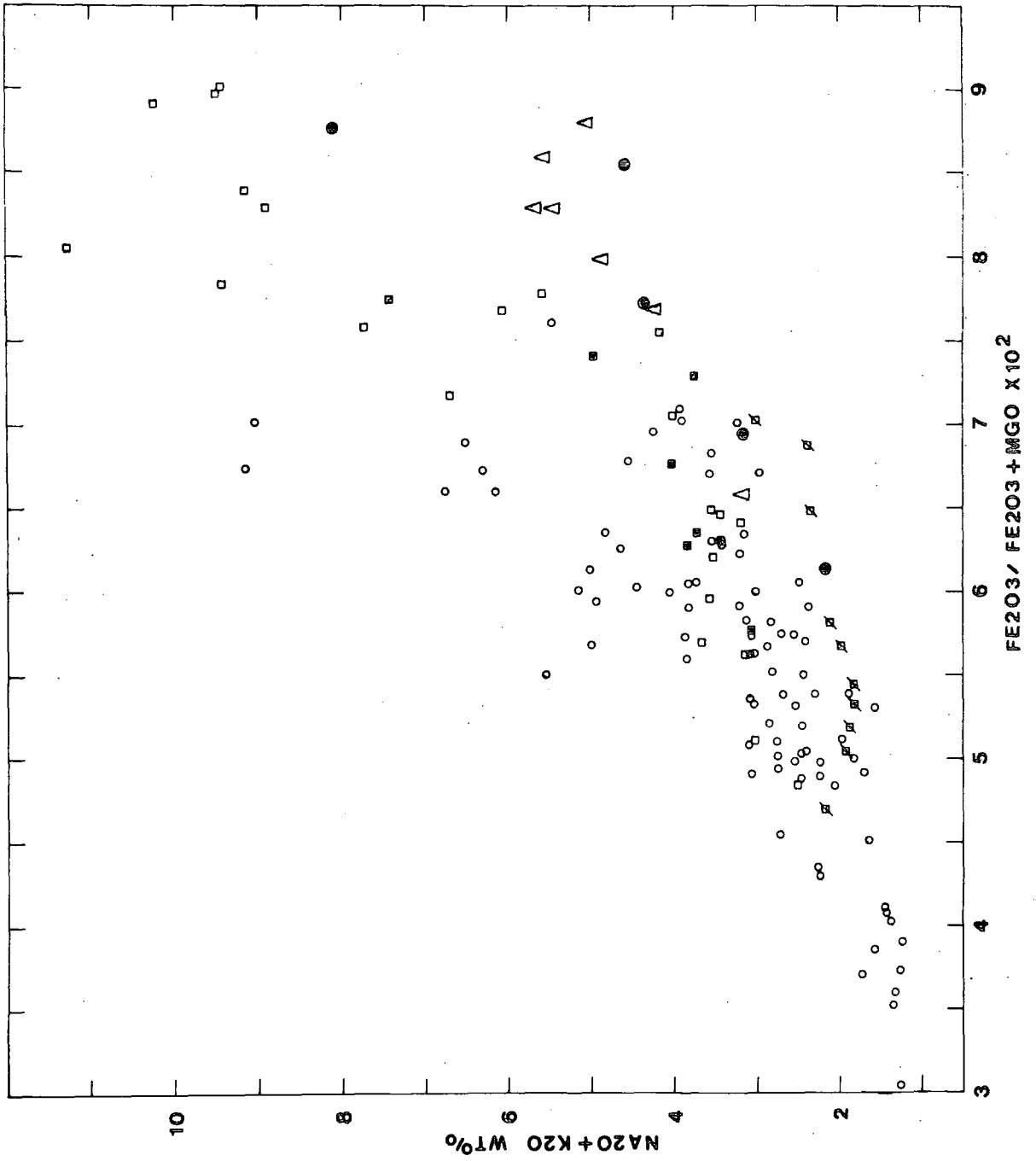
TABLE 8.1

SOME PROPOSED RHUM LAYERED SERIES PARENT MAGMAS
Analysis 1 Brown (1956, Table 8, anal.1)
Analysis 2-3 Gibb (1976, Table 1, B,c)

	1	2	3
SiO_2	46.80	46.54	45.64
Al_2O_3	18.60	14.77	13.11
Fe_2O_3	1.40	3.75	3.69
FeO	7.70	6.85	7.43
MgO	10.90	9.86	14.58
CaO	10.60	12.06	10.72
Na_2O	2.70	1.53	1.39
K_2O	0.30	0.14	0.13
TiO_2	0.80	1.17	0.78
P_2O_5	0.04	0.07	0.08
MnO	0.0	0.19	0.16
Cr_2O_3	0.04	440 ppm	0.14
Or	1.8	0.9	0.8
Ab	19.2	13.4	12.1
An⁻	37.8	34.1	29.9
Ni	2.0*	—	—
Di	11.9	22.0	19.4
Hy	—	15.8	10.8
Ol	23.2	8.2	22.2
Mt	2.7	3.1	3.3
Ilm	1.5	2.3	1.5
Ap	0.1	0.2	0.2

Wt% (label at left of Cr_2O_3 row)

*All norms calculated with a fixed Fe_2O_3/Fe_2O_3+FeO ratio of 0.25. Analysis 1 is hypersthene normative if the norm is calculated with the Fe_2O_3 and FeO values quoted by Brown (1956).

	Particle diameter	Viscosity (poises) 100	Viscosity (poises) 300	Viscosity (poises) 500	Viscosity (poises) 1000	Viscosity (poises) 3000
		cm/sec	cm/sec	cm/sec	cm/sec	cm/sec
Olivine (Fo85)	1 mm	0.2287	0.0762	0.0457	0.0228	0.0076
	3 mm	2.0580	0.6860	0.4116	0.2058	0.0686
Cr-spinel	0.3 mm	0.0848	0.0283	0.0170	0.0085	0.0028
	0.4 mm	0.1507	0.0502	0.0301	0.0151	0.0050

Table 8.2. Comparison of calculated settling rates (cm/sec) for olivines and Cr-spinels in the Rhum layered series to illustrate that olivine will settle much faster than the latter. For discussion of the calculation method see Appendix 8.1.

SUMMARY OF IMPORTANT POINTS

Several interesting facts concerning the Rhum minor intrusions have resulted from this investigation. A wide range of rock types came under scrutiny and the synthesis of their field relationships as expressed in Chapters 2 and 5 has allowed appraisal of the probable sequence of magma evolution on Rhum. The contrast between the Rhum sequence and that found in other well studied Hebridean centres (e.g. Skye, Thompson et al., 1972; Mull, Beckinsale et al., 1978) emphasises the complexity of mantle processes which can operate in a small area over a relatively short period of geological time.

The Discriminant Function Analysis technique applied to basalt classification in Chapter 3 has shown that there are real and distinct differences between the tholeiite, alkali olivine basalt and calc-alkali basalt magma types. Although the existence of basalts compositionally transitional between alkali olivine basalt and tholeiite basalt has been appreciated for several years this, statistical approach produced a method for numerically defining their transitional nature and allows for numeric comparisons of the departure of any basalt composition from the typical alkali olivine basalt or tholeiite basalt compositions.

The petrographic and mineralogical studies show that mineral textural and compositional variation in the Rhum

minor intrusions can be related to a variety of magmatic processes. The unusual texture of the minerals occurring in several of the dykes are similar to those produced in experimental charges and suggest that supercooling has played a role in the genesis of several of the Rhum dykes. Previous studies of compositional variation in spinel minerals has shown they are   sensitive indicators of magmatic change and providing the effects of primary and secondary variation can be disentangled they can be useful petrogenetic indicators. If future experimental studies concentrate on the roles of compositional variation and pressure in spinel genesis it is possible that this mineral type may offer great insight into magma genesis.

The geochemical data presented in Chapter 7 shows that liquids with approximately 15 wt% MgO were not uncommon on Rhum during the Tertiary and may alleviate several difficulties concerning the genesis of the Rhum layered peridotites and possibly the layered basic rocks in other Hebridean centres. Two principal trends are developed by the basic and intermediate rocks of Rhum, these being an iron enrichment - MgO depletion trend and an iron depletion - MgO depletion trend as exemplified in Fig. 7.2. These are broadly considered to reflect the differences between mantle and crustal petrogenetic processes. The petrogenetic discussion of these trends

in Chapter 7 attempted to distinguish between mantle
and crustal processes but the lack of more sophisticated
geochemical data (especially REE) precludes an unequivocal
interpretation.

References

Anderson F. W. and Dunham K. C. 1966. The Geology of
Northern Skye. Mem. Geol. Surv. U.K.

Aoki K. and Shiba I. 1973. Pyroxenes from Lherzolite
inclusions of Itinomegata. Lithos 6, 41-51.

Bailey E. B. 1945. Tertiary igneous tectonics of Rhum.
Quart. Jl Geol. Soc. Lond. 100, 165-191.

Bailey E. B. 1956. Hebridean notes: Rhum and Skye.
Lpool. Manchr. Geol. Jl 1, 420-426.

Barberi F., Bizouard H. and Varet J. 1971. Nature of the
clinopyroxene and iron enrichment in alkalic and
transitional basaltic magmas. Contrib. Mineral.
Petrol 33, 93-107.

Bass M. N. 1972. Occurrence of transitional abyssal
basalts. Lithos 5, 57-67.

Beckinsale R. D., Pankhurst R. J., Skelhorn R. R. and
Walsh J. N. 1978. Geochemistry and petrogenisis of the
early Tertiary lava pile of the Isle of Mull, Scotland.
Contrib. Mineral. Petrol. 66, 415-427.

Beddoe-Stephens B. 1977. The petrology and geochemistry
of the Rossland volcanic rocks, Southern British
Columbia. Unpublished Ph.D. Thesis, Univ. of Durham.

Biggar G. M. and Gibb F. G. F. 1976. Experimental re-
crystallisation of an ultrabasic dyke rock from Skye.
Prog. in Exp. Petrol. Rept 3 N.E.R.C. 216-217.

Binns P. E., McQuillin R. and Kenolty N. 1973. The Geology
of the sea of the Hebrides. Rept. of the Inst. of
Geological Sciences 73/14 London pp. 44.

Binns R. A., Duggan M. B. and Wilkinson J. G. E. 1970.
High Pressure megacrysts in alkaline lavas from
N. E. New South Wales. Am. Jl Sci. 269, 132-168.

Birch F., Schairer J. F., and Spicer H. C. 1942. Handbook
of physical constants. Spec. Pap. Geol. Soc. Am.
36, pp. 325.

Black G. P. 1952. The age relationships of the granophyre and
basalt of Orval, Isle of Rhum. Geol. Mag. 98, 106-112.

Black G. P. and Welsh W. 1961. The Torridonian succession of the Isle of Rhum. Geol. Mag. 98, 265-276.

Bottinga Y. and Weill D. F. 1970. Densities of liquid silicate systems calculated from partial molar volumes of oxide components. Am. Jl Sci. 269, 169-182.

Bott M. H. P. and Tuson J. 1973. Deep structure beneath the Tertiary volcanic regions of Skye, Mull and Ardnamurchan, North West Scotland. Nature Phys. Sci. 242, 114-116.

Bott M. H. P., Armour A. R., Himsworth, E. M., Murphy T. and Wylie G. 1979. An explosion seismology investigation of the continental margin west of the Hebrides, Scotland at 58°N. Tectonophys. 59, 217-231.

Bowen N. L. 1928. The evolution of igneous rocks. Princeton University Press, Princeton. N.J. pp. 332.

Brooks C. K. 1976. The Fe_2O_3/FeO ratio of basalt analyses: an appeal for a standardised procedure. Bull. Geol. Soc. Denmark. 25, 117-119.

Brown G. C. and Musset A. E. 1976. Evidence for two discrete centres in Skye. Nature 261, 218-219.

Brown G. M. 1956. The layered ultrabasic rocks of Rhum, Inner Hebrides. Phil. Trans. Roy Soc. B240, 1-53.

Brown G. M. 1957. Pyroxenes from the early and middle stages of fractionation of the Skaergaard intrusion, East Greenland. Miner. Mag. 31, 511-543.

Brown G. M. 1967. Mineralogy of basaltic rocks, in Hess H. H. and Poldervaart A. (Eds). Basalts, the Poldervaart treatise on rocks of basaltic composition. John Wiley and Sons, New York, 103-162.

Brown G. M., Emeleus C. H., Holland J. G. and Phillips R. 1970. Petrographic, mineralogic and X-ray fluorescence analysis of Lunar igneous type rocks and spherules. Science 167, 559-601.

Brown G. M., Peckett A., Emeleus C. H., Phillips R and Pinsent R. H. 1973. Petrology and mineralogy of Apollo 17 Mare basalts. Proc. 6th Lunar Sci. Conf. 1-13.

Bullerwell W. 1972. Geophysical studies relating to the Tertiary volcanic structure of the British Isles. Phil. Trans. Roy Soc. A271, 209

Cam$\wedge$bell I. G. and Borley G. D. 1974. The geochemistry of pyroxenes from the lower layered series of the Jimberlana intrusion, Western Australia. Contrib. Mineral. Petrol. 47, 282-297.

Carmichael I. S. E. 1967. The iron-titanium oxides of salic volcanic rocks and their associated ferro-magnesium silicates. Contrib. Mineral. Petrol. 14, 36-64.

Carmichael I. S. E., Nicholls J. and Smith A. L. 1970. Silica activity in igneous rocks. Am. Mineral. 55, 246-263.

Carmichael I. S. E., Turner F. J. and Verhoogen J. 1973. Igneous Petrology. McGraw Hill, New York.

Carter S. R., Evenson N. M., Hamilton P. J. and O'Nions R. K. 1978. Neodymium and strontium isotope evidence for crustal contamination of continental volcanics. Science 202, 743-746.

Cawthorn R. G., Ford G. E., Biggar G. M., Bravo M. S. and Clarke D. B. 1973. Determination of the liquid composition in experimental samples: Discrepancies between microprobe analyses and other methods. Earth Plan. Sci. Lett. 21, 1-5.

Clarke D. B. 1970. Tertiary basalts of Baffin Bay: Possible primary magma from the upper mantle. Contrib. Mineral. Petrol. 25, 203-224.

Clarke D. B. and O'Hara M. J. 1979. Nickel and the existence of high-Mgo liquids in nature. Earth Plan. Sci. Lett. 44, 153-158.

Coombs D. S. 1963. Trends and affinities of basaltic magmas and pyroxenes as illustrated on the Diopside-Olivine-Silica diagram. Mineral Soc. Am. Spec. Paper 1, 227-250.

Cox K. G. 1972. Tholeiites and alkali basalts: unimodal or bimodal population? Earth Plan. Sci. Lett. 16, 185-188.

Cox K. G. 1978. Komatiites and other high magnesia lavas: some problems. Phil. Trans. Roy. Soc. A288, 599

Deer W. A., Howie R. A. and Zussman J. 1966. An introduction to the rock forming minerals. Longman, London.

Deer W. A., Howie R. A. and Zussman J. 1979. Rock forming minerals, Vol. 2A, 2nd ed., Longmans London.

Donaldson C. H. 1974. Olivine crystal types in the Tertiary Harrisite rocks of the Rhum pluton and in some Archean spinifex rocks. Bull. Geol. Soc. Am. 85, 1721-1726.

Donaldson C. H. 1975. Ultrabasic breccias in layered intrusions - the Rhum complex. Jl Geol. 83, 33-45.

Donaldson C. H. 1976. An experimental investigation of olivine morphology. Contrib. Mineral. Petrol. 57, 187-213.

Donaldson C. H. 1977. Petrology of anorthite bearing gabbroic anorthosite dykes in North west Skye. Jl Pet. 18, 595-620.

Donaldson C. H. and Brown R. W. 1977. Refactory megacrysts and magnesian rich melt inclusions with spinel in oceanic tholeiites: indicators of magma mixing and parental magma composition. Earth Plan. Sci. Lett. 37, 81-89.

Donaldson C. H., Drever H. I. and Johnston R. 1973. Crystallisation of poikilo-macro-spherulitic feldspar in a Rhum peridotite. Nature Phys. Sci. 243, 69-70.

Drever H.I. Johnston R, 1966. A natural high-lime liquid more basic than basalt. Jl.Pet, 7, 414-420

Dunham A. C. 1962. The petrology and structure of the northern edge of the Tertiary Igneous Complex of Rhum. Unpublished D. Phil. Thesis Univ. of Oxford.

Dunham A. C. 1964. A petrographic and geochemical study of back veining and hybridisation at a gabbro-felsite contact in Coire Dubh, Isle of Rhum, Inverness-shire. Mineral. Mag. 33, 887-902.

Dunham A. C. 1965a. The nature and origin of the ground mass textures in felsites and granophyres from Rhum, Inverness-shire. Geol. Mag. 102, 8-23.

Dunham A. C. 1965b. A new type of banding in the ultrabasic rocks from central Rhum. Am. Mineral. 50, 1410-1420.

Dunham A. C. 1968. The felsites, granophyres, explosion breccias and tuffisites of the north-east margin of the Tertiary igneous complex of Rhum, Inverness-shire. Qt. Jl Geol. Soc. Lond.

Dunham A. C. 1970. The emplacement of the Tertiary igneous complex of Rhum. in Newall G. Rast N. (eds) Mechanism of Igneous Intrusions Geol Jl Spec issue 2, 23-32.

Dunham A. C. and Emeleus C. H. 1967. The Tertiary geology of Rhum, Inner Hebrides. Proc. Geol. Assoc. 78, 395-418.

Dunham A. C. and Wadsworth W. J. 1978. Cryptic variation in the Rhum layered intrusion. Mineral. Mag. 42, 347-356.

Dunham A. C., Emeleus C. H., Hudson J. D., Peacock D. and Wadsworth W. J. (in press). The Geology of the Small Isles, 2nd ed. Mem. Geol. Surv. UK.

Emeleus C. H. 1973. Granophyre pebbles in Tertiary conglomerate on the Isle of Canna, Inverness-shire. Scot. Jl. Geol. 9, 157-159.

Emeleus C. H. 1976. The Tertiary lavas of Rhum, Inverness-shire. Jl. Geol. Soc. Lond. 132. 700.

Emeleus C. H. and Forster R. M. 1979. Field guide to the Tertiary igneous rocks of Rhum, Inner Hebrides. Nature Conservancy Council. pp. 44.

Emeleus C. H. and Preston J. 1969. Field excursion guide to the Tertiary volcanic rocks of Ireland. I.A.V.C.E.I. Symposium (Oxford) 1969. Dormans, Belfast.

Emeleus C. H., Dunham A. C. and Thompson R. N. 1971. Iron-rich pigeonites from acid rocks in Tertiary igneous province of Scotland. Am. Mineral. 56, 940-951.

Esson J., Dunham A. C. and Thompson R. N. 1975. Low alkali, high calcium olivine tholeiite lavas from the Isle of Skye, Scotland. Jl Petrol. 16, 488-497.

Ferguson A. K. 1978. Ca-enrichment in olivines from volcanic rocks. Lithos. 11, 189-194.

Flanagan F. J. 1973. 1972 values for international geochemical reference samples. Geochim. et. Cosmochim. Acta 37, 1189-1200.

Floyd P. A. and Winchester J. 1975. Magma type and tectonic setting using immobile elements. Earth Plan. Sci. Lett. 27, 211-218.

Forster R. M. 1978. Preliminary atmospheric pressure melting relationships of some proposed Rhum parent magmas. Prog. in Exp. Petrol. Rept. 3 N.E.R.C. 200-201.

Gamble J. A. 1979. The geochemistry and petrogenesis of dolerites and gabbros from the Tertiary central volcanic complex of Slieve-Gullion, north-east Ireland. Contrib. Mineral. Petrol. 69, 5-20.

Gass I. G., Mallick D. I. J. and Cox K. G. 1973. Volcanic Islands of the Red Sea. Jl Geol. Soc. Lond. 129, 275-310.

Geike A. 1896. The Tertiary basalt plateaux of north-western Europe. Qt. Jl Geol. Soc. 52, 331-406.

Gibb F. G. F. 1968. Flow differentiation of the xenolithic ultrabasic dykes of the Cuillins and the Strathaird peninsula, Isle of Skye, Scotland. Jl Petrol. 9, 411-443.

Gibb F. G. F. 1971. Crystal-liquid relationships in some ultrabasic dykes and their petrological significance. Contrib. Mineral. Petrol. 30, 103-118.

Gibb F. G. F. 1973. The zoned pyroxenes of the Shiant Island sill, Scotland. Jl Petrol. 14, 203-230.

Gibb F. G. F. 1974. Supercooling and crystallisation of plagioclase from a basaltic magma. Mineral Mag. 39, 641-653.

Gibb F. G. F. 1976. Ultrabasic rocks of Rhum and Skye: the nature of the parent magma. Jl Geol. Soc. Lond. 132, 209-222.

Gibb F. G. F. and Henderson C. M. B. 1978. Possible higher pressure relics within titaniferous augites in a basic sill. Geol. Mag. 115, 55-62.

Gibson I. L., Mariner G., Mattey D. P., Thompson R. I. V. and Wood D. A. Is the extrusive portion of the oceanic crust vertically compositionally zoned? Bull. Geol. Soc. France. 17, 897-900.

Green D. C. 1970. Transitional basalts from the Eastern Australian Tertiary province. Bull. Volc. 33, 930-941.

Greenbaum D. 1977. The chromitferous rocks of the Troodos ophiolite complex. Econ. Geol. 72, 1176-1194.

Gunn B. M. 1971. Trace element partition during olivine fractionation of Hawaiian basalts. Chem. Geol. 8, 1-13.

Harker A. 1908a. The geology of the small isles of Inverness-shire. Mem. Geol. Surv. UK.

Harker A. 1908b. Geological survey of the United Kingdom. One inch map of Scotland sheet 60 (Republished colour printed 1971)

Hart S. R. and Davis K. E. 1978. Nickel partitioning between olivine and silicate melt. Earth. Plan. Sci. Lett. 40, 203-219.

Hatch F. H., Wells A. K. and Wells M. K. 1975. Petrology of the igneous rocks. George Allen and Unwin Ltd., London. pp 551.

Henderson P. 1975. Reaction trends shown by chrome spinels of the Rhum layered intrusion. Geochim. et. Cosmochim. Acta. 39, 1035-1044.

Henderson P. and Suddaby P. 1971. The nature and origin of the chrome-spinel of the Rhum layered intrusion. Contrib. Mineral. Petrol. 33, 21-31.

Henderson P. and Gejbels R. 1977. Trace element indicators of the genesis of the Rhum layered intrusion. Scot. Jl Geol. 12, 325-333.

Hermann A. G., Potts M. J. and Knake D. 1974. Geochemistry of the Rare Earth Elements in spilites from oceanic and continental crust. Contrib. Mineral. Petrol. 44, 1-16.

Hill R. and Roeder P. L. 1974. The crystallisation of spinel from basaltic liquid as a function of oxygen fugacity. Jl Geol. 82, 707-779.

Holland J. F. G. and Brindle D. W. 1966. A self consistent mass absorbtion correction for silicate analysis by X-ray Fluroescence. Spectrochim. Acta. 22, 2083-2093.

Holland J. G. and Brown G. M. 1971. Hebridean tholeiitic magmas: A geochemical study of the Ardnamurchan cone sheets. Contrib. Mineral. Petrol. 37, 139-160.

Hughes C. J. 1955. Petrographical and structural studies in south-east Rhum, Inverness-shire. Unpublished D. Phil. Thesis Univ. of Oxford.

Hughes C. J. 1960. The Southern Mountains Igneous Complex, Isle of Rhum. Q. Jl. Geol. Soc. Lond. 116, 111-138.

Humphris S. E. and Thomson G. 1978. Trace element mobility during hydro-thermal alteration of oceanic basalts. Geochim. et Cosmochim. Acta. 42, 127-136.

Humphris S. E., Morrison A. and Thompson R. N. 1978. Influence of rock crystallisation history upon subsequent Lanthanide mobility during hydrothermal alteration of basalts. Chem. Geol. 23, 125-137.

Irvine T. N. 1967. Chromium spinel as a petrogenic indicator. 2. Petrolog.ic implications. Canadian Jl Earth Sci. 4, 71-103.

Irvine T. N. and Baragar W. R. 1971. A guide to the chemical classification of the common volcanic rocks. Canadian Jl Earth Sci. 8, 523-548.

Jakobsson S. P., Jansonn J. and Shido F. 1979. Petrology of the western Reykjanes peninsula, Iceland. Jl Petrol. 19, 669-705.

Johannesson H. 1975. Structure and petrochemistry of the Reykjadular central volcano and the surrounding areas, Midwest Iceland. Unpublished Ph. D. Thesis Univ. of Durham.

Le Bas M. J. 1962. The role of aluminium of igneous clinopyroxenes with relationship to their parentage. Am. Jl Sci. 260, 267-288.

Lofgren G. E. 1974. An experimental study of plagioclase crystal morphology: isothermal crystallisation. Am. J. Sci. 274, 243-273.

MacGregor A. G. 1948. Problems of Carboniferous-Permian volcanicity in Scotland. Qt. Jl Geol. Soc. Lond. 104, 133-153.

MacDonald G. A. 1963. Physical properties of erupting Hawaiian magmas. Bull. Geol. Soc. Am. 74, 1071-1078.

Mattey D. P., Gibson I. L., Marriner G. F. and Thompson R. N. 1977. The diagnostic geochemistry, relative abundance and spatial distribution of high calcium, low alkali of olivine tholeiite dykes in lower Tertiary regional swarm of Skye, NW Scotland. Miner. Mag. 318, 273-286.

McBirney A. R. and Noyes R. M. Crystallisation and layering of the Skaergaard intrusion. Jl Petrol. 20, 487-554.

McDougall I. 1971. The geochronology and evolution of the young volcanic island of Reunion, Indian Ocean. Geochim. et. Cosmochim. Acta. 35, 261-288.

McQuillin R. and Tuson J. 1963. Gravity measurements over the Rhum Tertiary plutonic complex. Nature 199, 1276-1277.

Meighan I. G. 1979. The acid igneous rocks of the British Tertiary province. Bull. Geol. Surv. G.B. 70, 10-22.

Middlemost E. A. K. 1975. The Basalt Clan. Earth Sci. Rev. 11, 337-364.

Morrison M. A. 1978. Trace element contents of Hebridean basaltic magmas, their metamorphism and regional distribution: implications for the interpretation of ancient metabasic rocks. Earth Plan. Sci. Lett. 39, 407-416.

Murase T. and McBirney A. R. 1973. Properties of some common igneous rocks and their melts at high temperatures. Bull. Geol. Soc. Am. 84, 3563-3592.

Murata K. J. and Richter O. H. 1966. Chemistry of the lavas, 1959-60 eruption of Kilauea Volcano, Hawaii. Prof. Paper U.S. Geol. Surv. 537A A1-A26.

Nie N. H., Hedlai-Hull C., Jenkins J. G. Steinbrenner K. and Bent D.H. 1975. Statistical package for the social sciences. McGraw-Hill, New York.

Nisbett E. G. and Pearce J. A. 1977. Clinopyroxenes in mafic lavas from different tectonic settings. Contrib. Mineral. Petrol. 63, 149-160.

O'Hara M. J. 1968. The bearing of phase equilibria studies in synthetic and natural systems on the origin and evolution of basic and ultrabasic rocks. Earth Sci. Rev. 4, 69-133.

O'Hara, M. J., Saunders M. J. and Mercy E. L. P. 1975. Garnet peridotite primary ultrabasic magma and eclogite, interpretation of upper mantle processes in kimberlite. Phys. Chem. Earth 9, 571-604.

Pearce J. A. 1976. Statistical analysis of major element patterns in basalts. Jl Petrol. 17, 15-43.

Pearce J. A. and Cann J. R. 1971. Ophiolite origin investigated by discriminant analysis using Ti,Y and Zr. Earth Plan. Sci. Lett. 12, 339-349.

Pearce J. A. and Cann J. R. 1973. Tectonic setting of basic volcanic rocks determined using trace element analyses. Earth Plan. Sci. Lett. 19, 290-300.

Pearce J. A. and Flower M. F. J. 1976. The relative importance of petrogenetic variables in magma genesis at accreting plate margins: a preliminary investigation. Jl Geol. Soc. Lond. 134, 103-128.

Pinsent R. H. 1974. The emplacement and metamorphism of the Blue River ultra-mafic body, Cassiar district, British Columbia, Canada. Unpublished Ph. D. Thesis, Univ. of Durham.

Presnall D. C., Dixon S. A., Dixon J. R., O'Donell T. H., Brenner N. L., Schrock R. L. and Dycus D. W. 1978. Liquidus phase relations on the join Diopside-Forsterite-Anorthite from 1 atmosphere to 20 Kb: their bearing on the generation and crystallisation of basaltic magma. Contrib. Mineral. Petrol. 66, 203-220.

Preston J. 1967. A Tertiary feeder dyke in County Fermanagh, Northern Ireland. Proc. Roy Soc. Dublin. 3A 1-16.

Reeves M. J. 1971. Geochemistry and mineralogy of British Carboniferous seat earths from northern coalfields. Unpublished Ph. D. Thesis Univ. of Durham.

Richey J. E. 1948. Scotland: The Tertiary volcanic districts. Regional Geology Guide, Geol. Surv. UK.

Richey J. E. 1961. Scotland: The Tertiary volcanic districts. Regional Geology Guide, Geol. Surv. UK.

Richey J. E. and Thomas H. H. 1930. The geology of Arnamurchan, Northwest Mull and Coll. Mem. Geol. Surv. UK.

Ridley W. I. 1970. Some chemical features of basalts from the British Tertiary province. Earth Plan. Sci. Lett. 11, 435-439.

Ridley W. I. 1971. The petrology of some volcanic rocks from the British Tertiary province: The Islands of Rhum, Eigg, Canna and Muck. Contrib. Mineral. Petrol. 32, 251-266.

Ridley W. I. 1973. The petrology of volcanic rocks from the Small Isles of Inverness. Rept. of the Inst. of Geological Sciences 73/10 pp 55.

Ridley W. I. 1977. The crystallisation trends of spinels in Tertiary basalts in Rhum and Muck and their petrological significance. Contrib. Mineral. Petrol. 64, 243-255.

Ridley W. I., Rhodes, J. M., Reid A. M., Jakes P., Shih C. and Bass M. N. Basalts from Leg 6 of the deep-sea drilling project 1974. Jl Pet. 15, 140-159.

Robson G. R. and Barr K. G. 1964. The effects of stress and faulting and minor intrusions in the vicinity of the magma body. Bull. Volcanol. 27, 315-330.

Roeder P. L. and Emslie R. F. 1970. Olivine-liquid equilibrium. Contrib. Mineral. Petrol. 29, 275-289.

Roobol M. J. 1971. Some relations between common acid-basic
    associations. Geol. Mag. 108, 525-531.

Sato H. 1977. Nickel content of basaltic magmas: identification
    of primary magmas and measure of the degree of olivine
    fractionation. Lithos 10, 113-120.

Simkin T. and Smith J. V. 1970. Minor element distribution of
    olivine. Jl Geol. 78, 304-325.

Skelhorn R. R., Henderson P., Walsh J. N. and Longland P. J. N.
    The chilled margin of the Ben Buie layered gabbro, Isle
    of Mull. Scott. Jl Geol. 15, 161-167.

Smith R. E. and Smith S. E. 1976. Comments on the use of
    Ti, Zr, Y, Sr, K, P and Nb in the classification of
    basaltic magmas. Earth Plan.Sci. Lett. 32, 114-120.

Speight J. M. 1972. The form and structure of the Tertiary
    dyke swarms of Skye and Ardnamurchan. Unpublished Ph. D.
    Thesis City of London Polytechnic.

Stewart F. H. 1965. Tertiary igneous activity in the
    Geology of Scotland. in The Geology of Scotland (Ed
    G. Y. Craig) Oliver and Boyd pp 420.

Sweatman T. R. and Long J.U. P. 1969. Quantitative electron
    probe micro-analysis of the rock forming minerals.
    Jl Petrol. 10, 332-379.

Sun S. S., Nesbitt R. W., and Sharaskin A. V. 1979.
    Geochemical characteristics of mid-ocean ridge basalts.
    Earth Plan. Sci. Lett. 44, 119-138.

Taylor H. P. and Forrester R. W. 1971. Low ^{18}O rocks from
    the intrusive complexes of Skye, Mull and Ardnamurchan.
    Jl Petrol. 12, 465-497.

Thompson R. N. 1974a. Primary basalts and magma genesis,
    Skye, Northwest Scotland. Contrib. Mineral. Petrol. 45,
    317-341.

Thompson R. N. 1974b. Some high pressure pyroxenes.
    Miner. Mag. 37, 368-387.

Thompson R. N. 1978. British Tertiary Igneous Province, in
    Igneous rocks of the British Isles, D. S. Sutherland (ed)
    John Wiley and Sons, New York.

Thompson R. N., Esson J. and Dunham A. C. 1972. Major elemental
    chemical variation in the Eocene lavas of the Isle of Skye.
    Jl Pet. 13, 219-253.

Thornton C. P. and Tuttle O. F. 1960. Chemistry of igneous
    rocks: pt I, Differentiation Index. Am. Jl Sci. 258,
    664-684.

Tomkieff S. I. 1942. The Tertiary lavas of Rhum. Geol. Mag.
    79, 1-13.

Tyrell G. W. 1928. The Geology of Arran. Mem. Geol. Surv. UK.

Usselman T. M. and Hodge D. S. 1978. Thermal control of low
    pressure fractionation processes. Jl Vol. Geothem. Res.
    4, 265-281.

Verhoogen J. 1962. Distribution of titanium between silicates
    and oxide in igneous rocks. Am. Jl Sci. 260, 211-220.

Wadsworth W. J. 1961. Ultrabasic rocks of southwest Rhum,
    Inner Hebrides. Phil. Trans. Roy Soc. B244, 21-64.

Wadsworth W. J. 1973. Magmatic sediments. Minerals Sci. Eng.
    5, 25-35.

Wager L. R. and Brown G. M. 1968. Layered igneous rocks.
    Freeman, San Francisco.

Wager L. R., Brown G. M. and Wadsworth W. J. 1960. Types of
    igneous cumulates. Jl Petrol. 1, 73-85.

Wass S. Y. 1979. Multiple origins of clinopyroxenes in alkali
    basaltic rocks. Lithos 12, 115-132.

Watson E. B. 1979a. Calcium content of forsterite existing
    with silicate liquid in the system $Na_2O-CaO-MgO-Al_2O_3-$
    SiO_2. Am. Mineral. 64, 824-829.

Watson E. B. 1979b. Zircon saturation in felsic liquids.
    Experimental results and application to trace element
    geochemistry. Contrib. Mineral. Petrol. 70, 407-420.

Wilkinson J. F. G. 1967. The petrography of basaltic rocks
    in basalts. The Poldevaart treatise on rocks of
    basaltic composition, Eds H. H. Hess and A. Poldevaart.
    John Wiley and Sons, New York.

Williams H., Turner F. J. and Gilbert C. M. 1955. Petrography:
    An introduction to the study of rocks in thin section.
    Freeman, San Francisco.

Wood D. A. 1979. Dynamic partial melting. Its application
    to the petrogenesis of basalts erupted in Iceland, the
    Faroe Islands, the Isle of Skye (Scotland) and the
    Troodos massif (Cyprus). Geochim. et. Cosmochim Acta
    43, 1031-1047.

Wood D. A., Gibson I. L. and Thompson R. N. 1976.
    Elemental mobility during zeolite facies
    metamorphism of the Tertiary basalts of Eastern
    Iceland. Contrib. Mineral. Petrol. 55-241.

Wyllie P. J. 1967. Ultramafic and ultrabasic rocks.
    in Ultramafic and related rocks (Ed P. J. Wyllie).
    John Wiley, New York.

Yagi K. and Onuma K. 1967. The join Ca Mg Si_2O_6 —
    Ca Ti Al_2O_6 and its bearing on titanaugites.
    Jl Fac. Sci. Hokkaido Univ., ser 4, 8, 463-483.

Yoder H. S. and Tilley C. E. 1972. Origin of basaltic
    magmas: An experimental study of natural and
    synthetic rock systems. Jl Petrol. 3, 342-532.

Appendices

Note that all references cited in the appendices, except those in appendices 3.1 - 3.3, are included in the reference list for the main text. References in appendices 3.1 - 3.3 are located on p. 373 unless marked otherwise.

Appendix 1.1

List of publications made during the course of this study.

Forster, R.M. 1978. Preliminary atmospheric pressure
    melting relations of some proposed Rhum parent
    magmas. Prog. in Experimental Petrology, N.E.R.C.
    Rpt. 4, p.200-201.

Emeleus, C.H. & Forster, R.M. 1979. Field guide to
    the Tertiary Igneous rocks of Rhum. Nature
    Conservancy Council, pp.44.

Forster, R.M. The Tertiary minor intrusions of Rhum.
    In: Dunham et al. (in press). The Geology of the
    Small Isles of Inverness-shire. Mem. Geol. Surv.
    UK. 2nd edition.

Appendix 2.1 Strike orientations plotted in Fig 2.1

STRIKE (°)	270-279	280-289	290-299	300-309	310-319	320-329	330-339	340-349	350-359	0-9	10-19	20-29	30-39	40-49	50-59	60-69	70-79	80-89
ROSE 1			4	10	7	2	8	4		1		1			2	2	2	
ROSE 2	10	4	5	1	1	3	1	4	3	2	2	1	4	4	5	10	6	5
ROSE 3			1	1	3		5	13	5	20	12	8	2		2		1	
ROSE 4	1	3	4	6	8	5		1	2			1	1					
ROSE 5	14	12	8	16	7	7	4	1			2	3	3	4	4	5	3	5
ROSE 6	9	7	6	2	7	5	4	4	3	1		3	2	2	2	4		6
ROSE 7	1	1	4	2	1	1	1	1	2	1	2					1		
ROSE 8	5	6	3	10	3	1	1				2							
ROSE 9	6	5	10	6	1	5		3		2	3	4	9	7	9	3		2
ROSE 10	2	5	5	11				1		1	3	2	2	7	6	2		3
ROSE 11	2		1							1	4	1	2	2	1	1		1
ROSE 12			2	3		4	3	7	11	11	6	2	3		2			
ROSE 13	7	2	2	1				1		6		3		1		1	1	

Appendix 2.2

Strike and dip directions of the inclined
sheets included in Fig 2.1

Rose 1

Strike	Dip
175	60W
125	64SW
155	25NE
120	60SW
160	55E
80	50W
110	60S
5	50W
150	55NE
125	60SW
110	55N
125	65SW
135	30NE
135	50NE
20	55E

Rose 2

Strike	Dip
125	45SW
140	60SW
85	65S
110	35W
145	45SW
10	40W
55	65NW

Rose 3

Strike	Dip
160	50SW
10	55W
55	45N
15	60
15	60W
10	65E
165	60W

Rose 4

Strike	Dip
145	65NE
135	65NE
5	65W
145	65SW

Rose 5

Strike	Dip
20	30NW
130	70SW
100	40N
90	30N
105	15SW
50	30NW

Rose 5

Strike	Dip
155	55SW
60	55NW
40	60NW
100	65N
75	65N
90	55N
90	65N
60	45NW
90	45N
110	65N
90	65N
60	30NW
45	50NW
90	65S
80	50N
105	65S
30	50NW
80	55N
75	20N
105	60SW
125	55SW
125	55SW
100	60S
135	55NE
90	55N
20	60E
40	30NW
150	55NE
40	45NW
110	65SW
100	65SW
20	65NW
50	45NW
145	55SW
150	10NE
110	65SW
25	55W
105	60S
120	40NE
110	55S
60	60N
115	50W
95	40N

Rose 6

Strike	Dip
105	62N
90	55N

Strike	Dip
145	50NE
95	60N
105	50N
110	65N
65	65NW
65	60NW
135	35NE
25	60W
175	60W
115	50NE
45	50N
85	60W
30	50W
95	65N
55	40NE
105	65
130	60W
65	25N
50	20N
45	40NW
95	65N
25	40
50	25N
50	30N
90	45N
20	55W
50	40SE
60	50S
65	30S
20	20N
50	25N

Rose 9

Strike	Dip
95	40N
40	60NW
45	60NW
50	50
80	60S
80	60S
115	55S
140	25S

Rose 10 *

Strike	Dip
40	15W
105	60S
105	60S
175	50SW
70	25NW

* includes the parallel inclined sheets which were not plotted on 10

Strike	Dip
165	60E
10	60W
85	55S
30	15NW
30	35NW
45	25NW
10	15NW
45	20NW
85	15NW
135	20NE
125	60SW
115	25SW
80	30SE
110	45SW
135	50SW
155	30SW
105	40SW
110	55SW
110	45SW
115	45SW
145	45SW
115	45SW
110	45SW
85	20SW
110	65SW
125	45SW
125	45SW
115	40SW
120	40SW
115	40SW
105	30SW
130	35SW
105	40SW
120	50SW
120	50SW
115	40SW
125	15NE
125	45SW
115	70SW
110	30SW
110	35SW
105	30SW
1110	40SW
115	40SW
120	35SW
115	35SW
115	40SW
105	40SW
130	45SW
130	40SW
110	40SW
130	35SW
90	30SW
100	40SW

Strike	Dip
140	70SW
110	45SW
105	45SW
110	45SW
105	55SW

Rose 12

Strike	Dip
170	65E
140	45E
135	60E
0	60W
0	60W
50	25NW
5	45E
30	45SE
20	55SE
170	60E
170	60W
15	65E
170	65W
165	40W
100	25N
110	25NW

Appendix 3.1

DATA SOURCES FOR BASALT ANALYSES USED IN THE DISCRIMINANT
ANALYSIS WITH THE NUMBER OF ANALYSES USED FROM EACH SOURCE

I Tholeiites

Continental		Ocean Floor	
Brooks and Nielson (1978)	3	Baragar et al. (1977)	4
Cox and Horung (1966)	3	Cann (1970)	3
Cox et al. (1967)	2	Engel and Engel (1964)	2
Dunham and Kaye (1965)	5	Engel et al. (1965)	4
Holmes (1936)	1	Fisher et al. (1968)	2
Holmes and Harwood (1929)	1	Kay et al. (1970)	1
Lipman and Moench (1972)	3	Muir and Tilley (1966)	3
Sukeswala and Poldervart (1958)	2	Ridley et al. (1974)*	3
Wilkinson (1968)	4		

Oceanic island (includes Iceland)

Baker et al. (1974)	3	MacDonald and Katsura (1964)	4
Carmichael (1964)	5	McBirney and Williams (1969)	3
Gass et al. (1973)	3	Sigvald (1974)	5
Gunn et al. (1971)	6	Wood (1978)	3

II Alkaline

Continental		Oceanic (includes Grenada)	
Baker et al. (1973)	3	Arculus (1976)	4
Barber et al. (1970)	4	Baker (1969)	4
Brown and Carmichael (1971)	3	Baxter (1976)	3
Gass and Mallick (1968)	4	Gass et al. (1973)	3
Gibb and Henderson (1978)	4	Gunn and Watkins (1976)	2
Kesson (1973)	3	Gunn et al. (1970)	2
Lipman (1969)	4	Irrabalo (1969)	3
Saggerson (1970)	5	MacDonald and Katsura (1964)	4
		McBirney and Williams (1969)	3
		Strong (1972)	3

III Calk-alkaline

Beddoe-Stephens (1977)*	4	Keller (1974)	2
Brothers and Martin (1970)	7	Kuno (1960)	3
Fitton (1971)	4	Lowder and Carmichael (1970)	3
Gill (1970)	2	Lopez-Escobar and Frey (1977)	4
Gunn and Mooser (1970)	2	Nichols (1971)	7
Hemming (1974)	4	Smith and Carmichael (1968)	3
Jakes and Smith (1970)	1	Wise (1969)	5

IV World-wide transitional

Baker et al. (1977)	12	Hei . et al. (1966)	2
Bass (1972)*	2	Lipman and Moench (1972)	6
Cox et al. (1970)	4	Tonguy (1978)	3
Gass et al. (1973)	6	Waters (1961)	5
Green (1970)*	4		

V Hebridean

Beckinsale et al. (1978)*	11	Mitchell et al. (1976)	8
Holland (unpublished data)	16	Ridley (1973)*	47
Mattey et al. (1977)	25	Thompson et al. (1972)*	43

*Cited at end of main text

STATISTICS ON SOURCE BASALT COMPOSITIONS

THOLEIITE BASALTS   TOTAL NUMBER OF CASES=78

VARIABLE	NO OF CASES WITH VARIABLE	MEAN	ST-DEV	MAXIMUM	MINIMUM	SKEWNESS
SIO2	78	49.73	1.13	53.77	46.28	0.69
AL2O3	78	15.78	1.53	19.15	11.99	0.19
TOTALFEO	78	11.16	1.74	14.71	7.72	0.25
MGO	78	6.70	1.55	12.20	3.40	0.37
CAO	78	10.80	1.44	14.51	7.29	-0.18
NA2O	78	2.72	0.43	3.57	1.82	0.46
K2O	78	0.46	0.32	1.85	0.04	1.47
TIO2	78	1.97	0.83	4.04	0.47	0.62
MNO	78	0.19	0.04	0.34	0.11	1.22
P2O5	75	0.25	0.19	1.17	0.03	2.18
NI	52	98.27	67.68	350.00	15.00	2.02
CR	38	240.79	125.22	550.00	44.00	0.23
BA	43	107.88	84.30	310.00	5.00	0.38
NB	19	17.00	10.09	40.00	2.00	0.79
ZR	46	128.30	70.65	326.00	35.00	0.68
Y	35	32.29	14.23	62.00	10.00	0.26
SR	52	230.77	139.76	484.00	40.00	0.56
RB	34	9.53	6.22	26.00	1.00	0.59
ZN	18	100.17	25.55	141.00	57.00	-0.07

ALKALI OLIVINE BASALTS   TOTAL NUMBER OF CASES=62

VARIABLE	NO OF CASES WITH VARIABLE	MEAN	ST-DEV	MAXIMUM	MINIMUM	SKEWNESS
SIO2	62	47.39	1.79	52.88	44.68	1.29
AL2O3	62	15.61	1.41	17.94	10.27	-0.93
TOTALFEO	62	11.44	1.34	14.69	8.53	-0.05
MGO	62	7.87	2.63	15.14	3.71	0.59
CAO	62	10.08	1.50	13.05	6.18	-0.35
NA2O	62	3.27	0.85	5.97	1.98	1.00
K2O	62	1.01	0.50	2.40	0.16	0.25
TIO2	62	2.44	0.83	4.25	0.81	0.04
MNO	62	0.17	0.04	0.28	0.01	-0.03
P2O5	62	0.46	0.21	1.06	0.14	0.80
NI	25	182.76	134.79	495.00	26.00	0.67
CR	27	198.44	144.09	540.00	15.00	0.62
BA	42	363.20	170.63	720.00	48.00	0.44
NB	22	38.05	25.58	100.00	2.00	0.47
ZR	35	173.06	79.99	380.00	68.00	0.84
Y	27	29.59	12.28	60.00	15.00	0.86
SR	40	595.35	287.87	1500.00	261.00	1.95
RB	32	21.25	11.05	40.00	3.00	-0.20
ZN	19	83.42	15.85	114.00	50.00	-0.18

CALC-ALKALI BASALTS   TOTAL NUMBER OF CASES=51

VARIABLE	NO OF CASES WITH VARIABLE	MEAN	ST-DEV	MAXIMUM	MINIMUM	SKEWNESS
SIO2	51	50.49	0.97	52.21	48.54	-0.32
AL2O3	51	17.50	2.13	22.05	11.38	-1.00
TOTALFEO	51	9.49	1.32	12.86	7.35	0.99
MGO	51	6.53	1.87	11.33	3.12	0.71
CAO	51	10.69	1.52	13.77	7.77	0.14
NA2O	51	2.64	0.74	3.89	0.84	-0.49
K2O	51	1.01	0.70	3.33	0.22	1.76
TIO2	51	1.01	0.38	1.90	0.19	0.65
MNO	51	0.18	0.04	0.28	0.12	0.63
P2O5	46	0.23	0.13	0.47	0.03	0.04
NI	23	87.09	84.42	337.00	10.00	1.46
CR	25	148.28	155.46	634.00	10.00	1.58
BA	23	368.43	197.42	901.00	107.00	0.37
NB	14	5.86	4.02	13.00	1.00	0.47
ZR	28	71.95	45.44	158.00	19.00	0.75
Y	19	18.32	8.12	35.00	5.00	0.95
SR	23	586.52	226.43	984.00	130.00	-0.46
RB	22	47.86	45.68	152.00	5.00	1.50
ZN	19	84.68	16.12	138.00	71.00	2.32

Appendix 3.1

References

Arculus R. J. 1976. The geology and chemistry of the alkali basalt and andesite association of Grenada, Lesser Antilles island Arc. Geol. Soc. Am. Bull. 87, 612-624.

Baker B. H., Gordon G. G., Leeman P. W. and Lindstrom M. M. 1977. Geochemistry and petrogenesis of a basalt-benmoreite-trachyte suite from the southern part of the Gregory Rift, Kenya. Contrib. Mineral. Petrol. 64, 303-332.

Baker I. 1969. Petrology of the volcanic rocks of St Helena Island, South Atlantic. Geol. Soc. Am. Bull. 80, 1283-1310.

Baker P. E., Brosset R., Gass I. G. and Neary C. R. 1973. Jebel al Abyad: a recent alkalic volcanic complex in Western Saudi Arabia. Lithos 6, 291-303.

Baker P. E., Buckley F. and Holland J. G. 1974. Petrology and geochemistry of Easter Island. Contrib. Mineral. Petrol. 44, 85-100.

Baragar W. R. A., Plant A. G., Pringle, G. J. and Schau M. 1977. Petrology and alteration of selected units of Mid-Atlantic Ridge basalts sampled from sites 332 and 335 D.S.D.P. Canadian J. Earth Sci. 14, 837-874.

Barberi F., Borsi S., Ferrara G., Marinelli G. and Varet J. 1970. Relations between tectonics and magmatology in the northern Danakil Depression, Ethiopia. Phil. Trans. Roy. Soc. A257, 293-311.

Baxter A. N. 1976. Geochemistry and petrogenesis of primitive alkali basalt from Mauritius, Indian Ocean. Bull. Geol. Soc. Am. 87, 1028.

Brooks C. K. and Nielson T. E. D. 1978. Early stages in the differentiation of the Skaergaard magma as revealed by a closely related suite of dyke rocks. Lithos 11, 1-14.

Brothers R. N. and Martin K. R. 1970. The geology of Macauley Island, Kermadec Group, South West Pacific. Bull. Volc. 34, 330-346.

Brown F. H. and Carmichael I. S.E. 1971. Quaternary volcanology of the Lake Rudolf region: II The lavas of North Island, South Island and the barrier. Lithos 4, 305-323.

Cann J. R. 1969. Spilites from the Carlsberg Ridge, Indian Ocean. J. Pet. 10, 1-19.

Carmichael I. S. E. 1964. The petrology of Thingmuli, a
Tertiary volcano in eastern Iceland. J. Petrol. 5,
435-460.

Cox K. G. and Hornung G. 1966. The petrology of the Karroo
basalts of Basutoland. Am. Miner. 51, 1414-1422.

Cox K. G., Macdonald R. and Hornung G. 1967. Geochemical and
petrographic provinces in the Karroo basalts of Southern
Africa. Am. Miner. 52, 1451-1474.

Cox K. G., Gass I. G. and Mallick, D. I. J. 1970. The
peralkaline volcanic suite of Aden and Little Aden,
South Arabia. J. Petrol. 11, 433.

Dunham A. C. and Kaye, M. J. 1965. The petrology of the Little
Whin Sill, County Durham. Proc. Yorks. Geol. Soc. 35,
229-276.

Engel A. E. J. and Engel C. G. 1964. Igneous rocks of the
East Pacific Rise. Science 146, 477-485.

Engel A. E. J., Engel C. G. and Havens R. G. 1965. Chemical
characteristics of oceanic basalts and the upper mantle.
Geol. Soc. Am. Bull. 76, 719-734.

Fisher R. L., Engel C. G. and Hilde R. W. 1968. Basalts
dredged from the Amirante Ridge, Western Indian Ocean.
Deep Sea Res. 15, 521-534.

Fitton J. G. 1971. The petrogenesis of the calk-alkaline
Borrowdale Volcanic Group, Northern England. Unpublished
Ph.D. Thesis, University of Durham.

Gass I. G. and Mallick D. I. J. 1968. Jebel Khariz: an upper
Miocene strata volcano of comenditic affinity on the
south Arabian coast. Bull. Volc. 32, 33-88.

Gass I. G., Mallick D. I. J. and Cox K. G. 1973. Volcanic
islands of the Red Sea. Jl. Geol. Soc. Lond. 129, 275-310.

Gibb F. G. F. and Henderson C. M. B. 1978. The petrology of
the Dippin Sill, Arran. Scott. J. Geol. 14, 1-27.

Gill J. B. 1970. Geochemistry of Vitu Levu, Fiji and its
evolution as an island arc. Contrib. Mineral. Petrol.
27, 179-203.

Gunn B. M. and Mooser F. 1970. Geochemistry of the volcanics
of central Mexico. Bull. Volc. 34, 577-616.

Gunn B. M. and Watkins N. D. 1976. Geochemistry of the
Cape Verde Islands and Fernando de Noronha. Bull
Geol. Soc. Am. 78, 1089-1100.

Gunn B. M., Coy-Yll R., Watkins N. D., Abranson E. and
Nougier J. 1970. Geochemistry of an oceanite-ankaramite
basalt suite from East Island, Crozet Archipelago.
Contrib. Mineral. Petrol. 28, 319-339.

Gunn B. M., Abranson C. E., Nougier J., Watkins N. D. and
Hajash A. 1971. Amsterdam Island, an isolated volcano
in the Indian Ocean. Contrib. Mineral. Petrol. 32, 79-92.

Heier K. S., Chappell B. W., Arriens P. A. and Morgan J. W.
1966. The geochemistry of 4 Icelandic basalts. Norsk.
Geol. Tiddsk. 46, 427-431.

Hemming R. F. 1974. Geology and petrology of Rabaul Caldera,
Papua New Guinea. Bull. Geol. Soc. Am. 85, 1253-1264.

Holmes A. 1936. A record of new analyses of Tertiary igneous
rocks (Antrim and Staffa). Roy. Irish Acad. Proc. 43
Sec B no 8, 89-94.

Holmes A. and Harwood H. F. 1929. The tholeiite dykes of the
North of England. Miner. Mag. 22, 1-52.

Irrabolo E. 1969. Variation trends in basaltic rocks of the
Canary Isles. Bull. Volc. 33, 729-777.

Jakes P. and Smith I. E. 1970. High potassium calc-alkaline
lavas from Cape Nelson, Eastern Papua. Contrib. Miner.
Petrol. 28, 259-271.

Kay R., Hubbard N. J. and Gast P. W. 1970. Chemical
characteristics and origin of ocean ridge volcanic rocks.
J. Geophys. Res. 75, 1585-1613.

Keller J. 1974. Petrology of some volcanic rock series of the
Aeolian arc, southern Tyrrhenian Sea. Contrib. Mineral.
Petrol. 46, 27-47.

Kesson S. E. 1973. The primary geochemistry of the Morana
alkaline volcanics, south east Australia - evidence for
upper mantle hetereogeneity. Contrib. Mineral. Petrol.
42, 93-108.

Kuno H. 1960. High Alumina Basalt. J. Petrol. 1, 121-145.

Lipman P. W. 1969. Alkalic and tholeiitic basaltic magmatism related to the Rio Grande depression, southern Colorado and Northern New Mexico. Bull. Geol. Soc. Am. 80, 1343-1354.

Lipman P. W. and Moench R. H. 1972. Basalts of the Mount Taylor volcanic field, New Mexico. Bull. Geol. Soc. Am. 83, 1335-1344.

Lopez-Escobar L., Frey F. A. and Veraga M. 1977. Andesites and High Alumina basalts from the central-south Chile High Andes: Geochemical evidence bearing on their petrogenesis. Contrib. Mineral. Petrol. 63, 199-228.

Lowder G. G. and Carmichael I. S.E. 1970. The volcanoes and caldera of Talasea, New Britain, Geology and Petrology. Bull. Geol. Soc. Am. 81, 17-38.

MacDonald G. A. and Katsura T. 1964. Chemical compositions of Hawaiian lavas. J. Petrol. 5, 82-133.

McBirney A. R. and Williams H. 1969. Geology and petrology of the Galapagos Islands. Mem. Geol. Soc. Am. 118.

Mitchell J. G., Jones E. T. W. and Jones G. T. 1976. The composition and age of basalts dredged from the Blackstones igneous centre. Geol. Mag. 113, 525-533.

Muir I. D. and Tilley C. E. 1966. Basalts from the northern part of the Mid-Atlantic Ridge. Part II. J. Petrol. 7, 193-201.

Nichols I. A. 1971. Petrology of the Santorini Volcano, Cyclades, Greece. J. Petrol. 12, 67-119.

Saggerson E. P. 1970. The structural control and genesis of alkaline rocks in Central Kenya. Bull. Volc. 34, 38-76.

Sigualdson G. E. 1974. Basalts from the centre of the assumed Icelandic mantle plume. J. Petrol. 15, 487-524.

Smith I. A. and Carmichael I. S. E. 1968. Quaternary lavas from the southern cascades, Western U.S.A. Contrib. Mineral. Petrol. 19, 212-228.

Strong D. F. 1972. The petrology of the lavas of Grande Comore. J. Petrol. 13, 181-217.

Sukeswala R. N. and Poldervaart A. 1958. Deccan basalts from the Bombay area, India. Bull. Geol. Soc. Am. 69, 1475-1494.

Tonguy J. C. 1978. Tholeiitic basalt magmatism of Mount
     Etna. Contrib. Mineral. Petrol. 66, 51-57.

Waters A. C. 1961. Stratigraphic and lithologic variations
     in the Columbian River basalts. Am. J. Sci. 259, 583-611.

Wilkinson J. G. F. 1968. The magmatic affinities of some rocks
     from the Tweed shield volcano, SE Queensland - NE New
     South Wales. Geol. Mag. 105, 275-289.

Wise W. S. 1969. Geology and petrology of the Mt Hood area:
     a study of High Cascade volcanism. Bull. Geol. Soc. Am.
     80, 969-1006.

Wood D. A. 1978. Major and trace element variation in the
     Tertiary lavas of eastern Iceland and their significance
     with respect to the Iceland geochemical anomaly.
     J. Petrol. 19, 393-436.

Appendix 3.2

Discriminant function analysis

The analysis was performed using the procedure
discriminant in the Northern Universities Multiple
Access computer (NUMAC) SPSS statistical package
version 8 at Durham University (Nie et al., 1975).
The first stage in the analytical procedure was the
recalculation of Fe_2O_3 + FeO to total iron as FeO the
major oxides in all analyses were then normalised to
total 100%. The second stage in the analytical pro-
cedure was standardisation of the data variables (both
major oxide and trace elements) to Z scores by sub-
tracting the mean of the distribution for each variable
i and dividing by the standard deviation.

$$Zi = \frac{X_i - \overline{X}_i}{S_i}$$

This standardisation equally weights the variability
of say SiO_2 at 45-52 (wt %) and the variability of Rb
(0-50 ppm) about their respective common means. In
accordance with standard trace element procedure a Log_{10}
transformation was performed on the trace elements to
produce a normal population distribution.

Discriminant analysis then acts on these standardised
variables and forms one or more linear "functions in the

form:

$$D_i = d_{i1}Z_1 + d_{i2}Z_2 + \ldots\ldots dipZp$$

where D_i is the score on the discriminant function i,
the d's are weighting coefficients and the Z's are
the standardised values of p discriminating variables.
Option 1 of procedure Discriminant (Nie et al., op.cit)
was invoked to include cases with missing values.

The classification functions were in the form:

$$C_i = C_{i1}V_1 + C_{i2}V_2 + CipVP + CiO$$

where Ci is the classification score for each class,
the Cij's are the classification coefficients with
CiO being the constant and the V's are the raw scores
on the discriminating variables. A separate classif-
ication function was derived for each class and each
function weighted according to the size of the class.
These classification functions were derived from the
individual group covariance matrices.

Procedure discriminant produces two probability
statistics during the classification of a case into a
group. The value P(X/G) gives the probability of a
case in a group which has a location as far from the
group centroid (see below) as the case in question.
The value P(G/X) is the probability of that case
belonging to the group it has been classified into.

A high $P(G/X)$ value indicates that the case in question
is more likely to belong to that group than any of the
other groups and providing the $P(X/G)$ value is also high
the classification is valid. This latter probability
provides the necessary constraint on for example classi-
fication of an igneous suite which includes intermediate
rocks with high SiO_2. These would be preferentially
classified as tholeiite as opposed to alkali basalt
(in that SiO_2 is an important component in the discriminant
function) but they would lie a long way from the group
centroid (ie. low $P(X/G)$ and the mis-classification
would be detected.

The value known as the group centroid is the mean
of the discriminant score for each group on its
respective function(s),ie. the most likely situation of
a member of that group with respect to the discriminant
function(s).

Appendix 3.3

Standardised Canonical Discriminant Functions

MAJOR OXIDES ONLY

	FUNC 1	FUNC 2		FUNC 1
SiO_2	-2.55413	-2.30421	SiO_2	-2.45367
Al_2O_3	-2.15715	-1.89696	Al_2O_3	-1.71555
TOTALFEO	-2.00173	-2.24044	TOTALFEO	-1.81133
MgO	-2.20393	-2.82525	MgO	-1.64695
CaO	-2.13883	-2.34856	CaO	-1.70922
Na_2O	-0.52234	-1.03540	Na_2O	-0.11566
K_2O	-0.50462	-0.01291	K_2O	0.18248
TiO_2	-0.76063	-1.87916	TiO_2	-0.95737
MnO	-0.56885	0.06925	MnO	-0.42719
P_2O_5	0.21650	-0.01302	P_2O_5	0.01778

Group Centroid

	FUNC 1	FUNC 2	FUNC 1
Tholeiite	-0.77349	-0.97010	-1.53514
Alkali	2.15513	0.22543	1.93131
Calc-alkali	-1.43698	1.20963	

MAJOR OXIDES AND TRACE ELEMENTS

	FUNC 1	FUNC 2		FUNC 1
SiO_2	1.56944	1.87389	SiO_2	1.37565
Al_2O_3	1.14233	1.41384	Al_2O_3	0.70378
TOTALFEO	0.93003	1.73647	TOTALFEO	0.65459
MgO	0.89251	1.99830	MgO	0.17576
CaO	1.10176	1.80435	CaO	0.69055
Na_2O	0.11080	0.65778	Na_2O	-0.33114
K_2O	0.25193	-0.11967	K_2O	-0.40389
TiO_2	0.08724	1.54733	TiO_2	0.27646
MnO	0.67999	-0.07930	MnO	0.49545
P_2O_5	-0.21569	0.01949	P_2O_5	-0.10802
Ni	0.38956	0.30412	Ni	0.23780
Cr	0.51407	-0.45891	Cr	0.24169
Ba	-0.56523	-0.15776	Ba	-0.57506
Nb	0.32225	-0.19077	Nb	0.20345
Zr	-0.15130	0.14434	Zr	-0.06704
Y	-0.28276	0.19448	Y	-0.14930
Sr	-0.35734	0.71693	Sr	0.24242
Rb	0.13891	-0.18489	Rb	-0.05511
Zn	-0.01709	-0.32845	Zn	-0.11609

Group Centroid

	FUNC 1	FUNC 2		FUNC 1
Tholeiite	0.63726	1.02875	Tholeiite	-1.60125
Alkali	-2.31720	-0.44057	Alkali	-2.01447
Calc-alkali	1.84237	-1.31308		

Unstandardised Canonical Discriminant Functions

These are derived in an analogous manner to the standardised functions listed previously but will operate on data which has not been normalised to z scores providing the penultimate product is multiplied by the constant listed at the end of each discriminant function.

MAJOR OXIDES ONLY

	FUNC 1	FUNC 2		FUNC 1
SiO_2	-1.898049	-1.712328	SiO_2	-1.682596
Al_2O_3	-1.287582	-1.132277	Al_2O_3	-1.161031
TOTALFEO	-1.322826	-1.480578	TOTALFEO	-1.148963
MgO	-1.080723	-1.385393	MgO	-0.7849087
CaO	-1.445055	-1.586755	CaO	-1.165026
Na_2O	-0.7757832	-1.537783	Na_2O	-0.1787287
K_2O	-1.007275	-0.2576487E-01*	K_2O	0.4473243
TiO_2	-1.028659	-2.541340	TiO_2	-1.150076
MnO	-13.38699	1.629625	MnO	-9.857938
P_2O_5	0.7172462	-0.4312484E-01	P_2O5	0.6661001E-01
(CONSTANT)	158.4481	153.8755	(CONSTANT)	135.4631

MAJOR OXIDES AND TRACE ELEMENTS

	FUNC 1	FUNC 2		FUNC 1
SiO_2	1.166300	1.392542	SiO_2	0.9433487
Al_2O_3	0.6818425	0.8439041	Al_2O_3	0.4762943
TOTALFEO	0.6146039	1.147533	TOTALFEO	0.4152199
MgO	0.4376528	0.9798891	MgO	0.8376549E-01
CaO	0.7443850	1.219076	CaO	0.4706844
Na_2O	0.1645537	0.9769390	Na_2O	-0.5117261
K_2O	0.5028897	-0.2388704	K_2O	-0.9900758
TiO_2	0.1179788	2.092575	TiO_2	0.3321041
MnO	16.00260	-1.866279	MnO	11.43313
P_2O_5	-0.7145491	0.6455399E-01	P_2O_5	-0.4047525
Ni	0.1002807	0.7828676E-01	Ni	0.6129370E-01
Cr	0.1252376	0.1118012	Cr	0.5842955E-01
Ba	-0.1385052	-0.3865885E-01	Ba	-0.1435192
Nb	0.9957589E-01*	-0.5894766E-01	Nb	0.6130612E-01
Zr	-0.3798900E-01	0.3624231E-01	Zr	-0.1661615E-01
Y	-0.7689975E-01	0.5289183E-01	Y	-0.4003399E-01
Sr	-0.8600952E-01	0.1725599	Sr	0.5959392E-01
Rb	0.3864681E-01	-0.5143928E-01	Rb	-0.1561139E-01
Zn	-0.4727808E-02	-0.9085518E-01	Zn	-0.3299191E-01
(CONSTANT)	-89.35329	-120.9608	(CONSTANT)	-64.04783

*computer notation E-01 = 10^{-1}

Appendix 5.1

Specimen list with compositional type, location, enclosing country rock (CR), structal type (SR) and relevant cross-cutting relationships.

Key to compositional types.

1-12 Dolerite groups, F denotes a high variant.

HMG   High MgO Gabbro

LMG   Low MgO Gabbro

P   Peridotite

A   Acid

Key to country rocks

LA   Lavas

PE   Layered peridotites

MG   Marginal gabbros

GR   Granophyre

TU   Tuffisite

FE   Felsite

EX   Explosion breccia

TB   Torridonian inside MRF

TO   Torridonian outside MRF

LE   Lewisian gneiss

Key to structural types

DY   Dyke

IS   Inclined sheet

TCS   Thin conformable sheet

THC   Thick conformable sheet

PIS   Parallel inclined sheet

Pl   Plug

Spec	Type	Location	CR	ST	X-Cutting
10A76	4F	NM40849985	TO	DY	
12A76	7	Fig 2.11	EX	DY	Cuts an early gabbro
14A76	4F	NM40479978	TO	TCS	
15A76	8	NM40509982	TO	TCS	
16A76	8	NM40559984	TO	DY	
18A76	8	NM40619984	TO	TCS	
20A76	8	NM40669984	TO	DY	
21A76	4	NM40669984	TO	DY	Cuts 22A76
22A76	4	NM40719982	TO	TCS	
23A76	8	NM40839985	TO	TCS	
25A76	8F	NM40899986	TO	TCS	
26A76	4	NM40919986	TO	DY	
29A76	9	NM39459865	TO	TCS	
32A76	10	NM35489968	PE	DY	
35A76	8	NM35549975	GR	DY	
38A76	4F	NG55430048	TO	DY	Cuts 41A76
40A76	2	"	TO	DY	Cuts 38A76
41A76	4	"	TO	DY	
44A76	2	NG55370045	TO	DY	
46A76	2	NM39319828	TO	DY	Cut by MRF
47A76	4	NM39319829	TO	PIS	
48A76	8	"	TO	DY	
49A76	8	"	TO	PIS	
50A76	8	"	TO	DY	
51A76	8	NM39309831	TO	DY	
52A76	1	Fig 2.9	TO	DY	
53A76	1	"	TO	DY	
54A76	1	"	TO	DY	Cuts 50A76
55A76	9	NM39359835	TO	DY	
56A76	1	Fig 2.9	TO	DY	
60A76	4	NM39369839	TO	DY	
61A76	4	NM39569894	TO	PIS	
62A76	4	NM39579899	TO	PIS ?	
63A76	4	"	TO	PIS ?	
64A76	8	NM38389845	TO	PIS	
65A76	2	"	TO	PIS	
66A76	3	"	TO	PIS	
69A76	1	Fig 2.9	TO	DY	
70A76	2	NM39369841	TO	DY	
71A76	1	Fig 2.9	TO	DY	
72A76	3	NM39419847	TO	PIS	
73A76	3	NM "	TO	PIS	
74A76	3	"	TO	PIS	
75A76	8	NM39419846	TO	PIS	
76A76	9	NM39419845	TO	PIS	
77A76	1	Fig 2.9	TO	DY	Cuts PIS
79A76	8	NM39439850	TO	PIS	
81A76	9	NM39459852	TO	DY	
82A76	4	"	TO	DY	Cuts 81A76?
83A76	10F	NM "	TO	PIS	
85A76	1	Fig 2.9	TO	DY	
87A76	3	NM39459868	TO	PIS	
89A76	3	NM39469860	TO	PIS	
92A76	3	NM39439855	TO	PIS	

Spec	Type	Location	CR	ST	X-Cutting
93A76	2	NM39459859	TO	PIS	
94A76	4	NM39519877	TO	DY	Cuts 95A76,77316
95A76	4	NM "	TO	PIS	
77002	4F	NM41099646	TB	DY	
77003	8	NM40929550	PE	DY	
77004	8	NM40849574	PE	DY	
77005	11	NM40849575	PE	DY	
77006	8	NM40849576	PE	DY	
77007	8	NM40839580	PE	DY	
77008	11	NM40819593	PE	DY	
77010	4	Fig 2.8	GR	DY	
77011	4	"	GR	DY	
77012	4	"	GR	DY	
77013	4	NM "	GR	DY	
77014	7	"	GR	DY	Also on Fig 2.11
77015	4	"	GR	DY	
77017	1	"	GR-PE	DY	Alsoon Fig 2.9
77019	2	NM33559360	PE	DY	
77025	11F	NM35359716	PE	DY	Cuts Dornabac breccia
77024	1	Fig 2.9	PE	DY	
77031	HMG	Fig 2.11	TO	PL	
77032	4	NM39169725	PE	DY	
77033	HMG	Fig 2.11		PL	
77034	9	NM38599860	EX	DY	Cuts 77033
77035	4	"	EX	DY	Cuts 77033
77036	1	Fig 2.9	EX	DY	Cuts 77033
77039	2	NM38569866	EX	DY	Cuts 77033
77040	8	NM38499840	FE	DY	
77042	2	NM38509831	FE	DY	
77044	4	NM38519850	FE	DY	Cuts 77046
77046	3	"	FE	DY	
77047	7	Fig 2.11	FE	DY	
77048	3	NM38419852	FE	DY	Cuts 77047
77049	4F	NG35690130	TO	DY	Cuts 77361 (PP)
77051	P	Fig 2.11	TO	PL	
77052	1	Fig 2.9	TO	DY	Cuts 77051 (PP)
77054	P	Fig 2.11	TO	PL	
77055	P	Fig 2.11	TO	PL	
77056	5	NG34300221	TO	DY	Cuts 77055 (PP)
77058	10	NM39839399	FE	DY	
77061	8F	NM38549350	EX-FE	DY	Liq-liq contact with FE
77064	8	NM38619351	FE	DY	
77066	P	Fig 2.11	TO	PL	
77067	LMG	Fig 2.11	TO	PL	
77068	4	NG42200020	TO	DY	
77070	4	NG42290053	TO	TCS	
77071	4	NM38599349	FE	DY	
77073	4	NM38599349	FE	DY	
77075	8F	NM39369806	TB	DY	
77076	4	"	TB	DY	Cuts 77075
77077	1	Fig 2.9	TB	DY	Cuts 77075
77078	8	NM39429807	TB	DY	
77080	5	NM39309807	TB	DY	
77082	3	NM39359801	TB	DY	

Spec	Type	Location	CR	ST	X-Cutting
77084	2	NG32720202	TO	DY	
77086	4	NG32690204	TO	DY	
77087	4F	NG32840224	TO	DY	Cuts 77078
77088	9	"	TO	DY	
77089	P	Fig 2.11	TO	PL	
77090	10	NG36800395	TO	DY ?	
77091	4	"	TO	DY	
77092	8	Fig 2.11	TO	THC	Kilmory type
77093	1	Fig 2.9	TO	DY	
77095	1	"	TO	DY	
77097	P	Fig 2.11	TO	PL	
77098	HMG	"	TO	PL	Pos'n WRT MRF ?
77099	P	"	TO	PL	
77100	LMG	"	GR	PL	
77101	1	Fig 2.9	LE	DY	
77102	QG	Fig 2.11	TB-EX-LE		Dunham 1968 Pl 25
77103	QG	Fig 2.11	TB		
77104	HMG	Fig 2.11	TO	PL	Extremely fresh .
77105	8	"	TO	THC	Kilmory type
77107	1	Fig 2.9	TO	DY	
77108	8	Fig 2.11	TO	THC	Kilmory type
77109	P	Fig 2.11	TO	PL	
77116	2	NM38639356	FE	DY	
77120	4	NM38539381	TB	DY	
77121	2	NM38439248	EX	DY	
77122	2	NM38349260	EX	DY	
77123	2	"	EX	DY	
77124	8	NM38239354	EX	DY	
77125	4	Fig 2.6	FE	DY	Cuts 77335
77127	8F	"	FE		Liq-liq contact with FE
77132	12	NM36579176	TO-MG	IS	
77136	P	Fig 2.11	TO	PL	
77137	10	NM36639184	MG	DY	
77138	P	Fig 2.11	MG		
77145	8F	NM38559350	EX-FE	DY	Liq-liq contact with FE
77148	4	Fig 2.6	FE	DY	
77149	8	"	FE	DY	
77155	8	NM37889494	PE	DY	
77158	2	"	PE	DY	
77159	A	Fig 2.11	TB	DY	Cut by a basic dyke
77160	7	"	GR	DY	
77174	8F		TO	THC	Papadil type
77175	4	NM38029186	TO	DY	
77176	4	"	TO	DY	
77177	12	NM36759121	TO	IS	
77178	3	NM36769110	TO	DY	Cuts 77179?
77179	1	Fig 2.9	TO	DY	
77180	A	Fig 2.11	TO	DY	
77181	P	"	TO	PL	
77182	P	"	MG	PL	
77183	P	"	MG	PL	
77184	10	NM36159176	MG	DY	
77191	3	NM36119181	MG	DY	
77192	1	Fig 2.9	MG	DY	

Spec	Type	Location	CR	ST	X-Cutting
77196	1	Fig 2.9	MG	DY	
77197	1	"	MG	DY	
77204	4	NM36849140	TO	IS	Cuts 77245
77205	4	NM "	TO	IS	Cuts 77204,77245
77208	4	NM39379259	TO	DY	
77209	9	"	TB	DY	Cuts 77208
77210	4F	NM39439266	TB	DY	
77212	2	"	TB	DY	
77214	2	"	TB	DY	Cuts 77212
77215	4	NM39379259	TB	DY	
77221	1	Fig 2.9	MG	DY	
77224	1	Fig 2.9	PE	DY	
77225	1	"	MG	DY	
77231	4	NM34459826	GR	DY	
77235	1	Fig 2.9	MG	DY	
77236	1	"	MG	DY	
77237	1	"	MG	DY	
77239	A	Fig 2.11	GR	DY	
77240	2	NM33309562	GR	DY	
77241	A	Fig 2.11	GR	DY	
77243	8F	Fig 2.11	TO	THC	Cut by a Gp 7 DY
77244	8F	"	TO	THC	Papadil type
77245	2	NM36849140	TO	DY	Cut by 77205
77246	LMG	Fig 2.11	TO	PL	
77249	3	NM39259785	TB-TU	DY	Cuts 77251
77250	8	"	TB-TU	DY	
77251	3	"	TB-TU	DY	
77252	HMG	Fig 2.11	FE-MG	PL	
77256	HMG	Fig 2.11	TO	PL	
77257	HMG	"	TO	PL	
77258	7	"	TO	PL	
77259	P	"	TO	PL	
77261	LMG	"	TO	PL	
77264	FD	"	TO	PL	
77265	LMG	"	TO	PL	
77267	LMG	"	TO	PL	
77268	P	"	TO	PL	
77269	4	NG34790175	TO	TCS	
77270	LMG	Fig 2.11	TO	PL	
77271	8	"	TO	THC	Kilmory type
77272	8	"	TTO	THC	Kilmory type
77273	LMG	"	TO	PL	
77274	QD	"	TO	PL	
77279	11	NM36279973	PE	DY	
77280	HMG	Fig 2.11	PE	PL	
77281	P	"	GR	PL?	
77282	LMG	"	TO	PL	
77283	LMG	"	TO	PL	
77284	4	NG34920143	TO	TCS	Cut by 77268 (Pp)
77286	P	Fig 2.11	TO	PL	
77287	LMG	"	GR	PL	
77288	HMG	"	TO	PL	
77290	P	"	TB-EX	PL	

Spec	Type	Location	CR	ST	X-cutting
77292	HMG	Fig 2.11	EX	PL	
77295	HMG	"	EX	PL	
77296	LMG	"	TB	PL	
77306	8F	NM38559350	EX-FE	DY	Liq-liq contact with FE
77309	P	Fig 2.11	TO	PL	
77314	4	NM39189713	PE	DY	
77315	8	NM39069685	PE	DY	
77316	8	NM39409846	TO	PIS	
77318	3	"	TO	PIS	
77320	HMG	Fig 2.11	TO	PIS	
77321	1	Fig 2.9	TO	DY	Chill to 52A76
77322	4F	NM33459558	GR	DY	
77323	5	NM33129564	GR	DY	
77324	4	NM33109563	GR	DY	Cuts 77325
77325	8	"	GR	DY	
77327	4	NM33939562	PE	DY	
77330	4	Fig 2.6	FE	IS	Cuts 77335
77331	4	"	FE	DY	Cuts 77343,77149,77339,77333
77332	4	"	FEE	DY	
77333	4	"	FE	IS	
77334	4F	"	FE	DY	
77335	4	"	FE	IS	Cuts 77332
77337	4	"	FE	IS	Cuts 77149,77334,77335,77343
77339	8	"	FE	IS	Cuts 77343
77340	4	"	FE	IS	Cuts 77339
77341	1	"	FE	DY	Cuts 77339 Also on Fig 2.9
77342	11	"	FE	IS	Cuts 77339
77343	4	"	FE	DY	
77344	4	"	FE	DY	Cuts 77339,77343
77346	9	"	FE	DY	
77348	4	"	FE	IS	Cuts 77343,77350
77349	8	"	FE	DY	
77350	8	"	FE	DY	
77351	4	"	FE	IS	Cuts 77149
77352	2	"	FE	DY	Cuts 77149
77356	3	NM39409846	TO	PIS	
77359	4	NG35700416	TO	DY	
77360	4	"	TO	DY	Cuts 77359,cut by a THC
SR141	6		LA	DY	CHE pers collection
SR151	5		LA	DY	"
SR159	6		LA	DY	"
SR182	6		LA	DY	"
SR211	6		LA	DY	"
SR229	5		LA	DY	"
SR238	5		LA	DY	"
SR282	6		LA	DY	"
SR284	5		LA	DY	"

APPENDIX 6.1

ELECTRON MICROPROBE ANALYSIS

The machine used was a Cambridge Instrument Company Geoscan Mark II operated at an accelerating voltage of 15 KU and a specimen current of 40 nanoamps. The focussed beam diameter is in the order of 2-5 μ .

Samples were prepared as polished thin sections and where possible were simultaneously carbon coated with the standards to ensure a uniform carbon coat thickness. Both standards and samples were stored in a dessicator between analysing sessions to prevent deterioration of the carbon coat.

All analyses were made on a wavelength dispersive system with three analysing crystals - LiF, K.A.P. and P.E.T. Analyses prior to January 1979 were made using a single spectrometer, all subsequent analyses made simultaneous use of two spectrometers. The general analysing conditions for each element are shown in Table A6.1.

Data handling follows the general method described by Sweatman and Long (1969) and was performed by an on-line Varian 620 L/100 computer. The program Tim 3 (written by Dr. A. Peckett) performs a ZAF (Atomic number, Mass absorbtion, Fluorescence) correction on peak and background data for samples and standard. In general 4 to 6 ten-second count accumulations are obtained and averaged for each peak and background position, for each element. Background values determined for each mineral type were used throughout each analytical session.

Calculated detection limits for the elements in Table A6.1 are believed to be 200-500 pm and overall accuracy for the major constituents ($>$ 10 wt%) is estimated to be $\pm$2% (Pinsent, 1974).

TABLE A6.1

OPTIMUM ANALYSING CONDITIONS AND STANDARDS USED IN ELECTRON MICROPROBE ANALYSIS

Z	Element	Line	Analysing crystal	Counter	Peak	Background	Standard
11	Na	$K\alpha 1$	K.A.P.	Flow	$53°14'$	$\pm 2°$	Jadeite
12	Mg	"	"	"	$43°42'$	"	MgO
13	Al	"	"	"	$36°32'$	"	Al_2O_3
14	Si	"	P.E.T.	"	$109°18'$	"	Wollastonite
19	K	"	"	"	$50°20'$	"	K-feldspar
20	Ca	"	LiF	"	$113°02'$	"	Wollastonite
22	Ti	"	"	"	$86°05'$	"	TiO_2
24	Cr	"	"	"	$69°16'$	"	Cr_2O_3
25	Mn	"	"	"	$62°48'$	"	Rhodonite
26	Fe	"	"	"	$57°20'$	"	Fe
28	Ni	"	"	"	$48°34'$	"	Ni

APPENDIX 6.2

TABLE SHOWING WHICH MINERAL TYPES WERE ANALYSED IN EACH SPECIMEN
OL=OLIVINE, PL=PLAGIOCLASE, CP=CLINOPYROXENE,
OP=OPAQUE OXIDES, OPX=ORTHOPYROXENE, A=AMPHIBOLE
TY=SPECIMEN TYPE, GP=GABBRO PLUG, PP=PERIDOTITE PLUG

SPEC	TY	PHENOCRYSTS				GROUNDMASS					
		OL	PL	CP	OP	OL	PL	CP	OP	OPX	A
12A76	7		X				X	X			
32A76	10						X	X	X		
46A76	2						X	X	X		
52A76	1	X			X			X			
53A76	1	X					X	X			
55A76	9		X	X			X				
62A76	4			X				X			
60A76	1				X			X			
85A76	1	X			X		X	X			
95A76	4						X	X	X		
77227	8		X	X							
77023	11						X	X			
77024	1	X			X	X	X	X			
77039	2				X		X	X	X		
77044	4			X							
77047	7		X								
77052	1	X									
77058	10							X			
77067	GP							X			
77068	4							X	X		
77082	3		X	X			X	X	X		
77088	3		X					X			
77090	10		X					X			
77092	8			X			X	X			
77093	1	X			X	X	X	X			
77095	1	X			X		X	X			
77105	8		X	X			X	X			
77132	12						X				
77155	8						X	X	X		
77184	10				X						
77209	9			X							
77212	2						X	X			
77214	2		X	X			X	X	X		
77236	1										X
77251	3			X			X	X	X		
77258	7		X								
77268	PP					X					
77279	11						X	X	X		
77292	GP						X	X		X	
77321	1			X			X	X			
77341	1						X	X			
SR286	6							X			

Appendix 6.3

Table of mineral analyses. The specimens in each mineral type
are arranged in the ascending order of their respective dolerite
groups, with the gabbro and peridotite mineral analyses located
at the end of each section. Note that iron is given as Fe^{2+} in
all analyses,(including the opaque oxides), NA= not analysed.
Guide to analysis numbers.

The first 5 characters refer to the specimen number.

01,02 etc refer to the mineral analysis number for that specimen.

G and P refer to groundmass and phenocrysts respectively.

CLINOPYROXENES

	52A7601G	52A7602G	53A7601G	53A7602G	53A7603G	7732101G	7732103G	7734101G
WT.%								
SiO_2	47.33	46.34	48.56	47.89	47.47	43.62	44.06	45.52
TiO_2	2.45	2.16	1.02	1.95	2.53	3.88	3.53	2.42
Al_2O_3	6.15	6.32	6.62	6.89	7.54	8.56	9.05	8.86
Cr_2O_3	0.15	0.12	0.14	0.06	0.04	0.02	NA	NA
FeO	12.30	8.99	8.79	9.74	8.26	11.96	12.67	12.15
MnO	0.32	0.15	0.20	0.20	0.12	0.16	0.18	0.12
MgO	11.53	12.42	12.46	11.53	12.52	10.24	10.15	10.28
CaO	24.58	21.95	21.90	21.32	21.98	20.72	20.41	20.25
Na_2O	0.23	0.42	0.36	0.91	0.24	0.85	0.89	0.73
NiO	0.02	0.03	0.11	0.14	0.23	NA	NA	NA
TOTAL	98.54	98.67	101.06	99.89	104.65	98.99	98.04	98.43

ATOMIC PROPORTIONS BASED ON 6 OXYGENS

	52A7601G	52A7602G	53A7601G	53A7602G	53A7603G	7732101G	7732103G	7734101G
SI	1.797	1.755	1.798	1.825	1.749	1.684	1.691	1.745
TI	0.070	0.062	0.053	0.055	0.071	0.112	0.102	0.070
AL	0.275	0.284	0.289	0.272	0.328	0.388	0.409	0.399
CR	0.005	0.003	0.004	0.002	0.012	0.001	0.000	0.000
FE2	0.332	0.287	0.272	0.306	0.254	0.353	0.342	0.325
MN	0.001	0.005	0.006	0.006	0.004	0.005	0.006	0.004
MG	0.657	0.705	0.688	0.653	0.684	0.588	0.581	0.565
CA	0.847	0.898	0.869	0.851	0.875	0.854	0.830	0.830
NA	0.015	0.031	0.026	0.067	0.017	0.063	0.066	0.054
NI	0.001	0.001	0.003	0.004	0.007	0.000	0.000	0.000

ATOMIC PROPORTIONS

	52A7601G	52A7602G	53A7601G	53A7602G	53A7603G	7732101G	7732103G	7734101G
CA	46.13	47.50	47.51	47.30	48.11	47.59	47.62	47.58
FE	18.09	15.16	14.88	16.80	13.77	19.67	19.43	18.65
MG	35.78	37.34	37.60	35.90	38.12	32.75	32.95	33.67

MG-NUMBER

	52A7601G	52A7602G	53A7601G	53A7602G	53A7603G	7732101G	7732103G	7734101G
M/M+F	65.42	71.12	71.64	68.12	73.47	62.48	62.90	64.35

CLINOPYROXENES

	7734122G	7709531G	85A7601G	85A7602G	69A7632G	69A7633G	7702411G	7702412G
WT.%								
SIO2	45.72	45.16	49.21	49.45	48.61	48.59	47.66	47.40
TIO2	2.59	1.97	1.95	1.25	2.36	1.58	1.66	1.91
AL2O3	6.62	8.52	5.47	4.13	4.64	4.15	5.73	5.39
CR2O3	0.04	0.16	0.02	0.29	0.17	0.13	0.20	0.21
FEO	11.87	9.43	10.03	8.44	8.28	8.18	8.85	9.31
MNO	0.21	0.17	0.30	0.17	0.14	0.19	0.36	0.28
MGO	11.17	11.69	14.47	14.55	13.60	13.76	12.24	11.35
CAO	19.80	20.21	18.85	19.97	21.77	21.82	22.98	23.46
NA2O	0.65	0.55	0.40	0.33	0.40	0.22	0.55	0.47
NIO	NA	NA	NA	NA	0.19	0.15	NA	NA
TOTAL	98.67	97.84	100.70	98.58	100.16	98.77	100.43	100.08

ATOMIC PROPORTIONS BASED ON 6 OXYGENS

SI	1.762	1.735	1.824	1.866	1.816	1.843	1.798	1.791
TI	0.075	0.057	0.054	0.035	0.066	0.045	0.047	0.054
AL	0.301	0.385	0.239	0.184	0.204	0.185	0.254	0.271
CR	0.001	0.005	0.001	0.009	0.005	0.004	0.006	0.006
FE2	0.383	0.303	0.311	0.266	0.259	0.259	0.278	0.294
MN	0.007	0.005	0.009	0.005	0.004	0.006	0.011	0.009
MG	0.642	0.672	0.800	0.818	0.757	0.777	0.686	0.630
CA	0.818	0.832	0.749	0.807	0.871	0.885	0.925	0.934
NA	0.049	0.041	0.029	0.024	0.029	0.016	0.040	0.034
NI	0.000	0.000	0.000	0.000	0.006	0.005	0.000	0.000

ATOMIC PROPORTIONS

CA	44.39	46.11	40.27	42.67	46.17	46.09	48.98	50.00
FE	20.77	16.79	16.72	14.08	13.71	13.48	14.72	15.76
MG	34.84	37.10	43.01	43.25	40.12	40.43	36.29	34.24

MG-NUMBER

M/M+F.	62.65	68.84	72.00	75.45	74.54	74.99	71.14	68.48

CLINOPYROXENES

	46A7621G	46A7622G	7703901G	7703902G	7708401G	7708403G	7721281G	7721282G
WT.%								
SIO2	46.98	46.72	47.11	48.83	47.89	47.51	46.37	45.33
TIO2	1.45	1.33	1.67	0.95	1.52	1.38	1.73	1.72
AL2O3	6.28	5.64	5.81	4.41	5.75	4.58	5.87	5.88
CR2O3	NA	0.04	0.14	0.02	0.15	0.26	0.03	0.02
FEO	7.87	8.25	9.45	10.49	8.58	11.09	9.85	10.58
MNO	0.04	0.18	0.19	0.25	0.15	0.27	0.23	0.34
MGO	13.71	13.65	12.82	13.29	13.26	13.12	12.79	12.62
CAO	23.83	23.74	21.83	20.72	21.85	19.68	21.57	20.24
NA2O	0.45	0.46	0.50	0.53	0.36	0.54	0.57	0.70
NIO	0.08	0.04	NA	0.05	NA	NA	0.06	0.12
TOTAL	97.46	97.07	98.72	98.74	99.61	98.23	99.07	98.83
ATOMIC PROPORTIONS BASED ON 6 OXYGENS								
SI	1.797	1.801	1.796	1.836	1.823	1.828	1.772	1.777
TI	0.042	0.039	0.048	0.027	0.046	0.040	0.050	0.050
AL	0.274	0.256	0.261	0.199	0.255	0.228	0.264	0.266
CR	0.000	0.001	0.004	0.001	0.004	0.002	0.001	0.001
FE2	0.252	0.265	0.341	0.335	0.273	0.357	0.315	0.349
MN	0.010	0.006	0.006	0.006	0.005	0.009	0.007	0.011
MG	0.782	0.785	0.729	0.757	0.744	0.752	0.728	0.721
CA	0.854	0.857	0.859	0.849	0.881	0.811	0.883	0.832
NA	0.033	0.034	0.037	0.039	0.026	0.040	0.042	0.052
NI	0.003	0.001	0.000	0.002	0.000	0.000	0.002	0.003
ATOMIC PROPORTIONS								
CA	45.24	44.92	45.48	43.72	46.50	42.24	45.84	43.73
FE	13.34	13.95	15.95	17.27	14.25	18.58	16.34	18.35
MG	41.42	41.14	38.57	39.01	39.25	39.18	37.82	37.93
MG-NUMBER								
M/M+F	75.64	74.67	70.74	69.31	73.37	67.83	69.83	67.42

CLINOPYROXENES

	7721401P	7721402P	7721403P	7721404G	7721405P	7721406G	7721407G	7728231P
WT.%								
SIO2	51.31	51.27	51.36	49.16	49.25	49.57	48.69	46.59
TIO2	0.82	0.78	0.58	1.35	1.33	1.33	1.29	2.33
AL2O3	2.58	1.89	2.53	5.49	5.61	4.49	5.37	5.57
CR2O3	0.17	0.06	0.42	0.26	0.46	NA	0.18	0.17
FEO	9.50	10.17	7.31	7.51	6.50	10.01	7.94	8.91
MNO	0.21	0.19	0.15	0.11	0.15	0.17	0.13	0.14
MGO	15.24	14.91	17.29	14.68	13.80	12.95	14.08	12.51
CAO	19.69	19.56	19.31	21.88	22.01	21.21	21.55	21.42
NA2O	0.25	0.24	0.22	0.29	0.26	0.34	0.27	0.18
NIO	NA	NA	NA	NA	NA	NA	NA	NA
TOTAL	99.77	99.07	99.09	100.13	99.22	99.73	99.33	97.20

ATOMIC PROPORTIONS BASED ON 6 OXYGENS

	7721401P	7721402P	7721403P	7721404G	7721405P	7721406G	7721407G	7728231P
SI	1.915	1.932	1.910	1.827	1.838	1.863	1.824	1.812
TI	0.023	0.022	0.014	0.038	0.037	0.038	0.036	0.058
AL	0.113	0.084	0.111	0.240	0.247	0.199	0.238	0.254
CR	0.005	0.002	0.012	0.008	0.014	0.000	0.005	0.005
FE2	0.295	0.321	0.227	0.233	0.206	0.315	0.249	0.225
MN	0.007	0.006	0.005	0.003	0.005	0.005	0.004	0.005
MG	0.848	0.838	0.958	0.788	0.768	0.726	0.783	0.722
CA	0.787	0.790	0.769	0.871	0.882	0.854	0.867	0.886
NA	0.018	0.018	0.016	0.021	0.019	0.009	0.020	0.002
NI	0.000	0.000	0.000	0.000	0.000	0.000	0.000	0.000

ATOMIC PROPORTIONS

	7721401P	7721402P	7721403P	7721404G	7721405P	7721406G	7721407G	7728231P
CA	40.76	40.55	39.35	46.23	47.48	45.09	45.63	46.85
FE	15.35	16.45	11.63	12.38	11.11	16.61	13.12	15.45
MG	43.89	43.00	49.02	41.39	41.41	38.30	41.24	38.14

MG-NUMBER

	7721401P	7721402P	7721403P	7721404G	7721405P	7721406G	7721407G	7728231P
M/M+F	74.09	72.32	80.83	76.97	78.84	69.75	75.86	71.68

CLINOPYROXENES

	7708282P	7708284G	7725101G	7725102G	7725103P	7725104P	7704481P	7704483P
WT.%								
SIO2	47.56	47.12	51.63	46.60	51.37	49.28	51.19	51.71
TIO2	1.61	2.23	0.85	2.35	1.18	1.13	0.04	0.60
AL2O3	4.73	5.73	3.01	5.42	2.44	2.51	4.74	2.71
CR2O3	0.17	0.22	0.20	NA	0.10	NA	0.58	0.27
FEO	8.92	9.28	8.32	12.50	9.69	9.23	6.44	7.58
MNO	0.19	0.18	0.12	0.17	0.35	0.26	0.14	0.23
MGO	12.73	12.65	15.33	11.68	14.46	14.31	15.71	17.10
CAO	21.29	21.10	20.43	21.30	19.60	21.85	20.38	18.24
NA2O	0.00	0.00	0.00	0.00	0.30	0.00	0.26	0.26
NIO	NA	NA	NA	NA	NA	NA	0.10	0.05
TOTAL	97.28	98.37	99.90	98.02	97.85	98.57	100.48	98.53
ATOMIC PROPORTIONS BASED ON 6 OXYGENS								
SI	1.837	1.797	1.913	1.799	1.911	1.879	1.872	1.921
TI	0.047	0.066	0.024	0.068	0.034	0.032	0.026	0.010
AL	0.215	0.258	0.131	0.247	0.108	0.113	0.204	0.119
CR	0.005	0.007	0.006	0.000	0.003	0.000	0.017	0.008
FE2	0.287	0.293	0.258	0.349	0.309	0.294	0.197	0.236
MN	0.006	0.005	0.004	0.006	0.011	0.008	0.004	0.007
MG	0.731	0.719	0.847	0.672	0.823	0.813	0.856	0.947
CA	0.879	0.862	0.811	0.869	0.851	0.893	0.798	0.726
NA	0.000	0.000	0.000	0.000	0.000	0.000	0.018	0.019
NI	0.000	0.000	0.000	0.000	0.000	0.000	0.003	0.002
ATOMIC PROPORTIONS								
CA	46.34	46.09	42.34	45.97	41.46	44.63	43.12	38.05
FE	15.12	15.48	13.46	18.45	16.00	14.71	10.64	12.34
MG	38.54	38.44	44.20	35.57	42.55	40.56	46.24	49.60
MG-NUMBER								
M/M+F	71.83	71.29	76.66	65.84	72.68	73.43	81.30	80.07

CLINOPYROXENES

	7724404P	7706881G	7706882G	95A7501G	95A7602G	95A7603G	95A7604G	62A7601P
WT %								
SIO2	49.61	46.77	48.33	47.96	49.18	48.26	48.24	52.42
TIO2	1.43	2.41	1.32	1.54	1.43	2.19	2.19	0.80
AL2O3	6.31	5.14	4.79	5.58	4.48	4.67	4.07	3.20
CR2O3	0.06	0.03	NA	0.06	0.04	0.38	0.07	0.22
FEO	8.43	12.64	11.72	10.59	11.74	12.35	11.02	8.21
MNO	0.24	0.29	0.34	0.25	0.39	0.28	0.25	0.40
MGO	12.86	12.15	12.84	13.56	12.77	12.36	12.67	15.41
CAO	18.99	19.91	18.42	19.18	17.60	19.29	19.51	24.47
NA2O	0.86	0.41	0.68	0.48	0.45	0.45	0.60	0.30
NIO	NA	NA	NA	NA	NA	NA	NA	NA
TOTAL	98.76	99.35	98.38	99.22	98.08	100.13	99.01	98.99
ATOMIC PROPORTIONS BASED ON 6 OXYGENS								
SI	1.858	1.795	1.847	1.815	1.860	1.825	1.827	1.894
TI	0.040	0.058	0.038	0.044	0.041	0.062	0.062	0.025
AL	0.279	0.232	0.217	0.249	0.242	0.217	0.222	0.137
CR	0.002	0.001	0.000	0.002	0.001	0.002	0.002	0.007
FE2	0.263	0.406	0.377	0.335	0.375	0.391	0.378	0.258
MN	0.008	0.009	0.011	0.008	0.013	0.009	0.008	0.013
MG	0.718	0.695	0.734	0.771	0.728	0.697	0.682	0.841
CA	0.752	0.819	0.758	0.775	0.721	0.782	0.792	0.924
NA	0.062	0.031	0.051	0.035	0.033	0.033	0.051	0.022
NI	0.000	0.000	0.000	0.000	0.000	0.000	0.000	0.000
ATOMIC PROPORTIONS								
CA	43.72	42.65	42.57	41.19	39.53	41.82	42.78	42.86
FE	15.09	21.14	20.17	17.83	20.58	20.90	20.40	13.42
MG	41.19	36.21	39.26	40.98	39.90	37.28	36.82	43.72
MG-NUMBER								
M/M+F	73.18	63.14	66.06	69.69	65.97	64.08	64.35	75.52

CLINOPYROXENES

	62A7602P	62A7603G	62A7604G	62A7605G	SR28201G	SR28202G	SP28203G	12A7641G
WT.%								
SIO2	51.13	48.79	50.03	51.43	50.20	51.57	50.70	49.50
TIO2	0.88	1.54	1.48	0.82	1.75	0.69	0.73	1.54
AL2O3	3.15	4.23	4.62	3.35	4.65	2.31	4.25	5.27
CR2O3	0.18	0.04	0.05	0.23	0.39	0.15	0.32	0.09
FEO	8.02	11.14	8.64	6.47	8.04	8.24	7.82	9.13
MNO	0.54	0.84	0.54	0.40	0.22	0.30	0.18	0.23
MGO	14.87	13.04	14.32	15.19	15.11	16.08	15.02	13.91
CAO	20.27	19.65	20.53	20.85	19.83	19.39	19.69	20.07
NA2O	0.32	0.37	0.23	0.26	0.23	0.21	0.24	0.35
NIO	NA	NA	NA	NA	0.12	0.13	0.08	NA
TOTAL	99.34	99.64	100.44	99.00	99.84	99.07	99.03	100.79

ATOMIC PROPORTIONS BASED ON 6 OXYGENS

	62A7602P	62A7603G	62A7604G	62A7605G	SR28201G	SR28202G	SP28203G	12A7641G
SI	1.909	1.849	1.856	1.913	1.861	1.924	1.874	1.836
TI	0.025	0.044	0.041	0.023	0.029	0.019	0.020	0.043
AL	0.139	0.189	0.202	0.147	0.223	0.102	0.185	0.222
CR	0.005	0.001	0.001	0.007	0.011	0.004	0.009	0.003
FE2	0.253	0.353	0.268	0.201	0.249	0.257	0.242	0.283
MN	0.017	0.027	0.017	0.013	0.007	0.009	0.006	0.007
MG	0.828	0.737	0.792	0.842	0.835	0.894	0.877	0.769
CA	0.811	0.798	0.816	0.831	0.788	0.775	0.780	0.833
NA	0.023	0.027	0.017	0.019	0.017	0.015	0.017	0.025
NI	0.000	0.000	0.000	0.000	0.004	0.004	0.002	0.000

ATOMIC PROPORTIONS

	62A7602P	62A7603G	62A7604G	62A7605G	SR28201G	SR28202G	SP28203G	12A7641G
CA	42.94	42.27	43.50	44.33	42.08	40.24	41.07	44.20
FE	13.23	18.70	14.29	10.74	13.32	13.35	12.73	15.02
MG	43.83	39.02	42.21	44.93	44.60	46.42	46.20	40.78

MG-NUMBER

	62A7602P	62A7603G	62A7604G	62A7605G	SR28201G	SR28202G	SP28203G	12A7641G
M/M+F	76.81	67.60	74.71	80.71	77.01	77.67	78.40	73.09

CLINOPYROXENES

	12A7682G	12A7683G	7709201G	7709202G	7709203P	7709204P	7712501P	7715501G
WT %								
SIO2	49.62	50.25	52.57	53.36	53.26	53.09	53.59	51.61
TIO2	1.68	1.40	0.54	0.38	0.36	0.33	0.31	0.61
AL2O3	5.86	6.41	3.42	2.64	2.47	2.25	2.38	1.87
CR2O3	0.26	0.25	0.48	0.26	0.22	0.21	0.37	0.06
FEO	7.48	6.27	7.43	7.68	6.37	6.38	5.92	10.26
MNO	0.14	0.17	0.14	0.15	0.13	0.23	0.13	0.22
MGO	13.03	13.53	16.01	16.96	18.43	17.98	17.68	15.55
CAO	21.17	20.94	19.11	18.41	19.43	18.28	19.64	19.23
NA2O	0.31	0.38	0.22	0.21	0.22	0.27	0.17	0.33
NIO	NA	NA	NA	NA	NA	NA	0.18	NA
TOTAL	99.45	99.18	99.52	99.66	100.89	98.82	100.20	99.71

ATOMIC PROPORTIONS BASED ON 6 OXYGENS

SI	1.848	1.852	1.935	1.955	1.929	1.955	1.947	1.931
TI	0.045	0.042	0.015	0.010	0.010	0.009	0.008	0.017
AL	0.257	0.262	0.148	0.114	0.105	0.098	0.102	0.082
CR	0.008	0.008	0.002	0.022	0.006	0.006	0.011	0.002
FE2	0.233	0.194	0.229	0.235	0.193	0.197	0.180	0.321
MN	0.004	0.005	0.004	0.005	0.004	0.001	0.004	0.007
MG	0.724	0.747	0.879	0.926	0.995	0.987	0.958	0.867
CA	0.845	0.830	0.754	0.723	0.754	0.721	0.765	0.771
NA	0.022	0.022	0.016	0.015	0.015	0.019	0.012	0.022
NI	0.000	0.000	0.000	0.000	0.000	0.000	0.003	0.000

ATOMIC PROPORTIONS

CA	46.90	45.84	40.50	38.36	38.83	37.87	40.22	39.35
FE	12.93	10.97	12.29	12.49	9.94	10.32	9.46	16.39
MG	40.16	42.19	47.21	49.16	51.24	51.82	50.34	44.26

MG-NUMBER

M/M+F	75.64	79.37	79.34	79.74	83.76	83.40	84.18	72.98

CLINOPYROXENES

	7715502G	7715503G	7700601P	55A7601P	55A7602P	55A7603P	7720901P	7720902P
WT.%								
SIO2	49.23	49.15	51.80	51.33	51.28	51.33	50.83	50.70
TIO2	1.18	1.29	0.92	0.89	1.07	1.09	0.92	0.88
AL2O3	3.78	3.52	3.69	2.55	2.95	3.13	2.74	2.54
CR2O3	0.06	0.08	0.89	0.12	0.11	0.16	0.09	0.12
FEO	11.54	12.64	8.76	11.04	11.56	10.83	11.44	11.31
MNO	0.23	0.27	0.21	0.21	0.25	0.23	0.05	0.79
MGO	14.17	14.03	15.61	14.87	16.62	15.62	16.13	15.71
CAO	20.03	18.15	19.21	19.94	17.29	18.84	15.57	18.75
NA2O	0.42	0.43	0.09	0.26	0.33	0.30	0.24	0.19
NIO	NA	NA	NA	NA	NA	NA	NA	NA
TOTAL	99.44	99.93	100.29	100.28	100.56	100.60	99.01	101.28

ATOMIC PROPORTIONS BASED ON 6 OXYGENS

	7715502G	7715503G	7700601P	55A7601P	55A7602P	55A7603P	7720901P	7720902P
SI	1.855	1.867	1.888	1.910	1.896	1.890	1.901	1.888
TI	0.034	0.037	0.026	0.025	0.030	0.034	0.026	0.025
AL	0.169	0.161	0.157	0.116	0.129	0.135	0.121	0.116
CR	0.002	0.002	0.026	0.004	0.003	0.005	0.003	0.001
FE2	0.363	0.399	0.271	0.313	0.330	0.311	0.358	0.352
MN	0.007	0.009	0.007	0.007	0.008	0.007	0.030	0.025
MG	0.799	0.792	0.860	0.825	0.916	0.873	0.899	0.878
CA	0.812	0.734	0.761	0.796	0.685	0.748	0.664	0.747
NA	0.031	0.029	0.006	0.019	0.024	0.022	0.017	0.014
NI	0.000	0.000	0.000	0.000	0.000	0.000	0.000	0.000

ATOMIC PROPORTIONS

	7715502G	7715503G	7700601P	55A7601P	55A7602P	55A7603P	7720901P	7720902P
CA	41.76	38.18	40.22	41.15	35.48	38.70	34.57	37.93
FE	17.15	20.75	14.31	16.17	17.07	16.08	18.63	17.86
MG	41.09	41.06	45.47	42.69	47.45	45.21	46.81	44.21

MG-NUMBER

	7715502G	7715503G	7700601P	55A7601P	55A7602P	55A7603P	7720901P	7720902P
M/M+F	70.56	66.42	76.05	72.53	73.54	73.76	71.54	71.23

CLINOPYROXENES

	7720003P	7720004P	7705801G	7705802G	7709001G	7709002G	32A7601G	32A7602G
WT.%								
SIO2	51.55	52.01	48.36	47.98	46.14	46.45	46.96	45.58
TIO2	0.72	0.79	1.94	1.80	3.15	2.98	2.69	3.31
AL2O3	2.49	2.34	5.58	5.60	4.88	4.85	4.14	5.53
CR2O3	0.12	0.10	0.16	0.38	0.09	0.12	0.02	0.28
FEO	10.39	10.35	9.61	8.44	12.35	10.68	9.28	9.93
MNO	0.83	0.83	0.18	0.13	0.78	0.59	0.30	0.33
MGO	15.42	15.60	13.41	13.57	10.99	11.11	10.39	9.30
CAO	17.91	18.66	21.27	21.31	19.65	21.32	24.82	24.75
NA2O	0.24	0.25	0.41	0.47	0.49	0.00	0.64	0.24
NIO	NA	NA	NA	NA	NA	NA	NA	NA
TOTAL	100.67	100.93	100.92	99.68	98.52	98.10	99.24	99.32
ATOMIC PROPORTIONS BASED ON 6 OXYGENS								
SI	1.909	1.923	1.802	1.803	1.790	1.799	1.806	1.758
TI	0.020	0.022	0.054	0.051	0.092	0.087	0.078	0.096
AL	0.109	0.102	0.245	0.248	0.223	0.221	0.188	0.256
CR	0.004	0.003	0.005	0.011	0.003	0.004	0.001	0.009
FE2	0.322	0.320	0.299	0.255	0.401	0.346	0.298	0.320
MN	0.026	0.025	0.006	0.004	0.026	0.019	0.010	0.010
MG	0.906	0.860	0.745	0.750	0.636	0.641	0.596	0.535
CA	0.711	0.739	0.849	0.858	0.817	0.885	1.023	1.023
NA	0.017	0.018	0.030	0.034	0.037	0.000	0.048	0.018
NI	0.000	0.000	0.000	0.000	0.000	0.000	0.000	0.000
ATOMIC PROPORTIONS								
CA	36.65	38.52	44.85	45.56	44.08	47.26	53.36	54.47
FE	16.60	16.68	15.82	14.08	21.62	18.48	15.57	17.06
MG	46.75	44.80	39.34	40.36	34.30	34.26	31.07	28.47
MG-NUMBER								
M/M+F	73.80	72.87	71.32	74.13	61.33	64.96	66.62	62.54

CLINOPYROXENES

	7727901G	7727902G	7727903G	7727904G	7702301P	7702302P	7706701G	7706702G
WT %								
SIO2	50.99	49.76	51.61	50.27	47.64	47.71	51.37	49.72
TIO2	1.17	1.24	0.91	0.63	2.71	2.47	0.76	0.70
AL2O3	3.12	3.26	2.69	1.32	3.58	4.07	2.51	3.29
CR2O3	0.02	0.13	0.17	0.07	0.05	0.00	0.06	0.69
FEO	9.77	9.61	9.48	11.31	9.64	10.53	7.57	6.39
MNO	0.69	0.93	0.80	0.51	0.27	0.31	0.30	0.19
MGO	14.83	15.28	15.09	13.17	11.64	9.85	16.31	16.30
CAO	19.11	18.65	18.60	23.35	23.42	23.23	22.88	21.71
NA2O	0.29	0.29	0.34	0.31	0.37	0.36	0.31	0.21
NIO	NA	NA	NA	NA	NA	NA	0.17	0.12
TOTAL	99.99	98.96	99.69	101.04	98.62	98.33	103.24	99.32
ATOMIC PROPORTIONS BASED ON 6 OXYGENS								
SI	1.941	1.883	1.924	1.899	1.835	1.845	1.899	1.857
TI	0.033	0.034	0.026	0.018	0.058	0.072	0.021	0.020
AL	0.137	0.145	0.118	0.059	0.162	0.186	0.109	0.145
CR	0.001	0.004	0.005	0.002	0.002	0.000	0.002	0.020
FE2	0.305	0.304	0.296	0.357	0.310	0.341	0.234	0.200
MN	0.022	0.033	0.025	0.020	0.009	0.010	0.009	0.006
MG	0.824	0.849	0.839	0.742	0.668	0.568	0.899	0.907
CA	0.764	0.764	0.743	0.945	0.966	0.955	0.827	0.869
NA	0.021	0.021	0.025	0.023	0.028	0.027	0.022	0.015
NI	0.000	0.000	0.000	0.000	0.000	0.000	0.005	0.004
ATOMIC PROPORTIONS								
CA	40.35	39.84	39.58	46.24	49.69	51.23	42.20	43.97
FE	16.10	15.84	15.75	17.48	15.96	18.28	11.94	10.10
MG	43.56	44.32	44.67	36.28	34.35	30.48	45.86	45.93
MG-NUMBER								
M/M+F	73.01	73.66	73.94	67.49	68.28	62.51	79.34	81.97

CLINOPYROXENES

	7729201G	7729202G	7729203G	7726804G	7726805G	7726806G
WT.%						
SIO2	53.52	51.16	51.28	52.36	52.98	51.34
TIO2	0.72	0.87	0.86	0.56	0.55	0.56
AL2O3	2.42	2.45	2.05	4.02	3.77	3.71
CR2O3	0.15	0.02	0.06	1.43	1.32	1.29
FEO	10.05	11.06	11.06	4.43	4.45	4.50
MNO	0.36	0.34	0.38	0.28	0.17	0.17
MGO	15.36	14.42	14.76	16.34	16.09	15.39
CAO	18.72	19.21	19.36	21.42	21.38	21.59
NA2O	0.32	0.34	0.37	0.27	0.33	0.30
NIO	0.10	0.15	0.22	0.07	0.09	0.04
TOTAL	99.67	99.81	100.42	99.10	99.13	99.99

ATOMIC PROPORTIONS BASED ON 6 OXYGENS

	7729201G	7729202G	7729203G	7726804G	7726805G	7726806G
SI	1.898	1.918	1.914	1.866	1.885	1.883
TI	0.020	0.025	0.024	0.016	0.015	0.015
AL	0.137	0.139	0.090	0.176	0.164	0.160
CR	0.004	0.001	0.002	0.041	0.039	0.037
FE2	0.344	0.347	0.346	0.136	0.138	0.138
MN	0.011	0.011	0.012	0.009	0.005	0.005
MG	0.860	0.805	0.821	0.872	0.887	0.896
CA	0.753	0.754	0.774	0.850	0.847	0.853
NA	0.023	0.025	0.027	0.019	0.024	0.021
NI	0.006	0.005	0.007	0.002	0.003	0.001

ATOMIC PROPORTIONS

	7729201G	7729202G	7729203G	7726804G	7726805G	7726806G
CA	38.47	39.87	39.88	44.99	45.26	45.18
FE	17.58	18.11	17.82	7.22	7.35	7.32
MG	43.95	42.02	42.30	47.79	47.39	47.50

MG-NUMBER

	7729201G	7729202G	7729203G	7726804G	7726805G	7726806G
M/M+F	71.43	69.89	70.36	86.88	86.57	86.65

ORTHOPYROXENES IN THE EARLY (HIGH MGO) GABBROS

	7729204G	7729205G	7729206G
WT %			
SI02	52.52	53.45	53.22
TIO2	1.35	0.47	0.46
AL203	1.41	1.45	1.42
CR203	0.03	0.04	0.04
FEO	19.41	18.10	18.43
MNO	0.52	0.54	0.56
MGO	23.01	23.95	24.72
CAO	2.09	1.98	1.92
NA20	0.12	0.01	0.01
NIO	0.10	0.13	0.10
TOTAL	100.33	100.12	100.48

ATOMIC PROPORTIONS BASED ON 6 OXYGENS

SI	1.935	1.955	1.943
TI	0.029	0.013	0.013
AL	0.061	0.063	0.061
CR	0.001	0.001	0.001
FE2	0.598	0.554	0.560
MN	0.016	0.017	0.017
MG	1.264	1.307	1.345
CA	0.083	0.078	0.075
NA	0.007	0.001	0.001
NI	0.006	0.004	0.003

ATOMIC PROPORTIONS

CA	4.24	4.21	3.81
FE	30.76	28.58	27.93
MG	65.00	67.41	68.26

MG-NUMBER

M/M+F	67.88	70.22	70.96

AMPHIBOLES IN THE GROUP 1 (TYPE 3) PICRITES

	77236Ø1G	77236Ø2G	77236Ø3G
WT.%			
SIO2	42.44	41.37	41.87
TIO2	4.94	4.73	5.21
AL2O3	11.49	11.74	11.26
CR2O3	Ø.Ø3	Ø.15	Ø.Ø7
FEO	9.Ø3	8.75	8.88
MNO	Ø.14	Ø.12	Ø.14
MGO	14.97	15.Ø8	14.75
CAO	11.87	11.86	11.92
NA2O	3.13	2.97	2.5Ø
K2O	Ø.41	Ø.42	Ø.46
TOTAL	98.45	97.19	97.Ø6

ATOMIC PROPORTIONS BASED ON 23 OXYGENS

SI	6.152	6.Ø78	6.15Ø
TI	Ø.539	Ø.523	Ø.575
AL	1.963	2.Ø33	1.949
CR	Ø.ØØ3	Ø.Ø17	Ø.ØØ8
FE2	1.Ø95	1.Ø75	1.Ø91
MN	Ø.Ø17	Ø.Ø15	Ø.Ø17
MG	3.235	3.3Ø3	3.229
CA	1.844	1.867	1.876
NA	Ø.88Ø	Ø.846	Ø.712
K	Ø.Ø76	Ø.Ø79	Ø.Ø86

MG-NUMBER
| M/M+F | 74.71 | 75.44 | 74.75 |

OLIVINES   GROUP 1 TYPE 1

	52A7603P	52A7604P	53A7604P	53A7605P	53A7606P	53A7607P
WT %						
SIO2	40.88	40.94	40.65	38.50	39.54	40.60
CR2O3	0.09	0.11	0.11	0.00	0.00	0.10
FEO	11.10	11.26	12.88	13.23	14.54	12.90
MNO	0.17	0.15	0.20	0.16	0.22	0.23
MGO	47.73	46.99	46.37	46.45	45.36	45.85
CAO	0.33	0.37	0.34	0.32	0.40	0.36
NIO	0.36	0.37	0.43	0.46	0.34	0.39
TOTAL	100.66	100.19	100.98	99.12	100.40	100.43

ATOMIC PROPORTIONS BASED ON 4 OXYGENS

SI	0.996	1.002	0.995	0.965	0.984	0.999
CR	0.002	0.002	0.002	0.000	0.000	0.002
FE2	0.226	0.231	0.264	0.277	0.303	0.266
MN	0.004	0.003	0.004	0.003	0.005	0.005
MG	1.734	1.715	1.691	1.736	1.683	1.682
CA	0.009	0.010	0.009	0.009	0.011	0.009
NI	0.527	0.544	0.632	0.693	0.508	0.577

MG-NUMBER

| M/M+F | 88.46 | 88.15 | 86.52 | 86.22 | 84.76 | 86.37 |

OLIVINES GROUP 1 TYPE 2

	7705201P	7705223P	7709301P	7709302P	7709323P	7709304G	7709502P	7709503P
WT.%								
SIO2	41.98	41.85	43.52	39.65	39.77	39.76	39.66	39.63
FEO	12.94	11.95	12.82	11.87	11.35	14.84	12.76	12.79
MNO	0.27	0.19	0.19	0.17	0.15	0.27	0.18	0.22
MGO	46.85	47.34	46.95	48.10	47.04	44.83	46.88	47.14
CAO	0.32	0.28	0.36	0.35	0.40	0.67	0.36	0.38
NIO	0.37	0.38	0.32	0.40	0.35	0.25	0.37	0.36
TOTAL	100.66	101.96	101.25	100.54	99.06	100.58	100.21	100.52

ATOMIC PROPORTIONS BASED ON 4 OXYGENS

	7705201P	7705223P	7709301P	7709302P	7709323P	7709304G	7709502P	7709503P
SI	1.019	1.008	0.993	0.973	0.988	0.990	0.980	0.977
FE2	0.222	0.241	0.262	0.244	0.236	0.308	0.264	0.264
MN	0.004	0.004	0.004	0.004	0.003	0.006	0.004	0.005
MG	1.695	1.698	1.710	1.760	1.742	1.664	1.728	1.733
CA	0.008	0.007	0.009	0.009	0.011	0.018	0.010	0.010
NI	0.539	0.550	0.470	0.590	0.522	0.374	0.550	0.534

MG-NUMBER

	7705201P	7705223P	7709301P	7709302P	7709323P	7709304G	7709502P	7709503P
M/M+F	88.42	87.58	86.72	87.84	88.08	84.37	86.75	86.79

OLIVINES GROUP 1

	85A7632P	85A7633P	7702431P	7702432P	7702433P	7702435P	7702436P	7702437P
WT.%								
SIO2	42.45	39.85	38.95	39.55	37.45	38.34	38.76	37.84
FEO	11.68	13.98	21.62	22.02	21.82	23.13	22.31	21.75
MNO	0.13	0.22	0.39	0.36	0.36	0.44	0.47	0.42
MGO	45.23	45.21	38.86	38.72	38.91	38.47	38.64	39.12
CAO	0.33	0.44	0.32	0.42	0.44	0.24	0.51	0.27
NIO	0.34	0.33	0.22	0.15	0.21	0.18	0.20	0.20
TOTAL	99.16	100.04	100.36	99.22	98.79	100.80	100.89	99.60

ATOMIC PROPORTIONS BASED ON 4 OXYGENS

SI	1.033	0.992	1.003	1.021	0.976	0.991	0.997	0.986
FE2	0.242	0.291	0.465	0.432	0.488	0.520	0.480	0.474
MN	0.003	0.005	0.009	0.008	0.008	0.010	0.010	0.009
MG	1.739	1.677	1.491	1.491	1.527	1.483	1.482	1.519
CA	0.009	0.012	0.009	0.012	0.012	0.007	0.014	0.008
NI	0.507	0.494	0.340	0.233	0.332	0.280	0.309	0.313

MG-NUMBER

| M/M+F | 87.59 | 85.22 | 76.21 | 77.51 | 76.07 | 74.78 | 75.53 | 76.22 |

OLIVINES GROUP 1 AND PERIDOTITE PLUG

	7702410G	7726801P	7726802P	7726803P
WT.%				
SIO2	38.72	40.24	40.01	40.60
FEO	22.90	14.00	14.33	14.60
MNO	0.53	0.26	0.10	0.01
MGO	36.86	45.12	44.60	44.33
CAO	0.54	0.26	0.26	0.16
NIO	0.17	0.37	0.45	0.33
TOTAL	99.72	100.25	99.75	100.03

ATOMIC PROPORTIONS BASED ON 4 OXYGENS

SI	1.011	0.998	0.997	1.009
FE2	0.500	0.290	0.299	0.304
MN	0.012	0.005	0.002	0.000
MG	1.435	1.668	1.656	1.643
CA	0.015	0.007	0.007	0.004
NI	0.267	0.551	0.674	0.493

MG-NUMBER

M/M+F	74.15	85.17	84.73	84.40

PLAGIOCLASE

WT.%	53A7609G	85A7608G	85A7609G	7702415G	7702416G	7702417G	7709308G	7709511G
SIO2	49.02	49.55	50.23	50.30	58.92	51.34	49.75	48.70
AL2O3	30.68	30.24	30.23	29.08	25.16	30.09	28.93	30.24
FEO	0.57	0.80	0.79	0.52	0.51	0.79	1.74	1.42
MGO	ND	0.38	1.16	0.22	2.27	0.31	1.55	0.86
CAO	15.32	13.31	14.00	13.75	7.94	13.13	13.62	14.50
NA2O	2.64	3.24	2.65	3.78	6.26	3.93	2.70	2.68
K2O	0.26	0.10	0.09	0.09	0.23	0.11	0.05	0.04
TOTAL	98.37	98.12	99.16	98.73	99.25	99.70	98.34	98.49

ATOMIC PROPORTIONS BASED ON 32 OXYGENS

	53A7609G	85A7608G	85A7609G	7702415G	7702416G	7702417G	7709308G	7709511G
SI	9.129	9.217	9.240	9.320	10.601	9.390	9.273	9.085
AL	6.714	6.629	6.554	6.534	5.335	6.485	6.355	6.630
FE2	0.089	0.124	0.122	0.080	0.077	0.121	0.271	0.222
MG	0.000	0.244	0.318	0.061	0.072	0.085	0.431	0.239
CA	3.058	2.653	2.760	2.725	1.523	2.573	2.720	2.916
NA	1.026	1.169	0.949	1.356	2.184	1.394	0.976	0.969
K	0.014	0.024	0.021	0.021	0.053	0.026	0.012	0.010

ATOMIC PROPORTIONS

	53A7609G	85A7608G	85A7609G	7702415G	7702416G	7702417G	7709308G	7709511G
CA	74.62	68.99	73.99	66.43	40.51	64.45	73.36	74.87
NA	25.03	30.39	25.44	33.05	58.09	34.91	26.32	24.89
K	0.35	0.62	0.57	0.52	1.40	0.64	0.32	0.24

PLAGIOCLASE

	7732104G	7732105G	7734103G	7734104G	46A7608G	46A7609G	7723910G	7703811G
WT.%								
SIO2	52.36	52.39	47.55	48.55	48.88	55.23	51.23	52.55
AL203	27.07	26.88	32.43	29.92	32.74	27.33	28.38	28.74
FEO	1.87	2.24	1.36	1.61	0.76	0.92	1.39	1.29
MGO	1.07	0.92	1.05	0.94	0.18	0.49	0.86	0.94
CAO	11.62	12.53	15.25	15.39	14.65	10.59	14.13	13.93
NA20	4.67	5.49	3.43	2.79	3.17	4.75	3.59	3.23
K20	0.19	0.17	0.13	0.10	0.09	0.21	0.14	0.09
TOTAL	98.85	100.72	98.84	98.98	98.47	99.63	99.72	98.73
ATOMIC PROPORTIONS BASED ON 32 OXYGENS								
SI	9.693	9.636	8.898	9.050	9.102	10.015	9.432	9.381
AL	5.906	5.828	6.704	6.558	6.745	5.840	6.158	6.285
FE2	0.290	0.343	0.213	0.251	0.118	0.136	0.214	0.200
MG	0.295	0.251	0.293	0.261	0.050	0.132	0.236	0.249
CA	2.305	2.481	3.060	3.014	2.923	2.077	2.788	2.764
NA	1.676	1.952	1.121	1.008	1.145	1.670	1.282	1.162
K	0.045	0.040	0.031	0.024	0.021	0.049	0.033	0.021
ATOMIC PROPORTIONS								
CA	57.25	55.47	72.64	74.49	71.49	54.72	67.96	73.02
NA	41.64	43.64	26.62	24.92	27.99	44.00	31.24	29.44
K	1.11	0.89	0.74	0.59	0.52	1.28	0.80	0.54

PLAGIOCLASE

	7721204G	7721205G	7721206G	7708408P	7721405P	7721406G	7724107P	7721408P
WT.%								
SIO2	53.29	49.69	49.49	50.66	49.36	55.41	52.25	45.72
AL2O3	28.32	31.18	32.54	29.45	31.36	26.63	26.02	33.21
FEO	1.37	1.35	1.37	1.37	0.54	0.63	0.91	0.46
MGO	0.41	0.50	0.41	0.44	NA	NA	NA	NA
CAO	12.78	16.25	15.30	15.33	14.88	9.69	11.10	17.33
NA2O	4.53	2.85	2.65	3.12	3.92	6.96	6.47	2.31
K2O	0.49	0.24	0.01	0.39	0.09	0.14	0.49	0.38
TOTAL	100.79	102.58	99.17	100.18	100.15	99.46	97.74	99.81

ATOMIC PROPORTIONS BASED ON 32 OXYGENS

	7721204G	7721205G	7721206G	7708408P	7721405P	7721406G	7724107P	7721408P
SI	9.658	9.094	9.147	9.291	9.055	10.094	9.772	8.636
AL	6.049	6.549	6.652	6.365	6.780	5.717	5.933	7.234
FE2	0.208	0.207	0.165	0.167	0.083	0.096	0.142	0.071
MG	0.111	0.136	0.113	0.120	0.000	0.000	0.000	0.000
CA	2.482	3.189	2.971	3.013	2.925	1.891	2.225	3.432
NA	1.592	1.015	0.950	1.110	1.394	2.458	2.346	0.720
K	0.021	0.009	0.002	0.021	0.021	0.033	0.021	0.019

ATOMIC PROPORTIONS

	7721204G	7721205G	7721206G	7708408P	7721405P	7721406G	7724107P	7721408P
CA	60.61	75.69	75.73	72.71	67.39	43.16	48.44	82.28
NA	38.88	24.09	24.21	26.78	32.13	56.10	51.09	17.27
K	0.51	0.22	0.06	0.51	0.49	0.74	0.47	0.45

PLAGIOCLASE

	7721439P	7708205G	7708206G	7708206G	7708239G	7708212P	7725105G	7725106G
WT.%								
SIO2	52.24	49.34	53.67	49.52	54.31	46.51	49.05	52.43
AL2O3	29.14	30.93	28.33	30.49	28.21	32.79	30.82	31.36
FEO	0.65	0.67	1.05	0.63	0.60	0.50	0.64	0.62
MGO	NA	NA	NA	NA	NA	NA	NA	NA
CAO	12.93	14.48	11.11	14.07	10.82	16.65	14.44	14.44
NA2O	4.67	4.01	5.92	4.42	7.30	1.86	4.15	3.92
K2O	0.13	0.06	0.19	0.08	0.16	0.01	0.03	ND
TOTAL	97.96	99.49	100.27	99.31	101.40	98.54	99.13	100.47

ATOMIC PROPORTIONS BASED ON 32 OXYGENS

SI	9.391	9.105	9.753	9.173	9.775	8.733	9.001	9.101
AL	6.419	6.727	6.067	6.642	5.984	7.199	6.732	6.671
FE2	0.133	0.103	0.160	0.097	0.090	0.078	0.099	0.095
MG	0.000	0.000	0.000	0.000	0.000	0.000	0.000	0.000
CA	2.690	2.864	2.163	2.787	2.087	3.330	2.868	2.820
NA	1.693	1.435	2.086	1.584	2.548	0.673	1.491	1.385
K	0.031	0.014	0.044	0.019	0.037	0.002	0.007	0.000

ATOMIC PROPORTIONS

CA	63.04	66.40	50.39	63.48	44.67	83.14	65.68	67.06
NA	39.24	33.27	48.59	36.09	54.54	16.80	34.16	32.94
K	0.72	0.33	1.03	0.43	0.79	0.06	0.16	0.00

PLAGIOCLASE

	95A7605G	95A7606G	12A7604P	12A7605P	12A7606G	12A7607G	7734782P	7725801P
WT.%								
SIO2	57.22	58.52	46.85	46.95	59.01	59.12	45.52	47.32
AL2O3	25.81	24.63	32.48	32.38	25.04	24.99	33.98	32.01
FEO	0.72	1.21	0.55	0.30	1.41	1.38	0.58	0.54
MGO	0.12	0.79	0.25	ND	0.44	0.44	0.05	0.19
CAO	8.79	8.05	17.47	16.99	7.86	7.85	17.32	17.38
NA2O	6.42	5.52	1.33	1.79	5.94	6.72	1.56	1.31
K2O	0.19	0.17	ND	0.02	0.11	0.13	0.03	0.01
TOTAL	99.27	99.88	98.98	98.43	99.81	100.59	99.04	99.56
ATOMIC PROPORTIONS BASED ON 32 OXYGENS								
SI	10.356	10.532	8.715	8.767	10.585	10.557	7.865	8.729
AL	5.510	5.223	7.122	7.125	5.293	5.259	6.919	7.154
FE2	0.109	0.182	0.086	0.047	0.212	0.206	0.084	0.083
MG	0.032	0.212	0.069	0.000	0.118	0.126	2.331	0.052
CA	1.706	1.554	3.482	3.399	1.511	1.502	3.207	3.435
NA	2.255	2.268	0.498	0.648	2.066	2.327	0.523	0.469
K	0.044	0.039	0.000	0.005	0.025	0.030	0.007	0.002
ATOMIC PROPORTIONS								
CA	42.60	42.25	87.49	83.89	41.94	38.93	85.83	87.94
NA	56.30	58.74	12.51	15.99	57.36	60.30	13.99	12.20
K	1.10	1.01	0.00	0.12	0.70	0.77	0.18	0.06

PLAGIOCLASE

	7725802P	7725803P	7725804P	7709205G	7709206G	7710502P	7710503P	7710504P
WT.%								
SIO2	46.81	48.20	47.97	52.80	52.02	46.78	49.78	48.84
AL2O3	32.54	32.93	32.84	29.20	29.50	31.92	32.46	31.22
FEO	0.70	0.53	0.57	1.18	0.91	0.55	0.63	0.53
MGO	0.28	0.19	0.22	0.33	0.30	NA	NA	NA
CAO	16.69	16.70	16.75	13.17	13.34	19.03	15.18	15.05
NA2O	1.61	1.56	1.71	3.34	3.67	2.55	2.72	2.42
K2O	0.02	0.01	ND	0.17	0.18	0.08	0.12	0.20
TOTAL	98.65	100.12	100.06	100.19	99.92	100.91	98.89	99.15
ATOMIC PROPORTIONS BASED ON 32 OXYGENS								
SI	8.728	8.825	8.800	9.590	9.491	8.634	9.211	9.037
AL	7.150	7.105	7.100	6.250	6.343	6.943	6.642	6.828
FE2	0.109	0.081	0.087	0.179	0.139	0.085	0.097	0.082
MG	0.078	0.052	0.060	0.089	0.082	0.000	0.000	0.000
CA	3.334	3.276	3.293	2.553	2.608	3.763	3.010	3.182
NA	0.582	0.554	0.608	1.176	1.298	0.913	0.976	0.858
K	0.005	0.002	0.000	0.039	0.042	0.019	0.028	0.021
ATOMIC PROPORTIONS								
CA	85.03	85.49	84.41	67.83	66.05	80.16	74.98	78.15
NA	14.84	14.45	15.59	31.13	32.88	19.44	24.31	21.32
K	0.12	0.06	0.00	1.04	1.06	0.40	0.71	0.52

PLAGIOCLASE

	7717505P	7715504G	7715505G	7715506G	7715507G	7720604P	7720605P	55A7604P
WT.%								
SIO2	49.74	56.55	59.20	56.80	61.46	51.22	54.23	54.12
AL2O3	32.92	25.94	23.56	25.39	23.12	29.45	27.67	27.57
FEO	0.76	0.59	0.78	0.58	0.51	0.64	0.56	0.57
MGO	NA	NA	NA	NA	NA	NA	NA	NA
CAO	16.07	8.88	6.37	8.02	5.62	12.57	10.46	11.21
NA2O	2.72	6.52	7.90	6.59	8.05	5.38	7.24	5.11
K2O	0.09	0.44	0.73	0.47	0.81	0.37	0.14	0.22
TOTAL	100.30	98.92	98.54	98.25	99.57	99.63	100.60	98.60
ATOMIC PROPORTIONS BASED ON 32 OXYGENS								
SI	9.110	10.336	10.784	10.437	11.013	9.421	9.836	9.928
AL	6.674	5.571	5.058	5.482	4.882	6.383	5.914	5.955
FE2	0.116	0.090	0.119	0.089	0.076	0.098	0.130	0.087
MG	0.000	0.000	0.000	0.000	0.000	0.000	0.000	0.000
CA	3.154	1.734	1.243	1.574	1.079	2.477	2.033	2.202
NA	0.966	2.304	2.790	2.483	2.797	1.919	2.546	1.816
K	0.021	0.102	0.170	0.110	0.185	0.087	0.032	0.051
ATOMIC PROPORTIONS								
CA	76.16	41.88	29.58	37.78	26.57	55.26	44.08	54.11
NA	23.33	55.65	66.38	59.58	68.87	42.80	55.21	44.63
K	0.51	2.47	4.04	2.64	4.56	1.94	0.70	1.26

PLAGIOCLASE

	55A7605P	55A7606G	55A7607G	7709003P	7709004P	32A7601G	32A7602G	7702303G
WT.%								
SIO2	55.45	57.69	54.56	50.07	50.86	68.06	67.18	50.84
AL203	25.82	25.96	26.95	29.90	29.07	17.13	16.46	21.25
FEO	0.83	0.75	0.72	0.45	0.65	0.50	0.11	0.59
MGO	NA	NA	NA	0.13	0.28	NA	NA	NA
CAO	10.12	9.47	10.15	12.64	11.47	1.08	0.03	5.77
NA20	6.64	5.79	0.86	2.90	3.52	7.57	0.12	7.20
K20	0.26	0.30	0.20	0.20	0.22	0.44	15.18	0.36
TOTAL	99.12	99.97	93.44	96.29	96.07	94.78	99.08	96.01

ATOMIC PROPORTIONS BASED ON 32 OXYGENS

SI	10.157	10.378	10.317	9.421	9.577	12.402	12.398	11.119
AL	5.573	5.504	6.006	6.630	6.451	3.679	3.580	4.653
FE2	0.127	0.114	0.114	0.071	0.102	0.076	0.017	0.092
MG	0.000	0.000	0.000	0.036	0.079	0.000	0.000	0.000
CA	1.986	1.825	2.057	2.548	2.314	0.211	0.006	1.348
NA	2.358	2.020	0.315	1.058	1.285	2.675	0.043	2.594
K	0.061	0.059	0.048	0.048	0.053	0.102	3.574	0.085

ATOMIC PROPORTIONS

CA	45.09	45.64	84.98	69.73	63.36	7.06	0.16	33.47
NA	53.53	51.60	13.03	28.95	35.19	89.52	1.19	64.41
K	1.38	1.76	1.99	1.31	1.45	3.42	98.65	2.12

PLAGIOCLASE

	7702304G	7727906G	7713201G	7713202G	7713203G
WT.%					
SIO2	65.72	63.34	67.58	67.77	64.95
AL2O3	15.92	22.13	18.93	18.45	18.44
FEO	0.26	0.14	0.73	0.70	1.10
MGO	NA	NA	NA	NA	0.04
CAO	0.01	2.17	0.32	0.19	0.33
NA2O	0.14	6.92	6.01	5.58	5.67
K2O	15.04	0.11	6.81	8.02	6.86
TOTAL	97.29	94.81	100.38	100.71	98.39

ATOMIC PROPORTIONS BASED ON 32 OXYGENS

	7702304G	7727906G	7713201G	7713202G	7713203G
SI	12.403	11.579	12.030	12.082	11.898
AL	3.541	4.768	3.971	3.876	3.981
FE2	0.041	0.021	0.109	0.104	0.169
MG	0.000	0.000	0.000	0.000	0.011
CA	0.002	0.425	0.061	0.036	0.065
NA	0.051	2.453	2.074	1.929	2.369
K	3.621	0.025	1.547	1.624	1.603

ATOMIC PROPORTIONS

	7702304G	7727906G	7713201G	7713202G	7713203G
CA	0.06	14.64	1.66	0.96	1.60
NA	1.39	84.48	56.34	55.90	58.68
K	98.55	0.88	42.00	48.14	39.71

OPAQUE OXIDES: CHROME SPINELS

	52A7585P	52A7606P	52A7607P	52A7608P	69A7601P	7732137P	7709386P	7709387P
WT.%								
SI02	0.13	0.34	0.07	0.25	0.11	0.23	0.02	0.32
TI02	0.95	1.07	0.91	1.03	0.05	1.05	0.56	0.54
AL203	24.47	25.41	24.29	27.08	26.73	28.75	31.58	34.47
CR203	38.15	34.62	37.62	33.51	33.22	32.31	30.51	32.34
FE0	19.71	23.08	18.82	20.39	21.85	18.13	20.49	17.17
MNO	0.57	0.49	0.61	0.60	0.57	0.55	0.58	0.48
MGO	15.89	15.59	15.83	15.68	15.62	16.71	15.37	17.41
CAO	0.03	0.02	0.03	0.01	0.02	0.08	0.06	0.02
TOTAL	99.90	97.28	97.38	98.05	98.17	97.81	99.17	98.45
ATOMIC PROPORTIONS BASED ON 32 OXYGENS								
SI	0.033	0.088	0.024	0.017	0.037	0.075	0.006	0.087
AL	7.367	8.422	7.360	7.401	8.020	8.435	9.213	8.227
CR	6.347	6.731	6.450	7.076	7.047	7.436	8.077	7.353
FE2	13.467	9.701	13.568	9.263	9.264	8.839	8.254	8.016
MN	5.477	5.699	5.127	5.624	6.171	5.024	5.615	4.741
MG	7.293	0.245	7.345	0.296	0.283	0.258	0.282	0.233
CA	5.586	5.597	5.697	5.553	5.581	5.857	5.328	6.081
	7.591	8.403	8.585	0.199	0.401	1.573	1.166	7.392
MOLECULAR PROPORTIONS								
R02	0.13	0.08	0.09	0.07	0.15	0.31	0.03	0.03
R203	13.32	14.41	13.55	15.27	14.21	16.35	17.54	15.86
RO	86.55	85.59	86.35	84.67	85.65	83.34	82.43	83.12
MG-NUMBER								
M/M+F	2.73	2.46	2.81	3.09	2.97	2.94	3.28	2.58

OPAQUE OXIDES: CHROME SPINELS

	7709504P	7709505P	7709506P	7709507P	7709508P	7709509P	7709510P	85A7604P
WT.%								
SIO2	0.01	0.31	0.22	0.37	0.47	0.25	0.47	0.26
TIO2	0.68	1.06	0.81	0.56	0.65	0.61	0.63	7.68
AL203	32.82	29.11	29.72	33.93	32.14	29.09	33.57	24.47
CR203	29.19	29.47	31.96	28.33	32.07	31.82	27.07	37.04
FEO	18.54	22.07	19.35	18.93	17.49	19.10	18.68	19.49
MNO	0.72	0.37	0.41	0.49	0.53	0.57	0.64	0.33
MGO	15.66	15.42	16.30	16.34	17.13	15.84	16.63	15.27
CAO	0.02	0.03	0.04	0.17	0.26	0.11	0.14	0.47
TOTAL	98.62	97.52	98.31	99.22	98.74	98.28	98.73	98.38
ATOMIC PROPORTIONS BASED ON 32 OXYGENS								
SI	0.003	0.083	0.037	0.118	0.150	0.082	0.150	0.087
AL	0.258	0.412	0.312	0.247	0.244	0.234	0.237	0.268
CR	8.367	7.598	7.692	8.523	8.128	7.746	8.461	5.371
FE2	7.872	8.137	8.750	7.525	8.224	8.678	7.457	10.623
MN	5.054	6.172	5.366	5.093	4.727	5.344	5.244	5.527
MG	0.336	0.182	0.200	0.232	0.252	0.277	0.344	0.150
CA	5.756	5.448	5.612	5.561	5.856	5.535	5.680	5.478
	0.388	0.595	0.787	3.244	4.985	2.155	2.682	1.448
MOLECULAR PROPORTIONS								
RO2	0.01	0.31	0.03	0.51	0.65	0.34	0.65	0.35
R203	18.47	16.73	16.72	19.13	18.01	16.65	18.92	13.18
RO	81.51	83.26	83.25	80.35	81.34	83.01	80.43	85.47
MG-NUMBER								
M/M+F	4.10	2.19	2.24	2.99	3.05	3.39	3.92	1.39

OPAQUE OXIDES: CHROME SPINELS

	85A7605P	7703912P	7703913P	7718401P	7718402P	32A7505G	32A7607G	7702413P
WT.%								
SIO2	0.64	0.39	0.34	0.03	0.01	0.20	1.11	0.89
TIO2	0.54	0.71	18.37	1.69	0.38	1.91	13.05	1.12
AL203	29.95	25.65	1.37	19.61	27.30	1.50	0.64	15.45
CR203	29.69	34.24	0.54	22.53	20.40	7.15	0.01	24.62
FEO	21.49	17.86	67.12	44.61	39.02	76.12	74.14	47.05
MNO	0.24	0.65	2.06	1.19	0.68	0.99	0.07	0.84
MGO	14.57	15.62	0.35	4.60	7.48	0.26	0.45	5.52
CAO	0.18	NA	NA	0.05	0.04	0.09	0.22	NA
TOTAL	97.41	95.83	90.15	94.43	95.81	88.02	91.49	97.20
ATOMIC PROPORTIONS BASED ON 32 OXYGENS								
SI	0.212	0.038	0.114	0.011	0.003	0.082	0.385	0.312
AL	0.248	0.283	7.250	0.739	0.356	0.925	5.327	0.463
CR	7.786	7.135	0.363	5.517	7.427	0.487	0.175	4.453
FE2	8.161	9.697	0.151	6.705	5.855	2.456	0.204	7.226
MN	5.983	5.123	19.042	13.446	11.342	26.488	21.755	14.257
MG	0.118	0.328	1.028	0.631	0.348	0.646	0.501	0.430
CA	5.167	5.661	0.126	1.788	2.750	0.026	0.167	2.076
	1.582	0.030	0.020	1.059	0.825	2.222	4.580	0.030
MOLECULAR PROPORTIONS								
RO2	0.89	0.12	0.47	0.04	0.01	0.27	1.49	1.17
R203	16.98	15.11	15.69	12.12	16.05	2.32	12.66	9.18
RO	82.13	84.77	83.84	87.84	83.93	97.40	87.86	89.65
MG-NUMBER								
M/M+F	1.42	3.27	87.18	8.60	5.61	19.79	65.52	5.73

OPAQUE OXIDES: CHROME SPINELS

	7702414P	7726837P	7726838P	7726809P
WT.%				
SIO2	0.99	0.45	0.44	0.51
TIO2	1.49	1.25	1.48	1.54
AL2O3	12.68	19.62	18.63	18.68
CR2O3	21.67	35.93	36.86	36.35
FEO	54.28	27.28	28.40	28.63
MNO	0.76	0.72	0.90	0.78
MGO	3.50	12.02	12.12	12.13
CAO	NA	NA	NA	NA
TOTAL	95.37	97.27	99.03	98.62

ATOMIC PROPORTIONS BASED ON 32 OXYGENS

	7702414P	7726837P	7726838P	7726809P
SI	0.357	0.157	0.148	0.172
AL	0.634	0.528	0.587	0.613
CR	3.619	5.308	5.212	4.990
FE2	6.542	10.283	10.379	10.271
MN	15.598	7.928	8.099	8.193
MG	0.449	0.357	0.452	0.393
CA	1.354	4.403	4.372	4.391
	0.000	0.000	0.000	0.000

MOLECULAR PROPORTIONS

	7702414P	7726837P	7726838P	7726809P
RO2	1.32	0.52	0.56	0.56
R2O3	7.76	11.18	10.67	10.68
RO	90.93	88.22	88.77	88.66

MG-NUMBER

	7702414P	7726837P	7726838P	7726809P
M/M+F	5.88	3.45	4.17	3.68

OPAQUE OXIDES   "ILMENITES"

	46A7605G	46A7636G	7703908P	7703809P	7708406G	7725107G	95A7608G	95A7609G
WT.%								
SIO2	0.04	0.37	2.68	2.77	3.08	0.31	0.02	0.01
TIO2	4.17	8.64	18.74	15.87	15.76	42.31	18.97	17.95
AL2O3	0.28	0.90	2.28	2.33	3.81	0.00	1.23	0.11
CR2O3	0.09	0.05	0.08	0.03	0.07	0.00	0.09	0.04
FEO	84.01	77.64	67.34	65.79	67.37	54.40	71.64	73.22
MNO	0.45	0.75	1.47	1.11	1.95	2.68	1.64	1.60
MGO	0.02	0.38	1.26	2.47	3.54	0.00	0.07	0.00
CAO	0.05	0.00	0.00	0.00	0.00	0.00	0.12	0.00
NIO	0.00	0.41	0.13	0.13	0.13	0.00	0.00	0.00
TOTAL	89.11	89.14	93.98	90.50	92.71	99.40	93.78	92.93
ATOMIC PROPORTIONS BASED ON 6 OXYGENS								
SI	0.003	0.027	0.165	0.177	0.193	0.017	0.001	0.001
TI	0.242	0.469	0.866	0.754	0.741	1.699	0.926	0.921
AL	0.025	0.077	0.165	0.176	0.201	0.000	0.094	0.009
CR	0.005	0.003	0.004	0.002	0.003	0.000	0.005	0.002
FE2	5.427	4.690	3.462	3.523	3.522	2.446	3.891	4.089
MN	0.029	0.046	0.077	0.060	0.103	0.122	0.090	0.000
MG	0.002	0.041	0.115	0.236	0.050	0.000	0.007	0.000
CA	0.004	0.000	0.000	0.000	0.000	0.000	0.008	0.000
	0.000	1.780	0.480	0.500	0.488	0.000	0.000	0.000
MOLECULAR PROPORTIONS								
RO2	4.29	9.34	21.62	19.42	19.65	40.05	18.66	17.73
R2O3	0.27	0.75	1.77	1.83	2.99	0.00	0.99	0.11
RO	95.44	89.91	76.61	78.75	77.36	59.95	80.35	82.16
MG-NUMBER								
M/M+F	0.04	0.86	3.23	6.27	1.41	0.00	0.17	0.00

OPAQUE OXIDES   "ILMENITES"

	7706803G	7727907P	7727908P
WT.%			
SIO2	4.54	0.12	0.11
TIO2	16.30	45.25	47.53
AL2O3	4.13	0.35	0.32
CR2O3	0.16	0.13	0.13
FEO	68.06	46.82	45.32
MNO	0.06	4.13	4.00
MGO	0.83	1.17	1.63
CAO	0.00	0.13	0.10
NIO	0.20	0.00	0.00
TOTAL	94.28	98.04	99.14

ATOMIC PROPORTIONS BASED ON   6 OXYGENS

SI	0.272	0.006	0.006
TI	0.735	1.798	1.845
AL	0.292	0.022	0.019
CR	0.008	0.004	0.005
FE2	3.413	2.069	1.956
MN	0.003	0.185	0.175
MG	0.074	0.092	0.125
CA	0.000	0.006	0.006
	0.721	0.000	0.000

MOLECULAR PROPORTIONS

RO2	21.67	43.28	44.86
R2O3	3.22	0.31	0.30
RO	75.10	55.41	54.84

MG-NUMBER

M/M+F	2.13	4.25	5.02

OPAQUE OXIDES   "MAGNETITES"

	7721440G	7721440G	7708213G	7708214G	7725108G	7715508G	7715509G
WT.%							
SIO2	0.33	0.27	0.00	0.26	0.35	0.28	0.59
TIO2	19.36	22.19	33.08	6.28	1.60	23.05	19.99
AL2O3	0.37	1.27	0.00	0.00	0.00	1.02	1.53
CR2O3	0.12	ND	0.00	0.00	0.10	0.15	0.16
FEO	76.56	72.48	64.24	89.42	91.53	70.73	72.70
MNO	1.55	1.64	2.19	0.21	0.00	0.90	0.93
MGO	0.43	0.00	0.00	0.00	0.00	0.60	0.57
CAO	0.11	0.26	0.00	0.24	0.13	0.14	0.14
TOTAL	98.83	98.04	99.51	96.37	93.71	96.87	96.61
ATOMIC PROPORTIONS BASED ON 32 OXYGENS							
SI	0.109	0.088	0.000	0.098	0.140	0.091	0.195
TI	4.819	5.431	7.557	1.775	0.482	5.650	4.973
AL	0.144	0.462	0.000	0.000	0.000	0.392	0.596
CR	0.031	0.000	0.000	0.000	0.032	0.039	0.042
FE2	21.192	19.727	16.324	28.105	30.650	19.280	20.113
MN	0.435	0.452	0.564	0.067	0.000	0.248	0.261
MG	0.212	0.000	0.000	0.000	0.000	0.292	0.281
CA	0.039	0.091	0.000	0.081	0.056	0.049	0.050
MOLECULAR PROPORTIONS							
RO2	18.32	21.21	33.92	6.22	1.98	22.23	19.73
R2O3	0.33	0.88	0.00	0.00	0.05	0.83	1.22
RO	81.35	77.90	69.08	93.78	97.97	76.94	79.05
MG-NUMBER							
M/M+F	0.99	0.00	0.00	0.00	0.00	1.49	1.38

APPENDIX 7.1

X-ray Fluorescence Analysis

Samples were fragmented and stripped of weathering using a Cutrock Engineering hydraulic splitter. Further fragmentation to an aggregate of < 1cm chips was achieved with a Sturtevant 2"x 6" Roll Jaw Crusher. Grinding of this aggregate to a fine powder was accomplished in a Tema Laboratory Disc Mill with a tungsten-carbide grinding barrel. Grinding took 1-4 minutes.

Several grams of powder were then compressed into briquettes using a hydraulic press, operated at 800-900 kg/cm^2 (5-6 tons/$inch^2$). A few drops of an inert organic binding material (Mowiol) was added to the powder, prior to compression to aid cohesion.

Major and trace elements (excluding some Nb and Rb) were analysed on a Philips PW1212 automatic spectrometer into which the bricquettes were loaded by a Torrens Industries TE108 Automatic Sample Loader. Routine operating conditions for this machine are given by Reeves (1971).

The major and minor elements Si, Al, Fe, Mg, Na, K, Ti and P were determined in a single analytical session using a Cr target and an evacuated tube. Mn was determined separately using W radiation. The accumulation of counts for the unknowns was based on a 'fixed count' time for a

monitor. This minimises machine drift or instability.

Data handling was performed using an iterative procedure described by Holland and Brindle (1966) and Reeves (1971). Standards used in this calibration were the international standards, AGV1, BCR1, BR, DTS1, G1, GH, GR, PCC1, SY-1 and W-1 (for compositions see Flanagan, 1973). The departmental secondary standard Na-1 with 20-50 wt% Al_2O_3 was used to control Al_2O_3 calibration beyond the range of the international standards (17.25 wt%). K_2O in specimens with < 0.07 wt% K_2O was redetermined with longer (100 seconds) counting times to increase the precision of the K_2O determination at low concentrations.

Three checks were made to elucidate the scope of variation possible for each quoted major oxide determination thus giving an estimate of the precision of the procedures outlined above, these are as follows:

(1) Two separate briquettes were made from the same powdered sample (77192, an olivine phyric dolerite). The replicate analyses are presented in Table A7.1. Only small differences occur in the values quoted for the replicate determination excluding perhaps Na_2O which varies from 2.31-2.52 wt%.

(2) Two samples (52A76, 77047) which were analysed on the first day were re-analysed at the end of the last

day to estimate any variability within the run
due to machine instability. The replicate analyses
on these two specimens are also presented in Table
A7.1 where slight variations can be seen in the
values quoted for each element.

(3)   The percentage error due to the variation in the
counts of standards (each of which was analysed
four times during the run) were assessed for 6
representative standard compositions. The
compositions of these standards and the error for
each major oxide determination are presented on
Table A7.2. It is clear that although precision
declines with decreasing concentration the errors
on the standards in Table A7.2 are generally small.
An exception being the composition G1 which exhibits
larger errors.

The checks outlined above suggest that small variations
in run conditions over a period of days do occur but
these do not significantly affect the reliability of the
results. The reasons for the larger errors on G1 are
not clear but inhomogeneity within the briquette is one
possible explanation. It must be stressed that these
results are based on limited data and can only be viewed
as a rough guide to the precision of data produced by
the PW1212. A rigorous check of the precision of

PW1400 prior to its routine use as an operating instrument and the discontinued use of standard G1 is recommended.

The trace elements Ba, Nb, Zr, Y, Sr, Rb, Zn, Ni and Cr were determined using W radiation. Nb and Rb were redetermined on a PW1400 using Rh radiation and longer counting times (100 seconds) in samples with < 6 ppm and 10 ppm respectively. Peaks and backgrounds obtained for standards and unknowns were converted to the function (P/B-1). This function when plotted against standard concentrations produces a straight line from which unknown concentrations can be directly obtained. This calculation was performed using the program TRATIO (written by R.C.O. Gill). Mass absorbtion and matrix effects are compensated for by the (P/B-1) function using scattered background radiation as an internal standard. TRATIO also allows correction for the interferences of Sr Kα on Zr Kα, Rb Kα on Y Kα and Y Kα on Nb Kα using experimentally determined interference factors. The redetermined Nb and Rb values were calculated using the function (P/B-1), direct and were in tolerable agreement with the earlier determinations. The longer counting times over one peak and two background positions lowered the detection limit of these elements to 1 ppm with an estimated error of $\pm$0.5 ppm at this concentration.

The standards used were synthetic, spiked glasses produced by the Pilkington Research Laboratory for use in lunar investigations (Brown et al., 1970).

TABLE A3.1

REPLICATE DETERMINATIONS OF MAJOR OXIDE ANALYSES

Analyses 1 and 2: Analyses of two different bricquettes made from the same finely crushed sample
Analyses 3 and 4: Analyses of the same bricquette at the beginning and end of the same run
Analyses 5 and 6:   "   "   "   "   "   "   "   "   "   "   "   "   "   "

Spec.	1 77192(a)	2 77192(b)	Deviation from mean	3 77047	4 77047	Deviation from mean	5 52A76	6 52A76	Deviation from mean
SiO_2	46.54	46.61	$\pm$ 0.04	49.99	49.70	$\pm$ 0.15	41.18	41.21	$\pm$ 0.02
Al_2O_3	15.04	15.08	$\pm$ 0.02	18.94	18.95	$\pm$ 0.01	8.77	8.74	$\pm$ 0.02
Fe_2O_3*	11.20	11.02	$\pm$ 0.09	7.18	7.24	$\pm$ 0.03	12.16	12.15	$\pm$ 0.01
MgO	12.99	12.78	$\pm$ 0.11	5.62	5.66	$\pm$ 0.02	30.52	30.44	$\pm$ 0.04
CaO	10.05	10.02	$\pm$ 0.02	15.10	15.28	$\pm$ 0.09	5.58	5.64	$\pm$ 0.03
Na_2O	2.31	2.52	$\pm$ 0.11	1.98	1.98		0.62	0.67	$\pm$ 0.03
K_2O	0.46	0.46		0.08	0.08		0.14	0.14	
TiO_2	1.20	1.20		0.91	0.91		0.82	0.82	$\pm$ 0.01
MnO	0.16	0.17	$\pm$ 0.01	0.10	0.10		0.17	0.17	
P_2O_5	0.12	0.14	$\pm$ 0.01	0.08	0.09	$\pm$ 0.01	0.08	0.08	

BR Wt%	Comp	Mean Counts	Range of %ge error ($\pm$)	BCR1 Comp	Mean Counts	Range of %ge error($\pm$)
SiO2	38.20	67923	0.14-0.38	54.50	103424	0.22-0.29
Al3O3	10.20	86680	0.21-0.39	13.61	122427	0.21-0.48
Fe2O3	12.88	100780	0.35-0.53	13.40	114147	0.38-0.47
MgO	13.28	96292	0.93-1.29	3.46	19039	1.22-1.62
CaO	13.80	179566	0.51-0.55	6.92	86876	0.04-0.23
Na2O	3.05	28343	1.16-3.23	3.27	28572	0.44-0.96
K2O	1.40	56617	0.40-0.84	1.70	64615	0.67-0.86
TiO2	2.60	127306	0.25-0.46	2.20	116977	0.73-0.89
P2O5	1.04	13878	2.02-2.16	0.36	3804	2.70-3.19

W1 Wt%	Comp	Mean Counts	Range of %ge error($\pm$)	GR Comp	Mean Counts	Range of %ge error ($\pm$)
SiO2	52.64	94908	0.44-0.67	65.90	134043	0.94-1.12
Al2O3	15.00	141896	0.72-1.34	14.75	133556	0.37-0.44
Fe2O3	11.09	95819	0.21-0.33	4.05	39061	0.64-0.67
MgO	6.62	41064	1.08-1.61	2.40	22130	1.28-2.00
CaO	10.96	139079	0.35-0.53	2.50	30477	0.27-0.48
Na2O	2.15	20248	0.64-0.79	3.80	31562	1.04-1.69
K2O	0.64	26252	0.77-0.89	4.50	156947	0.41-0.43
TiO2	1.07	52847	0.46-0.72	0.65	37429	0.55-1.20
P2O5	0.14	1751	0.40-0.40	0.28	2794	9.24-13.28

DTS1 Wt%	Comp	Mean Counts	Range of %ge error ($\pm$)	G1 Comp	Mean Counts	Range of %ge error ($\pm$)
SiO2	40.50	57770	0.21-0.22	72.64	150040	2.65-3.63
Al2O3	0.24	2016	3.05-3.94	14.04	129702	6.06-6.39
Fe2O3	8.64	107481	0.68-0.40	1.94	17638	0.46-0.61
MgO	49.80	418756	0.94-1.24	0.38	4226	9.80-11.17
CaO	0.15	2456	1.75-2.61	1.39	16086	3.31-8.16
Na2O	0.01	788	11.37-16.19	3.32	28544	4.66-5.05
K2O	0.00	715	2.94-2.73	5.48	176739	5.58-6.01
TiO2	0.01	837	0.42-1.19	0.26	14419	1.47-3.19
P2O5	00.00	32	68.25-157.1	0.09	732	24.34-17.04

Table A3.2 Estimated precision of the major oxide determinations based on the range of error around the mean counts value

Appendix 7.2

Table of major oxide and trace element analyses.

These are arranged in ascending order of the dolerite groups with D.I.

followed by the high MgO gabbros, the low MgO gabbros and the

peridotite plug analyses. The CIPW norms are presented on p458

* indicates an analysis plotted in Chapter 7.

The following average analyses were also plotted in Chapter 7

Group 3

The average of 4 similar parallel inclined sheets,(72A76,73A76,

77318,77356).

Group 8

Average of 5 Kilmory thick conformable sheets,(77092.77105,77108,

77271,77272).

Average of 3 Papadil thick conformable sheets,(77174,77243,77244).

Average of 4 dykes with liquid-liquid contacts with felsite in

Stony Corrie, Dibidil,(77061,77127,77145,77306).

RHUM DOLERITE GROUPS 1-12

	52A76☆	53A76☆	54A76*	55A76	69A76*	71A76	77A76*	77077*	77179*	77321*
WT%										
SIO2	41.20	43.55	45.09	43.75	43.29	44.45	43.53	44.77	41.70	42.66
AL2O3	8.76	11.98	13.30	11.87	12.55	12.77	12.56	13.44	8.60	12.46
FE2O3	12.16	11.71	12.18	11.69	12.49	11.63	12.22	11.69	11.36	11.93
MGO	32.48	20.73	14.84	20.22	18.47	16.50	19.42	15.19	30.92	21.60
CAO	5.51	9.17	11.29	9.67	9.65	8.99	9.40	10.47	5.23	8.41
NA2O	0.65	1.02	1.56	1.01	1.36	1.13	3.96	2.00	0.25	1.15
K2O	0.14	0.31	0.09	0.23	0.12	0.13	0.63	0.29	0.72	0.20
TIO2	0.83	1.23	1.37	1.27	1.68	1.46	1.33	1.78	0.86	1.52
MNO	0.17	0.16	0.17	0.15	0.17	0.15	0.18	0.16	0.16	0.16
P2O5	0.08	0.15	0.15	0.15	0.22	0.10	0.15	0.21	0.11	0.23
PPM										
NI	1846	635	285	554	438	654	635	345	1771	659
CR	2628	1172	687	982	731	1258	1166	555	3083	4
BA	13	4	48	29	70	13	47	48	37	35
NB	4	4	4	5	9	3	4	4	4	5
ZR	51	98	93	90	124	73	120	144	59	153
Y	8	16	20	15	16	14	16	23	10	17
SR	107	200	159	194	298	159	192	269	109	276
RB	2	6	5	3	3	4	12	6	31	1
ZN	71	59	70	55	123	87	95	77	66	79
GROUP	1.1	1.1	1.1	1.1	1.1	1.1	1.1	1.1	1.1	1.1

RHUM DOLERITE GROUPS 1-12

	77341	77052	77093*	77095*	77101*	77107*	77224*	77192	77196	77197*
WT%										
SIO2	44.35	44.03	46.67	46.13	43.15	43.89	44.54	46.58	45.01	41.84
AL2O3	13.01	12.89	13.88	13.44	11.91	11.66	14.19	15.06	14.92	11.57
FE2O3	12.48	12.74	12.51	12.73	12.53	12.73	13.24	11.11	11.95	11.30
MGO	15.74	15.14	11.71	12.74	20.36	18.24	13.46	12.89	14.47	25.82
CAO	10.80	11.43	12.56	11.68	9.30	10.28	13.27	10.04	9.23	7.18
NA2O	1.27	1.20	1.92	1.75	1.04	1.35	2.55	2.42	2.02	1.00
K2O	0.48	0.10	0.06	0.06	0.20	0.12	0.23	0.45	0.55	0.17
TIO2	1.53	1.18	1.40	1.26	1.23	1.44	1.23	1.24	1.47	0.77
MNO	0.19	0.18	0.21	0.17	0.10	0.18	0.18	0.17	0.17	0.17
P2O5	0.15	0.09	0.10	0.09	0.09	0.12	0.11	0.13	0.21	0.08
PPM										
NI	385	600	391	548	928	622	430	367	453	1500
CR	1059	1364	1104	1288	1729	1385	914	868	936	3000
BA	51	77	10	19	30	30	53	302	217	28
NB	4	2	2	2	3	3	4	4	6	2
ZR	106	65	79	64	73	83	69	74	112	52
Y	19	12	24	16	15	16	25	17	19	14
SR	183	168	147	145	129	162	156	407	272	83
RB	25	6	2	2	8	4	2	5	8	3
ZN	153	79	80	78	72	74	98	74	86	74
GROUP	1.1	1.2	1.2	1.2	1.2	1.2	1.2	1.3	1.3	1.3

RHUM DOLERITE GROUPS 1-12

	77221	77225	77235	77236*	77237*	85A76	77017	77024*	77036	43A76
WT%										
SIO_2	42.25	43.98	44.96	41.63	46.09	43.40	43.75	44.41	44.74	46.78
AL_2O_3	13.26	13.07	15.35	12.39	15.19	9.21	13.23	14.96	13.34	14.66
FE_2O_3	12.53	12.24	11.43	12.40	10.66	11.56	13.47	11.72	12.59	10.92
MGO	20.20	15.77	12.43	21.24	12.76	28.44	14.87	15.55	15.28	13.35
CAO	9.25	9.02	11.22	8.88	10.45	5.50	10.54	9.93	10.39	11.35
NA_2O	1.83	2.64	2.56	1.69	2.55	0.82	1.89	2.19	1.58	1.62
K_2O	0.14	0.40	0.19	0.12	0.18	0.13	0.15	0.05	0.19	0.18
TIO_2	1.32	1.66	1.52	1.45	1.87	0.69	1.79	0.88	1.76	1.14
MNO	0.18	0.16	0.18	0.17	0.14	0.16	0.18	0.17	0.18	0.16
P_2O_5	0.15	0.16	0.17	0.25	0.09	0.09	0.16	0.08	0.16	0.13
PPM										
NI	890	513	364	1041	390	1500	413	717	351	243
CR	1263	893	814	1878	788	2559	696	1296	674	854
BA	17	48	34	29	140	27	75	11	46	27
NB	2	5	3	3	2	5	6	3	5	4
ZR	83	107	104	81	73	56	129	53	123	84
Y	17	18	16	33	15	13	17	13	20	18
SR	188	218	243	167	246	104	255	123	230	227
RB	3	17	8	0	3	6	2	1	3	7
ZN	82	45	75	53	64	75	87	77	88	72
GROUP	1.3	1.3	1.3	1.3	1.3	1	1	1	1	2

RHUM DOLERITE GROUPS 1-12

	44A76*	46A76*	65A76*	72A76	93A76	77019*	77039	77042	77084*	77116*
WT%										
SIO2	45.69	45.97	46.91	45.71	45.62	44.32	46.32	44.28	46.74	46.86
AL2O3	14.31	12.98	14.26	13.82	12.94	14.20	13.53	13.48	14.33	13.51
FE2O3	12.86	11.63	11.49	12.04	12.43	12.91	11.19	13.63	11.85	12.12
MGO	15.73	11.41	12.01	11.11	14.89	13.60	15.62	12.59	11.25	11.95
CAO	10.75	13.54	11.42	12.11	9.85	10.45	10.03	11.44	12.01	11.04
NA2O	1.28	2.15	2.16	2.35	1.65	2.17	1.70	2.13	1.86	2.12
K2O	0.35	0.25	0.10	0.19	0.33	0.31	0.33	0.11	0.13	0.36
TIO2	1.20	1.70	1.35	1.63	1.41	1.72	1.18	2.40	1.58	1.59
MNO	0.14	0.19	0.16	0.19	0.18	0.18	0.16	0.18	0.19	0.17
P2O5	0.09	0.18	0.14	0.15	0.13	0.15	0.13	0.16	0.11	0.14
PPM										
NI	368	176	143	148	335	372	425	283	284	214
CR	649	565	368	379	693	697	872	584	639	517
BA	140	46	56	47	82	70	58	92	54	112
NB	4	5	4	5	5	5	4	6	4	5
ZR	66	108	90	114	110	123	79	126	89	127
Y	15	16	14	23	17	17	18	21	17	22
SR	182	269	236	241	175	261	138	312	212	208
RB	10	4	4	8	9	6	5	4	1	12
ZN	52	58	73	102	104	76	76	96	79	101
GROUP	2	2	2	2	2	2	2	2	2	2

RHUM DOLERITE GROUPS 1-12

	77121	77122	77123	77158*	77212*	77214*	77240	77245	77352*	66A76*
WT%										
SIO2	45.53	44.98	45.89	45.54	45.41	47.19	44.95	45.85	45.48	47.18
AL2O3	13.74	12.87	13.76	14.34	14.73	14.56	14.41	15.49	14.15	13.01
FE2O3	12.26	12.73	12.16	12.24	12.75	11.89	12.54	11.52	12.48	12.23
MGO	14.83	14.99	13.58	13.29	11.28	10.26	13.59	11.64	12.84	12.28
CAO	18.45	17.98	11.37	10.89	12.22	12.29	11.78	11.95	11.78	10.52
NA2O	1.69	1.35	1.65	1.82	1.52	2.01	1.18	1.62	1.67	2.14
K2O	0.12	0.36	0.12	0.25	0.44	2.30	0.74	0.51	0.11	0.10
TIO2	1.12	1.45	1.31	1.61	1.76	1.26	1.47	1.17	1.34	1.45
MNO	0.18	0.19	0.17	0.17	0.18	0.17	0.21	0.17	0.17	0.16
P2O5	0.09	0.10	0.10	0.14	0.14	0.12	0.12	0.09	0.14	0.14
PPM										
NI	353	372	275	239	145	164	289	193	229	234
CR	811	895	661	516	374	404	618	373	458	476
BA	41	22	27	52	34	56	45	182	52	83
NB	4	5	3	4	4	4	4	3	4	5
ZR	72	91	82	123	113	77	83	52	85	116
Y	19	18	21	19	23	17	19	15	17	23
SR	138	154	178	230	172	203	179	228	147	194
RB	4	20	4	4	2	17	36	19	8	3
ZN	74	79	71	91	75	70	97	81	129	95
GROUP	2	2	2	2	2	2	2	2	2	3

RHUM DOLERITE GROUPS 1-12

	72A76	73A76	74A76	87A76*	89A76*	92A76	77046*	77048	77080	77082*
WT%										
SIO_2	48.56	48.66	47.24	47.51	48.31	47.13	48.39	47.48	48.63	48.42
AL_2O_3	14.01	13.92	13.77	14.48	14.07	14.18	14.21	13.83	14.33	14.13
FE_2O_3	12.34	11.72	12.21	11.74	11.86	11.82	11.68	11.51	11.46	11.61
MGO	12.67	11.31	12.82	11.31	12.25	11.49	11.17	11.61	10.25	10.73
CAO	12.05	12.38	11.28	12.00	12.16	11.28	10.16	10.95	10.85	10.68
NA_2O	2.28	2.30	2.48	2.33	2.59	2.13	2.23	2.12	2.57	2.18
K_2O	0.26	0.21	0.17	0.78	0.51	0.25	0.53	0.66	0.22	0.28
TIO_2	1.55	1.51	1.70	1.43	1.88	1.44	1.32	1.52	1.41	1.65
MNO	0.17	0.16	0.17	0.17	0.17	0.18	0.17	0.17	0.17	0.17
P_2O_5	0.17	0.13	0.15	0.16	0.21	0.12	0.13	0.15	0.12	0.16
PPM										
NI	152	148	147	192	133	179	186	241	113	153
CR	381	396	367	399	343	422	472	575	361	771
BA	107	126	73	134	156	91	125	139	116	142
NB	5	5	5	6	6	4	3	5	5	5
ZR	133	126	126	124	168	105	106	114	111	129
Y	24	19	22	23	22	19	21	25	22	23
SR	199	274	211	285	235	191	180	208	222	241
RB	8	8	8	67	26	13	15	21	5	7
ZN	99	90	93	91	84	82	101	91	90	99
GROUP	3	3	3	3	3	3	3	3	3	3

RHUM DOLERITE GROUPS 1-12

	77178	77191*	77249	77251	77318	77356	21A76	22A76*	41A76	47A76*
WT%										
SIO_2	45.13	46.24	46.95	46.57	48.12	48.41	48.66	47.55	47.63	48.63
AL_2O_3	14.93	15.29	13.68	14.14	13.93	13.96	13.91	13.59	14.71	13.54
FE_2O_3	12.92	11.47	12.66	11.93	12.53	11.91	12.42	13.44	13.36	11.09
MGO	12.32	11.43	11.33	11.97	13.32	12.86	9.11	8.73	8.36	9.81
CAO	9.55	10.91	10.25	10.63	10.51	10.54	11.52	11.09	11.43	11.51
NA_2O	3.17	2.43	2.47	2.28	2.47	2.34	2.41	2.29	2.40	2.25
K_2O	0.53	0.46	0.48	0.32	0.18	0.17	0.30	0.23	0.10	0.23
TIO_2	1.96	1.51	2.15	1.87	1.63	1.52	1.55	1.01	1.73	1.67
MNO	0.16	0.15	0.17	0.17	0.18	0.18	0.18	0.18	0.20	0.17
P_2O_5	0.28	0.16	0.24	0.20	0.13	0.14	0.14	0.18	0.10	0.17
PPM										
NI	144	175	160	182	146	134	125	93	98	105
CR	381	353	357	339	434	393	380	265	334	354
BA	314	128	137	93	103	115	136	82	46	93
NB	5	5	6	5	4	4	5	4	4	5
ZR	166	98	166	145	131	133	118	126	76	129
Y	26	18	24	22	20	23	22	25	27	22
SR	438	305	329	223	205	205	202	209	204	225
RB	21	5	9	6	6	5	8	3	13	13
ZN	83	76	102	97	113	98	76	72	114	87

| GROUP | 3 | 3 | 3 | 3 | 3 | 3 | 4 | 4 | 4 | 4 |

RHUM DOLERITE GROUPS 1-12

	60A76	61A75	62A76	63A76	77012	77013	77032	77035	77044*	77068*
WT%										
SIO2	45.69	47.04	46.96	46.87	47.01	47.53	48.00	48.87	47.81	46.64
AL2O3	13.90	13.78	14.06	13.83	14.34	15.03	13.64	14.28	14.56	14.31
FE2O3	12.23	13.48	13.15	13.42	12.64	11.87	12.79	11.97	12.39	12.77
MGO	9.46	9.40	9.47	9.58	9.56	9.76	8.80	9.25	8.97	10.05
CAO	11.17	11.78	12.09	11.94	11.95	10.70	11.08	10.64	11.48	10.72
NA2O	2.41	2.18	2.02	2.12	2.43	2.56	2.88	2.75	2.74	2.45
K2O	0.19	0.33	0.38	0.33	0.18	0.63	0.38	0.32	0.34	0.34
TIO2	1.63	1.66	1.56	1.50	1.63	1.59	1.95	1.61	1.68	1.45
MNO	0.18	0.20	0.20	0.19	0.20	0.17	0.18	0.17	0.18	0.19
P2O5	0.15	0.14	0.12	0.13	0.14	0.15	0.20	0.13	0.15	0.16
PPM										
NI	141	84	114	111	151	216	88	160	90	170
CR	382	335	369	350	373	526	284	465	332	314
BA	83	40	36	51	24	128	110	87	115	283
NB	5	4	4	3	4	4	5	5	4	3
ZR	138	67	60	61	101	146	139	129	119	80
Y	29	22	23	20	20	23	25	27	21	18
SR	179	212	211	217	213	218	213	217	225	314
RB	6	11	15	12	6	22	8	7	12	2
ZN	100	95	92	100	263	86	90	94	85	63
GROUP	4	4	4	4	4	4	4	4	4	4

RHUM DOLERITE GROUPS 1-12

	77076	77125	77148*	77175*	77176*	77204	77208	77231	77269	77284
WT%										
SIO2	48.15	47.67	46.83	46.83	46.82	47.21	45.91	47.30	47.66	46.17
AL2O3	13.49	14.04	14.53	14.64	15.21	13.92	15.37	14.82	14.35	15.24
FE2O3	12.59	12.53	12.87	13.88	14.26	13.83	13.20	12.37	13.10	12.41
MGO	8.83	8.95	9.57	9.52	9.39	9.79	9.23	9.55	8.35	9.40
CAO	11.64	12.68	11.95	9.76	9.38	9.97	12.31	11.83	11.87	12.84
NA2O	2.34	1.96	2.27	2.73	2.25	2.55	1.99	2.14	2.32	1.97
K2O	0.68	0.34	0.14	0.54	0.76	0.66	0.30	0.37	0.17	0.22
TIO2	1.89	1.51	1.50	1.67	1.75	1.68	1.65	1.55	1.75	1.78
MNO	0.19	0.20	0.18	0.22	0.17	0.19	0.18	0.17	0.18	0.18
P2O5	0.19	0.12	0.15	0.25	0.26	0.19	0.15	0.19	0.16	0.15
PPM										
NI	90	142	137	111	116	61	117	145	96	107
CR	200	397	383	94	267	61	294	363	331	391
BA	219	50	44	484	414	389	42	57	325	95
NB	4	3	3	5	5	6	4	3	4	4
ZR	127	68	92	145	153	150	106	99	103	111
Y	24	19	21	23	28	24	22	28	21	24
SR	280	195	158	469	445	269	188	267	271	242
RB	19	26	8	12	19	23	13	14	5	4
ZN	100	96	77	60	114	132	68	91	81	85
GROUP	4	4	4	4	4	4	4	4	4	4

RHUM DOLERITE GROUPS 1-12

	77327	77330*	77332	77333	77336	77337	77351	26A76*	82A76	04A76
WT%										
SIO2	47.19	47.74	47.28	48.12	46.21	47.27	47.45	46.58	47.43	47.33
AL2O3	14.21	13.67	14.51	14.15	14.75	14.63	14.41	13.02	13.51	15.81
FE2O3	13.52	12.52	12.45	12.31	12.62	12.54	12.36	13.13	13.54	12.33
MGO	9.58	9.28	9.74	9.78	9.46	9.49	9.33	9.68	8.52	8.23
CAO	9.85	12.48	11.19	11.58	11.47	11.44	11.85	11.85	10.91	11.32
NA2O	2.78	2.18	2.53	2.73	2.80	2.51	2.42	2.63	3.14	2.66
K2O	0.49	0.37	0.31	0.37	0.25	0.60	0.44	0.48	0.25	0.53
TIO2	1.38	1.46	1.63	1.41	2.03	1.61	1.42	1.84	2.13	1.73
MNO	0.19	0.19	0.19	0.20	0.18	0.20	0.19	0.19	0.24	0.16
P2O5	0.22	0.11	0.15	0.12	0.21	0.13	0.12	0.15	0.17	0.15
PPM										
NI	163	113	123	125	120	108	117	123	70	128
CR	335	359	329	377	291	327	386	297	171	317
BA	353	74	110	156	70	154	121	54	96	54
NB	5	4	5	3	6	5	4	4	6	4
ZR	137	88	123	83	149	123	89	95	159	128
Y	24	18	23	20	23	23	17	23	32	20
SR	396	207	213	197	282	245	211	231	218	282
RB	2	14	20	17	17	42	20	2	11	30
ZN	132	86	115	107	100	167	106	68	75	74
GROUP	4	4	4	4	4	4	4	4	4	4

RHUM DOLERITE GROUPS 1-12

	95A76☆	77010	77011	77015	77070	77071	77073	77074	77086	77091☆
WT%										
SIO2	47.73	47.32	46.84	47.47	46.36	46.33	46.88	46.55	46.72	46.57
AL2O3	15.72	13.09	13.86	14.36	13.68	13.47	14.53	14.81	14.93	13.75
FE2O3	12.61	13.32	13.37	13.14	13.09	15.12	12.69	12.84	12.51	12.62
MGO	8.24	8.24	8.81	8.16	7.82	8.33	9.56	9.77	8.92	8.59
CAO	10.57	11.47	11.28	11.21	12.87	11.67	10.53	10.48	11.92	13.78
NA2O	3.25	3.05	3.48	3.22	2.81	3.19	3.02	2.97	2.94	2.22
K2O	0.58	0.34	0.35	0.27	0.13	0.37	0.26	0.26	0.08	0.15
TIO2	1.56	1.91	1.94	1.86	1.96	2.41	1.86	1.86	1.59	1.87
MNO	0.18	0.21	0.20	0.20	0.21	0.22	0.18	0.19	0.22	0.19
P2O5	0.15	0.18	0.19	0.18	0.16	0.20	0.22	0.25	0.13	0.16
PPM										
NI	104	87	86	74	127	76	113	109	125	137
CR	279	279	282	293	362	158	258	365	341	378
BA	56	58	48	43	82	84	238	248	76	89
NB	4	5	5	5	4	5	6	6	4	4
ZR	123	133	131	132	94	146	142	136	99	124
Y	24	27	24	27	21	31	25	21	19	22
SR	248	205	209	209	286	215	322	317	228	203
RB	25	11	0	10	1	2	8	9	1	2
ZN	76	155	101	194	97	130	108	98	86	65
GROUP	4	4	4	4	4	4	4	4	4	4

WT%	77128	77225*	77215	77313	77314*	77324	77331*	77335	77342	77343
SIO_2	45.58	47.53	46.68	45.43	46.24	46.41	45.79	47.32	46.19	47.22
AL_2O_3	14.67	13.42	14.14	14.77	14.33	14.30	14.96	13.28	14.11	13.05
FE_2O_3	12.72	13.36	13.68	13.38	12.78	13.69	12.79	13.42	13.25	13.47
MGO	9.29	8.86	8.15	13.03	9.89	9.13	9.38	9.05	9.60	9.55
CAO	11.92	12.28	12.06	11.96	11.63	11.81	11.41	11.97	11.88	11.44
NA_2O	2.48	3.13	2.26	2.65	3.28	2.23	2.58	2.69	2.56	2.61
K_2O	2.35	2.92	2.61	3.44	2.89	2.47	2.24	2.24	2.15	2.28
TIO_2	1.83	2.45	1.84	1.71	1.73	1.87	1.49	1.77	1.94	1.79
MNO	2.18	2.22	2.18	2.19	2.19	2.21	2.21	2.24	2.21	2.24
P_2O_5	2.17	2.25	2.16	2.15	2.15	2.19	2.14	2.17	2.19	2.13
PPM										
NI	116	75	102	87	131	108	121	58	97	05
CR	343	187	374	342	287	276	312	124	349	349
BA	71	385	122	58	38	73	89	97	52	124
NB	3	8	4	4	4	4	4	3	4	4
ZR	122	203	129	118	113	123	97	113	125	124
Y	22	28	42	19	21	27	23	26	22	21
SR	268	387	252	227	225	246	168	245	237	227
RB	23	20	24	8	1	29	17	12	8	18
ZN	81	238	91	75	88	153	237	118	154	99
GROUP	4	4	4	4	4	4	4	4	4	4

RHUM DOLERITE GROUPS 1-12

	77344	77348	77359☆	13A76	14A76	38A76	77332	77049*	77087*	77210
WT%										
SIO2	47.56	47.06	47.42	47.82	46.12	47.28	47.31	45.75	47.65	46.47
AL2O3	15.77	14.84	14.35	12.87	13.17	14.66	14.65	13.59	13.47	14.34
FE2O3	11.73	12.07	12.26	16.31	15.69	13.98	14.39	15.45	15.34	14.91
MGO	8.49	9.84	9.34	6.82	7.58	7.52	7.31	7.29	7.46	7.61
CAO	11.68	11.14	11.71	12.12	12.87	10.28	11.36	12.62	9.83	11.42
NA2O	2.83	2.61	2.74	2.97	3.18	3.73	2.65	4.54	2.84	1.06
K2O	0.16	0.54	0.13	0.35	0.31	0.04	0.26	0.03	0.13	1.48
TIO2	1.45	1.57	1.70	2.70	2.72	2.15	2.19	2.32	2.81	1.97
MNO	0.17	0.18	0.18	0.24	0.22	0.20	0.21	0.22	0.23	0.23
P2O5	0.15	0.15	0.16	0.19	0.24	0.19	0.22	0.24	0.22	0.14
PPM										
NI	94	99	132	61	48	68	69	64	71	93
CR	298	307	603	56	244	98	178	71	139	223
BA	53	188	115	227	81	35	25	74	244	184
NB	4	5	4	7	6	5	5	5	6	3
ZR	97	120	122	173	178	149	143	159	181	111
Y	18	22	19	31	33	31	31	28	34	24
SR	221	231	216	241	259	375	212	249	284	183
RB	13	34	1	9	9	0	2	1	1	63
ZN	92	106	61	116	78	113	95	106	115	87
GROUP	4	4	4	4	4	4	4	4	4	4

RHUM DOLERITE GROUPS 1-12

	77322	77334	77363*	77356	77323	SR151	SR229	SR238	SR284	SR141
WT%										
SIO2	45.30	47.42	45.72	46.35	46.34	46.57	47.50	46.75	47.61	47.96
AL2O3	13.71	13.92	14.78	14.43	15.92	15.78	14.53	16.19	15.25	14.69
FE2O3	14.13	13.91	13.62	12.73	12.41	12.41	13.28	12.26	12.94	14.25
MGO	8.62	8.43	7.83	9.92	10.32	9.23	8.30	8.96	8.51	7.53
CAO	11.79	10.86	11.44	13.56	12.49	12.58	12.85	12.58	12.58	10.63
NA2O	2.85	2.83	3.38	1.72	2.31	2.16	1.96	2.34	1.82	2.72
K2O	0.20	0.39	0.29	0.48	0.35	0.45	0.35	0.05	0.25	0.12
TIO2	1.99	1.88	2.37	0.97	0.92	0.99	1.16	0.94	1.09	1.75
MNO	0.23	0.21	0.18	0.23	0.18	0.19	0.19	0.19	0.19	0.15
P2O5	0.17	0.13	0.20	0.07	0.08	0.08	0.10	0.08	0.13	0.18
PPM										
NI	67	54	76	163	176	149	93	147	128	306
CR	288	86	185	454	484	441	423	418	433	726
BA	95	137	66	29	24	272	45	173	68	72
NB	6	4	5	3	3	3	4	3	3	4
ZR	129	112	121	43	42	45	56	47	47	101
Y	23	25	22	21	21	25	24	23	23	23
SR	207	216	214	119	90	118	101	98	105	213
RB	7	22	0	2	1	2	2	2	1	2
ZN	330	123	86	76	74	85	77	74	0	0
GROUP	4	4	4	5	5	5	5	5	5	6

RHUM DOLERITE GROUPS 1-12

	SR159	SR182	SR211	SR282	12A76	77014	77047	77150	77258	16A76*
WT%										
SIO2	49.42	49.24	45.76	49.45	47.52	46.94	49.89	47.33	48.47	49.78
AL2O3	14.03	14.23	16.98	14.26	15.42	16.19	18.95	17.45	18.99	14.03
FE2O3	13.95	14.25	14.32	14.31	11.21	11.30	7.21	9.85	8.38	11.65
MGO	5.24	5.65	7.95	5.54	9.35	9.10	5.64	8.16	6.52	8.31
CAO	12.58	12.51	9.73	12.42	12.71	12.36	15.19	13.51	14.21	11.25
NA2O	2.96	3.11	3.28	2.97	2.41	2.41	1.98	1.72	1.67	2.49
K2O	0.67	0.73	0.11	0.74	0.23	0.54	0.48	0.54	0.66	0.64
TIO2	1.73	1.82	1.74	1.88	1.25	1.29	0.91	1.19	1.04	1.72
MNO	0.20	0.21	0.18	0.21	0.17	0.16	0.10	0.14	0.13	0.15
P2O5	0.21	0.23	0.19	0.22	0.11	0.11	0.09	0.13	0.09	0.16
PPM										
NI	55	44	122	45	121	134	63	112	70	144
CR	158	132	287	128	374	398	266	404	313	414
BA	261	254	21	253	47	102	35	115	125	173
NB	6	7	4	7	3	3	3	3	2	6
ZR	130	139	110	135	88	76	48	58	54	165
Y	37	43	27	39	19	17	11	12	14	27
SR	197	199	183	194	259	233	265	218	351	235
RB	15	16	1	16	9	17	6	14	27	14
ZN	109	109	103	117	75	68	45	52	50	81
GROUP	6	6	6	6	7	7	7	7	7	8

RHUM DOLERITE GROUPS 1-12

	18A76	22A76	23A76	35A76	48A76☆	49A76	50A76☆	51A76☆	64A76	70A76
WT%										
SIO2	51.75	52.71	50.69	52.76	49.78	49.36	50.67	52.41	52.11	49.95
AL2O3	13.56	13.41	13.45	14.53	14.22	13.31	13.83	14.12	14.38	13.42
FE2O3	11.85	12.21	11.91	12.41	12.69	11.34	12.76	12.29	10.78	11.97
MGO	7.52	7.48	8.16	4.94	10.80	10.47	9.11	7.18	7.45	8.01
CAO	10.78	10.09	10.37	8.22	10.90	11.12	10.01	10.21	8.87	10.69
NA2O	2.49	2.64	2.58	4.14	2.18	2.16	2.45	2.04	3.20	2.55
K2O	0.63	0.92	0.75	1.24	0.37	0.25	0.39	0.63	0.86	0.38
TIO2	1.79	1.83	1.84	2.13	1.44	1.65	1.58	1.92	1.96	1.78
MNO	0.18	0.18	0.17	0.20	0.15	0.16	0.15	0.18	0.15	0.19
P2O5	0.16	0.15	0.17	0.20	0.16	0.17	0.17	0.18	0.24	0.15
PPM										
NI	79	99	92	37	143	119	101	73	94	134
CR	271	332	256	49	347	346	361	168	255	313
BA	273	387	226	303	131	70	137	193	275	169
NB	6	5	6	8	4	5	5	6	6	5
ZR	173	172	175	225	131	154	158	173	204	143
Y	29	32	31	28	17	23	22	28	32	24
SR	210	232	239	229	234	235	242	209	246	282
RB	13	21	17	31	12	9	11	17	25	16
ZN	76	86	76	150	89	71	94	105	109	1041
GROUP	8	8	8	8	8	8	8	8	8	8

RHUM DOLERITE GROUPS 1-12

	77003	77004*	77006*	77007	77040	77075*	77078	77092	77105	77108
WT%										
SIO2	51.43	52.48	51.66	51.78	49.91	50.98	51.21	52.65	50.83	51.51
AL2O3	13.64	15.03	15.21	15.41	13.77	13.36	13.87	14.74	14.51	15.52
FE2O3	11.79	12.92	10.83	11.13	12.93	14.65	12.58	12.63	11.75	10.35
MGO	7.79	6.72	8.48	7.46	11.19	10.95	7.24	6.53	7.23	6.75
CAO	8.78	7.87	8.24	9.35	9.42	9.25	9.22	10.53	10.71	9.82
NA2O	3.34	4.23	3.49	3.18	2.42	2.47	2.95	2.86	2.82	3.25
K2O	0.95	0.82	0.35	0.95	0.93	0.57	0.64	0.67	0.70	1.20
TIO2	1.93	1.73	1.43	1.51	1.19	1.45	1.86	1.07	1.17	1.19
MNO	0.16	0.14	0.14	0.16	0.16	0.15	0.23	0.15	0.22	0.15
P2O5	0.19	0.20	0.18	0.17	0.12	0.15	0.23	0.11	0.12	0.24
PPM										
NI	62	88	177	113	270	253	63	47	49	74
CR	134	197	344	314	643	628	166	115	114	247
BA	331	453	262	281	218	241	252	253	237	487
NB	8	8	8	6	5	6	8	4	4	5
ZR	193	199	159	141	130	152	228	83	88	120
Y	26	28	19	18	24	21	37	24	22	19
SR	256	266	321	277	190	255	236	247	243	381
RB	24	28	9	16	33	16	19	12	9	21
ZN	109	89	87	84	100	101	126	74	82	75
GROUP	8	8	8	8	8	8	8	8	8	8

446

RHUM DOLERITE GROUPS 1-12

	77124	77145	77149	77250	77281	77272	77316	77325	77339	77349
WT%										
SIO2	52.16	49.53	49.53	52.17	52.86	53.27	49.72	53.51	52.36	49.45
AL2O3	14.07	12.73	13.59	13.34	14.74	15.21	14.38	13.84	15.25	14.36
FE2O3	12.55	15.68	11.77	14.53	11.10	12.55	12.73	11.99	12.55	11.13
MGO	5.92	5.94	9.51	6.84	5.16	6.42	6.94	5.89	7.85	9.73
CAO	7.21	9.35	11.05	8.97	13.48	13.47	9.78	7.63	7.02	12.46
NA2O	3.49	3.01	2.33	2.01	2.53	2.59	3.53	3.74	3.26	2.49
K2O	1.59	2.89	0.46	2.48	0.75	0.79	0.75	1.17	1.23	0.53
TIO2	2.46	2.41	1.40	2.32	1.27	1.02	1.83	1.67	1.49	1.53
MNO	0.18	0.23	0.18	0.22	0.20	0.16	0.19	0.23	0.15	0.18
P2O5	0.26	0.23	0.10	0.25	0.10	0.12	0.19	0.34	0.14	0.16
PPM										
NI	19	36	122	21	45	39	71	28	122	147
CR	36	85	354	79	108	99	126	161	263	365
BA	396	259	182	271	267	265	180	459	462	231
NB	9	5	6	6	4	4	6	9	7	8
ZR	224	155	119	160	93	88	166	325	164	157
Y	29	32	23	29	22	24	27	56	21	28
SR	239	239	214	261	196	207	236	199	285	226
RB	36	35	29	27	18	19	28	44	53	24
ZN	131	123	107	196	93	63	124	286	123	128
GROUP	8	8	8	8	8	8	8	8	8	8

RHUM DOLERITE GROUPS 1=12

	77358	15A76	25A76*	75A76	77061	77064	77127	77148	77155*	77243
WT%										
SIO2	49.82	52.53	49.86	52.74	52.45	49.92	50.51	51.61	49.28	49.17
AL2O3	13.32	13.42	13.34	13.37	13.25	13.09	13.56	12.54	13.85	13.87
FE2O3	11.90	13.95	14.63	14.32	14.53	13.11	14.39	14.05	14.24	14.23
MGO	9.63	6.22	6.14	6.52	6.26	6.72	6.34	6.82	6.58	7.42
CAO	12.75	9.76	9.44	8.52	8.53	12.42	8.64	8.77	10.49	9.93
NA2O	2.38	2.68	2.95	3.62	3.34	3.44	3.58	2.60	2.85	2.55
K2O	0.49	1.03	0.94	0.97	0.63	0.42	0.34	1.14	0.59	0.77
TIO2	1.37	2.14	2.31	2.51	2.23	2.01	2.29	2.03	1.81	1.68
MNO	0.20	0.19	0.24	0.20	0.24	0.19	0.21	0.21	0.22	0.21
P2O5	0.12	0.22	0.19	0.23	0.27	0.18	0.25	0.22	0.17	0.17
PPM										
NI	123	73	53	28	31	66	27	18	45	28
CR.	354	124	106	52	93	177	88	33	138	34
BA	265	387	442	294	274	216	285	347	231	171
NB	3	7	7	8	3	6	4	6	6	4
ZR	163	182	186	219	159	179	175	176	126	127
Y	26	35	32	32	33	29	35	28	36	24
SR	223	321	329	231	251	217	245	272	183	244
RB	25	24	25	31	29	11	29	36	16	20
ZN	100	87	121	137	123	104	142	127	97	99
GROUP	8	8	8	8	8	8	8	8	8	8

RHUM DOLERITE GROUPS 1-12

	77346	32A75*	83A76*	77058*	77090*	77137	77184	77005	77008*	77023
WT%										
SIO2	54.72	46.34	47.74	47.79	47.88	47.49	46.26	52.27	53.71	48.04
AL2O3	14.30	15.76	13.34	15.37	16.04	14.65	15.24	15.18	14.80	13.46
FE2O3	12.05	13.27	15.06	12.38	12.06	11.85	12.12	11.08	11.03	16.04
MGO	5.61	10.05	6.93	8.53	8.96	11.52	9.09	5.66	4.96	5.05
CAO	8.16	6.81	8.99	9.90	9.32	7.30	8.56	7.60	6.97	8.40
NA2O	3.30	3.55	3.20	3.19	2.97	3.25	4.53	4.58	5.60	4.20
K2O	1.16	1.44	1.05	0.54	0.91	1.46	1.01	1.58	0.91	1.29
TIO2	1.38	2.16	2.45	1.73	1.49	1.88	1.92	1.71	1.69	2.04
MNO	0.14	0.18	0.22	0.17	0.16	0.14	0.17	0.14	0.11	0.22
P2O5	0.16	0.43	0.21	0.29	0.21	0.46	0.39	0.20	0.21	0.35
PPM										
NI	128	173	42	124	124	248	199	95	48	18
CR	218	207	63	224	145	267	357	182	69	23
BA	471	487	266	515	571	878	367	476	325	474
NB	7	9	6	7	4	11	9	8	8	8
ZR	197	207	176	139	135	258	169	189	215	262
Y	23	25	30	23	21	28	26	25	26	36
SR	255	526	241	401	435	452	327	252	258	314
RB	37	22	55	16	13	27	15	26	16	20
ZN	108	132	213	153	87	120	112	97	23	145
GROUP	9	10	10	10	10	10	10	11	11	11

RHUM DOLERITE GROUPS 1-12

	77244	77306	77315	29A76☆	55A76☆	76A76☆	81A76☆	77034☆	77388	77209
WT%										
SIO2	51.71	49.16	49.71	55.11	57.59	54.43	57.43	55.13	52.94	55.28
AL2O3	13.45	12.88	13.22	13.21	13.92	14.13	13.69	14.49	13.79	14.22
FE2O3	13.85	15.71	13.32	11.32	8.85	10.56	9.33	10.07	13.42	10.95
MGO	5.88	6.17	7.43	7.15	5.88	6.04	5.56	6.81	6.27	4.57
CAO	7.58	9.38	9.58	7.69	6.78	7.61	7.34	7.33	7.31	7.35
NA2O	2.95	3.05	3.31	2.69	3.64	3.49	3.99	3.58	3.27	3.64
K2O	1.37	0.82	0.91	1.16	1.53	1.34	0.57	1.35	2.18	1.82
TIO2	1.97	2.49	2.31	1.56	1.54	2.01	1.79	1.34	2.32	1.74
MNO	0.17	0.23	0.20	0.23	0.12	0.16	0.14	0.14	0.20	0.16
P2O5	0.22	0.22	0.23	0.16	0.22	0.25	0.18	0.16	0.31	0.22
PPM										
NI	24	23	39	97	71	57	79	167	28	42
CR	128	84	71	247	163	141	96	367	138	99
BA	392	289	230	294	551	440	373	421	336	558
NB	6	5	6	8	9	9	9	7	8	9
ZR	166	152	202	289	266	293	314	191	296	465
Y	21	29	37	37	34	39	35	24	44	32
SR	276	258	223	295	280	282	293	286	393	276
RB	37	30	23	54	45	39	30	34	2	42
ZN	132	159	119	114	110	125	52	97	123	103
GROUP	8	8	8	9	9	9	9	9	9	9

RHUM DOLERITE GROUPS 1-12

	77279*	77342*	77132*	77177*
	53.20	49.35	56.86	54.?3
	14.81	14.27	16.54	17.45
	11.37	12.45	7.10	9.14
	5.83	6.02	3.?2	4.43
	5.59	3.?1	4.76	3.?4
	4.3?	4.26	4.85	4.26
	2.47	2.75	4.18	4.93
	1.99	2.63	1.?4	1.69
	0.16	0.19	0.12	0.15
	0.27	0.75	0.?4	0.92
	35	?	3	5
	35	28	1	37
	759	915	1524	1233
	11	11	23	22
	285	344	465	462
	3?	3?	41	44
	258	459	431	314
	49	61	6?	93
	128	172	136	119
GROUP	11	11	12	12

RHUM GABBRO PLUGS

	77031*	77033*	77134*	77256	77257	77292*	77205	77320*	77252	77284
WT%										
SIO2	49.95	49.24	47.42	46.10	47.15	48.98	48.78	46.15	43.78	43.85
AL2O3	14.82	14.39	15.94	15.68	15.12	15.74	15.38	15.44	14.22	15.41
FE2O3	13.37	13.02	9.97	11.39	10.52	11.47	13.58	12.14	11.65	13.47
MGO	10.71	11.22	10.48	11.03	11.95	9.74	10.36	11.68	17.23	13.46
CAO	10.18	12.14	12.95	13.32	11.57	9.99	10.22	10.45	9.19	9.97
NA2O	2.18	2.02	1.58	2.92	2.28	2.49	2.58	2.36	2.05	2.44
K2O	0.56	0.13	0.17	0.38	0.22	0.16	0.44	0.23	0.16	0.21
TIO2	1.02	0.52	0.96	1.80	0.95	1.17	1.56	1.27	1.41	1.68
MNO	0.15	0.16	0.14	0.16	0.16	0.17	0.14	0.16	0.15	0.18
P2O5	0.08	0.10	0.09	0.24	0.10	0.09	0.25	0.12	0.15	0.17
PPM										
NI	157	95	289	152	215	41	126	174	422	374
CR	447	337	785	319	833	158	347	321	858	720
BA	101	72	51	71	72	117	118	97	105	76
NB	6	2	3	4	0	2	1	1	0	1
ZR	86	16	61	144	56	33	146	79	83	115
Y	17	9	12	20	15	10	24	19	16	17
SR	149	277	193	330	181	323	256	184	288	253
RB	14	2	3	6	6	3	10	7	3	3
ZN	56	64	46	47	60	76	44	86	66	103

452

RHUM GABBRO PLUGS

	77288	77067	77098	77100	77246*	77261	77265	77267*	77270	77273
WT%										
SIO2	46.82	52.29	49.35	49.49	47.63	48.50	46.75	49.68	48.33	47.74
AL2O3	15.24	15.25	14.25	13.78	13.65	15.59	15.27	14.32	16.32	15.13
FE2O3	8.05	11.47	10.15	11.49	14.33	12.94	13.84	10.85	11.03	12.68
MGO	14.91	7.17	7.27	7.83	7.29	6.40	8.32	6.38	8.21	7.91
CAO	13.28	9.72	13.26	12.68	11.48	9.72	13.89	11.87	9.46	12.50
NA2O	3.96	3.64	3.45	2.88	2.69	3.44	3.19	3.92	3.28	3.63
K2O	0.05	2.69	0.32	0.32	0.55	1.04	2.11	0.58	0.07	0.25
TIO2	0.54	1.43	1.64	1.58	1.98	1.03	2.03	2.05	1.52	1.84
MNO	0.11	0.16	0.15	0.18	0.20	0.16	0.18	0.15	0.16	0.17
P2O5	0.07	0.17	0.15	0.18	0.20	0.31	0.22	0.19	0.22	0.22
PPM										
NI	337	92	91	88	69	58	122	72	78	96
CR	1955	395	146	434	124	189	277	326	226	221
BA	52	156	42	53	395	473	56	120	328	85
NB	3	4	4	5	1	4	5	2	6	3
ZR	30	128	57	125	120	160	128	118	131	121
Y	5	23	18	22	21	27	21	18	20	20
SR	199	272	281	234	360	517	592	300	488	304
RB	0	11	8	8	11	27	2	9	21	5
ZN	34	35	47	53	104	72	79	58	66	64

453

	77282	77283	77287	77296	77102*	77103*	77274*	77264*	33A76	77163
WT%										
SIO2	49.24	48.43	47.96	48.06	51.81	51.42	53.71	58.15	51.22	51.41
AL2O3	14.28	14.67	16.23	15.19	14.47	13.84	14.81	14.18	13.77	14.67
FE2O3	11.44	12.04	11.26	12.02	12.99	13.42	12.71	12.26	10.25	14.47
MGO	7.42	8.26	8.86	8.53	6.92	5.72	4.25	2.69	6.94	7.88
CAO	12.21	11.15	12.18	11.44	10.17	9.43	5.84	3.99	12.78	12.64
NA2O	3.14	2.89	3.42	3.28	2.44	3.38	4.59	4.03	2.53	2.62
K2O	0.33	0.87	0.44	0.18	0.87	1.01	1.52	2.36	0.57	0.54
TIO2	1.83	1.55	1.51	1.98	1.69	2.17	2.22	1.97	1.67	1.52
MNO	0.15	0.17	0.14	0.17	0.17	0.21	0.18	0.17	0.15	0.19
P2O5	0.18	0.15	0.18	0.31	0.16	0.24	0.20	0.25	0.13	0.12
PPM										
NI	78	77	133	81	93	32	4	4	68	126
CR	49	258	318	325	227	25	5	8	118	207
BA	79	125	132	58	228	272	351	431	131	224
NB	8	4	5	3	8	6	8	12	5	9
ZR	82	96	165	175	159	182	256	359	98	135
Y	19	22	23	26	25	33	32	57	24	25
SR	249	314	348	221	237	198	222	178	238	223
RB	6	21	9	7	24	25	46	58	11	12
ZN	53	72	69	53	61	107	98	168	52	87

RHUM GABBROS

	77328	77353
WT%		
SIO2	49.85	45.49
AL2O3	18.64	27.18
FE2O3	5.71	8.57
MGO	7.12	17.83
CAO	15.07	12.96
NA2O	1.78	1.38
K2O	0.08	7.03
TIO2	3.53	7.43
HNO	0.08	2.11
P2O5	0.07	7.03
PPM		
NI	88	272
CR	416	358
BA	39	32
NB	8	1
ZR	28	4
Y	6	4
SR	307	283
RB	1	1
ZN	16	33

PERIDOTITE PLUGS

	77181	77182	77183	77259	77268	77281	77286	77290	77389	77357
WT%										
SIO2	41.37	43.61	43.89	41.67	41.43	42.13	41.24	43.03	41.37	39.63
AL2O3	9.19	13.38	13.44	9.82	7.53	6.90	8.00	6.84	0.14	4.38
FE2O3	12.68	14.43	12.70	11.82	11.26	13.98	11.03	11.79	13.76	11.81
MGO	29.71	25.60	28.65	28.76	32.71	35.16	32.91	36.76	32.11	41.91
CAO	5.13	6.22	5.39	5.99	5.97	3.78	4.55	3.42	5.22	1.95
NA2O	0.82	0.76	1.15	1.02	0.53	0.47	0.66	0.65	1.09	0.18
K2O	0.12	0.15	0.17	0.09	0.07	0.07	0.07	0.04	0.12	0.03
TIO2	0.77	0.57	0.73	0.62	0.33	0.32	0.47	0.28	0.32	0.24
MNO	0.18	0.22	0.18	0.16	0.17	0.20	0.17	0.18	0.17	0.17
P2O5	0.18	0.08	0.10	0.09	0.06	0.06	0.05	0.04	0.06	0.04
PPM										
NI	1500	1233	1446	1476	1796	2247	1887	2306	1823	2465
CR	2559	2394	2854	2214	3235	3399	2565	2799	3170	2885
BA	22	91	65	27	25	36	14	15	42	16
NB	2	1	1	3	0	0	0	1	0	2
ZR	53	28	44	43	20	19	30	13	19	19
Y	10	2	6	8	4	5	6	6	4	1
SR	112	132	147	98	45	55	58	30	55	22
RB	3	4	4	1	0	4	2	0	4	1
ZN	66	110	85	72	67	68	77	77	68	70

PERIDOTITE PLUGS

	77051	77054	77055	77066	77089	77097	77099	77129	77136	77138
WT%										
SIO2	42.73	41.90	42.78	41.47	42.14	41.26	39.38	40.75	40.27	42.37
AL2O3	5.49	7.44	5.29	8.36	10.81	10.16	5.53	7.70	7.34	6.71
FE2O3	12.13	12.55	11.31	12.95	12.83	12.12	12.53	11.52	14.18	12.65
MGO	37.71	35.67	38.76	32.77	27.56	28.69	37.72	34.24	32.26	34.87
CAO	3.77	4.11	3.04	5.43	6.57	5.81	3.39	4.29	4.17	4.14
NA2O	0.37	0.74	0.29	0.78	1.15	1.01	0.54	0.62	0.81	0.48
K2O	0.30	0.10	0.06	0.14	0.10	0.10	0.12	0.13	0.13	0.13
TIO2	0.28	0.27	0.29	0.58	0.64	0.65	0.59	0.57	0.61	0.52
MNO	0.18	0.16	0.18	0.19	0.16	0.18	0.18	0.17	0.20	0.19
P2O5	0.04	0.03	0.06	0.07	0.07	0.07	0.06	0.08	0.09	0.06
PPM										
NI	2411	2535	2483	1727	1742	1523	2393	2035	1429	1842
CR	3528	3257	4456	2563	3466	2632	2668	3161	2215	2852
BA	23	29	18	45	42	21	0	10	43	25
NB	2	4	4	1	2	8	1	2	3	1
ZR	16	14	23	34	42	34	26	38	41	31
Y	4	5	5	7	11	9	5	7	8	7
SR	32	32	35	72	80	83	73	104	103	69
RB	4	5	4	1	3	2	1	3	5	1
ZN	70	47	58	75	69	78	76	74	105	76

Table of CIPW Norms.

These were calculated using the program NORMCAL, written by
R.C.O.Gill, with a fixed Fe2O3 / FeO ratio of 0.25.DI refers to
the Thornton-Tuttle (1960) Differentiation Index.

RHUM DOLERITE GROUPS 1-12   CIPW NORMS

	52A76*	53A76*	54A76*	56A76	69A76*	71A76	77A76*	77077*	77179*	77321*	77341	77052
ORTHOCLASE	0.8	1.8	0.5	1.4	0.7	0.8	3.8	1.7	4.3	1.2	2.9	0.6
ALBITE	5.6	8.7	13.3	8.6	11.6	9.7	8.2	14.5	2.1	9.9	10.9	10.3
ANORTHITE	28.8	27.5	29.3	27.4	28.1	29.7	28.4	27.1	28.7	27.4	28.7	29.8
NEPHELINE	0.0	0.0	0.0	0.0	0.0	0.0	0.0	1.4	0.0	0.0	0.0	0.0
DIOPSIDE	5.7	13.9	21.1	15.9	15.0	11.7	12.5	19.2	3.8	13.5	19.6	21.6
HYPERSTHENE	0.7	2.9	2.8	3.5	0.9	9.0	3.5	0.0	4.3	1.0	1.4	0.6
OLIVINE	62.1	39.3	26.7	37.2	36.5	33.8	37.4	29.0	59.9	43.4	32.0	31.2
MAGNETITE	3.3	3.1	3.3	3.1	3.4	3.1	3.3	3.1	3.1	3.2	3.4	3.4
ILMENITE	1.6	2.4	2.6	2.4	3.2	2.0	2.6	3.4	1.6	2.9	2.9	2.3
APATITE	0.2	0.4	0.4	0.4	0.5	0.2	0.4	0.5	0.3	0.6	0.4	0.2
DIFF. INDEX	6.4	10.6	13.9	10.0	12.3	10.4	12.0	17.6	6.4	11.1	13.7	10.9

	77093*	77095*	77101*	77107*	77224*	77192	77196	77197*	77221	77225	77235	77236*
ORTHOCLASE	0.4	0.4	1.2	0.7	1.4	2.7	3.3	1.8	0.8	2.4	1.1	0.7
ALBITE	16.4	15.0	8.9	11.5	13.9	19.6	17.2	6.1	9.5	10.5	14.3	6.1
ANORTHITE	29.4	28.9	27.5	25.7	26.9	29.1	30.0	26.4	27.8	22.9	30.1	26.5
NEPHELINE	0.0	0.0	0.0	0.0	4.3	0.6	0.0	1.7	3.3	6.6	4.1	4.3
DIOPSIDE	26.6	23.4	14.7	20.0	19.3	16.3	11.7	7.1	18.0	20.6	20.0	13.3
HYPERSTHENE	4.4	5.4	1.5	0.0	0.0	0.0	0.0	0.0	0.0	0.0	0.0	0.0
OLIVINE	16.5	20.9	40.2	35.6	28.1	26.1	31.0	52.9	42.2	33.2	23.9	42.9
MAGNETITE	3.4	3.4	3.4	3.4	3.6	3.0	3.2	3.0	3.4	3.3	3.1	3.0
ILMENITE	2.7	2.4	2.4	2.8	2.4	2.3	2.5	1.5	2.5	3.2	2.9	2.0
APATITE	0.2	0.2	0.2	0.3	0.3	0.3	0.5	0.2	0.4	0.4	0.4	0.0
DIFF. INDEX	16.8	15.3	10.1	12.2	19.6	22.9	20.5	8.9	13.7	19.4	19.5	11.3

RHUM DOLERITE GROUPS 1-12 CIPW NORMS

	77237*	85A76	77017	77024*	77035	40A76	44A76*	46A76*	65A76*	73A76	93A76	77019*
ORTHOCLASE	1.1	0.8	0.9	0.3	1.1	1.1	2.1	1.5	0.6	1.1	1.8	1.9
ALBITE	19.6	7.8	12.9	14.8	13.5	13.8	9.2	12.4	18.4	17.5	14.1	14.8
ANORTHITE	29.7	21.3	27.4	31.2	29.8	32.5	33.5	25.3	29.2	28.2	27.3	28.4
NEPHELINE	1.2	0.0	1.8	2.5	0.0	0.0	0.0	3.2	0.0	0.0	0.0	2.5
DIOPSIDE	17.6	4.5	19.6	14.5	17.6	18.8	15.8	33.3	21.8	25.4	17.8	18.5
HYPERSTHENE	0.0	10.7	0.0	0.0	4.6	13.4	10.8	0.0	4.1	3.1	12.5	0.0
OLIVINE	24.0	51.1	30.0	32.5	27.0	18.0	23.6	17.5	19.8	17.9	21.1	27.5
MAGNETITE	2.9	3.1	3.6	3.2	3.4	2.0	2.9	3.1	3.1	3.2	3.2	3.5
ILMENITE	3.6	1.3	3.4	1.7	3.4	2.2	1.9	3.3	2.6	3.2	2.7	3.3
APATITE	0.2	0.2	0.4	0.2	0.4	0.3	0.2	0.4	0.3	0.4	0.3	0.4
DIFF. INDEX	21.8	7.8	15.5	16.8	14.6	14.9	11.3	17.1	19.0	18.7	15.9	18.3

	77093*	77095*	77101*	77107*	77224*	77192	77196	77197*	77221	77225	77235	77236*
ORTHOCLASE	0.4	0.4	1.2	0.7	1.4	2.7	3.3	1.0	0.8	2.4	1.1	0.7
ALBITE	16.4	15.0	8.9	11.5	13.9	19.6	17.2	6.1	9.5	18.5	14.3	6.7
ANORTHITE	29.4	28.9	27.5	25.7	26.9	29.1	30.3	26.4	27.8	22.9	30.1	26.1
NEPHELINE	0.0	0.0	0.0	0.0	4.3	0.6	0.0	1.7	3.3	6.6	4.1	4.5
DIOPSIDE	26.6	23.4	14.7	20.0	19.3	16.3	11.7	7.1	18.0	20.6	23.0	13.3
HYPERSTHENE	4.4	5.4	1.5	0.0	0.0	0.0	0.0	0.0	0.0	0.0	0.0	0.0
OLIVINE	16.5	20.9	42.2	35.6	28.1	26.1	31.0	52.9	42.2	38.2	23.0	42.4
MAGNETITE	3.4	3.4	3.4	3.4	3.6	3.0	3.2	3.2	3.0	3.0	3.9	3.6
ILMENITE	2.7	2.4	3.4	2.8	2.4	2.3	2.8	1.5	2.5	3.3	3.9	3.6
APATITE	0.2	0.2	0.2	0.3	0.3	0.3	0.5	0.2	0.4	0.4	0.4	0.6
DIFF. INDEX	16.8	15.3	10.1	12.2	19.6	22.9	20.5	8.9	13.7	19.4	19.5	11.3

RHUM DOLERITE GROUPS 1-12   CIPW NORMS

	77352*	66A76*	72A76	73A76	74A76	87A76*	89A75*	92A76	77046*	77248	77280	77082*
ORTHOCLASE	2.7	0.6	1.5	1.3	1.2	4.7	3.2	1.5	3.2	3.9	1.3	1.7
ALBITE	13.7	18.3	19.5	19.6	21.2	19.9	22.1	18.2	19.1	18.1	21.9	18.6
ANORTHITE	31.4	28.3	27.5	27.3	26.2	27.0	25.5	28.7	27.5	26.5	27.2	28.2
DIOPSIDE	21.2	18.9	17.6	19.2	23.7	17.8	19.4	21.8	18.2	22.0	21.3	19.5
HYPERSTHENE	4.9	9.6	17.6	15.5	2.6	4.7	8.9	5.5	12.1	4.3	8.9	15.3
OLIVINE	21.9	17.9	9.6	10.8	18.4	19.7	13.8	18.1	14.1	18.7	13.3	10.0
MAGNETITE	3.4	3.3	3.3	2.9	3.3	3.2	3.2	3.2	3.1	3.1	3.1	3.2
ILMENITE	2.6	3.8	3.4	2.9	3.3	2.7	3.6	2.8	2.5	2.9	2.3	3.2
APATITE	0.3	0.3	0.4	0.3	0.4	0.4	0.5	0.3	0.3	0.4	0.3	0.4
DIFF. INDEX	14.3	18.9	21.0	20.9	22.2	24.6	25.2	19.7	22.2	22.0	23.3	20.3

	77178	77191*	77249	77251	77318	77356
ORTHOCLASE	3.0	2.7	2.9	1.9	1.1	1.0
ALBITE	21.8	18.3	21.1	18.8	21.1	19.7
ANORTHITE	25.2	29.9	25.1	28.0	26.6	27.5
NEPHELINE	2.9	1.2	0.0	0.0	0.9	0.0
DIOPSIDE	17.3	19.1	20.1	19.2	21.0	19.0
HYPERSTHENE	0.0	0.0	4.0	4.0	10.1	14.4
OLIVINE	21.9	22.4	16.8	19.9	12.7	11.3
MAGNETITE	3.5	3.1	3.4	3.2	3.4	3.2
ILMENITE	3.8	2.9	4.1	3.6	3.1	2.9
APATITE	0.7	0.4	0.5	0.5	0.3	0.3
DIFF. INDEX	27.7	22.2	24.0	20.7	22.2	20.7

RHUM DOLERITE GROUPS 1-12 CIPW NORMS

	77056	77323	SR151	SR229	SR238	SR284	SR141	SR159	SR182	SR211	SR282	12A76
ORTHOCLASE	0.5	0.3	0.3	0.4	0.3	0.3	0.7	4.0	4.4	0.7	4.4	1.4
ALBITE	14.5	17.2	18.5	16.8	17.4	15.6	23.3	25.3	26.6	25.3	25.4	17.2
ANORTHITE	31.8	34.6	33.5	31.8	35.2	33.1	27.8	23.3	23.8	32.6	23.7	32.7
NEPHELINE	0.0	0.0	0.0	0.0	0.0	0.0	0.0	0.0	0.0	0.6	0.0	0.0
DIOPSIDE	29.0	22.2	23.6	26.8	22.2	24.3	20.0	23.4	23.0	12.2	22.5	24.5
HYPERSTHENE	1.9	1.4	0.8	9.7	4.2	13.4	11.7	18.3	7.7	0.0	12.1	6.0
OLIVINE	16.8	19.1	18.0	9.3	15.4	7.5	8.9	6.0	7.1	21.1	3.9	12.6
MAGNETITE	3.4	3.2	3.3	3.6	3.3	3.5	3.8	3.8	3.8	3.9	3.9	3.0
ILMENITE	1.9	1.8	1.9	2.2	1.8	2.1	3.4	3.3	3.5	3.3	3.6	2.4
APATITE	0.2	0.2	0.2	0.2	0.2	0.2	0.4	0.5	0.6	0.5	0.5	0.3
DIFF. INDEX	15.0	17.5	18.8	17.1	17.7	15.0	24.0	29.3	31.0	26.5	29.8	18.5

	77014	77047	77163	77258	16A76*	18A76	20A76	23A76	35A76	48A76*	49A75	53A76*
QUARTZ	0.0	1.0	0.0	0.0	0.0	1.2	0.0	0.0	0.0	0.0	0.0	0.0
ORTHOCLASE	3.2	0.5	3.2	3.0	3.8	3.8	5.5	4.5	7.4	2.2	1.5	2.3
ALBITE	17.2	16.8	14.7	14.2	21.3	21.3	22.6	21.4	35.0	18.6	18.4	20.9
ANORTHITE	33.9	42.8	38.6	42.4	25.5	24.2	22.2	23.5	17.7	28.2	26.1	25.7
DIOPSIDE	22.1	26.2	22.9	22.7	23.4	23.4	22.2	22.2	18.3	20.4	22.9	22.4
HYPERSTHENE	1.8	8.8	4.5	7.9	14.4	19.2	18.4	21.2	9.3	15.6	18.9	21.2
OLIVINE	16.1	0.0	13.9	4.4	4.8	0.0	1.9	0.1	4.3	9.1	5.5	1.1
MAGNETITE	3.0	1.9	2.6	2.2	3.1	3.2	3.3	3.2	3.3	2.9	3.0	2.9
ILMENITE	2.5	1.7	2.3	2.0	3.3	3.4	3.5	3.5	4.1	2.8	3.2	3.0
APATITE	0.3	0.2	0.2	0.2	0.4	0.4	0.4	0.4	0.5	0.4	0.4	0.4
DIFF. INDEX	20.4	18.3	17.9	18.2	25.1	26.2	28.0	25.8	42.4	20.8	19.9	23.2

RHUM DOLERITE GROUPS 1-12   CIPW NORMS

	51A76*	64A76	79A76	77003	77004*	77006*	77007	77040	77075*	77078	77092	77105
QUARTZ	0.0	0.6	0.0	0.0	0.0	0.0	0.0	0.0	0.0	0.7	1.0	0.0
ORTHOCLASE	3.6	5.1	2.3	5.7	4.9	2.1	5.7	5.4	3.4	3.8	4.0	4.2
ALBITE	25.1	27.3	21.8	28.5	35.9	29.8	27.2	28.7	21.1	25.3	24.4	24.1
ANORTHITE	23.0	22.5	24.3	19.6	19.9	25.0	24.1	24.3	23.9	22.0	25.6	25.1
DIOPSIDE	21.4	16.5	22.9	18.8	14.8	12.2	17.6	17.8	17.2	17.8	21.5	22.8
HYPERSTHENE	16.3	20.8	18.0	15.5	11.4	20.9	13.4	14.4	24.3	22.0	17.3	14.3
OLIVINE	2.4	0.0	3.7	4.5	6.5	4.0	5.9	12.0	4.1	3.0	0.0	4.3
MAGNETITE	3.3	2.9	3.2	3.2	2.9	2.9	3.0	2.9	2.9	3.4	2.9	3.2
ILMENITE	3.6	3.8	3.4	3.7	3.3	2.7	2.9	2.3	2.8	3.6	2.1	2.1
APATITE	0.4	0.6	0.4	0.5	0.5	0.4	0.4	0.3	0.4	0.6	0.3	0.2
DIFF. INDEX	28.7	33.0	24.1	34.2	40.7	31.0	32.8	26.0	24.5	29.8	30.3	28.3

	77108	77124	77145	77149	77250	77281	77272	77316	77325	77339	77349	77350
QUARTZ	0.0	0.5	0.0	0.0	0.0	3.0	4.2	0.0	1.6	0.0	0.0	0.0
ORTHOCLASE	7.2	9.5	5.3	2.7	2.9	4.5	4.7	4.5	7.0	7.0	3.2	2.9
ALBITE	27.8	29.8	25.8	19.0	24.0	21.6	22.1	29.9	32.0	27.8	21.3	20.3
ANORTHITE	24.4	18.2	18.8	25.8	22.1	26.0	27.2	21.5	17.7	23.0	26.7	24.5
DIOPSIDE	18.9	13.3	22.1	23.5	17.5	20.4	23.0	21.5	15.0	12.7	19.0	23.2
HYPERSTHENE	9.7	19.9	15.1	14.8	22.8	17.4	16.7	3.1	19.6	28.5	13.9	16.4
OLIVINE	6.5	0.0	2.5	7.3	0.0	0.0	0.0	12.1	0.0	2.6	8.8	6.6
MAGNETITE	2.8	3.4	4.2	3.2	3.0	3.0	2.8	3.4	3.2	2.8	3.0	3.2
ILMENITE	2.3	4.7	4.6	2.7	4.5	2.1	2.0	3.5	3.2	2.9	2.9	2.6
APATITE	0.6	0.6	0.6	0.2	0.6	0.2	0.3	0.5	0.8	0.3	0.4	0.3
DIFF. INDEX	35.0	39.8	31.1	22.7	28.7	29.9	31.1	34.4	40.5	35.2	24.4	23.3

RHUM DOLERITE GROUPS 1-12   CIPW NORMS

	15A76	25A76*	75A76	77061	77064	77127	77148	77155A	77243	77244	77306	77315
QUARTZ	1.2	0.0	0.0	0.4	0.0	0.0	2.4	0.0	0.0	1.1	0.0	0.0
ORTHOCLASE	6.2	5.6	5.8	3.8	2.5	2.0	6.8	4.1	4.6	8.2	4.8	5.4
ALBITE	22.3	25.3	31.0	28.6	29.4	30.7	22.3	24.4	21.8	25.2	26.1	24.3
ANORTHITE	22.2	20.5	17.5	19.5	21.7	20.2	19.4	23.2	24.4	19.5	19.3	18.2
DIOPSIDE	21.6	21.1	19.4	19.0	22.4	17.6	19.0	23.3	20.0	13.6	21.8	23.0
HYPERSTHENE	19.2	16.6	8.9	19.2	8.9	10.0	21.8	19.2	16.3	24.2	13.9	6.5
OLIVINE	0.0	2.0	8.1	1.1	7.3	1.6	0.0	7.0	5.4	0.0	4.7	9.8
MAGNETITE	3.8	3.9	3.8	3.9	3.5	3.9	3.8	3.8	3.8	3.7	4.7	3.6
ILMENITE	4.1	4.4	4.8	4.3	3.9	4.2	3.9	3.5	3.2	3.8	4.2	3.6
APATITE	0.5	0.5	0.6	0.6	0.4	0.6	0.5	0.4	0.4	0.5	0.5	0.6
DIFF. INDEX	29.6	30.9	36.8	32.4	31.9	32.7	31.5	28.5	26.4	34.5	30.9	33.7

	29A76*	55A76*	76A76*	81A76*	77034*	77088	77209	77346	32A76*	83A76*	77058*	77090*
QUARTZ	7.3	7.3	3.8	8.1	2.8	6.0	4.3	3.7	0.0	0.0	0.0	0.0
ORTHOCLASE	6.3	9.1	8.0	4.0	8.0	1.0	12.9	6.0	8.6	6.3	3.8	5.4
ALBITE	23.0	31.0	29.8	34.0	30.5	28.0	31.1	28.2	23.1	19.2	26.0	28.0
ANORTHITE	21.0	17.3	19.1	17.6	18.5	22.7	17.2	21.0	24.4	27.4	26.3	25.4
NEPHELINE	0.0	0.0	0.0	0.0	0.0	0.0	0.0	0.0	0.0	0.0	0.0	0.0
DIOPSIDE	13.4	12.3	14.1	14.6	13.9	9.8	14.9	15.3	6.7	20.3	17.7	14.0
HYPERSTHENE	22.5	17.1	18.0	15.5	20.5	23.7	14.8	19.2	0.0	1.5	0.0	0.0
OLIVINE	0.0	0.0	0.0	0.0	0.0	0.0	0.0	0.0	25.3	15.8	18.4	20.1
MAGNETITE	3.2	2.9	3.8	3.3	2.7	3.6	3.3	2.7	3.6	4.3	3.3	3.2
ILMENITE	3.2	2.9	3.8	3.3	2.7	3.6	3.3	2.7	3.6	4.3	3.3	3.2
APATITE	0.4	0.5	0.6	0.4	0.4	0.7	0.5	0.4	1.0	0.5	0.7	0.5
DIFF. INDEX	36.6	47.5	41.5	46.1	41.4	35.0	46.2	38.8	36.2	33.7	30.6	30.8

RHUM DOLERITE GROUPS 1-12   CIPW NORMS

	77137	77184	77005	77008*	77023	77279*	77342*	77132*	77177*
CORUNDUM	0.0	0.0	0.0	0.0	0.0	0.0	0.0	0.0	1.9
ORTHOCLASE	8.7	6.0	9.4	5.4	7.7	14.7	12.2	24.8	29.3
ALBITE	25.1	18.7	37.8	46.5	30.0	36.7	29.8	41.3	36.3
ANORTHITE	21.3	18.4	15.3	12.7	14.3	13.9	13.9	11.1	8.9
NEPHELINE	1.4	10.8	2.7	0.7	3.3	0.0	3.5	0.0	0.0
DIOPSIDE	9.9	18.2	15.7	17.2	21.3	19.0	17.4	5.9	0.0
HYPERSTHENE	0.0	0.0	0.0	0.0	0.0	7.7	0.0	7.5	5.0
OLIVINE	25.7	28.2	12.3	13.8	12.6	9.3	12.9	2.2	10.7
MAGNETITE	3.2	3.3	3.0	3.0	4.3	3.1	3.3	1.9	2.5
ILMENITE	3.6	3.7	3.3	3.2	5.7	3.8	5.0	3.3	3.2
APATITE	1.1	0.7	0.5	0.5	0.8	0.6	1.8	2.0	2.2
DIFF. INDEX	35.3	35.6	47.9	52.7	41.3	51.5	45.6	66.1	65.6

	21A76	22A76*	41A76	47A76*	60A76	61A76	62A76	63A76	77012	77013	77032	77035
ORTHOCLASE	2.3	1.2	1.1	1.2	1.1	2.0	2.3	2.0	0.6	3.8	2.3	1.9
ALBITE	20.6	19.6	21.3	19.2	20.6	18.7	17.3	18.1	20.8	21.9	24.5	23.5
ANORTHITE	26.2	26.5	28.7	26.5	26.8	27.1	28.5	27.5	28.2	27.9	23.4	25.9
DIOPSIDE	25.2	26.4	22.3	24.3	22.8	25.2	25.5	25.6	25.0	20.0	25.0	21.5
HYPERSTHENE	8.9	8.4	8.0	14.0	13.2	5.3	5.2	4.2	1.9	1.4	2.2	8.9
OLIVINE	10.2	10.2	11.2	7.9	8.6	14.6	14.5	15.5	16.7	18.5	14.7	11.7
MAGNETITE	3.2	3.6	3.5	3.2	3.3	3.6	3.5	3.6	3.4	3.2	3.4	3.2
ILMENITE	3.0	3.7	3.3	3.2	3.1	3.2	3.0	3.1	3.1	3.0	3.7	3.1
APATITE	0.3	0.4	0.5	0.4	0.4	0.3	0.3	0.3	0.3	0.4	0.5	0.3
DIFF. INDEX	22.9	20.8	22.4	20.4	21.7	20.6	19.5	20.1	21.4	25.6	26.9	25.4

RHUM DOLERITE GROUPS 1-12   CIPW NORMS

	77044*	77068*	77076	77125	77148*	77175*	77176*	77204	77208	77231	77269	77284
ORTHOCLASE	2.0	2.0	4.1	2.0	0.8	3.0	4.5	3.0	1.8	2.2	1.2	1.3
ALBITE	23.4	21.0	20.0	16.8	19.4	23.4	19.3	21.8	17.0	18.3	19.7	16.8
ANORTHITE	26.7	27.3	24.6	28.8	29.5	26.5	29.5	24.9	32.5	31.0	28.6	32.4
DIOPSIDE	24.2	20.6	25.4	27.7	23.9	16.9	12.6	19.4	21.0	22.7	24.3	24.9
HYPERSTHENE	0.6	0.2	5.0	7.8	3.4	2.7	11.3	3.9	3.2	6.3	9.6	2.2
OLIVINE	16.2	22.3	11.5	10.3	16.3	24.0	15.0	18.6	16.9	13.9	9.4	15.2
MAGNETITE	3.3	3.4	3.4	3.4	3.4	3.7	3.8	3.7	3.6	3.2	3.6	3.3
ILMENITE	3.2	2.8	3.6	2.9	2.9	3.2	3.0	3.2	3.2	3.0	3.4	3.4
APATITE	0.4	0.4	0.5	0.2	0.4	0.6	0.6	0.5	0.4	0.5	0.4	0.4
DIFF. INDEX	25.4	23.1	24.1	18.8	20.2	26.4	23.8	25.8	18.8	22.5	23.7	18.2

	77327	77330*	77332	77333	77335	77337	77351	26A76*	82A76	94A76	95A76*	77010
ORTHOCLASE	2.9	2.2	1.0	2.2	1.5	3.6	2.6	0.5	1.5	3.5	3.5	2.0
ALBITE	23.8	18.6	21.5	17.4	20.1	21.5	20.7	23.8	25.1	22.2	23.9	22.9
ANORTHITE	25.1	26.7	27.6	28.7	27.2	27.1	27.4	26.2	22.3	29.8	24.9	23.7
NEPHELINE	0.0	0.0	0.0	0.0	2.1	0.0	0.0	0.0	1.0	0.0	2.1	1.7
DIOPSIDE	18.6	28.5	22.3	23.2	23.4	22.2	25.3	26.2	25.5	21.0	22.0	26.6
HYPERSTHENE	3.2	4.1	2.3	12.3	0.0	0.0	0.4	0.0	0.0	0.0	0.0	0.0
OLIVINE	18.6	13.4	17.4	10.0	17.9	18.7	17.3	18.0	16.5	16.3	16.6	15.3
MAGNETITE	3.7	3.4	3.3	3.3	3.4	3.4	3.3	3.5	3.7	3.2	3.4	3.6
ILMENITE	3.6	2.8	3.1	2.7	3.9	3.1	2.7	3.5	4.1	3.3	3.2	3.7
APATITE	0.5	0.3	0.4	0.3	0.5	0.3	0.3	0.4	0.4	0.4	0.4	0.4
DIFF. INDEX	26.7	20.8	23.5	19.6	23.7	25.0	23.3	22.2	27.5	26.0	29.5	26.7

RHUM DOLERITE GROUPS 1-12   CIPW NORMS

	77011	77015	77070	77071	77073	77074	77086	77091*	77120	77205*	77215	77313
ORTHOCLASE	2.3	1.6	2.8	0.4	1.6	1.6	0.5	0.9	2.1	5.4	4.8	2.6
ALBITE	22.6	23.9	18.6	24.8	23.8	23.1	20.6	16.9	19.8	22.7	18.3	14.2
ANORTHITE	22.3	24.2	24.6	22.5	26.3	26.5	27.6	27.4	28.2	20.1	25.3	25.5
NEPHELINE	3.9	2.0	2.9	1.4	1.1	1.2	2.5	1.1	0.7	2.2	3.7	4.6
DIOPSIDE	26.9	25.1	31.8	24.3	20.3	19.7	25.4	33.3	24.8	24.2	27.1	27.2
OLIVINE	16.3	15.6	13.3	17.4	19.4	20.2	16.8	13.3	17.1	17.2	15.4	18.7
MAGNETITE	3.6	3.5	3.8	4.1	3.4	3.5	3.4	3.4	3.4	3.6	3.7	3.6
ILMENITE	3.7	3.6	3.8	4.6	3.6	3.6	3.1	3.6	3.5	3.9	3.5	3.3
APATITE	0.5	0.4	0.4	0.5	0.5	0.6	0.3	0.4	0.4	0.6	0.4	0.4
DIFF. INDEX	26.8	27.5	22.4	26.6	26.4	25.9	23.5	18.9	22.7	30.3	23.6	21.4

	77314*	77324	77331*	77335	77340	77343	77344	77348	77359*	13A76	14A76	38A76
ORTHOCLASE	0.5	2.8	1.4	1.4	0.9	1.7	1.0	3.2	0.8	2.2	1.9	0.2
ALBITE	19.1	18.5	21.5	22.0	20.1	22.0	23.5	20.5	23.2	24.6	23.7	27.8
ANORTHITE	25.6	28.2	26.8	23.5	26.9	25.8	30.1	27.5	26.7	21.5	21.5	23.4
NEPHELINE	3.6	0.3	0.3	0.6	1.0	0.2	0.3	1.0	0.1	2.0	1.5	2.2
DIOPSIDE	25.7	24.3	22.3	28.8	25.2	24.8	22.2	22.2	25.4	23.2	25.9	22.0
HYPERSTHENE	0.0	0.0	0.0	0.0	0.0	0.0	0.0	0.0	0.0	11.7	0.0	0.0
OLIVINE	18.4	18.2	19.0	16.3	18.2	18.3	16.4	19.1	17.2	6.0	15.6	16.0
MAGNETITE	3.0	3.7	3.4	3.6	3.5	3.5	3.2	3.2	3.3	4.3	4.2	3.8
ILMENITE	3.3	3.6	2.9	3.4	3.7	3.4	2.8	3.0	3.3	5.2	5.2	4.1
APATITE	0.4	0.5	0.3	0.4	0.5	0.3	0.4	0.4	0.4	0.5	0.6	0.5
DIFF. INDEX	23.2	21.6	23.2	24.0	22.0	23.9	24.9	24.7	24.1	26.8	27.0	30.3

RHUM GABBRO PLUGS   CIPW NORMS

	77031*	77033*	77124*	77256	77257	77292*	77295	77320*	77252	77280	77288	77467
ORTHOCLASE	3.3	0.6	1.0	2.3	1.3	1.0	2.5	1.1	1.0	1.3	2.3	4.1
ALBITE	18.6	17.2	15.0	24.3	19.2	21.3	22.0	24.2	13.3	14.3	8.2	31.1
ANORTHITE	29.2	34.1	34.8	28.8	30.6	31.6	29.3	31.2	29.4	29.9	37.4	23.5
NEPHELINE	0.0	0.0	0.0	2.6	0.0	0.0	0.0	0.0	2.3	3.4	0.0	0.0
DIOPSIDE	17.0	24.1	23.6	17.1	21.4	14.4	16.2	16.5	12.5	15.3	22.7	19.7
HYPERSTHENE	19.2	13.2	4.5	0.0	0.0	16.9	11.6	0.2	0.0	0.0	0.5	2.6
OLIVINE	7.6	10.6	15.2	22.0	22.4	9.3	11.8	24.6	35.4	28.8	18.7	12.8
MAGNETITE	2.8	2.7	2.7	3.1	2.8	3.1	2.8	3.3	3.1	3.5	2.2	3.1
ILMENITE	2.0	1.2	1.8	3.4	1.8	2.2	3.0	2.4	2.7	3.2	1.8	2.7
APATITE	0.2	0.2	0.2	0.6	0.2	0.2	0.6	0.3	0.4	0.4	0.2	0.4
DIFF. INDEX	21.9	17.8	17.1	25.0	20.7	22.2	24.6	21.5	16.5	18.9	8.5	35.2

	77002	77049*	77087*	77210	77322	77334	77360*
ORTHOCLASE	0.4	0.2	0.8	0.4	1.2	2.3	0.5
ALBITE	22.7	21.1	24.3	16.8	20.3	24.2	23.7
ANORTHITE	28.2	16.8	23.9	26.4	24.3	24.4	26.5
NEPHELINE	0.0	9.7	0.0	0.0	0.0	0.0	1.4
DIOPSIDE	21.2	28.9	19.7	23.0	27.5	23.0	24.1
HYPERSTHENE	10.2	0.0	15.0	1.5	0.0	0.8	2.0
OLIVINE	8.8	14.2	6.2	15.8	16.4	16.7	15.5
MAGNETITE	3.9	4.2	4.1	4.0	3.8	3.7	3.7
ILMENITE	4.2	4.5	5.4	3.8	3.8	3.6	4.0
APATITE	0.5	0.5	0.5	0.3	0.4	0.3	0.5
DIFF. INDEX	23.0	30.9	25.1	25.2	23.7	26.6	25.7

RHUM GABBRO PLUGS   CIPW NORMS

	77098	77108	77246*	77261	77265	77267*	77270	77273	77282	77283	77287	77296
ORTHOCLASE	1.0	1.9	3.3	6.2	0.7	3.5	5.8	1.5	1.8	5.2	2.6	1.1
ALBITE	22.9	24.6	23.0	28.0	24.5	26.5	26.3	26.4	26.3	23.1	25.5	26.2
ANORTHITE	22.6	23.9	23.0	24.5	27.3	19.0	27.3	24.6	24.2	24.7	27.0	26.8
NEPHELINE	3.6	0.0	0.0	0.5	1.5	3.8	0.0	2.3	2.3	0.9	2.0	0.6
DIOPSIDE	34.6	31.2	25.9	18.2	21.3	31.1	15.2	21.8	29.1	24.5	17.7	23.0
HYPERSTHENE	0.0	0.0	3.5	0.0	0.0	0.0	0.0	0.0	0.0	0.0	0.0	0.0
OLIVINE	8.2	11.4	12.1	14.6	17.0	7.9	17.8	15.9	11.3	15.0	18.0	14.9
MAGNETITE	2.7	3.1	3.9	3.5	3.5	2.9	3.2	3.4	3.1	3.2	3.0	2.9
ILMENITE	3.1	3.0	3.8	3.7	3.0	3.0	3.1	3.5	3.5	3.0	2.9	3.8
APATITE	0.4	0.4	0.7	0.7	0.5	0.5	0.5	0.5	0.4	0.4	0.4	0.7
DIFF. INDEX	28.3	26.5	26.3	34.8	26.7	33.7	32.1	34.3	28.4	29.2	30.1	27.9

RHUM GABBRO PLUGS   CIPW NORMS

	77182*	77183*	77274*	77264*	33A76	77163	77328	77353
QUARTZ	2.5	4.1	3.3	9.6	0.7	4.7	4.1	3.8
ORTHOCLASE	5.2	6.4	9.5	14.1	3.4	3.8	8.5	3.2
ALBITE	23.8	28.9	39.2	34.5	21.6	22.4	15.1	11.8
ANORTHITE	26.2	19.8	15.2	13.6	24.7	27.6	42.9	49.1
DIOPSIDE	24.5	19.0	12.1	4.0	31.2	26.7	25.6	12.4
HYPERSTHENE	18.2	17.1	12.2	16.6	12.2	24.2	12.7	3.7
OLIVINE	0.0	0.0	0.0	0.0	0.0	0.0	0.0	19.7
MAGNETITE	3.0	3.5	3.4	3.3	2.8	2.8	1.8	2.3
ILMENITE	3.2	4.2	4.3	3.8	3.2	2.9	1.2	0.8
APATITE	2.4	0.5	0.7	0.6	0.3	0.2	0.2	4.1
DIFF. INDEX	28.6	35.8	49.1	58.1	25.7	26.1	15.7	11.9

PERIDOTITE PLUGS CIPW NORMS

	77051*	77054*	77055	77066	77089	77097	77099	77189	77136	77138	77181	77182
ORTHOCLASE	0.5	0.6	0.4	0.8	0.6	0.6	0.0	0.8	0.8	0.6	0.7	0.9
ALBITE	3.2	3.1	2.5	6.6	7.0	6.0	3.0	4.1	5.1	3.3	7.0	5.4
ANORTHITE	13.2	16.8	13.1	19.1	24.2	23.1	12.0	18.0	16.2	16.0	21.3	24.8
LEUCITE	0.0	0.0	0.0	0.0	0.0	0.0	0.0	0.0	0.0	0.0	0.0	0.0
NEPHELINE	0.0	1.7	0.0	0.0	1.5	1.4	3.0	0.6	1.0	0.4	0.0	0.6
DIOPSIDE	1.5	2.8	1.4	6.1	6.5	4.4	2.8	2.3	3.0	3.4	2.9	4.7
HYPERSTHENE	2.0	0.0	2.7	0.0	0.0	0.0	0.0	0.0	0.0	0.0	1.8	0.0
OLIVINE	75.7	71.5	76.3	62.6	55.8	59.8	76.7	69.8	68.7	71.7	61.3	58.4
CAL ORTHOSIL	0.0	0.0	0.0	0.0	0.0	0.0	0.0	0.0	0.0	0.0	0.0	0.0
MAGNETITE	3.3	2.8	3.0	3.5	2.9	3.3	3.4	3.1	3.8	3.4	3.4	3.0
ILMENITE	0.5	0.5	0.6	1.1	1.2	1.2	1.1	1.1	1.2	1.0	1.5	1.1
APATITE	0.1	0.1	0.1	0.2	0.2	0.2	0.1	0.2	0.2	0.1	0.2	0.2
DIFF. INDEX	3.7	5.4	2.8	7.5	9.1	8.0	3.5	5.5	6.9	4.3	7.7	6.9

PERIDOTITE PLUGS CIPW NORMS

	77183	77259	77268	77281	77286	77290	77309	77357
CORUNDUM	0.0	0.0	0.0	0.0	0.0	0.0	0.0	0.3
ORTHOCLASE	1.0	0.5	0.4	0.4	0.4	0.2	0.7	0.2
ALBITE	5.7	6.7	2.9	4.0	5.6	2.0	2.8	1.4
ANORTHITE	22.0	22.2	18.1	16.6	18.8	15.7	19.9	9.5
NEPHELINE	2.2	1.7	0.0	0.0	0.0	2.0	3.5	0.0
DIOPSIDE	3.5	5.7	9.0	1.5	2.9	0.0	4.6	0.0
HYPERSTHENE	0.0	0.0	0.0	7.8	0.0	0.0	0.0	0.0
OLIVINE	60.5	59.2	64.9	66.0	67.2	75.4	64.8	84.8
MAGNETITE	3.4	3.2	3.0	2.9	3.2	3.2	2.9	3.2
ILMENITE	1.4	1.2	0.6	0.6	0.9	0.5	0.6	0.5
APATITE	0.2	0.2	0.1	0.1	0.1	0.1	0.1	0.1
DIFF. INDEX	9.0	8.3	4.2	4.4	6.1	4.2	7.1	1.7

Appendix 8.1

Calculated olivine and spinel settling rates in

basaltic magmas.

The behaviour of fluids interacting with dispersed

particles can be predicted from the Reynolds Number (N_R)

of the system. This is the ratio of inertial force to

viscous force and can be expressed as follows:

$$N_R = \frac{UL\rho}{\mu}$$

where U is the relative velocity of fluid and particles

(cm sec^{-1})

   L is the particle diameter (cm)

   ρ is the density of the fluid (g cm^{-3})

   μ is the viscosity of the fluid (poises)

Large values of Reynolds Number ($N_R > 10,000$) imply only

slightly viscous behaviour and the development of turbulent

flow, while small values indicate highly viscous behaviour

and the operation of a laminar flow regime.

Natural systems involving magma and crystals have very

small Reynolds Number (< 0.1) and under these circumstances

it has been suggested that Stokes Law may be used to estimate

the settling velocity of crystals in a basaltic liquid

(Wadsworth 1973, Donaldson 1974). The assumption that

basalt liquidus phases will sink in a basalt liquid is a

fundamental premise of the cumulus theory in igneous

systems advocated by Wager and co-workers (e.g. Wager et al., 1960, Wager and Brown, 1968) which has recently been challenged by McBirney and Noyes (1979). These authors note that the olivine crystals in the KilaueaIki 1959 crater lava lake in Hawaii had not settled in the years following this lake's emplacement and suggested that Stokes Law was not applicable to crystals in igneous melts. It is beyond the scope of this thesis to reassess the role of crystal settling in the genesis of the Rhum layered peridotites. However, it may be pertinent that the mafic parent advocated in Chapter 8 of this thesis would be less viscous than a basalt parent and consequently may be less susceptible to the criticisms of the role of crystal settling in the Skaergaard parent levelled by McBirney and Noyes (1979).

Stokes Law may be stated as follows:

$$U = \frac{D^2 (\rho_P - \rho_F)g}{18\mu}$$

where U is the terminal settling velocity of the particle (cm sec^{-1})

D is the particle diameter (cm)

ρ_P is the particle density (gm cm^{-3})

ρ_F is the fluid density (gm cm^{-3})

g is the acceleration due to gravity (980 cm sec^{-2})

μ is the viscosity of the fluid (poises)

and is applicable to streamline motion of spherical

particles. The olivines and chromites in the Rhum layered

series are not spherical but Wadsworth (1973) suggests that

providing the grains do not have extreme shapes the calculated

results for a sphere of equivalent diameter hold reasonably

well (within 20%). In addition the lack of data concerning

magma density and viscosity introduce more uncertainty into

the results presented in Table 8.2 consequently these

figures can only be viewed on a comparative basis (ie. large

olivines will settle faster than small olivines).

The mineral density value ρP at $1000^{\circ}C$ for olivine

(Fo85) and Cr-spinel used in the calculations was 3.22 and

4.53 respectively (Birch et al., 1942). Various estimates

for magma viscosity ranging from 300 to approximately 3000

poises have been made (Macdonald 1963, Bottinga and Weill

1970, McBirney and Noyes 1979) so the calculations were made

for a range of magma viscosities. Various estimates have

also been made for magma densities (ρF), these are: 2.7-

2.8 Dunham and Emeleus (1967), 2.64-2.78 Bottinga and

Weill (1970), 2.58 Wadsworth (1973). The calculations

made here assumed a magma density of 2.8, whilst this may

lead to difficulties with respect to the cumulus theory in

that plagioclase may not sink in a magma of this density it

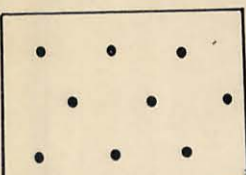does not affect the conclusion drawn from Table 8.2 that

olivine will sink much faster than Cr-spinel. The settling rates for both minerals will increase if a lower magma density value had been chosen. A comparison of olivine and spinel settling rates in a magma of density 2.5 and 2.8 respectively is made below to illustrate this point.
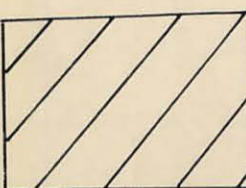
Mineral type	ρ_P	ρ_F	Particle diameter	Viscosity (poises)	Settling rate	
Ol	3.22	2.8	1 mm	300	0.0762	cm/sec
Ol	"	2.5	1 mm	"	0.1307	"
Ol	"	2.8	3 mm	"	0.6860	"
Ol	"	2.5	3 mm	"	1.1760	"
Cr-Sp		2.8	0.3 mm	"	0.0283	"
Cr-Sp		2.5	0.3 mm	"	0.0332	"
Cr-Sp		2.8	0.4 mm	"	0.0502	"
Cr-Sp		2.5	0.4 mm	"	0.0589	"

The particle diameters for Cr-spinel and olivines were measured in three thin sections from the Unit 11/ Unit 12 junction in the Durham University collections. The olivines range from 0.8-3.0mm in size and the largest spinels were 0.4mm diameter.

FIG 2.1 RHUM DYKE STRIKE ORIENTATIONS
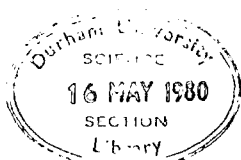
KEY

TORRIDONIAN AND TRIASSIC OUTSIDE THE MAIN RING FAULT

ACID AND ASSOCIATED ROCKS

U LAYERED ULTRABASIC ROCKS

L LAVAS

APPROXIMATE LOCATION OF TRAVERSE
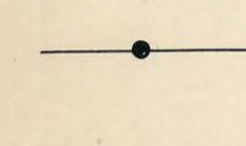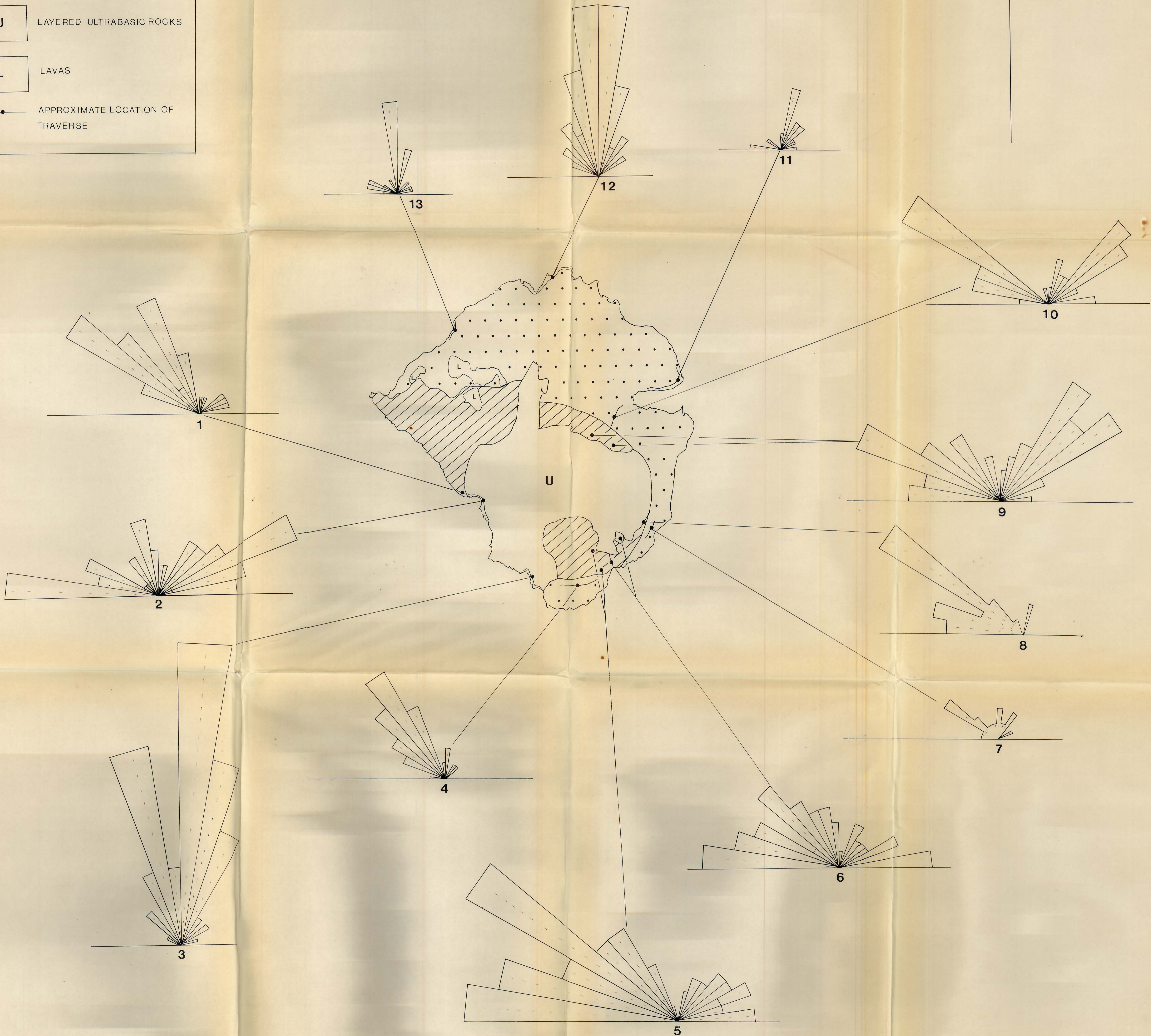
N

Fig. 2.11 Location map of some Rhum minor intrusions.

KEY

L	LAVAS AND CONGLOMERATES
U	LAYERED ULTRABASIC ROCKS
A	ACID AND ASSOCIATED ROCKS
Tr	TRIASSIC
T	TORRIDONIAN OUTSIDE THE MAIN RING FAULT
⬭	GABBRO PLUG
⬭	PERIDOTITE PLUG
▱	ACID DYKE
▱	THICK CONFORMABLE SHEET
▱	BIG FELDSPAR DYKE
77123	SPECIMEN NUMBER